Development of mathematical models of everyday life factors on glycaemia, identifiable in outpatients with type 1 diabetes

---

A thesis
submitted in partial fulfilment
of the requirements for the degree
of
Doctor of Philosophy
by
Erin Mansell

Department of Mechanical Engineering
University of Canterbury
2017

To my Dad,

whose legacy includes my love of knowledge,

wisdom,

and truth.

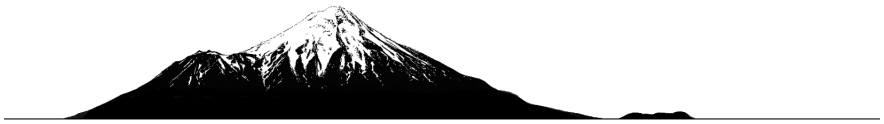

Foreward

Type 1 diabetes mellitus is an autoimmune disorder in which a lack of insulin is detrimental to the regulation of blood glucose. People with the disease must take doses of insulin to compensate. However, many endogenous and environmental stimuli alter glucose metabolism and sensitivity to insulin in the day to day life of the individual. The ability to understand, quantify and model such factors has great potential to improve glycaemic control.

The individualised nature of both the presence of and response to everyday stimuli inclines the research needs towards models that can be used in the outpatient environment. The unique challenges around the quantity and quality of outpatient data necessitates consideration to the practical identifiability of behaviours and parameters in the model. Hence, this work works towards modelling everyday life effects in a manner that is robust to poorer data. In particular:

Chapter 1 introduces the clinical concepts around type 1 diabetes along with some of the underlying physiological concepts of glucose homoeostasis.

Chapter 2 briefly reviews the history of mathematical modelling of glycaemia.

Chapter 3 introduces concepts around model fitting, identifying model parameters, and especially the need for considering practical identifiability.

Chapter 4 reviews the literature for justification and explanation of the effects of nutritional variation, psychological state, physical activity and metabolic rhythms on glycaemia. The review also covers current methods

and technologies for quantifying the presence or effect of these factors and mathematical models developed to date.

Chapter 5 introduces the high quality clinical data that has been obtained for model building and evaluation.

Chapter 6 details a range of models developed for the appearance of plasma insulin from subcutaneous insulin infusion, and an extensive analysis to compare the performance of the models.

Chapter 7 presents a data-driven modelling technique used to ascertain the nature of the effect of mild to moderate exercise on plasma insulin and glucose concentration.

Chapter 8 builds on the data-driven information with simplistic differential models for insulin and glucose using basis functions to model the effects of exercise.

Chapter 9 explores *in silico* the potential for everyday life effects to be identified in diary-style outpatient data.

Chapter 10 presents a method for further *in silico* analysis of the identifiability during model recovery.

Chapter 11 details a preliminary exploration of a potential method for evaluating *a priori* practical identifiability.

Chapter 12 analyses the effect of pre-analytical glucose decay on diagnosis rates of gestational diabetes.

Chapter 13 summarises the findings of the research.

Chapter 14 suggests opportunities for future work.

Acknowledgments

My supervisor, Dr. Paul Docherty, deserves a tremendous amount of praise and thanks. If I had to guess, I'd say he's easily in the upper quartile of supervisors. He's guided me through this whole thesis journey, passing on knowledge, wisdom and reassurance, all with good (and also bad) humour.

Further thanks to my co-supervisors: Dist. Prof. Geoff Chase, for advising and editing my work on numerous occasions (only one of which required a coffee bribe), and Dr. Sid Becker for always cheering me up.

Thanks to Dr. Signe Schmidt and the rest of the group in Denmark for gifting some amazing data and for continued collaboration. Also thanks to Dr. Helen Lunt and those at the Christchurch Diabetes Clinic for introducing me to clinical aspects of diabetes research.

I would like to thank my office mates Sophie, Jeremy and Bradley, for interrupting my days with banter and other interesting conversation topics.

Much appreciation goes towards my two flat-families for making home life awesome. Buzzy, Daniel, Megan, Jai, Tristan, Wilma and Danielle have honestly been the best people to come home to. We've shared a lot of laughs and plenty of deep and meaningfuls. Equally, much appreciation to my actual family, Mum, Scott and Lachlan, my church family, friends and mentors for supporting and encouraging me, praying for me, and just generally being awesome people to hang out with.

Of course, the most praise belongs to God the Father of my Lord Jesus Christ, who's Spirit has been with me through good times and bad, grown and challenged me, encouraged and loved me. He is endlessly faithful, good and merciful.

Abstract

Insulin therapy for type 1 diabetes mellitus is used to manage and maintain near normal blood glucose. However, this therapy balances treating hyperglycaemia and avoiding hypoglycaemia, both of which have negative health consequences. Optimal insulin doses are often uncertain in everyday life. Factors that are often overlooked can noticeably alter the metabolism of glucose and insulin, which can confound glycaemic control. Four major categories of everyday life factors have been reviewed in depth in the literature: nutritional variability, psychological effects, physical activity and metabolic rhythms.

Physiological mathematical models have long been used to study, observe and control glycaemia. However, relatively little physiological modelling of everyday outpatient factors has been carried out. Clinical data of subjects with type 1 diabetes experiencing everyday life events such as exercise, meals, snacks and insulin boluses was used as the basis for model development. In particular, the inclusion of the appearance of insulin from subcutaneous infusion, and the effect of exercise on plasma insulin and glucose concentration have been modelled. The insulin system was modelled with multiple physiological compartments while the effect of exercise was initially modelled with a data-driven autoregressive technique before basis models were developed.

Practical identifiability was considered to be a mathematically limiting factor for model complexity and specificity given that high quality data is generally not available in the outpatient environment. Hence, model development strongly considered practical identifiability. For example, a number of analyses were employed to determine which of multiple options for the insulin model had the optimal complexity. The result was that one of the simpler models had the best compromise between fit, parameter

robustness and prediction ability. Furthermore, since practical identifiability is a relatively new field with no formal analyses, two possible evaluation techniques were explored. One technique with an analytical *a priori* nature and the other using retroactive computational methods.

An *in silico* Monte Carlo analysis was carried out to test the potential model recovery of exercise, stress fatigue and insulin sensitivity in outpatient glycaemia. It was found that sparse, irregular and noisy data could be overcome as the data accumulated to provide a clearer picture of patient status. Variation in parameters decreased with increasing data according to the $1/\sqrt{n}$ rule, indicating that measurement error and other sources of noise introduced did not obscure parameter estimation. This proof of concept represents a pathway toward personalisable glycaemic models that can be fitted to the individual's responses, and be used to predict their response to treatment. Ultimately, sound modelling of everyday life factors would improve the quality of life for sufferers of diabetes by improving control and decreasing the burden of disease management.

Table of Contents

List of Figures

List of Tables

Abbreviations

Clinical

T1DM	type 1 diabetes mellitus
T2DM	type 2 diabetes mellitus
GDM	gestational diabetes mellitus
OGTT	oral glucose tolerance test
CGM	continuous glucose monitor
IAsp	insulin aspart
BMI	body mass index
GI	glycaemic index
HAPO	Hypoglycaemia and Adverse Pregnancy Outcomes
IADPSG	International Association of Diabetes and Pregnancy Study Group

Physiological

IR	insulin resistance
SI	insulin sensitivity
IV	intravenous
SC	subcutaneous
GE	gastric emptying
EGP	endogenous glucose production
HR	heart rate
VO_2max	peak oxygen uptake
EE	energy expenditure
GIP	glucose-dependent insulinotropic peptide
GLP-1	glucagon-like peptide 1
R_a	rate of appearance

Statistical and Analytical

R	correlation coefficient
R^2	coefficient of determination
CV	coefficient of variation
CI	confidence interval
p	probability value with respect to statistical significance
Q_1, Q_2, Q_3	quartiles
CDF	cumulative distribution function
PCA	principle component analysis
ANOVA	analysis of variance
ROC	receiver operating characteristic
TP	true positive
TN	true negative
FP	false positive
FN	false negative
AIC	Akaike information criterion

Modelling

NARX	nonlinear autoregressive exogenous
AC	auto-correlative
CC	cross-correlative
MC	Monte Carlo

Computational

CPU	central processing unit
RAM	random access memory
NaN	not-a-number

Part I

Background

Chapter I

Type 1 diabetes

1.1 Introduction

Type 1 diabetes mellitus (T1DM) is a metabolic disorder resulting from the autoimmune destruction of pancreatic β-cells and subsequent lack of insulin secretion (Atkinson and Eisenbarth, 2001). Insulin is necessary to regulate blood glucose, without which high glucose levels result. Untreated, T1DM is fatal. Hence, exogenous forms of insulin are usually injected or infused subcutaneously. The disease often onsets in childhood, although it can develop at any age, and is estimated to account for 5-10% of all cases of diabetes (American Diabetes Association, 2006).

Prior to the 1850s diabetes was diagnosed by tasting urine, since the large quantities of glucose cleared by the kidneys was easily detectable. The 1920s saw both commercially available urinary glucose tests and the emergence of laboratory-based blood glucose measurement (Gale, 2002). More recently, testing the presence of particular antibodies has proved to be a good predictor of T1DM onset prior to the presentation of other clinical symptoms (Sosenko et al., 2013; Atkinson and Eisenbarth, 2001).

Both reported and apparent incidence of T1DM has significantly increased over the last couple of centuries (Gale, 2002) and even in the last couple of decades (The DIAMOND Project Group, 2006). The pathology of T1DM is considered to arise from a complex interaction between both risk-increasing and protective genetic factors and a variety of environmental influences, ultimately resulting in the production of auto-antibodies that target and destroy β-cells (Atkinson and Eisenbarth, 2001). The environmental factors

in particular are not well understood but the primary areas investigated are viral infections, infant diet and toxins. The fast increasing disease incidence draws much research interest to uncovering and therefore responding with preventative measures for environmental risk factors (The DIAMOND Project Group, 2006).

A related and much more common disorder is type 2 diabetes mellitus (T2DM) which is likewise characterised by high blood glucose and accounts for 90-95% of diabetes cases (American Diabetes Association, 2006). Unlike T1DM, this form of diabetes is usually due to a combination of insulin resistance and defective insulin secretion. Recent research indicates onset of T2DM to be caused by over-production of insulin (Pories and Dohm, 2012). Basal glucose production is subsequently higher to compensate for chronic hyperinsulinaemia. Combined with other environmental and genetic risk factors affecting insulin secretion and sensitivity, the postprandial insulin response becomes blunted, resulting in hyperglycaemia. As the disease progresses, β-cell production deteriorates and insulin secretion reduces. Hence, late-stage T2DM presents similarly to T1DM.

1.2 Glucose homoeostasis

Glucose is a simple monosaccharide sugar with the molecular formula $C_6H_{12}O_6$. Glucose is an essential nutrient for humans and absorbed as a major component of most dietary sources of carbohydrates. Glucose is also synthesised in the liver from other non-carbohydrate substrates. The circulatory system delivers glucose to all other organs in the body where it is metabolised to release usable energy. The central nervous system, smooth muscle and red blood cells are able to absorb glucose directly, but most other tissues such as skeletal muscle and fat rely on insulin to facilitate glucose transport into the cell (Cherrington, 1999). Since glucose is primarily transported throughout the body via the bloodstream, it is critical that glucose is present in the blood in appropriate concentrations.

The normal (euglycaemic) range for glucose is pictured in Figure 1.1.

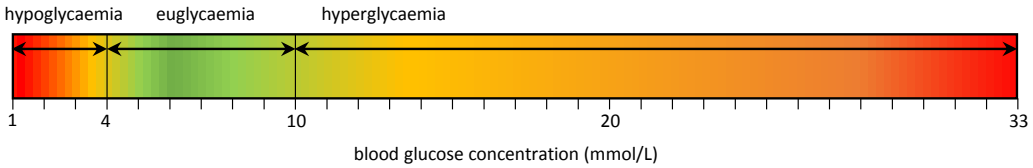

Figure 1.1: A diagram representing the full range of blood glucose, showing euglycaemia, hypoglycaemia and hyperglycaemia. Note that the euglycaemic range is relatively small and off-centred compared to the full range (Kovatchev et al., 1997).

Glucose < 3.9 mmol/L is hypoglycaemia (Kovatchev et al., 1997) which can be caused by excess exogenous insulin, and is generally accompanied by unpleasant symptoms such as anxiety, cognitive dysfunction and seizures (Cryer et al., 2003). Hypoglycaemia can be fatal or cause permanent brain damage due to energy starvation of the central nervous system. Frequent exposure to these blood glucose levels reduces an individual's hypoglycaemic awareness and therefore reduces their ability to take corrective action (Cryer et al., 2003). Glucose > 10 mmol/L is considered hyperglycaemia (Kovatchev et al., 1997). Chronic but mild hyperglycaemia tends to result in complications such as neuropathy, kidney disease, hypertension and heart disease (De Boer et al., 2008; Shankar et al., 2007; Retnakaran and Zinman, 2008; Rubin and Peyrot, 1999). Extreme hyperglycaemia associated with ketoacidosis and cerebral edema can be fatal (Atkinson and Eisenbarth, 2001).

Glucose concentration requires constant bodily regulation to remain at euglycaemic levels. The large quantity of incoming glucose from ingested meals is typically the most major disturbance. In healthy individuals, fasting glucose levels are around 4-5 mmol/L. Following a meal, blood glucose concentration may reach 7-10 mmol/L or higher for some individuals consuming meals with a large glycaemic load. Within 1-2 hours the concentration will be under 7 mmol/L again, progressing to fasted

levels. This glycaemic regulation is achieved through multiple concurrent mechanisms (Figure 1.2).

1.2.1 Insulin and peripheral uptake

Insulin is a peptide hormone secreted from the β cells of the pancreas. The primary function of insulin is to facilitate glucose transport into muscle and fat tissue to be stored and metabolised for energy. Insulin therefore has the dual primary purpose of reducing blood glucose concentration and thus mitigating postprandial hyperglycaemia. Secretion of insulin typically increases in response to sensory information from the gut (Cernea, 2011) and rising glucose levels (Cherrington, 1999). Likewise, low blood glucose and also high insulin concentrations reduce insulin secretion.

From the plasma, insulin diffuses into the extracellular interstitial space in peripheral muscle and fat tissues. There it docks to insulin receptors on the surface of a cell. Through a complex process, the insulin acts on the receptor to stimulate a new glucose transporter to be expressed in the cell membrane. The new transporter increases the rate of glucose transport into the cell, also promoting glycogen formation. After the insulin molecule has fulfilled its purpose it may be degraded by the cell or released. The liver and kidneys clear most of the insulin in circulation.

The efficacy of insulin in increasing glucose transport into insulin sensitive tissues at a given time is dependent on a large number of factors, generally lumped together as a single whole-scale notion termed insulin sensitivity. The equivalent but inverse property termed insulin resistance was more commonly referred to in historical literature. In the short term, insulin sensitivity is influenced by the likes of daily metabolic rhythms (Hinshaw et al., 2013), stress (Rizza et al., 1982), physical activity (Borghouts and Keizer, 2000), and menstrual cycles (Lunt and Brown, 1996). Longer term insulin sensitivity changes are correlated to factors such as age, obesity (Montastier et al., 2014), puberty (Hannon et al., 2006), and pregnancy (Cousins, 1991).

As previously stated, individuals with T1DM lack insulin. Autoimmune destruction of the insulin-creating β cells in the pathogenesis of T1DM may occur over a short or long period of time (American Diabetes Association, 2006). Shorter onset is more typical of children and adolescents while longer onset is more typical in adults. Those with established T1DM have negligible insulin secretion. Without insulin, hyperglycaemia persists and insufficient glucose reaches insulin-sensitive tissues.

1.2.2 Hepatic and renal balance

At the basal state, the liver and the kidney produce and release glucose into the plasma from stored sources (Cherrington, 1999). The liver performs this endogenous glucose production (EGP) though two metabolic processes: glycogenolysis and gluconeogenesis. Glycogenolysis cleaves glucose monomers from glycogen, a glucose polysaccharide. Gluconeogenesis metabolises non-carbohydrates such as pyruvate, lipids and lactate into glucose. The kidney only produces glucose through gluconeogenesis but also reabsorbs glucose back into the bloodstream that would otherwise be destined for the urine (Gerich, 2010).

Following a meal containing carbohydrates, a third of incoming glucose is taken up as it passes through the liver, both stored as glycogen and utilised for energy (Cherrington, 1999). The high gradient of glucose in the portal vein (from the intestine to the liver) compared to arterial concentration, as well as the increased presence of plasma insulin and glucose all promote hepatic glucose uptake. Insulin also reduces EGP in the liver by decreasing glycogenolysis directly and gluconeogenesis indirectly. Therefore net hepatic glucose output remains negative until plasma glucose, plasma insulin and the portal vein glucose gradient have lowered.

Several other hormones regulate the action of the liver, post-prandially and otherwise. Glucagon is a hormone secreted in α cells of the pancreas that promotes hepatic EGP (Cherrington, 1999; Gerich, 2010). Glucagon serves

to protect against hypoglycaemia, for example being secreted more when insulin is released due to fat intake rather than glucose absorption (Carr et al., 2008). Thus insulin and glucagon together mediate much of the liver's glucoregulatory response. The catecholamines, secreted from the adrenal glands in a state of stress, also have a range of effects on both the liver and kidney such as promoting renal glucose release, insulin suppression, and glucagon secretion (Gerich, 2010). Additionally, in Cherrington (1999)'s animal model, epinephrine and norepinephrine independently promoted glycogenolysis, and epinephrine also promoted gluconeogenesis.

As previously stated, people with T1DM must rely entirely on exogenously administered insulin. As a result, EGP is less tightly controlled, though still regulated by the remaining mechanisms. Furthermore, people with diabetes of both types tend to have hyperinsulinaemia. The effect of this is perhaps most notable during moderate aerobic exercise. High insulin concentrations that are not down-regulated for exercise tend to cause a shortfall in EGP that eventually results in hypoglycaemia (Yardley et al., 2013; Sonnenberg et al., 1990). On the other hand, in the absence of sufficient insulin, glucose uptake in the liver and kidney are vital for ameliorating the extent of postprandial hyperglycaemia.

1.2.3 The incretin effect

Incretins are glucoregulatory hormones secreted from the enterocyte cells lining the small intestine in response to the presence of nutrients (Hayes et al., 2014; Ahrén, 2013; Cernea, 2011). The two main incretins are glucagon-like peptide-1 (GLP-1) and glucose-dependent insulinotropic peptide (GIP). The primary effect of both incretins is to stimulate glucose-dependent insulin secretion (Cernea, 2011; Karstoft et al., 2015). The 'incretin effect' is defined as fraction of insulin secretion after an oral dose of glucose that does not appear for an equivalent intravenous infusion (Ahrén, 2013; Hayes et al., 2014). The magnitude of the response is dependent on calorific intake (Alsalim et al., 2015) since fat, protein and

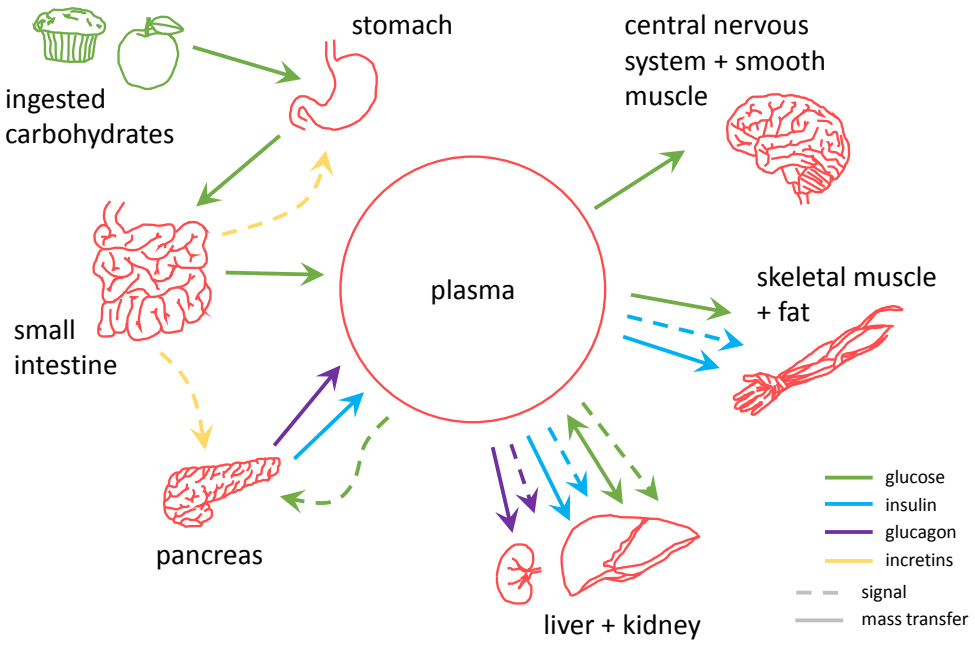

Figure 1.2: A schematic of healthy glucose homeostasis showing the movement of glucose into and out of various tissues through the plasma, as well as hormonal signalling between organs.

carbohydrate all stimulate the secretion of both incretins (Rijkelijkhuizen et al., 2010; Carr et al., 2008; Kameyama et al., 2014).

The effects of both GIP and GLP-1 are complex and multifaceted. Both stimulate glucose dependent insulin secretion (in those with functioning β cells) and likewise decrease glucose-dependent glucagon secretion (Cernea, 2011; Hayes et al., 2014). Although in some conditions GIP can instead increase glucagon secretion (Carr et al., 2008; Hayes et al., 2014). Beyond pancreatic effects, GLP-1 decreases the gastric emptying rate and increases satiety (Hayes et al., 2014; Cernea, 2011). GLP-1 also appears to increase insulin-independent muscular glucose uptake (Hayes et al., 2014; Karstoft et al., 2015; Abdulla et al., 2014; Johnson et al., 2007; Meneilly et al., 2001) and may suppress EGP (Hayes et al., 2014; Prigeon et al., 2003; Karstoft et al., 2015). GIP also potentially increases blood flow (Karstoft et al., 2015). There are mixed opinions in the literature as to whether individuals

with T1DM have normal or impaired incretin secretion (Vilsbøll et al., 2003; Kamoi et al., 2011; Lugari et al., 2000; Zibar et al., 2015).

1.3 Diabetes therapy

The discovery of insulin in 1921 heralded the treatment of T1DM (Atkinson and Eisenbarth, 2001). Initially, insulin was thought to be a cure, however the complexity of treatment soon became clear. Prior to this point the disease was considered to have 100% mortality for children in particular. Younger children typically survived for less than 2 years after onset, and older children sometimes survived 3-6 years (American Diabetes Association, 2006). T1DM is still fatal in some developing countries such as in Sub-Saharan Africa where treatment is not readily available or affordable. Even in developed countries fatalities still occur, especially in cases of delayed diagnosis in young children (Atkinson and Eisenbarth, 2001).

Initially, people were treated with porcine insulin which is very similar in structure to human insulin. In the years following, a number of manufactured human insulins were developed. Manufactured insulins vary in structure to achieve different purposes. Human insulin is typically stored in the pancreas as a hexameric group (Kang et al., 1991). However, the monomer is the active form used elsewhere in the body. While the hexamer is the most stable form of insulin, it takes some time to break into dimers then monomers. Hence, some manufactured insulins have certain sequences in the protein structure altered to discourage hexamer formation and therefore act more rapidly (Home et al., 1999). This is particularly useful to administer in conjunction with a meal. Other insulins are further bound in crystalline structures to slow breakdown into monomers (Roach and Woodworth, 2002). These longer-acting insulins are useful for mimicking the basal rate of insulin release throughout the day observed in healthy individuals.

The most common therapy involves multiple daily subcutaneous (SC)

injections of these different types of insulin (Atkinson and Eisenbarth, 2001). Outpatients consult with clinicians regularly to monitor and optimise their treatment regimes. The goal with longer-acting insulins is to create a smooth basal profile to minimise differences throughout the day. Depending on the half life of the insulin, this may require more than one injection per day. Outpatients will also inject quantity of rapid-acting insulin with meals based on the estimated quantity of carbohydrates in the meal. At any other time, rapid-acting insulin may also be injected to lower blood glucose according to a ratio of glucose levels to insulin units.

More recently, insulin pumps have become a mainstream form of treatment (Stephens, 2015). These pumps are installed with a needle into the subcutaneous tissue that is replaced every few days. Pumps tend to contain only a rapid-acting form of insulin but have the ability to titrate the contents at a slow rate throughout the day for a basal profile, as well as being able to deliver large boluses for meals or correction. The pumps can be programmed to supply a variable basis profile throughout the day in accordance with a person's circadian rhythm of glucose tolerance. The pumps also store the owner's insulin ratios and are able to make basic recommendations based on input information.

A significant amount of research has been carried out in the field of decision support based on mathematical modelling, both for self managed blood glucose monitoring with multiple daily injections (Wong et al., 2008c, 2009), clinically monitored care for the critically ill (Chase et al., 2011; Pappada et al., 2013; Lin et al., 2011; Pielmeier et al., 2010), and for a closed loop system utilising insulin pumps and continuous glucose monitors (Bequette, 2012; Cobelli et al., 2011; Hovorka et al., 2011, 2013; Kovatchev et al., 2009). Mathematical modelling will be covered more extensively in Chapter 2. The goal of decision support in T1DM is to reduce the burden of disease management and improve patient safety. The burden of disease management is associated with decreased perceived quality of life (Rubin and Peyrot, 1999, 2001). Additionally, fear of hypoglycaemia tends to result in those with T1DM tending toward hyperglycaemia and missing out

on the benefits of euglycaemia (Atkinson and Eisenbarth, 2001).

Despite the amount of research carried out to date, many challenges remain for delivering effective and personalised care to those with diabetes. In particular, there are a vast number of variable stimuli that an individual encounters throughout the day in an outpatient environment. Examples include differing levels of glucose demand depending on physical activity, changes in insulin sensitivity based on mood, and different patterns of incoming glucose from ingested food. Research around these factors is reviewed in Chapter 4. The manner in which many environmental stimuli affect glycaemia is complex and often not well understood. The uncertainties created by such factors continue to confound treatment at times for most individuals. Some people, termed by clinicians as being "brittle", are particularly susceptible to poor glycaemic control due to daily variabilities. These individuals would benefit most from advances in understanding and modelling around the effects of various environmental stimuli on glycaemia.

Chapter II

Physiological modelling

Mathematical modelling of physiological processes has become a standard method for studying these processes and developing new integrated technologies. This is particularly true in the field of diabetes research and glycaemic control. This chapter overviews some of the historical development of glycaemic models. By no means is the content covered exhaustive, due to the sheer quantity of research carried out in the field. Additionally, the overview will focus mostly on insulin kinetics and glucose-insulin dynamics rather than insulin secretion models.

2.1 Early models (1960s-1970s)

There have been a lot of glycaemic models developed over the years and it can be difficult to trace them all through the literature. Some of the earliest research was carried out in the 1960s by the Ackerman group (Ackerman et al., 1964; Gatewood et al., 1968). This group fit linear differential models to oral glucose tolerance tests with the purpose of distinguishing between healthy and mildly diabetic responses. Ackerman et al. (1964) defined their system as:

$$\dot{H} = -l_1 H + l_2 + l_3 G \tag{2.1}$$

$$\dot{G} = -l_4 G + l_5 - l_6 H - I \tag{2.2}$$

where H is plasma insulin concentration, G is plasma glucose concentration, l_1 is the insulin clearance rate, l_2 is basal insulin secretion, l_3 is the glucose-dependent insulin secretion rate, l_4 is the insulin-independent glucose disposal rate, l_5 is glucose production, l_6 is the insulin-dependent glucose disposal rate and I is the appearance of glucose from oral loads. An estimate was used for the plasma glucose profile from oral loads, despite a

relative lack of data to validate the model (Gatewood et al., 1968).

Much of the subsequent research into modelling insulin and glucose utilised multiple tracer technologies to measure the contributions of different organs in the production and disposal of insulin and glucose and under certain conditions. These types of experiments significantly increased the inherent complexity involved. By 1974, three compartment models had been proposed for each of insulin and glucose by the group of Sherwin et al. (1974) and Insel et al. (1974). The insulin model compartments described hepatic, plasma and extra-vascular concentrations. Sherwin et al. proposed three different model arrangements for the interactions between and clearances from each of the compartments. Insel et al. fit tracer data to the three compartment model that included insulin dependent and independent glucose disposal. Some other early contributors to insulin models were Frost et al. (1973) and Tranberg and Dencker (1978). The model of Frost et al. was non-linear having both linear and saturable clearance from the plasma compartment. In contrast, Tranberg and Dencker used only linear clearance from the plasma. Another contributor to glucose models in this period was Radziuk et al. (1978) who simplified prior 3-compartment glucose tracer models to a 2-compartment model.

2.2 The Bergman Minimal Model (1979)

In contrast to many of the complex models prior, perhaps the most notable glycaemic model developed is the Bergman et al. (1979) Minimal Model. The model is described:

$$\frac{dG}{dt} = -(p_1 + X(t))G(t) + p_1 G_b \tag{2.3}$$

$$\frac{dX}{dt} = -p_2 X(t) + p_3(I(t) - I_b) \tag{2.4}$$

$$\frac{dI}{dt} = -n(I(t) - I_b) + \gamma t|G(t) - h| \tag{2.5}$$

where G is the plasma glucose concentration, X is the insulin action, and I is the plasma insulin. The b subscript indicates a basal level parameter,

while the p and n terms are rate constants, and h is the target glycaemia relating to a critical glucose level for insulin secretion. The associated insulin sensitivity (S_I) can be calculated as p_3/p_2.

The Minimal Model has formed the basis for a large amount of glycaemic modelling research and application. The model and variations of it are in use (Campioni et al., 2009; Cobelli et al., 2014; Breton, 2008; Roy and Parker, 2007; Erichsen et al., 2004). However, the Minimal Model has drawn much criticism. This criticism is partially directed at just how minimal the model is in terms of some of the physiological assumptions and simplifications made (Chase et al., 2006; Palumbo et al., 2013) but also in terms of the lack of robust parameter solutions obtained when fitting the model to experimental data (Palumbo et al., 2013; Docherty et al., 2011; Cobelli et al., 1998; Quon et al., 1994). More recent legacies of the Minimal Model have addressed concerns around parameter robustness by using Bayesian estimation methods which penalise parameters for taking on values outside an expected range (Cobelli et al., 1999; Pillonetto et al., 2002, 2003).

2.3 The Sorensen physiologic model (1985)

Sorensen (1985) developed an incredibly extensive whole-body glucose metabolism model using a large number of simultaneous differential equations, based on the earlier work of Guyton et al. (1978). The model includes mass balances of glucose throughout several compartments: brain, heart and lungs, gut, liver, kidney, and periphery. Sources and sinks for glucose mass are considered in each compartment. An example of this glucose balance for the liver is:

$$V_L^G \frac{dG_L}{dt} = Q_A^G G_H + Q_G^G G_G - Q_L^G G_L + r_{HGP} - r_{HGU} \tag{2.6}$$

where V_L^G is the glucose distribution volume of the liver, G_L is the glucose concentration in the liver, Q_A^G is the blood flow rate in the hepatic artery, G_H is the glucose concentration in the heart and lungs, G_G is the glucose

concentration in the gut and Q_G the blood flow rate in the gut, Q_L is the blood flow rate in the liver, r_{HGP} is the hepatic EGP while r_HGU is the hepatic glucose uptake.

This equation alone hints at the complexity of the entire model with the interactions between the various organs. In particular, Sorensen (1985) modelled glucose in the brain, heart and lungs, gut, liver, kidney, and periphery. In addition to glucose balance equations, there are insulin balance equations for all of the same areas, as well as a mass balance for plasma glucagon. Altogether there are sixteen differential equations.

Sorensen calibrated the model to a 70 kg male and populated the vast number of variables with information from the literature. This is an example of a bottom-up modelling approach that focuses on including all contributing physiological processes, big or small, to achieve the observed outcomes. This is in contrast to more minimal approaches that aim to include the major contributing factors and achieve concordance with outcomes through model fitting to account for patient variability. The bottom-up approach tends to be less conducive to dealing with patient variability. The inherent complexity in the Sorensen model has resulted in comparatively sparse use in research (Kovacs et al., 2008). However, some independent research utilised a modified version of the model (Parker et al., 2000; Kovacs et al., 2008) or used it for simulation (Markakis et al., 2008).

2.4 Intensive care (2000s)

Much of the more recent research dedicated to glycaemic model development has been motivated by the need for safe and effective glycaemic control in intensive care units. The bodies of the critically ill are under sufficient medical stress to cause substantial insulin resistance and associated hyperglycaemia. Hyperglycaemia in this cohort significantly impacts on mortality and recovery times (Chase et al., 2006). Thus, mathematical modelling has been used to optimise insulin therapy for patient health and safety, recovery time, and nurse workload.

Three notable models were developed for use in critical care in the 2000s (Chase et al., 2006). The first by Chee et al. (2003) is not a physiological model as such but a proportional-integral-derivative control model. The model prescribes different doses based on the patient's blood glucose. The dose characteristics are subject to change according to integral and derivative control tactics.

The second model was physiological model developed for T1DM control model by (Hovorka et al., 2004), and later modified for critical care (Plank et al., 2006). The model seeks a comprehensive description of the physiology:

$$\dot{Q}_1(t) = -\left(\frac{F_{01}^c}{V_G G(t)} + x_1(t)\right) Q_1(t) + k_{12} Q_2(t) - F_R + U_G(t) + EGP_0(1 - x_3(t)) \tag{2.7}$$

$$\dot{Q}_2(t) = x_1(t) Q_1(t) - (k_{12} + x_2(t)) Q_2(t) \quad y(t) G(t) = \frac{Q_1(t)}{V_G} \tag{2.8}$$

$$F_{01}^c = \begin{cases} F_{01} & \text{if } G \geq 4.5 \text{ mmol/L} \\ \frac{F_{01} G}{4.5} & \text{otherwise} \end{cases} \tag{2.9}$$

$$F_R = \begin{cases} 0.003(G - 9) V_G & \text{if } G \geq 9 \text{ mmol/L} \\ 0 & \text{otherwise} \end{cases} \tag{2.10}$$

$$U_G(t) = \frac{D_G A_G t \mathrm{e}^{-t/t_{\max,\mathrm{G}}}}{t^2} \tag{2.11}$$

$$\dot{S}_1(t) = u(t) - \frac{S_1(t)}{t_{\max,\mathrm{I}}} \tag{2.12}$$

$$\dot{S}_2(t) = \frac{S_1(t)}{t_{\max,\mathrm{I}}} - \frac{S_2(t)}{t_{\max,\mathrm{I}}} \tag{2.13}$$

$$\dot{I}(t) = \frac{S_2(t)}{V_1 t_{\max,\mathrm{I}}} - k_e I(t) \tag{2.14}$$

$$\dot{x}_1(t) = -k_{a1} x_1(t) + k_{b1} I(t) \tag{2.15}$$

$$\dot{x}_2(t) = -k_{a2} x_2(t) + k_{b2} I(t) \tag{2.16}$$

$$\dot{x}_3(t) = -k_{a3} x_3(t) + k_{b3} I(t) \tag{2.17}$$

where Q_1 and Q_2 are accessible and inaccessible glucose compartments, k_{12} is the transfer rate between these compartments, V_G is the distribution volume of Q_1, y and G are the measurable glucose concentration and EGP_0 is the equivalent EGP with no insulin present. F_{01}^c is total non-insulin-dependent glucose flux for ambient glucose concentration while F_R is renal clearance above 9 mmol/L. U_G is the incoming glucose from the gut based on digested carbohydrates (D_G), carbohydrate bioavailability (A_G) and the time period until maximum appearance in Q_1 ($t_{\max,\mathrm{G}}$). Insulin is modelled with two compartments (S_1 and S_2) to describe the absorption of subcutaneous short-acting insulin, where $u(t)$ the insulin infusion, $t_{\max,\mathrm{I}}$ is the time period until maximum appearance in the plasma (I), k_e is the elimination rate and V_I the plasma insulin distribution volume. The remaining compartments on which insulin acts are the EGP (x_1), distribution (x_2) and disposal (x_3), according to the activation and deactivation rates given by the k_a and k_b terms.

The final of the three models is that of Chase et al. (2006) which is based on the Minimal Model. The model is described:

$$\dot{G} = -p_G G - S_I(G + G_E)\frac{Q}{1 + \alpha_G Q} + P(t) \tag{2.18}$$

$$\dot{Q} = -kQ + kI \tag{2.19}$$

$$\dot{I} = -\frac{nI}{1 + \alpha_I I} + u_{ex}(t)/V \tag{2.20}$$

$$P(t_i < t < t_{i+1}) = \bar{P}_{i+1} + (P(t_i) - \bar{P}_{i+1})\mathrm{e}^{-k_{pd}(t-t_i)} \text{ where } \bar{P}_{i+1} < P(t_i) \tag{2.21}$$

$$P(t_i < t < t_{i+1}) = \bar{P}_{i+1} + (P(t_i) - \bar{P}_{i+1})\mathrm{e}^{-k_{pr}(t-t_i)} \text{ where } \bar{P}_{i+1} > P(t_i) \tag{2.22}$$

where G is plasma glucose above equilibrium glucose (G_E), Q is the interstitial insulin, cleared at a rate k, $I(t)$ is the plasma insulin with exogenous input ($u_{ex}(t)$), distribution volume (V) and clearance rate n. The action of insulin and insulin clearance are both saturated effects modelled using Michaelis-Menten functions with saturation parameters α_G and α_I. The endogenous glucose clearance is denoted p_G and the insulin

sensitivity is S_I. Total plasma glucose is $P(t)$, dependent on enteral feeding where k_{pr} and k_{pd} are increasing and decreasing feed rates, and $\bar{P}_i$ and $\bar{P_{i+1}}$ are steps in the enteral feed rates. The model has since been updated to include more complex nutritional mechanics (Lin et al., 2011).

2.5 Summary and present

Glycaemic modelling has been carried out extensively over the last 50 years. The earliest models were descriptive but relatively simple compared to some of the models that followed. As the models became more sophisticated, different groups have decided on approaches that varied on the scale of simple to complex. The Bergman et al. (1979) Minimal Model is considerably simpler than the Sorensen (1985) physiologic model, which has at least 22 differential equations. Glycaemic modelling was initially motivated by studying and controlling diabetes but also gained a focus in intensive care in the 2000s.

At present, work continues in earnest to develop a safe and effective closed-loop control strategy for people with diabetes. A keyword search of "artificial pancreas" in the abstract and citation database Scopus results in over 800 hits for content published in the 2010-2016 period alone. Models continue to be researched, developed and implemented in this field. Despite the research efforts and promising clinical trials, adequate closed-loop control for outpatients with diabetes has not yet been achieved, mainly attributed to limitations in continuous glucose monitoring systems (Hanazaki et al., 2016). Variabilities in glucose metabolism arising from the outpatient lifestyle such as stress and physical activity are also considered major challenges to control, closed-closed loop or otherwise (Ward et al., 2011; Breton, 2008). Hence, models are beginning to incorporate more of these types of features as research progresses.

The goal of the present work is not to focus on the fundamental modelling of glucose dynamics, but rather on incorporating everyday life effects into an existing model, and to address these particular challenges in glycaemic

control for the individual with T1DM. By nature, less fundamental aspects of glucose metabolism encountered in the outpatient environment are subject to large inter-patient variability. Hence, modelling strategies for this purpose require a high level of personalisability to be effective. This requires that such models be able to handle the kinds of behaviour and variability anticipated, and on top of that work effectively with outpatient data. Both criteria contribute their own sets of challenges. However, this work represents a natural progression of the long and wide legacy of glycaemic modelling to date.

Chapter III

Parameter identification and identifiability

This chapter introduces the ideas and methodologies around identification of model parameters and the identifiability of those parameters. Both concepts are used extensively throughout this thesis.

3.1 The inverse problem

The 'inverse problem' in science and engineering is the use of observational data to calculate an underlying causative factor in a representative model. In the context of physiological modelling, inverse problem methodologies optimise variables in the model to some criteria based on the data of measurable species. These optimised variables are the identified parameters which govern underlying physiological behaviour in a manner specific to that dataset. The value of identified parameters is dependent on the model, data and application.

A model, especially in physiology, can only ever be an approximation of the real processes occurring, due to the numerous inconsistent and variable factors that can affect biological systems. When considering models representing different approximations of the same system, it is perhaps intuitive to assume that parameters identified from complex approximations are more valuable and useful than those obtained from simpler, more errant approximations.

However, it is important to note that the usefulness of model complexity is entirely limited by the unique observability of modelled behaviours, with respect to the quality and quantity of data available. There is no use trying to quantify the underlying behaviour of effects that are too small compared

to measurement noise, or too poorly timed relative to when data is sampled. This is the essence of identifiability.

With regard to application, some parameters tend to be of high clinical relevance (such as insulin sensitivity in glycaemia), while other parameters tend to be less clinically relevant but support the optimisation process by accounting for other inter- or intra- personal variabilities. On occasion, a parameter will fall into neither category, especially in overly complex models.

3.2 Parameter identification

3.2.1 Optimisation

Optimisation of a parameter set, represented by the vector $\mathbf{x}$, is often carried out by minimising the 2-norm of an objective or cost function ($\mathbf{\Psi}$). This optimisation is described mathematically as:

$$\mathbf{x}_{opt} = \text{argmin}_{\mathbf{x}}(||\mathbf{\Psi}||_2) \tag{3.1}$$

In the context of fitting a model to a measured behaviour, for example blood glucose concentration (G), the objective function is the residual modelling error . Hence, the minimised function is the least squares sum of the residual, described:

$$||\mathbf{\Psi}||_2 = \sqrt{\sum_{S=1}^{n} (G_S - G(t_S))} \tag{3.2}$$

where G_S are the measured samples for $S = 1 \ldots n$, where n is the total number of samples. Likewise, $G(t_S)$ is the modelled blood glucose at the sample times.

A successfully obtained least squares solution will have minimal positive or negative bias in the residual error. For ideally formulated models, the residual error corresponds exactly to the measurement noise. Hence, least

squares optimisation is effective when noise in the measured behaviour is zero-mean with no significant outliers, and when all observable behaviours that do not correspond to noise are otherwise modelled.

3.2.2 Algorithms

Due to the typical non-linearity of inverse problems in physiological modelling, least squares optimisation cannot be carried out through simple linear regression. An iterative approach is required since the optimised parameters depend on the model forward simulation (Equation (3.2)) which in turn depends on the parameters in a way that cannot be simplified and resolved. For the blood glucose example, $\mathbf{x}_{opt} = f\left(G(t_S) = f(\mathbf{x})\right)$.

The present work has extensively utilised gradient descent algorithms to identify optimised parameters. Essentially, gradient descent operates on an objective surface of $||\mathbf{\Psi}||_2 = f(\mathbf{x})$ (Figure 3.1). At each iteration (i), $||\mathbf{\Psi}||_2$ is evaluated a step in the direction of each parameter from the current set $(\mathbf{x}_i)$. This information is used to decide which direction on the objective surface is downhill, and how far to step in that direction for the next set $(\mathbf{x}_{i+1})$. As with all numerical methods, the perturbation must be suitably small to attain acceptable accuracy in $\mathbf{x}_{opt}$. However, it must also be large enough relative to the quality of the forward simulation to avoid convergence to a local minima in a noisy objective surface that does not represent the least squares solution at the global minima.

The simplest gradient descent method is known as steepest descent, and takes a step downhill in proportion to the steepness. The method is relatively slow to converge but also very stable. Gauss-Newton is a second order gradient descent algorithm that converges must faster but is sometimes less stable. Levenberg-Marquardt is a further development on Gauss-Newton that improves stability by tending toward steepest descent when more stability is required, but maintaining the faster Gauss-Newton descent otherwise.

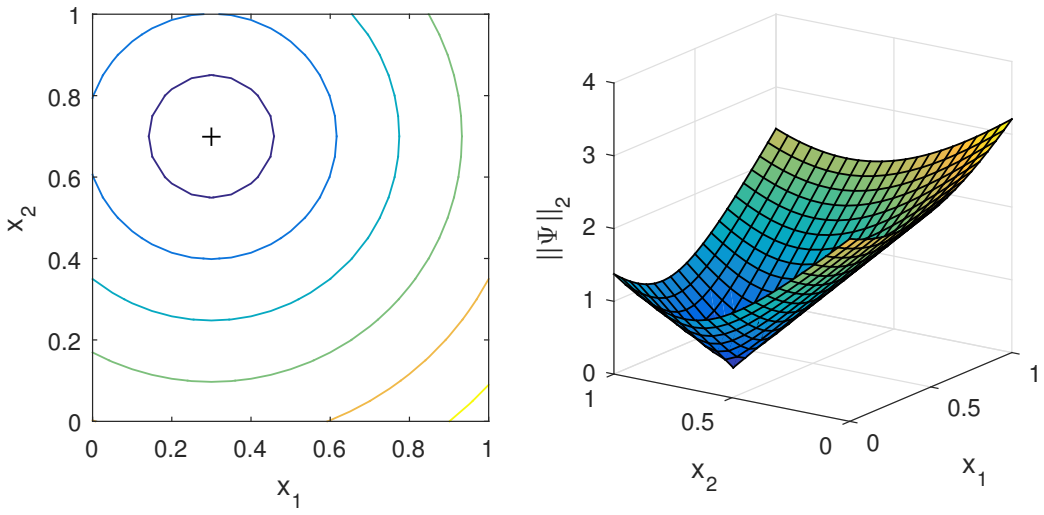

Figure 3.1: A contour plot (left) and surface plot (right) of an example objective surface for two parameters. Higher dimension objective surfaces (with three or more parameters) are harder to conceptualise visually but follow the same mathematical principles.

3.2.2.1 Gauss-Newton

Gauss-Newton iterations are carried out as follows:

$$\mathbf{x}_{i+1} = \mathbf{x}_i + (\mathbf{J}_i^{\mathrm{T}}\mathbf{J}_i)^{-1}(\mathbf{J}_i^{\mathrm{T}}\boldsymbol{\Psi}_i(\mathbf{x}_i)) \tag{3.3}$$

where $\mathbf{J}$ is the Jacobian, and is described:

$$\mathbf{J}_i = \left[\frac{\partial \Psi_S}{\partial x_j}\right]_i = \begin{bmatrix} \frac{\partial \Psi_1}{\partial x_1} & \frac{\partial \Psi_1}{\partial x_2} & \cdots & \frac{\partial \Psi_1}{\partial x_p} \\ \frac{\partial \Psi_2}{\partial x_1} & \frac{\partial \Psi_2}{\partial x_2} & \cdots & \frac{\partial \Psi_2}{\partial x_p} \\ \vdots & \vdots & \ddots & \vdots \\ \frac{\partial \Psi_n}{\partial x_1} & \frac{\partial \Psi_n}{\partial x_2} & \cdots & \frac{\partial \Psi_n}{\partial x_p} \end{bmatrix} \tag{3.4}$$

where j is the parameter index ($j = 1, 2, \ldots, p$) for p total parameters.
It is most simple to use a first order numerical approximation for the derivatives in the Jacobian:

$$\frac{\partial \Psi_S}{\partial x_j} = \frac{G(x_j + \delta x_j, t_S) - G(x_j, t_S)}{\delta x_j} \tag{3.5}$$

3.2.2.2 Levenberg-Marquardt

The Levenberg-Marquardt algorithm iterates to $\mathbf{x}_{opt}$ using Equation (3.6) and 3.7.

$$\mathbf{x}_{i+1} = \mathbf{x}_i + \mathbf{A}^{-1}(\mathbf{J}_i^{\mathrm{T}}\mathbf{\Psi}_i(\mathbf{x}_i)) \tag{3.6}$$

$$\mathbf{A} = \mathbf{J}_i^{\mathrm{T}}\mathbf{J}_i + \lambda_i \mathrm{diag}(\mathbf{J}_i^{\mathrm{T}}\mathbf{J}_i) \tag{3.7}$$

where λ is the damping parameter. Depending on the desired properties of the algorithm, λ is assigned different values as identification progresses. The larger it is, the closer to first order descent. The smaller it is, the closer to Gauss-Newton. Generally it is recommended to have some initial value, λ_0 with subsequent assignment of $\lambda_i = \lambda_{i-1}/v$ (where $v > 1$) if it achieved a greater decrease in $||\mathbf{\Psi}||_2$ than λ_{i-1}. If either option increased $||\mathbf{\Psi}||_2$, $\lambda_i = \lambda_{i-1}v^k$ would be assigned, increasing k until $||\mathbf{\Psi}||_2$ could be decreased. The revised parameter set $\mathbf{x}_i$ would therefore only be accepted once $||\mathbf{\Psi}_i||_2 < ||\mathbf{\Psi}_{i-1}||_2$.

3.2.3 Convergence

Since nonlinear inverse problems are solved iteratively, there is typically some criteria which define how many iterations are carried out. If there is a real solution and the system is stable, the parameter estimates will converge towards this real solution. A maximum number of iterations can be prescribed indiscriminately but it is usually more beneficial to include a tolerance-based convergence criterion as well. If satisfactory convergence occurs sooner than the maximum number of iterations, no unnecessary computational time is spent, and the maximum iterations can be assigned a conservatively large number.

Convergence is best measured in the object of interest, the parameter set itself, rather than a secondary feature like the modelled behaviour, which would be less sensitive to parameter convergence. Though there are many

variations, a sensible tolerance criterion might be:

$$\left|\left|\frac{\mathbf{x}_{i-1} - \mathbf{x}_i}{\mathbf{x}_{i-1}}\right|\right|_2 < 10^{-4} \tag{3.8}$$

When the criterion is true, the appropriate tolerance is reached and iterations cease. This criterion normalises convergence by the scale of each parameter. Thus, it ensures approximately 4 significant figures are reached in each parameter.

3.3 Identifiability

Identifiability is concerned with successfully modelling and identifying uniquely observable behaviours. The field of identifiability can be broadly split into two categories: structural and practical.

3.3.1 Structural identifiability

Structural or *a priori* identifiability is a well established field (Audoly et al., 1998, 2001; Bellman and Åström, 1970; Bellu et al., 2007; Pohjanpalo, 1978). This kind of identifiability is concerned with the model formulation and whether there is a unique solution of optimised parameters. Structurally identifiable models have a single global minima on the objective surface. Structural identifiability analysis methods assume perfect data, with at least as many observations as there are parameters. Insufficient observations for the number of parameters results in an under-defined solution.

A simple mathematical example of structural non-identifiability would be to use the model $\dot{X} = -(x_1 + x_2)X$ and attempt to identify both x_1 and x_2 as separate parameters. Least squares estimation of these parameters would result in a non-unique solution since there is no ability to distinguish the individual effects of the parameters. Whatever value x_1 was, x_2 could take on a value such that the desired net effect, as seen in the output behaviour, was modelled to the best fit. On the objective surface, this would be seen as a valley with an infinite line of solutions reaching minimum residual error.

Structural identifiability is reasonably intuitive, especially in such a simple example. Indeed, the formulation of the example model appears very redundant. However, in large models, non-identifiability can be subtle and hidden amongst the model complexity. Hence, several methods of detecting and confirming *a priori* identifiability have been developed (Audoly et al., 1998, 2001; Bellman and Åström, 1970; Bellu et al., 2007; Pohjanpalo, 1978). Model simplification can be used to remove a non-identifiable feature if necessary. In some scientific fields it is practical to combine several parameters into one non-dimensionalised parameter that can be identified, such as the Reynolds number in fluid mechanics. However, this approach may not be helpful when seeking to identify a specific physiological parameter.

3.3.2 Practical identifiability

Practical identifiability is an emerging field (Raue et al., 2009, 2012, 2014; Docherty et al., 2011; Saccomani, 2013). Though not as prevalent in the research community, it is arguably more important than structural identifiability, especially because of its less obvious and therefore more subversive nature. The concept of practical identifiability takes into consideration the role of data quality in the unique observability of behaviours (Raue et al., 2009; Docherty et al., 2011). While structural identifiability is discrete with either an affirmative or negative outcome, practical identifiability can be viewed somewhat more continuously.

Parameters that are practically non-identifiable can be unique in terms of model formulation, and thus pass as structurally identifiable. Therefore, for perfect data, there is a global minima on the objective surface. However, parameters prone to practical non-identifiability will tend to have large regions of shallow gradients surrounding the minima, spanning a large range in parameter values. The implication is that the noise in (inevitably) imperfect data obscures the true location of the global minima in the shallow region, and a wide range of parameter outcomes could result,

depending on the exact properties of the dataset.

To illustrate this concept, consider the model $y = x_1 \sin(t) + x_2 \sin(t + \phi)$ where $x_1 = 0.3$ and $x_2 = 0.7$. If the phase (ϕ) is $\frac{\pi}{2}$ then the contributions of the curves to y would be most apparent since one is at a maximum while the other is at zero and vice versa. If ϕ is either 0 or π then the model could be simplified to $y = (x_1 \pm x_2) \sin(t)$. The contributions of x_1 and x_2 would then be indistinguishable and thus structural non-identifiability is present. However, as the phase approaches but does not equal 0 or pi, practical non-identifiability increases and parameter estimates would become poorer.

Figure 3.2 shows a selection of parameter outcomes identified from data at three different phases. For each dataset, seven datapoints between 0 and 2π were taken with 20% noise applied. At $\phi = 0.5\pi$ there is maximum practical identifiability since this represents the greatest possible phase difference. Hence, the objective surface is conical and a relatively tight, circular grouping of identified parameters results. As the phase approaches π, the objective surface becomes progressively more elliptical. At $\phi = 0.95\pi$ the objective surface is an extremely long ellipse, though appears as a continuous valley within the reasonable range of parameter estimates. The identified parameters now cover a large range of possibilities and thus are no longer accurate or particularly useful.

In the example, when the phase was actually assigned to π, the parameter identification algorithm failed to identify either parameter, producing NaN results instead. This demonstrates how the effect of a structural non-identifiability tends to be obvious to a person using the model. In contrast, the $\phi = 0.95\pi$ model, with very low practical identifiability, still produced parameter estimates, many of which could appear reasonable to the model user in the context of use. However, the values obtained in practice could be very different from the underlying behaviours, negatively affecting treatment outcomes. Furthermore, the parameter identification also resulted in good adherence of the model to the data (not shown). Hence, the researcher could be deceived into believing that the model is

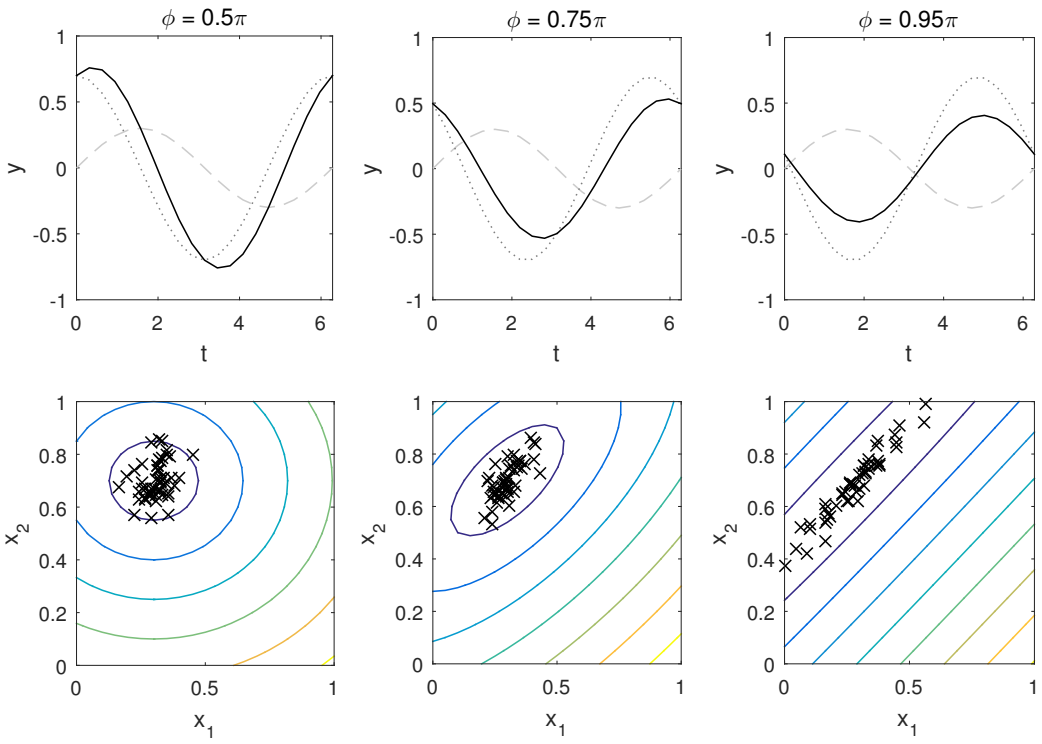

Figure 3.2: Decreasing practical identifiability from left to right as the phase approaches π. Top row: the simulated model (black) from the summed components (grey). Bottom row: The no-noise objective surface (—) with parameter estimates for 50 noisy datasets sampled from the model (+).

suitable for the given data, and that results are valid and useful when this is far from true.

Early research describing practical identifiability was presented by Raue et al. (2009). They presented a method for analysing both practical and structural identifiability for all parameters in an arbitrary model based on the flatness of likelihood profiles. Likelihood profiles are used in an alternative parameter identification process known as Maximum Likelihood Estimation. The likelihood profiles are similar to an objective surface in that the minimal value indicates the optimum parameter value. However, likelihood profiles are a more holistic representation of an individual parameter's objective function based on all the other factors involved.

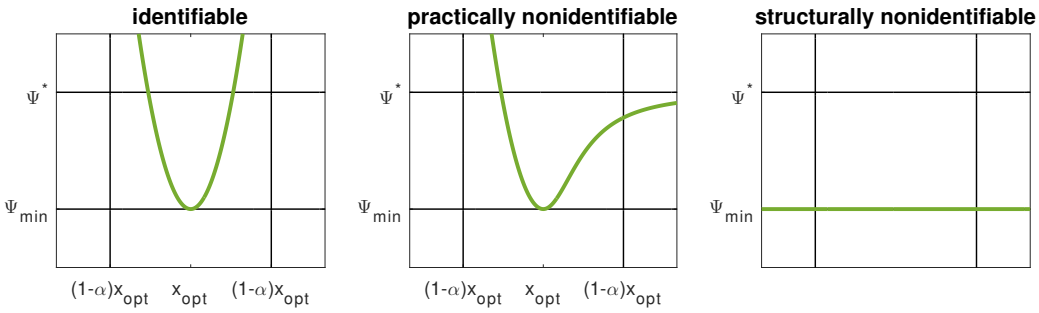

Figure 3.3: A demonstration of the method of Raue et al. (2009) to determine identifiability of a parameter using the maximum likelihood profile. An identifiable parameter (left) has a likelihood profile that exceeds the reference value (Ψ^*) outside the confidence interval. A practically non-identifiable parameter (middle) has a distinct optimum but does not reach the reference value outside the confidence interval. A structurally non-identifiable parameter (right) has a flat maximum likelihood profile as there are infinite optimum values.

Therefore, a totally flat likelihood profile indicates a structural non-identifiability the same way that an infinite trench does on a two-parameter objective surface. Likewise, if the likelihood function spans indefinitely from either end of the minima without exceeding a certain tolerance criterion, the parameter can be considered practically non-identifiable. Raue et al. uses a threshold corresponding to a likelihood-based 68% confidence interval, i.e. a parameter is considered practically non-identifiable if the 68% confidence interval is infinite. Figure 3.3 shows how the thresholds are used to determine identifiability.

Docherty et al. (2011) presented a graphical method for understanding and evaluating identifiability in mathematically separable behaviours scaled by the identified parameters. These behaviours are normalised by their respective means and compared graphically. The closer the normalised behaviours are, in particular at the sample times of the output data, the poorer the practical identifiability. This method has more limitations than that of Raue et al. but the advantage is that it can provide a clear picture (literally) of why some datasets are more suitable than others and which parameters might be better off as a single identified parameter. Docherty et

al. also demonstrates that the method lends itself toward tailoring clinical tests to optimise sampling times for accuracy and cost.

3.4 Implications

Solving the inverse problem is not always a simple matter of having a model and using it to quantify the desired properties. Obviously, some models are better approximations of real behaviours than others but the story is far from ending there. Appropriate and robust parameter identification methods are required to achieve good estimation. Additionally, the implications of practical identifiability are far reaching for the inverse problem. Some groups in the scientific community appear to prefer complex models, since they have the best chance to describe the system accurately. While it is generally true that model adherence to data is improved with complexity and parameterisation, parameter robustness suffers. Thus the sought after accuracy is not always upheld in the key parameter outcomes. In some cases, it is not the degree of complexity but an aspect of the model formulation that produces practical non-identifiability, such as with the Minimal Model of glucose dynamics. In either case, a good understanding of practical identifiability can prevent a model being used inappropriately, which is especially important where physiological modelling informs clinical decision making.

In the context of developing glycaemic models for outpatient use, practical identifiability is a hugely important consideration. The type of data that can be collected in the outpatient environment is incongruous with clinical or research-grade data. Hence, models developed using research-grade data cannot be translated directly to the outpatient and expected to perform in the same manner. Hence, the present work retains an awareness of the unique challenges of outpatients with regard to the development and use of glycaemic models.

Part II

Model building and evaluation

Chapter IV

Grey noise effects

This chapter reviews so-called "grey-noise" effects that, when unaccounted for, can introduce non-random systemic errors into glycaemic modelling outcomes. This review was published in the journal of Biomedical Signal and Processing (Mansell et al., 2017b) and presents physiological evidence to justify the presence of these grey-noise effects, technologies and methods that exist to quantify their presence or effect in some way, and previous efforts to model them by others in the field.

4.1 Motivation

Injecting exogenous insulin to restore normoglycaemia after a postprandial excursion is a necessary therapy for those with T1DM and is often beneficial for those with T2DM (Rubin and Peyrot, 2001). However, estimating optimal insulin doses can be difficult. The traditional factors determining a postprandial dose are meal carbohydrate content and nominal SI. However, a host of small confounding influences accompany these factors (Lovell-Smith et al., 2010; Lloyd et al., 1999; Nathan et al., 1981; Sonnenberg et al., 1990; Lunt and Brown, 1996; Van Cauter et al., 1997; Yardley et al., 2013; González-Ortiz et al., 2000). Uncertainty introduced by confounding factors can cause individuals to take conservative doses for fear of hypoglycaemia (Rubin and Peyrot, 2001), reinforcing mild hyperglycaemia and increased incidence of diabetic complications (Rubin and Peyrot, 2001; De Boer et al., 2008; Retnakaran and Zinman, 2008; Shankar et al., 2007).

Physiological modelling tends to involve identification of patient-specific physiological parameters from available data, either for a population or specific to the patient at that time. For glycaemic control applications,

these parameters are used in conjunction with measured data and prediction algorithms to determine an appropriate insulin dose to remediate glycaemic excursions to pre-defined targets. Thus, unmodelled, non-random factors that affect this identification impact control safety and quality, and thus compliance.

Comparatively simple models that contain few variables have proven to be effective for glycaemic prediction and control in critical care (Chase et al., 2008; Evans et al., 2011). These simple models work primarily because they can be robustly identified (Docherty et al., 2011; Saccomani, 2013). However, in outpatient diabetes there are significantly more environmental stimuli present. These stimuli have the potential to contribute confounding behaviours and variability to the glycaemic signal that are not measured or included in the model.

For example, psychological factors, such as stress and depression, have been shown to influence glycaemic outcomes, tending patients toward hyperglycaemia (Rubin and Peyrot, 2001; Surwit et al., 1992; Räikkönen et al., 1996; Lustman et al., 2000), and exercise is a major source of glycaemic disturbance and can potentially cause hypoglycaemia (Breton, 2008; Dalla Man et al., 2009; Roy and Parker, 2007). When factors such as exercise and stress are not modelled, they contribute to non-random grey noise' in the data and confound attempts to capture the patient's true glycaemic metabolism. Hence, capturing grey noise would ultimately lead to more precise prediction in glycaemic levels and thus, improved glycaemic control.

To fully and effectively model the glycaemic excursions of diabetes outpatients, the models employed should attempt to minimise (by design) the grey noise by including additional behaviours in conjunction with patient-specific parameters. However increasing the size and complexity of the models also increases risk of model structural (Audoly et al., 2001, 1998; Bellman and Åström, 1970; Bellu et al., 2007) and practical (Docherty et al., 2011; Saccomani, 2013; Raue et al., 2009, 2014)

non-identifiability. Parameters must be robustly identified for sensible estimation, and effective model-based treatment.

Glucose-insulin dynamic models are the core element of any glycaemic control algorithm and have already been extensively reviewed in the field (Carson and Cobelli, 2001; Chase et al., 2006, 2010; Palumbo et al., 2013). This chapter seeks to draw attention to important grey-noise effects in diabetes that can significantly affect management and interpretation of data, and to provide a qualitative assessment and comparison of the representative modelling efforts to date and their applicability to the outpatient environment. The background of literature evidence for each of these effects and any methods of measuring their presence are also explored, given that these aspects are critical for mathematical modelling and control strategies. The specific grey-noise effects considered are: variability in nutritional intake, psychological effects, physical activity and metabolic rhythms.

A literature review was carried out through extensive searches on the academic database Scopus, which includes access to PubMed and a range of other citation sources. Due to the wide range of topics within the scope of the research, no single or few search criteria were strictly applied. A more thorough and expedient approach was required where the focus of criteria shifted between the different grey-noise factors, and also between the fields of clinical research, development and use of measurement technologies, and mathematical model development and validation. The goal was to locate the foundational models for all general strategies used to model a specific grey-noise effect, as well as supporting measurement and evaluation technologies and science. This chapter therefore compiles and reviews the detectability, measurability and practical identifiability of certain grey-noise factors, relevant to modelling, understanding and predicting the glycaemic excursions of outpatients with diabetes.

4.2 Nutrition

4.2.1 Physiological sources of variability

The gastro-intestinal tract is a complex system for extracting nutritional components from ingested food. Meals typically contain differing quantities of water, carbohydrate, fat, protein, essential vitamins and minerals. After mastication, ingested food is ground into smaller particles in the stomach by gastric acid, digestive enzymes and mechanical contractions (Reinus and Simon, 2014). Gastric emptying (GE) then delivers the food to the intestine where it is combined with bile and pancreatic enzymes. Muscular contractions in the intestine mix, propel and further break-down the food (Reinus and Simon, 2014). Absorption of glucose and two other notable monosaccharide sugars, fructose and galactose, occurs through the intestine walls to the bloodstream via transporter proteins in the cell walls (Reinus and Simon, 2014; Bornhorst and Singh, 2014).

Many factors affect GE. Food composition and quantity has a large effect due to feedback signals for optimising intestinal nutrient absorption (Reinus and Simon, 2014; Goldenberg and Cummins, 1971; Macdonald, 1996). In particular, higher quantities of fat, glucose, energy, and acids in the food reduce GE rate (Reinus and Simon, 2014; Bornhorst and Singh, 2014; Goldenberg and Cummins, 1971; Macdonald, 1996; Velchik et al., 1989; Schvarcz et al., 1997). Studies appear to generally support these same observations in T1DM and T2DM (Schvarcz et al., 1997; Lodefalk et al., 2008; Gentilcore et al., 2006; Fraser et al., 1990; Samsom et al., 1997; Folwaczny et al., 2003; Kong et al., 1996). Food structure also has a large impact on GE. Starches with expanded or disperse matrices like bread and potato have been shown to empty faster than rice or pasta whose matrices are denser (Mourot et al., 1988; Mishra and Monro, 2012; Torsdottir et al., 1986).

GE rates also exhibit significant variability across and within individuals for equivalent meals (Lartigue et al., 1994). Those with diabetes are especially prone to variability, with 20-50% experiencing abnormally slow GE (Clark

and Nowak, 1994; Horowitz et al., 2002). This condition is known as gastroparesis and is perhaps due to chronic hyperglycaemia more than neuropathy (Folwaczny et al., 2003; Liu et al., 2007). However, its impact is variable across individuals and over time creating a grey-noise bias.

Most carbohydrates are not ingested as monosaccharides. Disaccharides, such as sucrose and lactose, must be cleaved by enzymes anchored to the cells lining the intestine before absorption can occur (Reinus and Simon, 2014; Mourad and Saadé, 2011). Starches are long, branching chains of covalently bonded glucose. These polysaccharides must be digested into oligosaccharides by pancreatic amylases before being processed further into singular glucose molecules at the intestinal wall (Reinus and Simon, 2014).

Amylase access to the starch substrate is a primary determinant of starch digestive rate and thus plasma glucose appearance (Mishra and Monro, 2012; Englyst et al., 2003; Englyst and Englyst, 2005). High levels of processing, weak and porous starch structures and low levels of dietary fibre typically contribute to rapid availability of glucose (Mishra and Monro, 2012; Englyst et al., 2003; Englyst and Englyst, 2005; Monro, 2013). Resistant starch and non-starch polysaccharides (e.g. cellulose) cannot be digested and absorbed as glucose, and are instead fermented by gut bacteria in the large intestine and absorbed as short-chain fatty acids, thus their effect is non-glycaemic (Reinus and Simon, 2014; Englyst and Englyst, 2005).

Absorption of monosaccharides is moderated by the expression of transporter proteins in the cells of the intestinal wall (Reinus and Simon, 2014; Mourad and Saadé, 2011). Transporter expression increases in response to intestinal glucose presence and insulin secretion (Mourad and Saadé, 2011). Studies have found diurnal rhythms of transporter expression in rats (Mourad and Saadé, 2011; Douard and Ferraris, 2008; Ferraris, 2001) and similar expression is hypothesised in humans. Increased transporter expression has been observed in diabetes Dyer et al. (2002) and obesity (Nguyen et al., 2015). Consequently, a common treatment for

T2DM involves partial transporter repression (Tahrani et al., 2013).

Finally, once absorbed, galactose and fructose provide limited contributions to glycaemia. The liver converts approximately 10-20% of galactose into free glucose (Gannon et al., 2001; Sunehag and Haymond, 2002; Ercan et al., 1993) and 29-54% of fructose into free glucose. However, reported rates vary widely, potentially depending on gender, exercise condition and health status (Sun and Empie, 2012), again contributing grey-noise and uncertainty.

4.2.2 Measurement of glucose appearance

Scintigraphy (gamma imaging of radio-labelled food) is considered the gold standard method to measure GE (Kar et al., 2014; Szarka and Camilleri, 2009). Studies show that GE of liquids typically follows exponential decay functions and is thus often described by half-emptying times (Reinus and Simon, 2014; Bornhorst and Singh, 2014; Lartigue et al., 1994; Siegel et al., 1988). Solids tend to exhibit a lag' period of slow emptying before exponential emptying takes over (Collins, 1991; Siegel et al., 1988; Bornhorst and Singh, 2014).

Glucose appearance trajectories from the intestine are difficult to measure or infer via plasma or capillary glucose concentration measurement, due in part to the obscuring effects of the hepatic regulatory response to meal ingestion. In particular, the hepatic glucose balance shifts from a steady output of glucose in the basal state to a net uptake during post-prandial periods (Cherrington, 1999). Insulin dynamics also obscure glucose appearance modelling when plasma glucose measurements are interpreted without consideration of specific insulin measurements. Thus, plasma glucose data provides only a net effect across these variable endogenous responses.

Glucose appearance can be modelled using data from double-tracer methods (Mari et al., 1994), which typically involve infusing one type of

labelled glucose ([^{3}H]glucose) intravenously while giving an oral dose that contains a different tracer element ([^{14}C]glucose) Mari et al. (1994). Together, the tracers allow the glucose appearance rate (R_a) to be distinguished from glucose clearance and EGP. This type of R_a data is considered to be gold-standard in the measurement of glucose appearance and has been used by multiple groups to validate candidate models (Wong et al., 2008c; Dalla Man et al., 2006). R_a can be expressed in units of mmol/min or mg/min, but in clinical trials is most often normalised by subject weight with units of mol/kg/min or mg/kg/min (Mari et al., 1994; Dalla Man et al., 2006; Elleri et al., 2013). R_a trajectory ($R_a(t)$) calculation requires glucose kinetic models, such as Steele's one-compartment model (Steele, 1959) or Mari's two-compartment model (Mari et al., 1994).

Evaluating the effect of food type on variability in glycaemic effect can be carried out through multiple methods. Glycaemic index (GI) is a long-standing and simple method that gives the relative area of a glycaemic excursion caused by a food normalised by that of a reference food of equivalent carbohydrate content, either glucose or white bread (Foster-Powell et al., 2002). Each food type must be tested across multiple subjects to mitigate the effect of inter-patient variability. In such studies, a cohort of subjects with diabetes are also often tested to account for physiological differences (Foster-Powell et al., 2002).

Glycaemic load is a later extension of GI that takes into account the carbohydrate density of a food for a more practical evaluation of glycaemic effect for regular portion sizes (Foster-Powell et al., 2002). Carbohydrate bioavailability' is another, more extensive, classification that divides carbohydrates into portions of rapidly available glucose, slowly available glucose and resistant starch (Mishra and Monro, 2012; Englyst et al., 2003; Englyst and Englyst, 2005; Monro, 2013). These quantities were determined via in vitro digestion rate measurements. Ultimately, solely carbohydrate focused evaluations have limited usefulness for mixed meals. In particular, a clinical study found no correlation between estimation GI and measured GI of common breakfasts due to the influence of fat and

protein content (Flint et al., 2004).

Elleri et al. (2013) calculated $R_a(t)$ for complex sugars and carbohydrates with high and low GI foods using a double tracer method with an enriched oral meal load. In a follow-up protocol, a controller was used to titrate intravenous glucose at a rate that would match the oral glucose excursions. The study itself did not propose novel model formulations for these food types, but noted the potential to do so. It appears to be the first study to quantify multiple modes of glucose absorption from different carbohydrates *in vivo*. The results are reproduced in Figure 4.1 to show the effect of slower available glucose compared to rapidly available glucose on $\mathrm{R_a}$ trajectories.

4.2.3 Models for glucose appearance

A summary of the nutritional models can be found in Table 4.1.

4.2.3.1 The minimal model

The minimal model of food absorption was developed by Worthington in 1997 (Worthington, 1997). Validation of Worthington's model was carried out using measured plasma glucose excursions in a subject with T1DM. Hence, insulin-mediated glucose clearance was assumed negligible. Worthington fitted models of varying complexity to glycaemic data for high and low GI meals, and proposed the one-compartment model with a delay (D) due to its minimal parameterisation and general adherence to data. This model is defined:

$$\frac{dC_1(t)}{dt} = P_X(t-D)\frac{G_V}{V_G} - k_a C_1(t) \tag{4.1}$$

where C_1 is a combined stomach and intestinal compartment, P_X is the mass of the ingested meal, G_V corresponds to the fraction of available glucose, V_G is the glucose distribution volume and k_a is the turnover rate. $\mathrm{R_a}$ is thus calculated as $k_a C_1$, normalised by subject mass if preferred.

The model is relatively minimal and does not aim to directly model observed physiological compartments, such as the stomach and intestine. Furthermore, the model was not validated on gold-standard R_a data as it was developed using glycaemic excursion data. The goal of the model was to develop measures for the specific glycaemic impact of different foods by characterising D, k_a and GV, as opposed to GI, which is impacted by glucose-insulin dynamics. A representative simulation of this model is pictured in Figure 4.1.

4.2.3.2 Piecewise emptying model

The Lehmann and Deutsch (1992) model features a piecewise stomach emptying function (G_{empt}) based on a linear increase to a maximum emptying rate (V_{max}), followed by constant rate and then linear decrease back to zero. Ascending and descending times (T_{asc} and T_{dec}) are usually 30 minutes each. Thus time spend at the maximum rate (T_{max}) based on the carbohydrate load (Ch) is defined as:

$$T_{max} = \frac{Ch}{V_{max}} - (T_{asc} + T_{dec}) \tag{4.2}$$

and the piecewise emptying rate is therefore given by:

$$G_{empt}(t) = \begin{cases} \frac{V_{max}}{T_{asc}} t; & t < T_{asc} \\ V_{max}; & T_{asc} < t \leq T_{asc} + T_{max} \\ V_{max} - \frac{V_{max}}{T_{dec}}(t - T_{asc} - T_{max}); & T_{asc} + T_{max} < t \leq T_{asc} + T_{max} + T_{dec} \end{cases} \tag{4.3}$$

The model is adjusted for small carbohydrate loads (approximately <10 grams) as there is too little food to allow time for the emptying rate to plateau. Thus there is no T_{max} and instead T_{asc} and T_{dec} are both defined as $2Ch/V_{max}$, rather than 30 minutes. The resulting function is triangular rather than trapezoidal.

Glucose in the gut was modelled with a linear differential compartment

defined as:

$$\frac{dG_{gut}(t)}{dt} = G_{empt}(t) - k_{abs}G_{gut}(t) \tag{4.4}$$

where k_{abs} is a constant emptying rate and thus the appearance rate would be $k_{abs}G_{gut}(t)$. An example of R_a from this model is included in Figure 4.1.

The model was developed to simulate a virtual patient for education in diabetes management as well as computational testing and analysis of treatment regiments (Lehmann and Deutsch, 1992). Thus all model parameters are defined at fixed values except for the input quantity of carbohydrate. The model accounts for some food-related variability by adjusting the model form with meals of low carbohydrate content, though an adjustment was mathematically necessary anyway. Further variability could be captured by altering the maximum emptying rate and intestinal absorption parameters. Moreover, using a fixed V_{max} would not account for strong GE dependence on factors such as quantity of carbohydrate, fat and protein and energy, demonstrated in the literature (Bornhorst and Singh, 2014; Reinus and Simon, 2014; Velchik et al., 1989; Goldenberg and Cummins, 1971; Schvarcz et al., 1997; Macdonald, 1996).

4.2.3.3 2-compartment model

Wong et al.'s model for clinical use in T1DM is a 2-compartment model that is based partially on the minimal model of Worthington (1997) and was validated on mixed-meal tracer glucose appearance data (Wong et al., 2008c). The first compartment (STO) represents the stomach, while the second (GUT) represents the gut with each emptying in an exponential decay. The model also includes a rate limitation in glucose/carbohydrate intake in the gut ($GABS_{max}$) based on experimental results. The model is defined as:

$$\frac{dSTO(t)}{dt} = -k_6 STO(t) + u_{CHO}(t) \tag{4.5}$$

$$\frac{dGUT(t)}{dt} = GABS(t) + k_6 STO(t) \tag{4.6}$$

$$GABS(t) = -\min(k_7 GUT(t), GABS_{max}) \tag{4.7}$$

where u_{CHO} is an impulse containing the carbohydrate mass in the meal, k_6 is the GE rate, and k_7 is the gut absorption rate. R_a can therefore be calculated as $GABS(t)/0.18$, and potentially further divided by subject mass.

This glucose appearance model aims to use *a priori* estimated values for all constants to inform therapeutic doses of insulin in conjunction with a wider model that includes glucose-insulin dynamics. The chapter discusses; but ultimately did not model, the effect of slowly digested carbohydrates due to the difficulty in predicting the various glycaemic indices of mixed meals. Figure 4.1 includes a representative simulation of this model.

4.2.3.4 3-compartment model

Dalla Man et al. (2006) developed a model to capture more complex digestive behaviours. Two compartments are used for solid (q_{sto1}) and liquid (q_{sto2}) phases in the stomach. The solids undergo grinding and enter the liquid phase and the liquid empties into the intestine. A third compartment (q_{gut}) is used for the small intestine. The model is defined:

$$\dot{q}_{sto1}(t) = -k_{21} q_{sto1}(t) + D\delta(t) \tag{4.8}$$

$$\dot{q}_{sto2}(t) = -k_{empt}(q_{sto}) q_{sto2}(t) + k_{21} q_{sto1}(t) \tag{4.9}$$

$$\dot{q}_{gut}(t) = -k_{abs} q_{gut}(t) + k_{empt}(q_{sto}) q_{sto2}(t) \tag{4.10}$$

$$R_a(t) = f k_{abs} q_{gut}(t) \tag{4.11}$$

where k_{21} is the grinding rate, D is the glucose content, $\delta(t)$ is an impulse function, k_{abs} is the absorption rate in the intestine and f is the fraction of glucose that appears from absorption. The k_{empt} parameter is a complex function of the stomach contents defined:

$$k_{empt}(q_{sto}) = k_{min} + \frac{k_{max} - k_{min}}{2}(\tanh(\alpha(q_{sto} - bD)) - \tanh(\beta(q_{sto} - cD)) + 2) \tag{4.12}$$

$$\alpha = \frac{2}{2D(1-b)} \tag{4.13}$$

$$\beta = \frac{5}{2Dc} \tag{4.14}$$

$$q_{sto} = q_{sto1} + q_{sto2} \tag{4.15}$$

where k_{min} and k_{max} are the minimum and maximum values of k_{empt}, c and b are shape parameters that specify when changes in k_{empt} occur relative to the fraction of the meal remaining in the stomach.

The complex changing emptying rate produces a secondary hump on $R_a(t)$ (seen in Figure 4.1) that is often observed experimentally. Initially, k_{empt} is large, but is quickly reduced, presumably imitating the feedback control from the small intestine as the first amount of glucose is absorbed. As the stomach empties, k_{empt} returns to its maximal value.

Dalla Man et al. (2006) optimised values for k_{max}, k_{min}, c, b and k_{abs} to fit the model to R_a data. The assumptions $k_{21} = k_{empt}$ and $k_{empt} > k_{abs}$ were made for structural identifiability. Still, it is worth noting that the authors found that for a quarter of the subjects, the c parameter was near zero, indicating that k_{empt} was initially at its minimal value. Assuming that $c = 0$ allowed the model to be simplified in these particular cases.

Dalla Man et al. noted that the second stomach compartment alone did not adequately fit the model to R_a data. Thus, the non-linear emptying rate function, rather than the additional compartment, is the defining feature of the model. Given a constant k_{empt} value, the two stomach compartments do not appear to produce significantly different $R_a(t)$ curves to a single compartment (seen in Figure 4.1).

4.2.3.5 Gastro-intestinal transit model

Salinari et al. (2011) presents a very thorough gastro-intestinal transit model for modelling R_a in Oral Glucose Tolerance Tests (OGTTs) that considers motility of carbohydrates along the small intestine. Glucose is

delivered to the intestine according to a GE function and then absorbed to the blood stream as it moves along the intestine. The authors present a simple form of the model, as well as a more extensive one that considers regional differences in transporter protein expression along the intestine (both seen in Figure 4.1). Like the 3-compartment model, the latter case accounts for the hump frequently observed on the descending path of R_a trajectories experimentally. Overall, it appears to be the first model that aims to capture the contributions of more complex behaviours in the intestine. The uniform absorption case with exponential GE can be simulated directly with:

$$R_a(t) = \begin{cases} fD\frac{k\gamma}{k-\gamma}(e^{-\gamma t} - e^{-kt}); & 0 \leq t \leq L/u \\ fD\frac{k\gamma}{k-\gamma}(e^{-\gamma L/u - k(t-L/u)} - e^{-kt}); & t > L/u \end{cases} \tag{4.16}$$

where D is the glucose bolus ingested, f is the loss coefficient, k is the GE rate constant, and γ is the intestinal glucose absorption rate. L is the length of the small intestine and u is the velocity of the glucose along the length. Thus, if the time exceeds L/u, some glucose will enter the large intestine and will not be absorbed.

Salinari et al.'s more complex model includes a power term in the gastric emptying function and two glucose transporters with different regional expression functions, and is defined:

$$R_a = f \int_0^L \gamma(z) q(z,t) dz \tag{4.17}$$

where the absorption rates ($\gamma(z)$) are a function of a space co-ordinate (z) and $q(z,t)$ is the quantity of glucose in the intestine as a function of space and time and is given by the equation:

$$q(z,t) = \begin{cases} q_0 \left(t - \frac{z}{u}\right) e^{-\frac{1}{u}\int_0^z \gamma(z')dz'}; & 0 \leq t - \frac{z}{u} \\ 0; & \text{elsewhere} \end{cases} \tag{4.18}$$

where u is the velocity of the glucose as with the uniform case and q_0 is the intestinal content at the entrance of the intestine, which is a function of gastric emptying, defined:

$$q(z = 0, t) = q_0(t) = \frac{1}{u}\eta(t) \tag{4.19}$$

where η is the delivery of glucose to the intestine due to power-exponential emptying and is given by:

$$\eta(t) = D\beta k^{\beta} t^{\beta-1} e^{-(kt)^{\beta}} \tag{4.20}$$

where β is the power constant. For the non-uniform case, the absorption rate is considered to be the sum of absorption rates for two separate transporters: $\gamma(z) = \gamma_1(z) + \gamma_2(z)$. Gaussian functions can be used to approximate γ_{1-2} in the absence of data.

Salinari et al. intended for the model to be used for identification of physiological parameters from OGTT data. *A priori* values had to be assumed for most constants in the nutritional model, except the GE rate (k), which was identified, and a scaling factor (c) for the Gaussian transport rate functions (γ_{1-2}). The scale of γ_2 was identified ($c_2 = c$) and the scale of γ_2 was assumed to be half that value ($c_1 = 0.5c_2$).

4.2.4 Implications for modelling nutritional intake

Appearance of glucose from nutrition is subject to a wide range of grey-noise variability and uncertainty due to the complexity of gastro-intestinal processes, inter- and intra- subject variation, and effects from the food structure and composition. These factors, when unmodelled, increase grey noise in model-based identification and prediction. Models of varying complexity were presented. Overall, each candidate nutritional models exhibits similar behaviour (in Figure 4.1). Since control of glycaemic excursions is of primary interest to researchers, the integrated form of $R_a(t)$, is particularly relevant, and more effectively demonstrates the similarity of the models.

The general glucose appearance trajectory can be captured even with the comparative simplicity of the minimal model of Equation (4.1). Modelling complex behaviours can give insight into the rates of particular and important physiological processes, especially in the presence of high quality

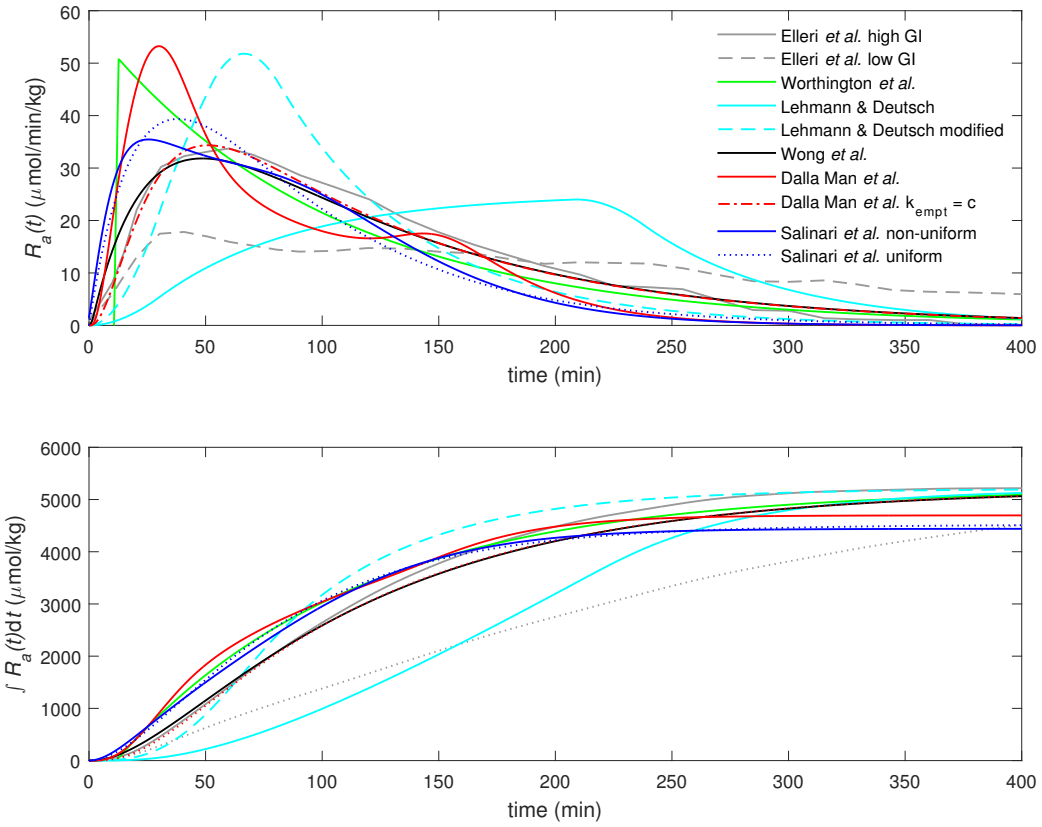

Figure 4.1: A summary comparison of six model types for 75g carbohydrate inputs and an 80kg subject: the minimal model (Worthington, 1997); the piecewise emptying model Lehmann and Deutsch (1992) both as in the literature and with a modified emptying rate; the 2 compartment model (Wong et al., 2008c); the 3 compartment model with complex GE rate (Dalla Man et al., 2006); the 3 compartment model with constant GE rate (Dalla Man et al., 2006) with parameters modified for comparison to the Wong et al. (2008c) model; the uniform and non-uniform absorption transit models (Salinari et al., 2011). Also included is the tracer data for high and low glycaemic meals (Elleri et al., 2013), scaled to achieve a similar overall glucose appearance per subject mass to the simulated models.

clinical data. Furthermore, complex modelling approaches can yield insight into particular dysfunctions or etiologies. However, predictive capabilities of a model for post-prandial glycaemic outcomes will likely be limited by intra-individual and food variability, rather than the complexity of the model, as these uncertainties significantly outweigh the added precision.

This concept is demonstrated in Figure 4.1, which also includes scaled versions of Elleri et al.'s tracer data for high and low GI meals. Most model simulations are similar to each other and the high GI data. The exception to this is the piecewise emptying model, which is largely due to the author's choice of fixed emptying rate coupled with a simulated carbohydrate load larger than generally prescribed for that model. Using a modified emptying rate brings the simulated model trajectory closer to those of the other models (Figure 4.1). In contrast to the majority of the models, the low GI data stands out with a significantly different trajectory. Hence, food structure and composition contributes to potentially recoverable grey noise in the measured data. If the influence of GI and other such factors is not modelled, this variance in glycaemic excursions will be incorrectly captured in other overall metabolic model parameters, and prediction precision will be harmed.

The many physiological and environmental sources of nutritional variability could perhaps be lumped into variables that capture the general behaviour. In this case, it appears that nominal appearance rate and glucose quantity are dominant features that could be parameterised to capture the general trend in glucose excursion caused by nutritional and subject variability, utilising *a priori* information, where possible, for prediction applications. At present, tools such as GI and carbohydrate availability are used to study and predict the glycaemic effect of a given meal (Englyst et al., 2003; Englyst and Englyst, 2005; Flint et al., 2004; Mishra and Monro, 2012; Monro, 2013). The fat and protein content of nutrition has shown a confounding effect on GI (Flint et al., 2004). Hence, the nature of the confounding effects needs to be quantified to provide the necessary *a priori* information to fully capture the glucose appearance of typical meals.

4.3 Psychological effects

4.3.1 Stress and similar factors

It is well recognised that medical and emotional stress affects glucose regulation (Klonoff, 2007; Lloyd et al., 1999; Räikkönen et al., 1996; Surwit et al., 1992; Xiu et al., 2014; Ramkissoon and Vehí, 2015). These effects are attributed to the release of a number of hormones, particularly cortisol (Xiu et al., 2014). More than three decades ago, Rizza et al. (1982) observed glycaemic responses alongside a cortisol infusion, which reduced hepatic and peripheral insulin sensitivity. A number of other experiments have also been carried out to determine the relationship between stress stimuli and glycaemia in T1DM subjects (Lloyd et al., 1999; Surwit et al., 1992; Ward et al., 2011; Rizza et al., 1982). While clear correlation was found between medical stress and hyperglycaemia, mixed results exist for the effect of psychological stress. Surwit et al. (1992) found some studies showed that psychological stress correlated with both hyperglycaemia and hypoglycaemia, while other studies exhibited no effect. This discrepancy could potentially be due to differing or ambiguous definitions of stress across studies and the possible presence of autonomic neuropathy in some individuals, which can reduce sympathetic responses to stress (Surwit et al., 1992).

In general, stress appears to be consistently associated with poor glycaemic control (Lloyd et al., 1999). Studies using exogenous cortisol as a stimulus found reduced insulin sensitivity signals (Surwit et al., 1992; Ward et al., 2011; Rizza et al., 1982). Depression is also associated with poor glycaemic control and a high incidence of hyperglycaemia (Nathan et al., 1981; Lustman et al., 2000). Since cortisol levels are elevated in depression and linked to insulin resistance (Nathan et al., 1981), it follows that depression would be linked to insulin resistance, although the strength of this link is unconfirmed.

4.3.2 Measurement of stress

The effect of stress has been measured by calculating SI values changing in response to a cortisol stimulus (Ward et al., 2011). Ward et al. tested a stress-compensating closed-loop glycaemic control algorithm in subjects taking oral hydrocortisone doses that were equivalent to moderate stress (Ward et al., 2011). Their results showed that model-identified SI was reduced by around 40-50% several hours after hydrocortisone doses leading to significant changes in insulin requirements for glycaemic control.

Stress levels can be measured using a number of methods other than subjective surveys. Recent technological advances have seen a rise in in the ability to measure indicators of stress in an outpatient environment. Several groups have performed research into measuring galvanic skin responses, which are altered in response to psychological stress as a sympathetic nervous response (De Santos Sierra et al., 2011; Saha et al., 2014; Luharuka et al., 2003). Their devices are able to provide continuous, digital data and can also be combined with heart rate monitors for very successful stress detection (De Santos Sierra et al., 2011). This technology would be less effective in diabetes due to reduced sympathetic nerve response and reduced skin moisture (Surwit et al., 1992; Goetsch et al., 1993). However, it could be useful in younger individuals and those that have little neuropathy. Another technology has emerged that can take quick and easy salivary cortisol measurements with a small device connected to a smartphone (Zangheri et al., 2015; Choi et al., 2014). The simplicity and cost effectiveness of the technology both add to outpatient usability. Therefore, there is great potential to measure stress and similar psychological disturbances on a day to day or more frequent basis, if necessary, in the near future.

4.3.3 Implications for modelling psychological effects

Stress and depression have significant impact effect on glycaemic regulation. Some studies have shown that stress is often concurrent with reduced SI (Surwit et al., 1992; Lloyd et al., 1999; Rizza et al., 1982). However, there

appears to be a lack of glycaemic models that incorporate stress, and thus this important contribution to grey-noise is typically overlooked.

Mansell et al. (2015d) modelled stress as a constant multiplicative reduction in SI appearing on certain days (Chapter 9). Considering more short-term effects, Ward et al. (2011) shows a delay between the administration of oral hydrocortisone and changes in SI. It is apparent that the specific bioavailability of the hydrocortisone compared to endogenous forms of cortisol has a significant but not yet quantified effect on glycaemic control. Given the mixed results of clinical studies of the effect of psychological stress and the emergence of sensors to measure its indicators, this research area may soon attract more interest and see the development of data-driven models. Accounting for psychological effects could reduce a large source of grey noise and enable tangible improvements in model-based glycaemic control in diabetes.

4.4 Physical activity

4.4.1 Physiological effects of physical activity

The acute effect of exercise is a major metabolic disturbance and thus can contribute grey noise in diabetes modelling. Moderate or aerobic exercise typically burns muscle glycogen stores in the first 5-10 minutes before relying on glucose released from the liver and fatty acids from fatty tissue (Yardley et al., 2013). In healthy individuals, insulin levels decrease and glucagon levels increase to stimulate the additional hepatic EGP required to maintain normoglycaemia (Yardley et al., 2013; Sonnenberg et al., 1990). During and after prolonged exercise, glycogen stores become depleted and hypoglycaemia can occur.

However, individuals with diabetes are typically in a state of hyperinsulinemia that prevents adequate hepatic response resulting in more readily occurring exercise induced hypoglycaemia (Yardley et al., 2013; Sonnenberg et al., 1990). Even post-exercise, elevated muscle clearance of glucose can persist for 2 hours and increased SI has been observed for

upwards of 16 hours due to increased peripheral sensitivity and increased non-insulin mediated uptake (Borghouts and Keizer, 2000; Magkos et al., 2008). These factors can lead to hypoglycaemic events hours after exercise has ended. High intensity anaerobic or resistance forms of exercise are less dependent on insulin and glucagon reactions, since the release of catecholamines stimulates a 5-10-fold increase in hepatic EGP (Yardley et al., 2013). Therefore, anaerobic and resistance forms of exercise, even included in routines with aerobic exercise, can reduce the likelihood of acute or late hypoglycaemia (Yardley et al., 2013).

4.4.2 Measurement of physical activity

Measurement of exercise is generally thought of in terms of energy expenditure (EE) and intensity. EE for aerobic respiration can be evaluated by measuring the gas exchange occurring within an individual. The rates at which oxygen is inspired and carbon dioxide is expired are highly correlated with energy consumption (Schrack et al., 2010). However, anaerobic respiration does not rely on O_2 and does not produce CO_2, so other methods must be used to estimate anaerobic EE (Scott, 2006).

Traditionally, the Douglas Bag method has been used as the gold-standard test for aerobic EE over a range of intensities. This method involves collecting exhaled gas via a face mask and analysing the oxygen and carbon dioxide content. However it is limited to a clinical environment due to the necessity of physical or chemical analysis of exhaled gas (Wenzel et al., 1990). Recent advances in technology have enabled portable, real-time analysis of gas exchange with a device known as the K4b^2 (Schrack et al., 2010). The device is considered effective and reliable for measurement in an outpatient environment (Veluswamy et al., 2015). However, the K4b^2 requires that exercise is undertaken while wearing a face mask and is thus not feasible for daily outpatient use.

Other less direct measures of physical activity can estimate EE. Heart rate is considered to have reasonable correlation with EE (Strath et al., 2000)

and can be supplemented with motion sensors for improved precision (Strath et al., 2002). Accelerometers have reasonable overall correlation with EE, but lack accuracy across different activities (Bassett D.R et al., 2000; Yumiko et al., 2002). Furthermore, measurements are dependent on the sensor location on the body relative to the activity (Kim et al., 2014). Regardless, accelerometers may be accurate enough to evaluate a level of EE in the average non-athlete individual depending on the application (Yumiko et al., 2002).

Self-recorded physical activity questionnaires have also been shown to correlate reasonably well to EE for moderate and vigorous exercise (Kurtze et al., 2007) and thus may be suitable for capturing the effect of exercise on glycaemia. Pedometers can give a good indication presence of physical activity, but cannot effectively delineate intense exercise from low-intensity walking (Dai et al., 2008). The ActiReg system combines body position sensing with motion sensing to estimate EE during low intensity activities and can also be supplemented with heart rate measurement for better estimation during higher intensity activities (Hustvedt et al., 2004). The advantage of movement monitors is the relative ease of data collection in an outpatient environment. In particular, the recent prevalence of smart-phones containing accelerometers vastly improves this data collection ability. However, the disadvantages of movement monitors are the low accuracy and precision. Those involving additional heart rate measurement appear to be the most accurate (Hustvedt et al., 2004; Strath et al., 2002).

The relative intensity of aerobic exercise is usually evaluated as a percentage of either peak oxygen uptake (VO_2max) or the oxygen uptake reserve ($VO_2R = VO_2max - VO_2rest$) (Mann et al., 2013). Direct measurement of VO_2max is time-consuming, difficult and not done daily (Beutner et al., 2015; Kumar et al., 2012). Thus, several other methods of indirect measurement have been developed (Beutner et al., 2015; Sykes and Roberts, 2004; Uth et al., 2004). Notably, the heart rate reserve can be used to estimate VO_2max (Uth et al., 2004) and heart rate relative to the heart rate reserve can be used as a measure of exercise intensity on its own

(Mann et al., 2013).

4.4.3 Models of exercise

A summary of exercise models can be found in Table 4.1.

4.4.3.1 Heart rate model

Breton (2008) developed a functional exercise model as an extension to the minimal model of glycaemic dynamics . The model was tested on a patient with T1DM and utilised a heart rate monitor as a measured input for exercise. Based on heart rate (HR), energy consumption (Y) is modelled:

$$\dot{Y} = -\frac{1}{\tau_{HR}}Y + \frac{1}{\tau_{HR}}(HR - HR_b) \tag{4.21}$$

where the subscript b indicates a basal heart rate and the rate parameter τ_{HR} was set as 5 minutes for a delay.

Insulin action (Z, synonymous with SI) can be modelled to mimic activation of glucose transporters, which increases with exercise, increasing apparent SI (Dalla Man et al., 2009):

$$\dot{Z} = -\left(f(Y) + \frac{1}{\tau}\right)Z + f(Y) \tag{4.22}$$

$$f(Y) = \frac{\left(\frac{Y}{\alpha HR_b}\right)^n}{1 + \left(\frac{Y}{\alpha HR_b}\right)^n} \tag{4.23}$$

Both n and τ are used to filter out random non-exercise induced changes in heart rate (Breton, 2008). These effects of energy consumption and modified insulin action appear in the plasma glucose (G) compartment that also includes insulin action (X) and glucose appearance from food (D):

$$\dot{G} = -p_1(G - G_b) - (1 + \alpha Z)XG - \beta YG + \frac{D}{V_g} \tag{4.24}$$

where α and β modify the size of the effects and were intended to be identified along with other glycaemic parameters, such as p_1, V_g, and G_b,

using a combination of least-squares and Bayesian influence (Breton, 2008). The use of Bayesian adaptation of parameter values implies that this model, as defined by Breton (2008), can yield impractical results due to low practical identifiability (Docherty et al., 2011; Cobelli et al., 1998; Erichsen et al., 2004; Cobelli et al., 1999; Pillonetto et al., 2002).

Figure 4.2 shows an example simulation of the effects of this exercise model. Breton notes that their experimental data did not cover enough time to explore the dynamics of post-exercise recovery in insulin sensitivity. Dalla Man et al. (2009) augmented it with increased peripheral tissue glucose utilisation post-exercise and a dependency of insulin action on the EE during exercise, with a concomitant increase in the number of identified parameters.

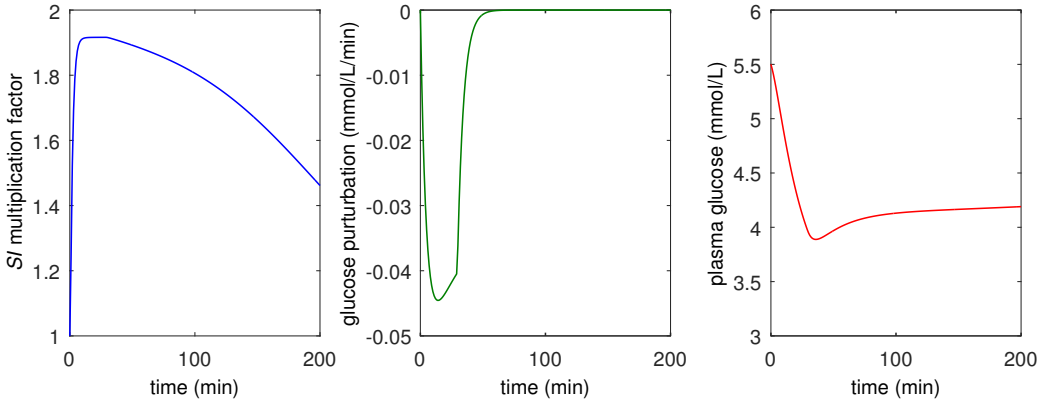

Figure 4.2: An example simulation of the Breton et al. model for 30 minutes of exercise with the SI multiplication factor $(1 + \alpha Z)$ pictured left, the rate of perturbation in plasma glucose (βYG) pictured middle and the resulting plasma glucose trajectory from a non-basal starting value pictured right.

4.4.3.2 $\text{PVO}_2^{\text{max}}$ *model*

Roy and Parker developed an exercise model as an extension of the minimal model Roy and Parker (2007). The power at maximum oxygen consumption ($\text{PVO}_2^{\text{max}}$) was used to modulate the insulin signal. Additionally, rather than

use $\mathrm{PVO}_2^{\max}$ as a measured quantity, it was modelled:

$$\frac{dPVO_2^{max}}{dt} = -0.8PVO_2^{max}(t) + 0.8u_3(t) \tag{4.25}$$

where $u_3(t)$ is ultimate exercise intensity (ranging from 0-92%) above basal (8%). Equation (4.25) effectively models a small delay between the targeted exercise intensity and the actual $\mathrm{PVO}_2^{\max}$. The plasma insulin compartment of the minimal model (I) is augmented by a variable (I_e), which is a function of $\mathrm{PVO}_2^{\max}$:

$$\frac{dI}{dt} = -nI(t) + p_4u_1(t) - I - e(t) \tag{4.26}$$

$$\frac{dI_e}{dt} = a_5PVO_2^{max}(t) - a_6I_e(t) \tag{4.27}$$

where u_1 is the exogenous insulin input. Population values were used by Roy and Parker for parameters n and p_4, while a_5 and a_6 were identified from plasma insulin assays in healthy individuals undergoing exercise in a clinical trial.

Roy and Parker also modelled hepatic EGP (G_{prod}) and peripheral glucose uptake (G_{up}) as a function of $\mathrm{PVO}_2^{\max}$:

$$\frac{dG_{prod}}{dt} = a_1PVO_2^{max}(t) - a_2G_{prod}(t) \tag{4.28}$$

$$\frac{dG_{up}}{dt} = a_3PVO_2^{max}(t) - a_4G_{up}(t) \tag{4.29}$$

where a_{1-4} were identified from multiple tracer data of EGP and glucose disappearance in healthy subjects undergoing exercise in a clinical trial. Model simulations were then compared to subjects with T1DM in a similar trial. Roy and Parker also modelled the decrease in EGP as a result of glycogen depletion (G_{gly}) as a function that was zero until a critical threshold was reached and also returned to zero in the post-exercise period.

The modified plasma glucose compartment was then defined:

$$\frac{dG}{dt} = -p_1(G(t) - G_b) - X(t)G(t) + \frac{D}{V_g} + \frac{W}{V_g}\left(G_{prod}(t) - G_{gly}(t) - G_{ip}(t)\right) \tag{4.30}$$

where W is weight of subject.

Figure 4.3 shows an example simulation of the model. It is evident from the figure and Equations (4.28) and (4.29) that G_{prod} and G_{up} cannot be easily delineated using data of their net effect on glycaemia if multiple tracer data were not available. Hence, for outpatient application, only one, rather than two, compartments could be used to model this net behaviour to maintain structural identifiability.

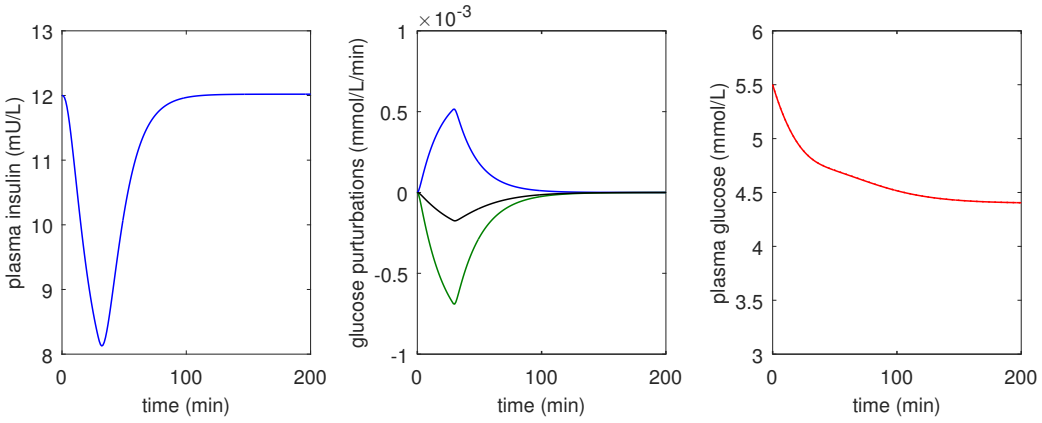

Figure 4.3: An example simulation of the Roy and Parker model for 30 minutes of exercise with the plasma insulin pictured left, glucose perturbation rates (note that G_{gly} is neglected) pictured middle and the resulting plasma glucose trajectory pictured right.

The reduction in plasma insulin with exercise is debated. Some literature indicates this behaviour occurs as a glucoregulatory response in healthy individuals to stimulate additional hepatic production, but cannot be regulated in individuals with T1DM (Sonnenberg et al., 1990; Yardley et al., 2013). Furthermore, increased plasma insulin has been observed

during exercise in T1DM suggesting increased mobilisation from subcutaneous depots of slow acting exogenous insulin (Mallad et al., 2015). Thus, the validation of the plasma insulin model against healthy individuals is not necessarily directly transferable across into diabetes.

4.4.3.3 Curviliniear insulin resistance model

Magkos et al. (2008) measured insulin resistance (IR, inverse to SI) the day after intense exercise in a clinical study. Reduced IR the morning after evening exercise was proposed to be related to EE as a curvilinear function shown in Figure 4.4. There was also a tendency for higher initial IR values to reduce to a greater extent (Magkos et al., 2008). It should be noted that there was a substantial amount of inter-subject variability.

While the model indicates that exercise reduces IR, a large portion of the subjects experienced an increase. The authors also noted that a large EE was required for appreciable changes. In the context of the study, this information led to the conclusion that relying on acute effects of exercise was not a practical means of improving insulin sensitivity. Overall, the study was underpowered to yield a statistically significant means of predicting changes in IR the day after exercise. However, the data shows a probable effect of exercise, and may be useful in further development of exercise models for glycaemic control, especially if more rigorous validation can be carried out.

4.4.4 Implications for modelling physical activity

The effect of exercise on glycaemia has been well recorded (Sonnenberg et al., 1990; Yardley et al., 2013; Mallad et al., 2015; Mayer-Davis et al., 1998; Borghouts and Keizer, 2000). Exercise is a particularly important factor due to its tendency to cause hypoglycaemia even well after exercise has ended (Sonnenberg et al., 1990; Yardley et al., 2013; Borghouts and Keizer, 2000). Clinical experiments have shown that compensating for exercise with planned reductions in insulin dose is an effective means of reducing hypoglycaemic risk (Sonnenberg et al., 1990). Such trials

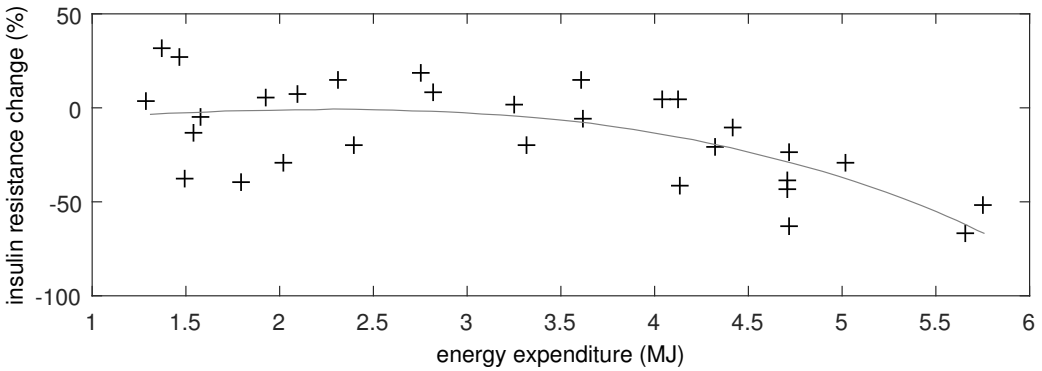

Figure 4.4: Data (+) and model (—) for changes in next-day insulin resistance as a function of EE in exercise in healthy subjects. Figure reproduced from Magkos et al. (2008)

demonstrate the benefit of a reduction in exercise-induced grey noise. Thus, including exercise in model-based prediction has great potential for safe-guarding patients with diabetes against hypoglycaemia and giving greater confidence in engaging in physical activity.

Some of the exercise models considered here use data that is unlikely to be available in an outpatient setting, such as PVO_2^{max} (Roy and Parker, 2007) or insulin resistance (Magkos et al., 2008). Given the sparse sampling regimen that could be expected in outpatient diabetes glucose control, models that capture the effects of exercise on glycaemia must be sparsely parameterised. However, the exercise model of Breton (2008) utilises the heart rate input data and thus could potentially be incorporated into an algorithm for the control of glycaemia. The model is also relatively simple and does not require a great deal of parameterisation and thus would not require prohibitively large data sets to confidently identify. Hence, the model is likely to be practically identifiable.

Some aspects of the effect of exercise have been explored in the models reviewed. Both Breton's heart rate-based model and Roy and Parker's PVO_2^{max}-based model are validated in high resolution, short term data that does not extend particularly far beyond the exercise period. The need for

models that capture post-exercise glucose excursions is highlighted by Magkos et al.'s clinical data and model for next-day IR. However, next day IR does not provide a precise picture of the whole post-exercise effect either. To capture exercise-induced grey noise in outpatient diabetes, further understanding of the immediate and delayed effects of exercise on glycaemia is needed.

Anaerobic exercise has a confounding influence and has not been modelled as often as aerobic exercise. In particular, anaerobic exercise does not correlate well with traditional means of measuring EE (Scott, 2006). Furthermore, anaerobic exercise seems to have a contrary glycaemic effect to aerobic exercise as it has been shown to reduce the risk of hypoglycaemia (Yardley et al., 2013). Thus, anaerobic exercise still presents a significant source of grey-noise that should be accounted for to improve glycaemic control.

4.5 Metabolic rhythm

Glucose regulation is also subject to circadian and other metabolic rhythms (Van Cauter et al., 1997). This section focuses on circadian rhythms in SI as a dominant, and thus measurable effect.

4.5.1 Circadian rhythms in glycaemic indicators

Section 4.2.1 described the presence of circadian rhythms in glucose transporters in the intestine. Overall glucose tolerance also tends to be lower in the afternoon and evening than in the morning in healthy individuals. Thus the term 'afternoon diabetes' emerged to describe the increased possibility of a false-positive diagnosis of glucose intolerance in the afternoon (Van Cauter et al., 1997). There are mixed results regarding the role of insulin sensitivity in this phenomenon (Sensi and Capani, 1976; Carroll and Nestel, 1973), but the evidence generally supports a reduced SI in the afternoon, along with reduced glucose utilisation and insulin secretion (Van Cauter et al., 1997). Oddly, this pattern appears to be reversed in diabetes with glucose tolerance and insulin sensitivity improving

from morning to evening for both T1DM and T2DM (Van Cauter et al., 1997; Visentin et al., 2015). This observation is part of the so-called 'dawn phenomenon'.

4.5.2 Measurement of circadian rhythms

Circadian metabolic rhythms tend not to be directly measurable. Early observations arose from differing glucose tolerance results to the same oral glucose challenge at different times of day (Van Cauter et al., 1997). More recently, mathematical models and multiple tracer methods have been used to study changes in SI and EGP and uptake at different times of the day (Van Cauter et al., 1997; Sensi and Capani, 1976; Carroll and Nestel, 1973; Visentin et al., 2015).

Hinshaw et al. (2013) recently calculated distinct SI values for breakfast, lunch and dinner in subjects with T1DM compared to healthy subjects. The mean result for the cohort with diabetes showed a large increase in SI from breakfast to lunch and a slight decrease by dinner, an opposite pattern to the healthy cohort. Hinshaw et al. noted that the unexpectedly large inter-subject variability in SI patterns reduced the power of the study to make conclusions for the whole T1DM population. However, this variability also perhaps suggests a greater need for personalisation in control algorithms using identifiable models and easily obtained data to minimise the impact of this effect.

4.5.3 Models of circadian SI rhythms

Several circadian SI models have been utilised (Toffanin et al., 2013; Fabietti et al., 2006; Mansell et al., 2015d). A summary of these models can be found in Table 4.1.

4.5.3.1 Piecewise model

Toffanin et al. (2013) used many literature references to determine several fixed points for their multiplication factor (y) . The $y(t)$ function was created by interpolating t and y with a cyclic piecewise cubic Hermite interpolating

polynomial based on:

$$t = [0, 2, 3, 8, 11.5, 15, 22, 24] \tag{4.31}$$

$$y = [1.4, 0.8, 0.6, 0.4, 0.8, 1, 1, 1.4] \tag{4.32}$$

where t is the time in hours.

The model was not used in any identification scheme, but as part of a virtual patient and control algorithm for *in silico* trials. Toffanin et al. parameterised the model via reference to various published reports. They noted the proposed model was for cases when patient-specific information was not available, but would become redundant with patient-specific clinical testing.

4.5.3.2 Sinusoidal model

Fabietti et al. (2006) used a simple sinusoid to model circadian SI. SI is multiplied by a function:

$$P_{circ} = 1 + A_c \sin\left(\frac{\pi t}{12} + P_c\right) \tag{4.33}$$

where A_c is the amplitude and P_c is the phase and t is the time in hours.

A_c, P_c and the nominal SI parameters were all identified from available data. Fabietti et al. noted problems with identifying A_c since the experiments were only 4-6 hours and the parameter would sometimes exceed 1, indicating a negative SI at some times. This result strongly suggests practical non-identifiability occurred in this study due to a lack of information in the data set. In particular, with only a small portion of the SI path recorded, there would be a greater trade-off between all of the parameters due to the nature of the function and not being able to observe the entire function. A longer experiment, in particular one lasting several days, would be required to remediate this issue (Mansell et al., 2015d). Importantly, the resultant time of lowest identified sensitivity averaged around 6am, which is consistent with literature (Fabietti et al., 2006),

providing some confidence.

4.5.3.3 Variable basis model

Mansell et al. (2015d) used a series of linear basis functions to model a circadian rhythm in SI:

$$SI(t) = SI_1 g_1(t) + SI_2 g_2(t) + SI_3 g_3(t) \tag{4.34}$$

where g_{1-3} are overlapping triangular basis functions, pictured Figure 4.5, and SI_{1-3} are parameters that can be identified from sparse diary data stretching over weeks or months.

The model prioritises flexibility for identifying patient-specific rhythms. More basis functions could be added to create a more detailed model, but at the expense of identifiability. Since there are typically 3 meals during the day, there are 3 unique glycaemic disturbances with which to perform parameter identification, particularly for sparse data. Hence, the model was designed to maximise practical identifiability of its parameters, while maintaining flexibility to capture various SI profiles.

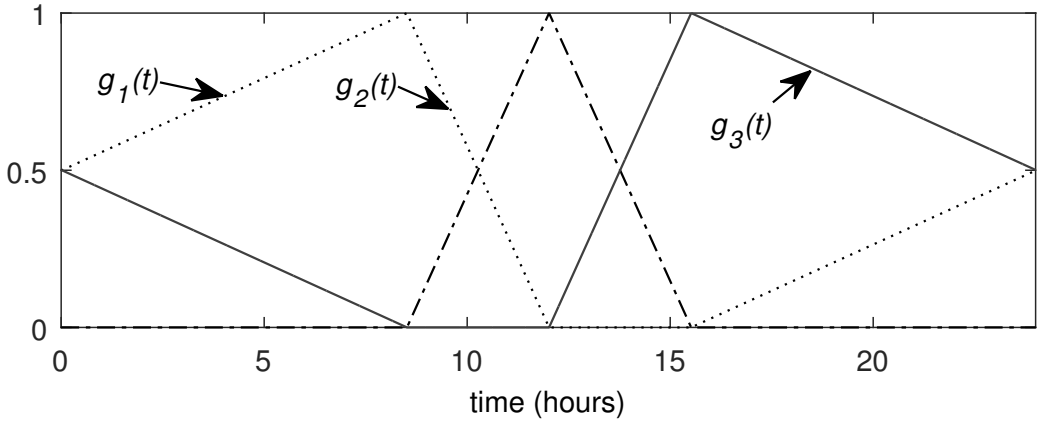

Figure 4.5: Basis functions for Mansell et al.'s variable-basis circadian SI model

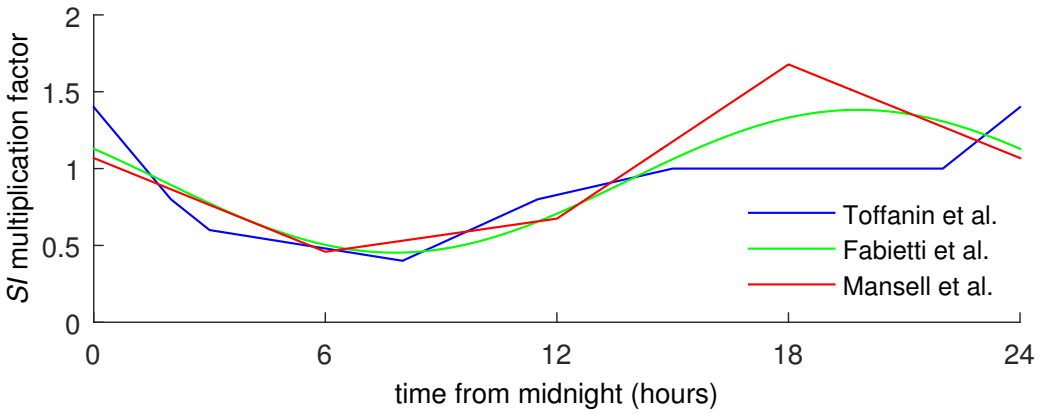

Figure 4.6: A comparison of circadian SI models: Toffanin et al.'s piecewise model, Fabietti et al.'s sinusoidal model and our variable basis model, with the latter two models fit to the first

4.5.4 Implications for modelling circadian rhythms in SI

Some models for circadian rhythms in metabolic function, particularly its effect on insulin sensitivity, have been developed. Figure 4.6 shows a comparison of the Fabietti et al. and Mansell et al. models fit to the Toffannin et al. piecewise model. The Toffanin et al. (2013) model uses information from the literature to populate all hours of the day with specific values for SI. This approach could be effective if the information proves to be applicable to a wide range of individuals, or if reliable clinical measurements of individual circadian rhythms could be taken and then used in diabetes outpatients. However, despite the specificity of Toffanin et al.'s piecewise model, the literature suggests a great deal of uncertainty in the shape of individual circadian SI rhythms (Van Cauter et al., 1997).

Due to the range of effects that could influence SI over the course of any single day, data would ideally be captured over multiple days to achieve sensible estimation of the rhythm. Both Fabietti et al.'s sinusoidal model and Mansell et al.'s variable basis model could be used effectively with long-term data. Since patient data and the majority of glycaemic excursions occur during waking hours, the data is not necessarily distributed in such a way that would benefit identification of Toffanin et

al.s' sinusoidal approximation (Toffanin et al., 2013; Docherty et al., 2011). Thus, model features occurring during the night would suffer from practical non-identifiability. The Mansell et al. model overcomes this issue by design, by placing identified features during the daylight hours.

4.6 Discussion

This chapter yielded information on several distinct, highly variable, grey-noise factors in outpatient diabetes, and their implications for modelling and control. In particular, a representative selection of foundational models for postprandial appearance of glucose in the bloodstream were identified and discussed, along with similar foundation models for the effects of exercise, stress, and circadian metabolic rhythms. A summary of these models is found in Table 4.1. While the models vary significantly in complexity, each are well suited for a particular purpose, though not all would be useful in the context of outpatient diabetes management.

This chapter has also examined the critical and relevant methods of quantifying and measuring these variables or their effect in terms of which are well suited for outpatients, which is relevant to the kinds of models that could be used in practice. Thus, models that rely on clinically available methods and data would be limited to use in clinical environments. Equally, very complex models with respect to the quality or quantity of data available tend to be vulnerable to mathematical non-identifiability, thus leading to clinical misinterpretation and prediction error, and are thus not easily suited for use in regular glycaemic management for inpatients or outpatients.

There is potential to capture contributions to grey-noise in glucose appearance from nutrition. Food structure affects the digestibility of carbohydrates and their resulting bioavailability. In general, more processed foods result in smaller particle size and thus, more rapidly available glucose (Mourot et al., 1988; Mishra and Monro, 2012; Torsdottir et al., 1986;

Englyst et al., 2003; Englyst and Englyst, 2005). Composition of a meal, particularly the fat and protein content, affects the rate of gastric emptying due to physiological feedback control from the small intestine (Bornhorst and Singh, 2014)(Reinus and Simon, 2014; Velchik et al., 1989; Goldenberg and Cummins, 1971; Schvarcz et al., 1997; Macdonald, 1996; Lodefalk et al., 2008; Gentilcore et al., 2006; Fraser et al., 1990; Samsom et al., 1997; Folwaczny et al., 2003; Schvarcz et al., 1997; Kong et al., 1996). Intra- and inter- subject variability is large, especially in diabetes where gastroparesis occurs (Clark and Nowak, 1994; Fraser et al., 1990; Horowitz et al., 2002; Kong et al., 1996; Lartigue et al., 1994). The nutritional models of glucose appearance considered here vary in complexity (Worthington, 1997; Wong et al., 2008c; Dalla Man et al., 2006; Lehmann and Deutsch, 1992). When considering the sparse nature of data expected in outpatient diabetes, only models that require few patient-specific parameters may be of use when attempting to capture the patient state. While each of these models has been developed using differing data resolution and quality, all analyses used data that was of a higher quality and resolution than may be expected in clinical practice. Hence, further research must be undertaken to establish the optimal model and *a priori* parameter combination that could capture patient state under the limited measurements available in an outpatient setting.

Psychological states, such as stress and depression, are a source of grey noise as they are known to affect glycaemia but are infrequently modelled in control applications (Klonoff, 2007; Lloyd et al., 1999; Räikkönen et al., 1996; Surwit et al., 1992; Xiu et al., 2014; Ramkissoon and Vehí, 2015). It is suspected that stress and depression cause elevated levels of cortisol and other hormones which reduce SI (Rizza et al., 1982). However, there are conflicting results in clinical trials as to the glycaemic effect of stress and depression (Surwit et al., 1992). Recent advances in measuring the presence of stress by simple, non-invasive means (Zangheri et al., 2015; Choi et al., 2014; De Santos Sierra et al., 2011; Saha et al., 2014; Luharuka et al., 2003) may allow further adaptations to model based capture of glycaemia.

Physical activity frequently results in hypoglycaemia in diabetes (Yardley et al., 2013; Sonnenberg et al., 1990; Borghouts and Keizer, 2000). This hypoglycaemia is thought to be the result of insufficient compensation by EGP to meet increased demands during exercise due to general hyperinsulinaemia (Yardley et al., 2013; Sonnenberg et al., 1990), as well as increased peripheral insulin sensitivity and glucose uptake lasting many hours after exercise (Borghouts and Keizer, 2000; Magkos et al., 2008). To maximise the applicability of exercise models in outpatient settings, they should utilise physical activity metrics such as heart rate or motion sensing (Strath et al., 2000, 2002; Bassett D.R et al., 2000; Yumiko et al., 2002; Kim et al., 2014). Additionally, the models should be extended over a post-exercise period of at least 16 hours, and must be robustly identifiable. None of the models reviewed completely fulfil these criteria. In particular, both the Breton and the Roy and Parker models were not validated beyond an hour post-exercise. Additionally, the Roy and Parker model required gold standard multiple tracer data to identify certain parameters, and would thus be too detailed and over-parameterised for outpatient data. Magkos et al.'s model had some clinical relevance but lacked validation power and seemed too sparsely parameterised.

Studies suggest that in diabetes, the insulin sensitivity is often lower in the morning than the evening (Van Cauter et al., 1997)Visentin et al. (2015). Clinical trials show substantial inter-subject variability in patterns of model-identified SI between breakfast, lunch and dinner (Visentin et al., 2015; Hinshaw et al., 2013). Several models that aim to capture or simulate circadian rhythms in SI are considered (Fabietti et al., 2006; Toffanin et al., 2013; Mansell et al., 2015d). The Toffanin et al. model was constructed with fixed points based on clinical studies while the Mansell et al. and Fabietti et al. models were created for data-driven identification. Given the large amount of inter-subject variation, useful models should be flexible and able to be identified over a number of days to increase the certainty of results and minimise grey noise. Furthermore, practical identifiability could be optimised by identifying parameters describing day-time behaviours, as the glycaemic perturbations which allow SI to be

identified are largely driven by meal times.

To maximise prediction capability, it is critical to ensure that model parameters are identified with confidence. Hence, candidate models must be as practically identifiable as possible, while maintaining the ability to capture the important characteristics of glycaemic excursions. In general, identifiability is maximised when there are a minimum of parameters in the candidate model (Raue et al., 2009, 2012, 2014). However, the necessity of modelling factors to reduce grey noise is apparent in this chapter. The challenge is to balance minimal parameterisation with capturing as many observable factors as possible. Ultimately, this modelling strategy should reduce uncertainties allowing for lower and more precise control targets. Increased confidence in glycaemic control protocols and a corresponding reduction in chronic hyperglycaemia should improve the quality of life for individuals living with diabetes.

4.7 Summary

This chapter examines several important and often overlooked grey-noise factors that affect glycaemia and glycaemic management in outpatient diabetes. Clinical literature has clearly shown that sources of variability around nutritional intake, physical activity, emotional stress and circadian metabolic rhythms are physiologically relevant factors affecting individual glycaemic excursions in diabetes. Hence, ignoring the presence of these factors could contribute significant and systemic grey noise to analytical or predictive modelling outcomes, as well as to management in general.

Therefore, there is significant potential benefit to be gained from including these factors in models when it is possible to measure the relevant stimuli. Methods to detect or measure the presence of these factors have been reviewed and discussed with respect to their applicability in aiding modelling and their potential clinical use in care. Previous efforts modelling these grey-noise factors are presented, compared and discussed with regard to applicability in outpatient diabetes. Practical identifiability is considered

to be a mathematically limiting factor for model complexity and specificity given that high quality data is generally not available in the outpatient environment. Hence, not all models would perform well in an outpatient context. However, each model considered may be effective when used for the purpose it was developed, whether that be for clinical diagnosis, disease pathology, or inpatient care.

Table 4.1: A summary of grey-noise effect models and their defining features

Section	Model	Year	Features
4.2.3	Worthington's minimal model	1997	• single linear compartment with delay
	Lehmann and Deutsch's piecewise emptying model	1992	• trapezoidal piecewise GE function • single linear gut compartment
	Wong et al.'s 2 compartment model	2008	• linear stomach and gut compartments
	Dalla Man et al.'s 3 compartment model	2006	• two stomach compartments for solid to liquid phases • non-linear GE rate function depending on total stomach content • one linear gut compartment
	Salinari et al.'s gastrointestinal transit model	2011	• stomach compartment with power-exponential GE function • partial differential equation for gut with movement/absorption along one spatial direction • regional expression of two gut glucose transporters approximated with Gaussian functions
4.3.3	Mansell et al.'s stress model	2015	• simple step function for multiplicative reduction of SI during stress
4.4.3	Breton's heart rate model	2008	• energy consumption modelled from heart rate • insulin action increased with exercise • energy consumption increases glucose disposal
	Roy and Parker's exercise model	2007	• PVO_2^{max} modelled from prescribed exercise intensity • glucose production and uptake compartments based on PVO_2^{max} affecting plasma glucose • glycogen depletion function for prolonged exercise affecting plasma glucose
	Magkos et al.'s curvilinear IR model	2008	• next day change in IR correlated to EE during exercise by a curvilinear function
4.5.3	Toffanin et al.'s piecewise SI model	2013	• piecewise interpolation of values interpreted from literature over 24hr period • lowest in early morning, middle in afternoon and evening, peak at midnight
	Fabietti et al.'s sinusoidal SI model	2006	• simple sinusoid with 24hr period
	Mansell et al's variable basis model	2015	• sum of three overlapping triangular basis functions over 24hr period • each basis function scaled by different value

Chapter V

Everyday life events data

This chapter describes the data used for the remaining chapters in Part II. The data was collected as part of a study designed by a group of clinicians and modellers in Denmark, and was kindly provided to us in the spirit of collaboration. Hence, this chapter is essentially the content of their work published in Schmidt et al. (2012) and Duun-Henriksen et al. (2013).

As Schmidt et al. (2012) describes in their paper, mathematical modelling is invaluable to the diabetes research field, and is used for developing control algorithms, performing research simulations, and predicting glucose for decision support. However, much of the data used historically for developing models has not reflected the everyday life of a heterogeneous cohort of individuals with T1DM, and the inherent variabilities therein. Hence, Schmidt et al. (2012) aimed to collect data for model-building that observed subjects with T1DM on subcutaneous infusion of insulin undergoing a series of everyday life events in a controlled clinical research environment.

5.1 Study Design

5.1.1 Participants

Twelve subjects were recruited from an outpatient diabetes clinic (subject characteristics given in Table 5.1). All patients had been treated with a SC infusion of insulin aspart (IAsp, Novo Nordisk, Bagsværd, Denmark) via pump for at least six months.

Table 5.1: Relevant characteristics for the recruited subjects.

Subject	Sex	Age (years)	Diabetes duration (years)	BMI (kg/m^2)	HbA1c (mmol/mol)	Total daily insulin (U/kg/day)	Resting HR (BPM)
1	F	51	43	23.1	46	0.45	58
2	M	41	8	22.2	52	0.61	62
3	F	35	26	26.9	52	0.50	68
4	F	26	13	21.4	50	0.72	49
5	M	31	23	23.5	40	0.73	64
6	M	49	7	25.1	43	0.47	69
7	F	25	8	23.8	52	0.76	63
8	F	29	19	32.6	53	0.67	52
9	F	38	13	20.3	51	0.57	73
10	F	34	12	34.7	54	0.78	60
11	F	29	14	24.4	49	0.66	53
12	F	23	12	23.3	54	0.62	47

5.1.2 Protocol

Each subject attended two study days, providing a total of 24 separate sets of data. On each of these study days, subjects participated in a unique schedule of three main events at 0, 150 and 300 minutes. These events varied in type (meal with or without insulin, insulin bolus, exercise or snack) and some events varied in magnitude (large or small insulin bolus, mild or moderate exercise). The possible schedules can be traced through the three tiers pictured in 5.1.

Out of the 24 study days, twenty included an exercise event, half at mild and half at moderate intensity. Thirteen of the exercise events occurred at Event 2 and the remaining seven at Event 3. Eight schedules contained a snack at Event 3. The remaining 2nd and 3rd events were insulin boluses, half of which were small and half large.

Subjects arrived two hours before the first event for a stabilisation period (-120 to 0 minutes). During this time glucose levels were brought to stable euglycaemic levels if necessary using small insulin boluses or intravenously administered glucose. The time period after the third event until discharge

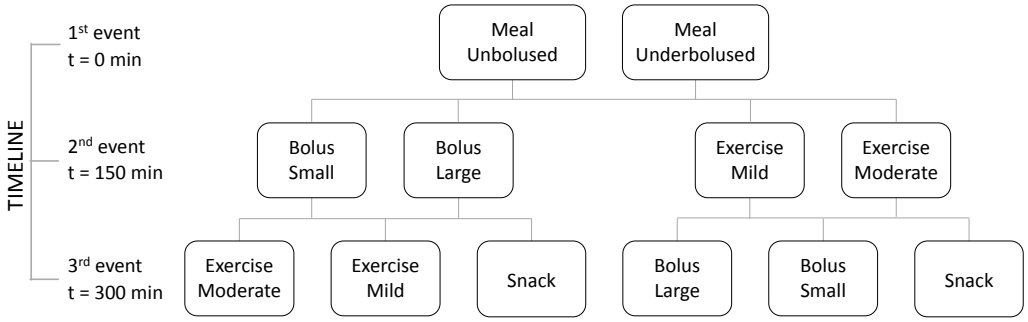

Figure 5.1: The trial structure indicating the possible combinations of first, second and third tier events

was also used to stabilise subjects (300 to 420 minutes). The total observation time was nine hours, from 8am to 4pm.

The meal provided at Event 1 contained one gram of carbohydrate per kilogram of the subject's body weight, and had an energy composition of 52% carbohydrates, 18% protein and 30% fat. The snack scheduled for some subjects at Event 3 contained 0.4 grams of carbohydrate per kilogram of body weight, and an energy composition of 89% carbohydrates and 11% protein. The carbohydrates in both the meal and snack have a high glycaemic index.

Exercise was carried out by treadmill running, where the speed of the treadmill was adjusted to achieve a prescribed HR. Prescribed HR for each of mild and moderate exercise intensity was chosen as a fraction of the HR reserve, i.e. $\mathrm{HR} = \mathrm{HR}_{\mathrm{rest}} + \%\mathrm{intensity}(\mathrm{HR}_{\mathrm{max}} - \mathrm{HR}_{\mathrm{rest}})$ where $\mathrm{HR}_{\mathrm{rest}}$ is the resting heart rate and $\mathrm{HR}_{\mathrm{max}}$ is the maximum heart rate, and the intensity for mild and moderate exercise is 50% and 75%, respectively.

At Event 1, insulin boluses with meals were either absent or given at half the required amount based on the subjects normal insulin to carbohydrate ratio. Boluses separate to meals (Event 2 or 3) were either small or large, defined as that estimated to cause a 3 or 6 mmol/L drop in blood glucose, respectively.

5.1.3 Measurements

A large range of variables were measured over the course of the study days. Subjects wore a continuous glucose monitor (Paradigm Real-Time, Medtronic) which gave a glucose reading every five minutes. Subjects also wore an ActiHeart® (CamNtech Ltd., Cambridge, UK) heart rate measurement device with readings every minute.

Blood samples were drawn at regular intervals to measure other relevant species. Blood glucose was analysed every ten minutes using the YSI2300 STAT Plus (Yellow Springs Instruments, Yellow Springs, OH). Three ten-minute insulin measurements were analysed after an event, otherwise every 30 minutes, using LOCI-technology (Novo Nordisk A/S, Måløv, Denmark). At the same time as insulin, the concentrations of glucagon, cortisol, growth hormone, epinephrine and norepinephrine were analysed.

Other relevant information was recorded for anything taken by the subjects during the study day. These inputs were food intake, intravenous glucose, subcutaneous insulin infusion, along with prescribed exercise. All measurements and inputs were recorded with respect to the relevant time.

5.2 Data and discussion

Figure 5.2 and Figure 5.3 are examples of the kind of input and output data obtained from two separate test days for the same subject. The type of data is ideal for the development of mathematical models. The data is of clinical-grade quality, considering the range of measured species, the equipment used, and relatively high sampling frequencies, but aims to capture much of the everyday variabilities expected in an outpatient environment. The large range of measured species, especially the various hormones analysed, provides numerous avenues for research for the effect of various environmental stimuli on these hormones, and the subsequent effect of the hormones on blood glucose and insulin dynamics.

From a dynamic modelling perspective, the variety in order of events is

useful for distinguishing different effects. For example, having some meals without boluses, some with, and some boluses alone allows for good observability of the independent effects of the meal and insulin boluses on blood glucose. For an event like exercise, it occurs at a variety of glucose and insulin concentrations across and within subjects, again providing a range of contexts to distinguish the effect of exercise specifically.

A disadvantage is the long postprandial period from the Event 1 meal. Rate of appearance studies have shown that the tail end of glucose from a meal with highly glycaemic carbohydrates can still be entering the bloodstream 300-400 minutes after initial ingestion (Elleri et al., 2013; Dalla Man et al., 2006). Since this event is present in all datasets, it could be more difficult to distinguish the effects of some other events occurring during this post-prandial period. However, this reflects everyday outpatient reality that, aside from first thing in the morning before breakfast, most hours of the day are spent well within 300-400 minutes of some form of food ingestion.

The sampling frequency of all the measured species appears to be appropriate for capturing most important glycaemic and insulinaemic dynamics reasonably well. While more data is generally better, the burden of cost for an increased sampling rate is a limiting factor. Additionally, since the primary dynamics appear to be reasonably observable as is, additional data may contribute mostly to further observation of measurement noise more than anything else.

Overall, the high quality data from Schmidt et al. (2012) and Duun-Henriksen et al. (2013) provides a unique opportunity for model development in T1DM. The subjects had T1DM and experienced a range of stimuli approximating their normal environment.

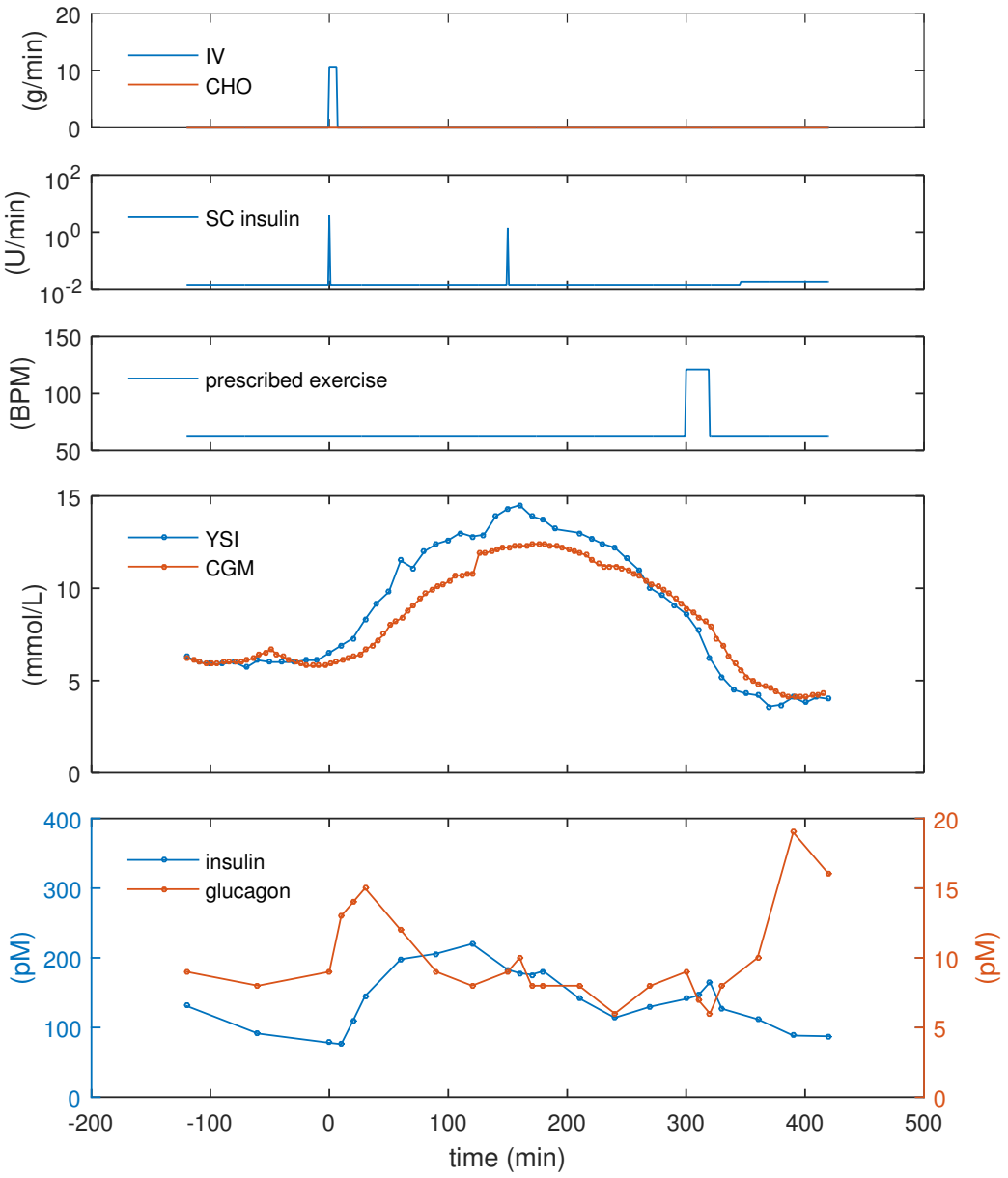

Figure 5.2: A visual representation of results from trial 2a (subject 2, study day 1) reproduced from Duun-Henriksen et al. (2013). Note that the subcutaneous insulin infusion is above zero as per the patient's normal pump settings.

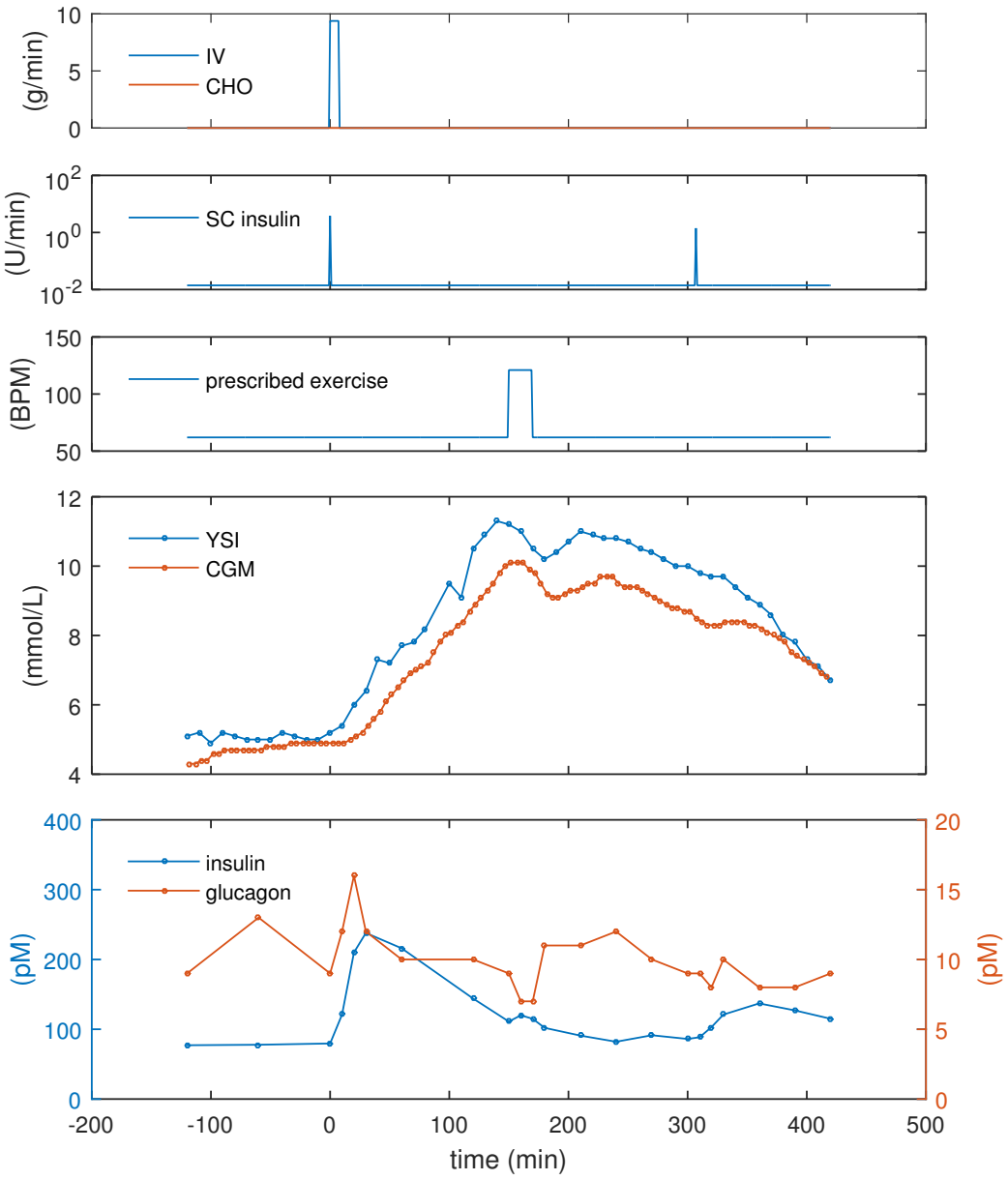

Figure 5.3: A visual representation of results from trial 2b (subject 2, study day 2) reproduced from Duun-Henriksen et al. (2013). Note that the subcutaneous insulin infusion is above zero as per the patient's normal pump settings.

Chapter VI

Subcutaneous insulin modelling

This chapter presents the model-building and evaluation process for a continuously infused subcutaneous insulin aspart model. While the underlying pharmacokinetics are inevitably complex, it is recognised that model complexity does not always contribute positively to model performance. Hence, a range of models of increasing complexity are compared and evaluated for performance with the available data. The content of this chapter is in review at the Journal of Pharmacokinetics and Pharmacodynamics.

6.1 Motivation

Subcutaneous administration is the typical route of insulin therapy for outpatients with T1DM and is sometimes used in T2DM. Appearance of insulin in plasma and the active interstitial regions is slower than intravenous (IV) administration of insulin, which peaks briefly before dissipating. Use of IV bolus administration for outpatients is unfeasible due to health risks and practical difficulties. Modelling IV insulin appearance is trivial. In contrast, modelling the appearance of insulin in plasma after SC insulin administration is difficult. In particular, SC insulin exhibits kinetic delays that are difficult to predict and quantify.

An injected insulin bolus disperses rapidly into the small fluid volume between fat cells (Rasmussen et al., 2014). The insulin is then subject to self-association reactions in addition to absorption kinetics (Lindholm and Jacobsen, 2001; Home et al., 1999). Pharmaceutical human insulin is typically stored as a six unit hexamer (Kang et al., 1991). Hexamers are thought to be either absorbed directly to the plasma at a slow rate (Kang et al., 1991) or drained lymphatically (Rasmussen et al., 2014). More

significantly, SC dilution cleaves hexamers to dimers, and single unit monomers. Both dimers and monomers appear to be readily absorbed (Kang et al., 1991; Rasmussen et al., 2014; Lindholm and Jacobsen, 2001; Home et al., 1999). However, absorption rates are strongly dependent on factors that affect blood flow. For example, temperature, injection depth and physical activity have been known to affect the absorption rates (Kang et al., 1991; Rasmussen et al., 2014).

The insulin analogue IAsp has been engineered with a molecular substitution that discourages self-association into hexamers and therefore exhibits a faster glycaemic response than soluble human insulin (Lindholm and Jacobsen, 2001; Home et al., 1999). Thus, while hexamers are the predominant insulin form in a vial of IAsp, these hexamers disassociate rapidly post-injection (Rasmussen et al., 2014; Lindholm and Jacobsen, 2001). Kang et al. (1991) suggest that SC hexamers are negligible in IAsp, that dimers become the predominant insulin form immediately and that the latter phase of IAsp is likely entirely monomeric due to lower concentrations. Furthermore, the monomer to dimer equilibrium constant in IAsp has been found to be 200-300 times smaller than in human insulin (Brems et al., 1992).

There have been multiple efforts to model the pharmacokinetics of various insulin types and insulin delivery strategies (Wilinska et al., 2005; Wong et al., 2008a,b; Li and Johnson, 2009; Lehmann et al., 2009; Nilam et al., 2007; Song et al., 2014; Li and Kuang, 2009). A range of candidate models have been developed for continuous SC IAsp infusion. These were compared and validated on a heterogeneous dataset that was collected in a clinical-grade environment that mimicked outpatient conditions (Chapter 5). Effective models must be robust to the typical variation expected within and between patients. Furthermore, models must be well-suited to the quality of data they would be coupled with to ensure successful parameter identification (Docherty et al., 2011; Raue et al., 2009; Saccomani, 2013).

6.2 Methods

6.2.1 Data selection and processing

Datasets that contained exercise in the second event tier were omitted from the analysis. Only 11 data sets remained, and within these, datasets with exercise in the third tier were truncated. These datasets covered 9 subjects (2/7 M/F, 33±8 years).

6.2.2 Models

Literature suggests that a multi-compartmental, potentially non-linear approach may be appropriate to represent the association and absorption kinetics of insulin (Eaton et al., 1980; Kang et al., 1991; Home et al., 1999; Lindholm and Jacobsen, 2001; Li and Johnson, 2009; Wilinska et al., 2005; Li and Kuang, 2009). However, the intentional reduction in dissociation half-life for IAsp could allow a much simpler model than required for other insulin types. The models developed are permutations of a large, generic model. This general model has three SC compartments (U_{S1-3}, [mU]), modelled by:

$$\dot{U}_{S1}(t) = U_X(t) - (k_1 + k_{13})U_{S1}(t) - \frac{k_2 U_{S1}(t)}{1 + \alpha_U U_{S1}(t)} \tag{6.1}$$

$$\dot{U}_{S2}(t) = \frac{k_2 U_{S1}(t)}{1 + \alpha_U U_{S1}(t)} - (k_2 + k_{23})U_{S2}(t) \tag{6.2}$$

$$\dot{U}_{S3}(t) = k_{13}U_{S1}(t) + k_{23}U_{S2}(t) - k_3 U_{S3}(t) \tag{6.3}$$

$$U_{ST}(t) = k_1 U_{S1}(t) + k_2 U_{S2}(t) + k_3 U_{S3}(t) \tag{6.4}$$

where k terms are transfer rates [min^{-1}]; α_U saturates the transfer rate between U_{S1} and U_{S2} [mU^{-1}]; and U_{ST} is the transfer rate of all insulin states from the subcutis to plasma [$\text{mU} \cdot \text{min}^{-1}$].

Plasma and interstitial dynamics are modelled by the 3-compartment model of Fisk et al. (2016) that was based on the 2-compartment ICING model (Lin et al., 2011). Insulin diffusion occurs between plasma (I), active interstitial (Q) and passive interstitial (Q_P) compartments. Clearance

occurs from the plasma and active interstitial compartments. The Fisk et al. model is described:

$$\dot{I}(t) = \frac{U_{ST}(t)}{V_I} - n_K I(t) - \frac{n_L I(t)}{1 + \alpha_I I(t)} - n_I(I(t) - Q(t)) - n_{I_p}(I(t) - Q_P(t)) \tag{6.5}$$

$$\dot{Q} = n_I \frac{V_I}{V_Q}(I(t) - Q(t)) - n_C Q(t) \tag{6.6}$$

$$\dot{Q}_P(t) = n_{I_p} \frac{V_I}{V_P}(I(t) - Q_P(t)) \tag{6.7}$$

where n_K is the renal clearance coefficient [min^{-1}]; n_L is the hepatic clearance coefficient [min^{-1}] that is saturated by α_I [$\text{L} \cdot \text{mU}^{-1}$]; n_C is the interstitial clearance rate [min^{-1}]; plasma-interstitium transport rates are labelled n_Q and n_P for active and passive, respectively [min^{-1}]; V_I, V_Q and V_P describe plasma, active interstitium and passive interstitium volumes of distribution, respectively [L].

The following candidate models were developed to represent specific simplifications of the large and highly detailed model Figure 6.1.

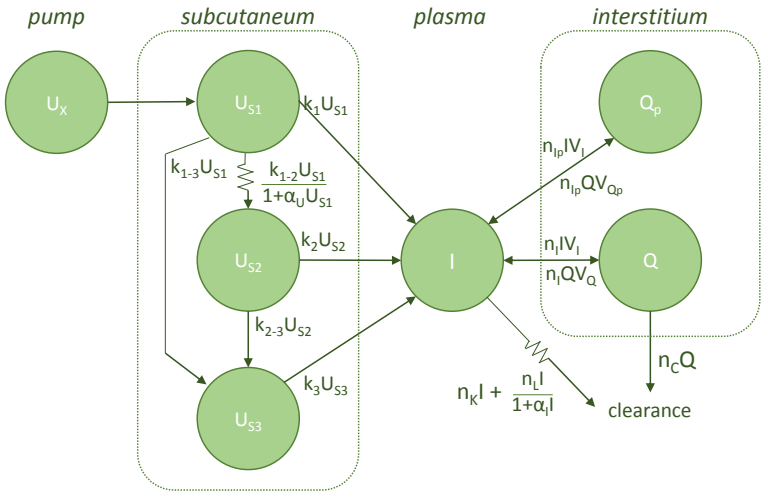

Figure 6.1: Pathway diagram for the full model showing rates of mass transfer between compartments

Model 1 (M1) is the simplest of all the models, including only a single linear compartment for SC insulin, and a single plasma compartment with linear clearance. Transport rate from the subcutis and hepatic clearance rate from the plasma are identified: $\mathbf{x} = [k_1, n_L]^{\mathrm{T}}$

Model 2 (M2) retains the simplicity of the M1 plasma compartment but insulin passes a second SC compartment before transportation to the plasma. Transport rates for both SC compartments are equal and identified as one parameter along with the clearance rate from plasma: $\mathbf{x} = [k_{12}, n_L]^{\mathrm{T}}, k_2 = k_{12}$

Model 3 (M3) has the same SC structure as M2 but introduces an interstitial insulin compartment paired with the plasma compartment. Insulin is cleared hepatically and renally from the plasma and also in the interstitium. Several functions interrelate interstitial-plasma transport and clearance rates and only interstitial clearance is identified along with the SC rate parameters: $\mathbf{x} = [k_{12}, n_C]^{\mathrm{T}}, k_2 = k_{12}$

Model 4 (M4) introduces nonlinear transport across SC compartments and identifies a transition from SC to the plasma. The saturation term creating this nonlinearity is *a priori* but the SC transport rates are no longer treated as equal and are identified separately: $\mathbf{x} = [k_{12}, k_2, n_C]^{\mathrm{T}}$

Model 5 (M5) introduces *a priori* nonlinear hepatic clearance from the plasma but is otherwise the same as M4: $\mathbf{x} = [k_{12}, k_2, n_C]^{\mathrm{T}}$

Model 6 (M6) adds a passive interstitial compartment that contains, but does not clear insulin. All passive compartment parameters are *a priori*. Active interstitial clearance is still identified along with the SC transport rates as before. Furthermore, the SC nonlinear saturation term is also identified: $\mathbf{x} = [k_{12}, k_2, \alpha_U, n_C]^{\mathrm{T}}$

Model 7 (M7) returns to the plasma-interstitial system of M5, neglecting

the passive interstitial compartment, but adds a third SC compartment. The first two compartments feed into the third compartment identified at a fixed ratio. The transport rate to the plasma, now from the third compartment, is also identified: $\mathbf{x} = [k_{12}, k_{13}, k_3, n_C]^{\mathrm{T}}, k_{23} = 0.66k_{13}$

Model 8 (M8) contains the SC system of M7 but again includes the passive interstitium of M6. M8 is the most complex model and contains three SC compartments from which three parameters are identified, a plasma compartment, a passive interstitial compartment, and an active interstitial compartment from which clearance is identified: $\mathbf{x} = [k_{12}, k_{13}, k_3, n_C]^{\mathrm{T}}, k_{23} = 0.66k_{13}$

Specifications for which parameters were identified and any *a priori* assigned values for each model are given in Table 6.1. In all cases plasma volume was assumed to be 3L, while interstitial volumes were predefined fractions of the subject weight (Fisk et al., 2016; Lin et al., 2011). Particular ratios (f_{n_K}, f_{n_L} and f_{n_Q}) defined relationships between clearance and transport rates for the plasma-interstitial system for some model permutations (Fisk et al., 2016; Lin et al., 2011). These ratios are defined:

$$f_{n_K} = \frac{4n_C V_Q}{2V_I} \tag{6.8}$$

$$f_{n_L} = \frac{7.5n_C V_Q}{2V_I} \tag{6.9}$$

$$f_{n_Q} = \frac{V_Q}{V_I n_C} \tag{6.10}$$

Linear, un-paired differential equations were simulated via analytical solutions with trapezoidal integration for computational simplicity. For nonlinear differential equations, left-hand numerical integration was used for nonlinear terms, while remaining terms were integrated trapezoidally. This ensured rapid integration while retaining precision. For interdependent compartments, i.e. plasma and interstitium, iterations were carried out between the species until satisfactory convergence in plasma

insulin was detected as:

$$\frac{||\mathbf{I_i} - \mathbf{I_{i-1}}||_2}{||\mathbf{I_i}||_2} < 10^{-6} \tag{6.11}$$

SC species were simulated for an additional few hours before the experimental start time to utilise information recorded about boluses used in the night or early morning. Starting point values for all species were simulated as steady state values given the parameters and initial concentrations in parent species.

6.2.3 Analysis methodology

6.2.3.1 Parameter estimation

Parameters were estimated for individual datasets using a Levenberg-Marquardt gradient descent algorithm (Chapter 3).

Table 6.1: Specifications for parameters in each model permutation

	Model	1	2	3	4	5	6	7	8
Parameter	k_1	ID	0	0	0	0	0	0	0
	k_{12}	0	ID	ID	ID	ID	ID	ID	ID
	k_{13}	0	0	0	0	0	0	ID	ID
	k_2	0	k_{12}	k_{12}	ID	ID	ID	0	0
	k_{23}	0	0	0	0	0	0	$0.66k_{13}$	$0.66k_{13}$
	k_3	0	0	0	0	0	0	ID	ID
	α_U	0	0	0	0.002	0.002	ID	0.002	0.002
	n_K	0	0	f_{n_K}	f_{n_K}	f_{n_K}	f_{n_K}	f_{n_K}	f_{n_K}
	n_L	ID	ID	f_{n_L}	f_{n_L}	f_{n_L}	f_{n_L}	f_{n_L}	f_{n_L}
	α_I	0	0	0	0	0.0017	0.0017	0.0017	0.0017
	n_I	0	0	f_{n_I}	f_{n_I}	f_{n_I}	f_{n_I}	f_{n_I}	f_{n_I}
	n_C	0	0	ID	ID	ID	ID	ID	ID
	n_{I_p}	0	0	0	0	0	n_I	0	n_I
	V_Q	0	0	$0.1w$	$0.1w$	$0.1w$	$0.058w$	$0.1w$	$0.058w$
	V_P	0	0	0	0	0	$0.09w$	0	$0.09w$
	V_I	3	3	3	3	3	3	3	3

Optimisation minimised the least squares of the insulin residuals:

$$||\mathbf{\Psi}||_2 = \sqrt{\sum_s \left(I_s - I(\mathbf{x}, t_s)\right)^2} \tag{6.12}$$

where $\mathbf{x}_{opt}$ is the optimal parameter values, I_s is the s^{th} insulin data measurement and $I(t_s)$ is the modelled plasma insulin at the time of the s^{th} sample.

Starting parameter values for the algorithm were $\mathbf{x}_0 = [0.01, 0.05, 0.05, 0.05, 0.5, 0.05]^{\mathrm{T}}$ and perturbations were $\Delta\mathbf{x} = [10^{-5}, 10^{-5}, 10^{-5}, 10^{-5}, 10^{-6}]^{\mathrm{T}}$. A maximum of 250 iterations were allowed to reach the convergence criterion:

$$\frac{||\mathbf{x}_i - \mathbf{x}_{i-1}||}{||\mathbf{x}_i||} < 10^{-5} \tag{6.13}$$

6.2.3.2 Goodness of fit

The candidate models' ability to capture the observed behaviour was assessed. Overall goodness of fit was evaluated with the coefficient of determination (R^2) across all datasets and compared across models. Additionally, residual error patterns in the post-bolus period were collated from all datasets to investigate the presence of any consistent bias indicating mismodelled behaviour.

6.2.3.3 Parameterisation

The degree of parameterisation was evaluated to ensure that the model did not attempt to fit kinetics that were more likely to be measurement noise. The Akaike Information Criterion (AIC) is based on information theory, and evaluates the trade-off between fitting capability and complexity. Typically, a model with the lowest AIC score is considered optimal. The AIC value for

small sample sizes is given by:

$$\mathrm{AIC} = 2k - 2\ln(L) + \frac{2k(k+1)}{n-k-1} \tag{6.14}$$

$$\ln(L) = -n\ln(\sigma) - \frac{n}{2}\ln(2\pi) - \frac{1}{2\sigma^2}\sum_{s=1}^{n}\Psi_{\mathrm{s}}^2 \tag{6.15}$$

where k is the number of parameters, n is the sample size, σ is the reported standard deviation of the measurement noise, derived from Petersen et al. (2010).

AIC was calculated for individual datasets to compare medians and interquartile ranges between models. In a related analysis, cumulative distribution functions (CDFs) of residual error collated from all datasets were created for each model and compared to the distribution expected from assay error alone. In theory, a perfectly parameterised model would yield a residual distribution that was just outside that of the reported measurement error. Such an outcome would imply that real behaviours are captured, and that the model was not adhering to measurement noise.

Knowledge of measurement noise was required for both parameterisation analyses. Published information for assay variance at different serum insulin concentrations (Petersen et al., 2010) was interpolated to simulate error at the concentration of each measured data point. For AIC, variance of this simulated error was calculated and averaged over 1000 simulations. The mean CDF of 1000 error simulations was used in the CDF analysis.

6.2.3.4 Practical identifiability

Robust parameter estimation is essential for utilisation of models in prescriptive clinical applications. Lack of robustness can be attributed to practical non-identifiability. Identified model parameter values describing similar but distinct behaviours can trade off if measurement noise in the data is sufficient (Raue et al., 2009; Docherty et al., 2011). Few formal methods of measuring practical non-identifiability have been developed. For

this application a boot-strapping methodology was employed. Robust parameters should be insensitive to small changes in the content of a dataset. Thus, for a data set with n datapoints, n parameter identification runs were undertaken with each run having one data point removed (i.e. with $n-1$ data). The coefficient of variation (CV) in $\mathbf{x}$ due to the down-sampled datasets was calculated ($\text{CV}_i = \frac{\sigma_{x_j}}{x_j} \times 100\%$). Median and interquartile values of CV were calculated across the eleven datasets for each parameter in each model.

6.2.3.5 Predictability

An analysis was carried out to test the predictive capabilities of each model. M1-8 were fit to each dataset excluding the last two hours of output data. Identified parameters were then used to predict the last two hours of plasma insulin. Residual error between the predictions and a linear interpolation of the data for all datasets was plotted for visual interpretation. For quantitative evaluation, mean absolute residual error over all datasets was calculated for each model.

6.3 Results

All models were successfully fit to the experimental data. Figure 6.2 shows a typical result. M1 had the lowest R^2 (Table 6.2), while the remaining models achieved similar goodness of fit (Figure 6.3a). Goodness of fit generally increased with complexity and M8 performed the best ($R^2 = 0.92$). Post-bolus residual patterns exhibited insignificant bias for models M2-M8 (Figure 6.4). However, M1 exhibited some consistent bias, indicating failure to capture some dynamics.

M8 achieved the lowest median AIC score Table 6.2. However, M4 achieved the lowest mean AIC score (Figure 6.3b). M2-8 have very similar AIC scores. No model residual CDFs were within the reported measurement noise (Figure 6.3c). Degree of conformity to the assay CDF increased roughly in the order of model complexity with M1 being the most distant from the assay error and M7 and M8 being very similar and the closest.

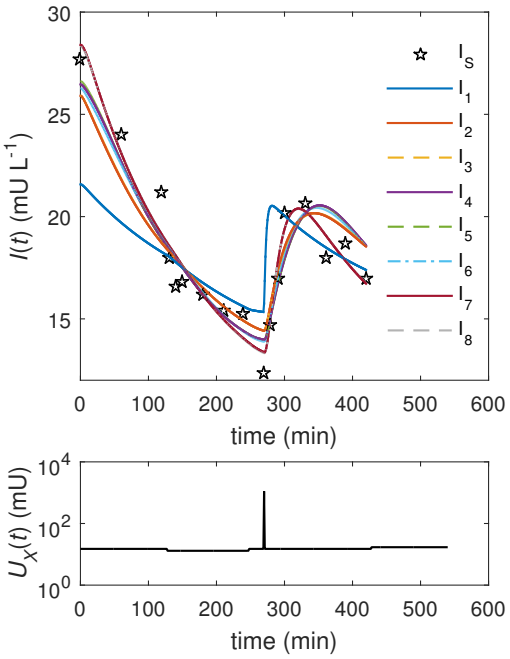

Figure 6.2: A typical result for model fitting plasma insulin for a dataset. Note log-scale in $U_X(t)$ and that the subject took a bolus not long before the experiment began

The CV of parameter estimates across bootstrap permutations were lowest for M2-3 (Table 6.3). M4-5 had similar results to M3 for the n_C parameter but higher CV in subsequent parameters. M6-8 had median CVs exceeding 20% in many parameters with large interquartile ranges.

On occasion, the convergence criteria was not reached before 250 iterations had elapsed. This convergence failure occurred for M7 in one of the 11 datasets in the original parameter estimation exercise. During the bootstrap analysis with 212 dataset permutations, convergence failure occurred six times for M6 and 19 times for M7.

The predictability analysis yielded similar minimal prediction errors for M2-8 while the errors for M1 were larger (Table 6.4, Figure 6.5). M3 predicted best with lowest mean error and tightest visible distribution of

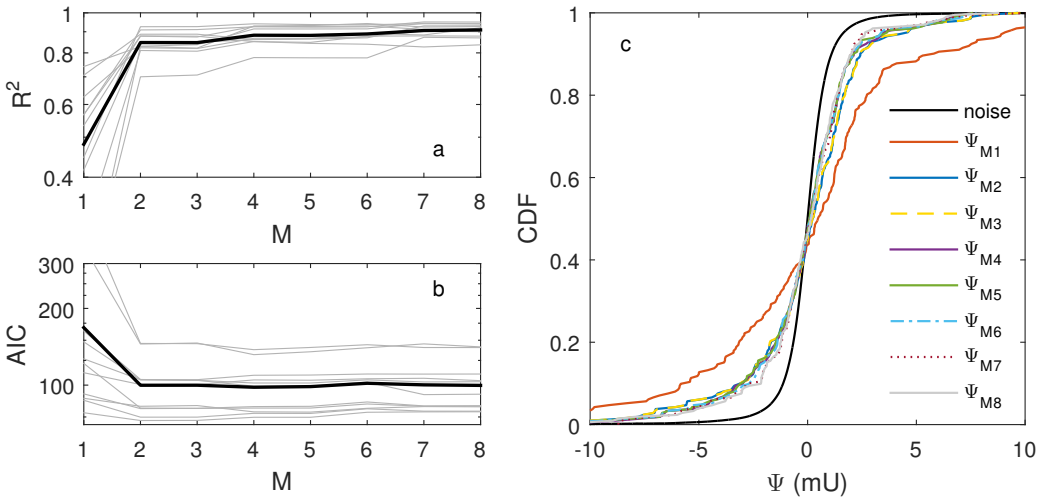

Figure 6.3: Analysis results: a) all (grey) and mean(black) R^2 values for datasets at each model; b) all (grey) and mean (black) AIC values for datasets at each model; c) collated residual CDFs for each model against simulated noise

residual trajectories. Convergence failure occurred once with each of M6-8 during this analysis.

6.4 Discussion

All models were generally capable of fitting the data. M8, the most complex model, achieved highest goodness of fit ($R^2 = 0.92$, Table 6.2). M1, the least complex model, was worst fitting model ($R^2 = 0.53$). This finding follows the expected trend of fitting capability improving with parameterisation and model detail. Post-bolus residuals (Figure 6.4) provide information on the suitability of the model forms for the capturing insulin responses and the efficacy of the identification process. As expected, post-bolus patterns did not differ significantly across models with the same underlying SC model. M1 yielded a repeated bias immediately after the bolus, indicating it was incapable of capturing the kinetics of post-bolus plasma insulin.

The net-zero bias of residuals shown in Figure 6.4 imply that the parameter

Table 6.2: Median, lower (Q_1) and upper (Q_3) quartiles for R^2 and AIC values for each model across the datasets

Model	R^2	(Q_1, Q_3)	AIC	(Q_1, Q_3)
M1	0.53	(0.32,0.61)	122	(89.7,159)
M2	0.85	(0.82,0.89)	101	(81.0,105)
M3	0.85	(0.82,0.89)	101	(81.1,105)
M4	0.87	(0.85,0.93)	99.1	(79.2,108)
M5	0.87	(0.85,0.93)	99.2	(79.1,108)
M6	0.89	(0.87,0.92)	102	(81.9,109)
M7	0.91	(0.88,0.94)	91.8	(82.4,109)
M8	0.92	(0.88,0.94)	92.1	(82.4,109)

identification process was generally robust and led to model simulations that adhered to the measured data. However, the non-zero incidence of failed convergence after 250 iterations for M6-8 during the bootstrapping and prediction exercises implies isolated cases of unstable parameter identification or that the particular parameter sets yielded practically non-identifiable model parameters. Practical non-identifiability can occur if the data contains insufficient information to quantify a particular model parameter's behaviour, or to delineate the behaviour of two or more model parameters. Practical non-identifiability results in very high CV values for some parameters. Models that produced a non-zero incidence of failed converge (M6-8) yielded the highest parameter CV values (Table 6.3). Thus, the parameter trade-off in M6-8 appears to have limited the ability of the parameter identification methodology to determine accurate Jacobian gradient directions, preventing descent on the objective surface with respect to certain parameters. This means that M6-8 have insufficient practical model identifiability to provide robust and reliable parameters.

The CDF comparison allowed a similar parameterisation analysis to AIC. The Akaike criteria implies that ideal model parameterisation leads to model fit residual CDFs as close as possible to the measurement error CDF. Model fit residual CDF within the measurement error envelope implies that the data has been over-fitted' and thus that the model is over parameterised. Over-parameterised models ultimately lead to poor

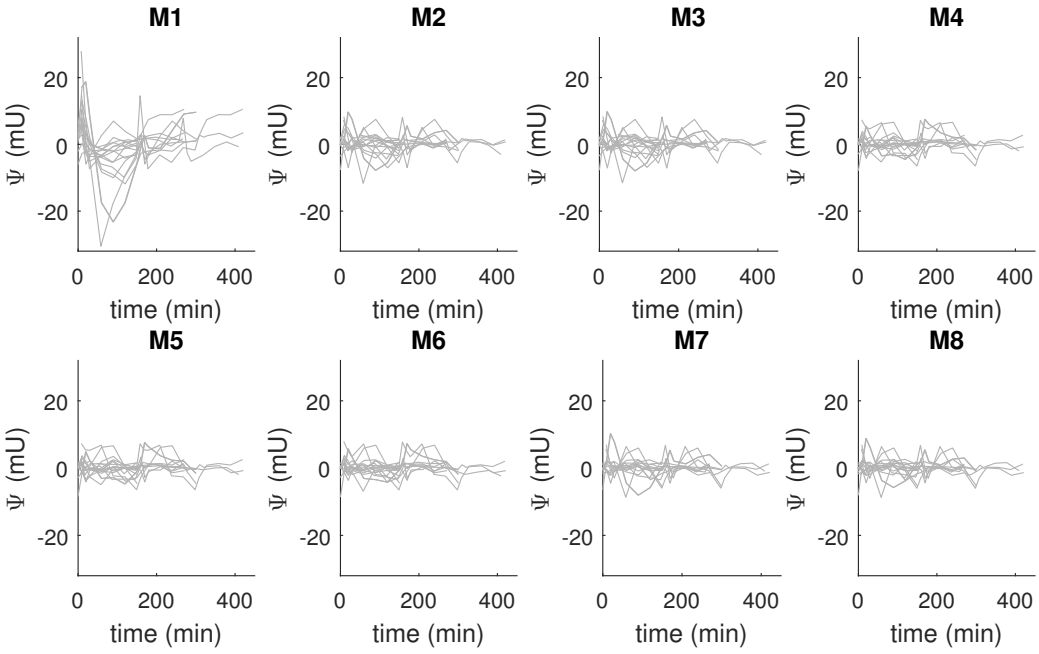

Figure 6.4: Post bolus residual trajectories of collated post-bolus residual behaviour across all datasets and for each model

prediction, classification and diagnosis of parameter values. The CDFs in Figure 6.3 indicated that none of the candidate models were over-fitted. Despite the potential for further parameterisation, the AIC analysis indicated that when trading off fit and model complexity M4 was the best choice based on lowest mean result (Figure 6.3b) or M7 based on the lowest median result (Table 6.2). This dichotomous outcome across summary statistics for the AIC metrics demonstrates that the optimal model was difficult to determine. A much larger sample size would be needed to confidently rank the top models according to the AIC criterion. The close AIC medians and ranges across the models, particularly M2-8, implied similar performance. The CDFs and R^2 results of M2-8 are also reasonably close.

The bootstrap analysis revealed that M2 and M3 were the most robust models (Table 6.3), with median parameter CVs not exceeding 2%. In contrast, M6-8 yielded multiple median parameter CVs in excess of 20%

Table 6.3: Median, lower (Q_1) and upper (Q_3) quartiles for CV [%] for parameter estimates across all permutations of datasets for each model in the bootstrap analysis

Model	M1	M2	M3	M4	M5	M6	M7	M8
x_1	n_L	n_L	n_C	n_C	n_C	n_C	n_C	n_C
CV_{x_1}	1.2	0.6	0.6	0.7	0.6	1.6	23	12
Q_1, Q_3	0.7,1.7	0.5,0.9	0.5,0.9	0.5,1.0	0.4,1.2	0.8,14	20,28	3.1,27
x_2	k_1	k_{12}	k_{12}	k_{12}	k_{12}	k_{12}	k_{12}	k_{12}
CV_{x_2}	8.0	1.7	1.7	5.1	5.8	40	16	11
Q_1, Q_3	6.4,13	1.5,2.1	1.5,2.2	2.6,10	2.7,12	27,157	11,28	4.3,18
x_3				k_2	k_2	k_2	k_{13}	k_{13}
CV_{x_3}				4.8	5.1	23	27	23
Q_1, Q_3				2.5,39	3.0,23	6.6,57	21,108	12,87
x_4						α_U	k_3	k_3
CV_{x_4}						64	25	4.4
Q_1, Q_3						39,150	3.1,32	2.7,24

Table 6.4: Mean absolute residuals with each model for predicted outcome of the last 2 hours of the experiment based on identification of prior data

Model	M1	M2	M3	M4	M5	M6	M7	M8
$\overline{\lvert\Psi^*\rvert}$ [mU/L]	5.01	2.23	2.07	2.33	2.39	2.95	2.45	2.82

and large interquartile ranges. This indicates that these models are too sensitive to small variations in data to yield unique parameter estimates that are indicative of the underlying pharmacokinetic behaviour of the participants. Hence, the M6-8 formulations lead to parameter estimates that have ambiguous utility in prediction or diagnosis. Furthermore, these models sometimes did not converge to the data within 250 iterations of the Levenberg-Marquardt scheme used during the bootstrap-like and prediction analyses. Levenberg-Marquardt is generally considered a robust parameter identification system due to its ability to transition between quick second order and robust first order convergence based on the behaviour of previous iterations.

The data used in this analysis followed a cohort of individuals with

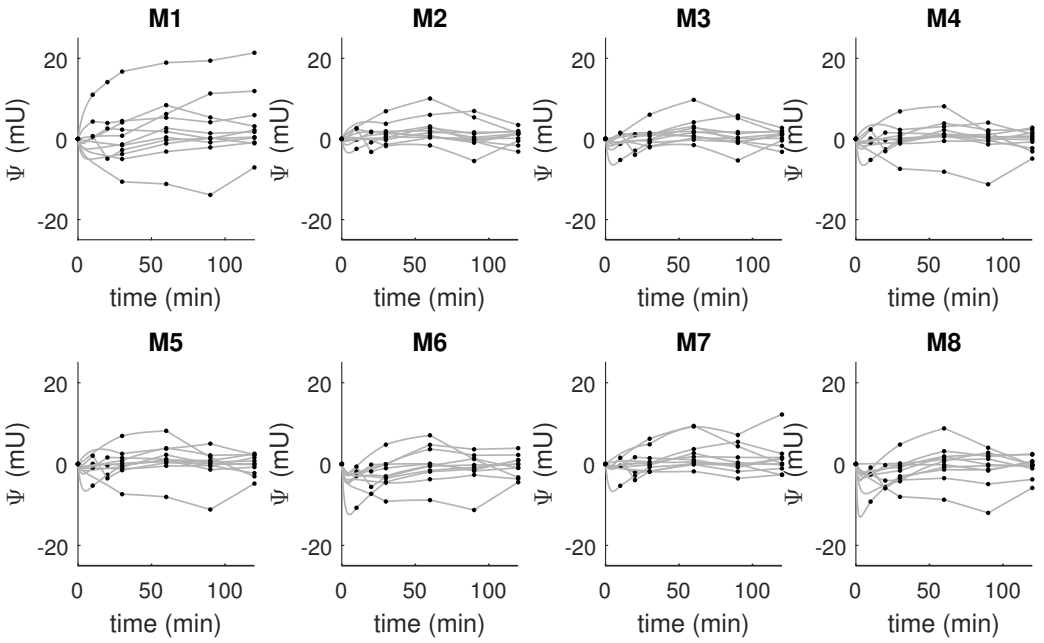

Figure 6.5: Residual error between 2 hour predictions and the actual data (at datapoints, black, at linear data interpolation, grey)

established T1DM. Thus, zero endogenous insulin secretion was assumed. This allowed analyses that did not require determination of the endogenous insulin signal. Even if undertaken with C-peptide data and an assumption of equimolar secretion, determining endogenous secretion would ultimately incorporate another contribution of measurement error into the analysis, reducing clarity in the appearance of insulin in plasma. There is some ambiguity whether the pharmacokinetics of SC insulin in T1DM is relevant in T2DM. Individuals with T2DM often experience a period of insulin hypersecretion prior to hyposecretion that occurs when the disease is established (Pories and Dohm, 2012). Thus, determining appearance of SC insulin in those with T2DM may require deconvolution of the appearance profile from hypersecretion of endogenous insulin. It is possible that such a deconvolution would introduce uncertainty greater than that caused by assuming equivalent SC kinetics across individuals with T1DM and T2DM.

Insulin measurements were taken at 10 minute intervals immediately after

the bolus administration. Higher data resolution would yield more robust estimates of non-linear appearance effects. However, Figure 6.4 shows that the general form of the plasma insulin excursions could be well quantified by the sampling rate. The non-linear effects of appearance may be of primary interest to pharmacokinetic studies of drug composition. However, the general form of the plasma insulin excursion captured by M2-M8 is of primary importance for projects aiming to control glycaemia. Changes in glucose are approximately proportional to area under the insulin curve. Hence, for glycaemic regulation, the most critical factors to determine are appropriate insulin rise time, peak levels, and decay rate.

Eight models of differing nature and complexity have been analysed. Models M1 to M7 are simplifications of M8 which contains terms for all reported significant mechanisms of SC appearance in plasma. The simplifications are achieved by fixing parameters *a priori*, defining relationships between parameters and effectively removing compartments. The models provided unique compromises of parameter robustness and fitting accuracy. Table 6.5 summarises the outcomes for all of the models highlights the value of M3 as the most robust model that also provides acceptable R^2 values. These outcomes imply that the best prediction and control could be achieved with M3. Table 6.5 also shows that M8 adheres to the measured data better than all other candidate models. However, M8 also exhibited relatively high parameter variance implying that it would have limited use in determining robust parameter estimates.

6.5 Summary

This modelling exercise considered eight permutations of an insulin pharmacokinetic model. The models had different levels of parameterisation, and different compartmental approaches. Increased parameterisation and complexity generally led to lower parameter estimation precision but better adherence to measured data. In contrast, models with fewer identified parameters had poorer model fitting, but led to improved identified parameter precision, and associated improvements in

plasma insulin prediction. The optimal model for parameter robustness and prediction incorporated a two compartment SC depot and a two compartment plasma-interstitial system.

Table 6.5: Summary of model performance across key metrics; underlined text indicates particularly poor outcomes

Model	R^2	AIC	Prediction $\overline{\lvert\Psi^*\rvert}$	CV of model parameters	Residuals	Potential value based on analysis
M1	*0.53*	122	*5.01*	1.2,8.0	*systemic bias*	*Too simplistic*
M2	0.85	101	2.23	0.6,1.7	unbiased	*No benefits over M3*
M3	0.85	101	2,07	0.6,1.7	unbiased	**Best prediction and parameter robustness**
M4	0.87	99.1	2.33	0.7,5.1,4.8	unbiased	Acceptable compromise of robustness and model fitting
M5	0.87	99.2	2.39	0.6,5.8,5.1	unbiased	Reasonable compromise of robustness and model fitting
M6	0.89	103	2.95	1.6,*40,23,64*	unbiased	*Poor practical identifiability*
M7	0.91	91.7	2.45	*23,16,27,25*	unbiased	*Poor practical identifiability*
M8	0.92	92.1	2.82	*12,11,23*,4.4	unbiased	**Best fit but poor parameter robustness**

Chapter VII

Autoregressive modelling of exercise

This chapter presents a data-driven autoregressive modelling approach to reveal the effect of mild to moderate exercise on insulin and glucose independently. This work was presented as a conference abstract and poster at the New Zealand Society for the Society for the Study of Diabetes Annual Scientific Meeting (Mansell et al., 2016)

7.1 Motivation

Exercise causes a disturbance to glycaemic control in T1DM and can result in hypoglycaemia without compensatory treatment (Sonnenberg et al., 1990; Brazeau et al., 2008). In healthy individuals, decreases in insulin secretion during exercise signal the liver to increase EGP for additional peripheral glucose demand (Sonnenberg et al., 1990). Since those with established T1DM lack endogenous insulin, this pathway for modulating hepatic EGP during exercise is impaired, though catecholamine hormones are still active (Yardley et al., 2013). Furthermore, some literature suggests that the plasma concentration of exogenous insulin increases during exercise in T1DM Koivisto and Felig (1978); Sonnenberg et al. (1990), further reducing glucose concentration. Hence, the insulin-glucose dynamics during exercise have implications for glycaemic management in T1DM.

In this chapter, Nonlinear AutoRegressive eXogenous (NARX) modelling has been used to delineate the effect of exercise on both insulin and glucose concentrations in T1DM. NARX is a non-parametric form of modelling that allows a model to be trained to imitate the relationship between model input and output data without specific knowledge of the physiological processes that link the stimuli and behaviour.

7.2 Methods

7.2.1 Data processing

Of the 24 trials from 12 subjects (3/9 M/F, 34±9 yrs), only 20 contained the necessary exercise periods for this study. During these trials, patients ran on a treadmill for approximately 20 minutes at either a mild or moderate level. These levels corresponded to target heart rates 50% and 75% of the interval between resting and maximum heart rate, respectively. The glucose data was truncated to exclude three hours following the morning meal and four datasets were excluded altogether due to a scheduled afternoon snack. Thus, meal glucose appearance could be neglected.

NARX is typically applied where input and output data sampling rates are equal and consistent. This is mathematically appropriate since NARX formulations are independent of time. The insulin and glucose measurements (I_{data} and G_{data}) were taken at sampling rates that were much lower than the one-minute resolution of insulin pump data, meal intake and prescribed exercise. Hence, the insulin and glucose data were interpolated with a Hermite cubic polynomial to increase the resolution of output data to equate the sampling rates.

Prescribed exercise was given in terms of a target heart-rate ($HR(t)$), elevated during the exercise period and at resting (HR_{rest}) otherwise. Subject information for maximum heart rate (HR_{max}) was used to normalise the exercise data array into a unit of intensity ($e(t)$) based on the formula:

$$e(t) = \frac{HR(t) - HR_{rest}}{HR_{max} - HR_{rest}} \tag{7.1}$$

Exercise data was then converted into an impulse located at the start of the exercise period (t_{e0}) based on the formula:

$$E(t) = \begin{cases} \int_{t_0}^{t_{n-1}} e(t)dt, & \text{at } t = t_{e0} \\ \text{zero}, & \text{otherwise} \end{cases} \tag{7.2}$$

where $n-1$ is the total number of minutes in the experiment. Integrating $e(t)$ means that the impulse is essentially a measure of energy expenditure.

7.2.2 Model formulation

NARX modelling correlates output behaviour to input stimuli. Interpolated insulin ($I(t)$) and glucose ($G(t)$) concentration were treated as the output behaviours for the two respective models. Continuous SC infusion ($U(t)$) and the exercise function ($E(t)$) were treated as input stimuli for the insulin model, as well as past insulin. The product of insulin and glucose ($I(t)G(t)$), intravenous glucose ($V(t)$), $E(t)$ and past glucose were input stimuli for the glucose model.

The insulin model is described:

$$\begin{aligned} I_t = a_I I_{t-1} + \sum_{k=1}^{100} b_{UI,k} U_{t+1-k} \\ + \sum_{j=1}^{60} b_{EI,j} E_{t+1-j} + c_I \end{aligned} \tag{7.3}$$

where a_I is the insulin auto-correlative (AC) term, $b_{UI,1\to100}$ are cross-correlative (CC) terms for SC insulin over 100 minutes, $b_{EI,1\to60}$ are the CC terms for exercise over 60 minutes, and c_I is the steady state offset.

The glucose model is described:

$$\begin{aligned} G_t = a_G G_{t-1} + b_{IG} I G_{t-1} + c_G \\ + \sum_{k=1}^{25} b_{VG,k} V_{t+1-k} + \sum_{j=1}^{60} b_{EG,j} E_{t+1-j} \end{aligned} \tag{7.4}$$

where a_G is the glucose AC term, b_{IG} is the CC term for the glucose-insulin product, $b_{VG,1\to25}$ are the CC terms for intravenous glucose over 20 minutes, $b_{EG,1\to60}$ are the CC terms for exercise over 60 minutes, and c_G is the steady-state offset.

Multiple parameters were used to correlate present I and G to the input stimuli legacy, since their effects were not expected to be instantaneous. In particular, SC insulin has significant kinetic delays before plasma appearance. The spike in glucose introduced by intravenous administration was not adequately represented by interpolation of the 10 minute resolution glucose samples. Hence, the interpolated behaviour needed to be modelled. Exercise input was modelled as an impulse so that the response, both during and after exercise, could be observed as one time-dependent effect. In all these cases, a continuous set of correlation parameters accounts for the appearance rate of these inputs in the output behaviours over a given period of time.

7.2.3 Parameter identification

Multiple linear regression was used to solve the parameters in each model. The $\mathbf{Ax} = \mathbf{b}$ matrix equation for insulin model is described:

$$\begin{aligned}[\mathbf{I}_{t-1}, \mathbf{U}_t, \mathbf{U}_{t-1}, \cdots, \mathbf{U}_{t-99}, \mathbf{E}_t, \mathbf{E}_{t-1}, \cdots, \mathbf{E}_{t-59}, \mathbf{1}] \\ * [a_I, \mathbf{b}_{UI}, \mathbf{b}_{EI}, c_I]^T = \mathbf{I}_t\end{aligned} \tag{7.5}$$

where all $\mathbf{I}$, $\mathbf{U}$ and $\mathbf{E}$ terms are $n-1 \times 1$ arrays of data, $\mathbf{b}_{\mathrm{UI}}$ is a 1×100 array of parameters, $\mathbf{b}_{\mathrm{EI}}$ is a 1×60 array of parameters, and $\mathbf{1}$ is a $n-1 \times 1$ array of ones.

Likewise, the matrix equation for the glucose model is described:

$$\begin{aligned}[\mathbf{G}_{t-1}, \mathbf{I}_{t-1}\mathbf{G}_{t-1}, \mathbf{V}_t, \mathbf{V}_{t-1}, \cdots, \mathbf{V}_{t-24}, \mathbf{E}_t, \mathbf{E}_{t-1}, \\ \cdots, E_{t-59}, \mathbf{1}] * [a_G, b_{IG}, \mathbf{b}_{VG}, \mathbf{b}_{EG}, c_G]^T = \mathbf{G}_t\end{aligned} \tag{7.6}$$

where all $\mathbf{G}$, $\mathbf{I}$, $\mathbf{V}$ and $\mathbf{E}$ terms are $n-1 \times 1$ arrays of data, n is the duration of the experimental data used, $\mathbf{b}_{\mathrm{VG}}$ is a 1×25 array of parameters

and $\mathbf{b}_{\mathrm{EG}}$ is a 1×60 array of parameters.

Values for $U_{-99} \rightarrow U_{-1}$ were populated from pump settings and recorded boluses that may have been administered before the experiment. Values for $E_{-59} \rightarrow E_{-1}$ and $V_{-24} \rightarrow V_{-1}$ were zero. When no IV glucose was given, $\mathbf{V}$ arrays and $\mathbf{b}_{VG}$ were excluded from the glucose equation. In two cases, IV glucose was administered within the 60 minute exercise observation window, and at no other time. To avoid structural non-identifiability, these datasets were truncated at the point of IV introduction. Identified CC coefficients for exercise ($\mathbf{b}_{EI}$ and $\mathbf{b}_{EG}$) for each dataset were compared across datasets. Cumulative integrals of these coefficients were compared.

7.3 Results

The exercise-insulin CC terms are shown in Figure 7.1. During exercise, $\mathbf{b}_{EI}$ was generally positive, greater at first, and generally negative post-exercise, tending toward zeros at the end. Distinct nodes are visible in $\mathbf{b}_{EI}$ at 10, 20, 30 minutes. The integrated $\mathbf{b}_{EI}$ profiles show an approximate net zero effect of exercise on insulin in most datasets.

The exercise-glucose CC terms are shown in Figure 7.2. The rate of glucose deficit in $\mathbf{b}_{EG}$ increases with exercise duration and returns to zero over the post-exercise period. Nodes in $\mathbf{b}_{EG}$ occur every 10 minutes. The integrated $\mathbf{b}_{EG}$ profiles show a net-negative effect of exercise on glucose.

Along with the sought after exercise CC coefficients, those for SC insulin infusion and intravenous glucose boluses are shown in Figure 7.3 and Figure 7.4, respectively. With the exception of one stray trajectory, most datasets produced a SC profile with a positive rate in the first half an hour, tapering to zero between 30 and 100 minutes. Therefore the integrated effect of SC input was net-positive by 100 minutes for these datasets. For the few datasets with IV glucose, the CC coefficients followed a somewhat sinusoidal trajectory with a period of 10 minutes. The remaining AC and CC terms for both the insulin and glucose models are presented in

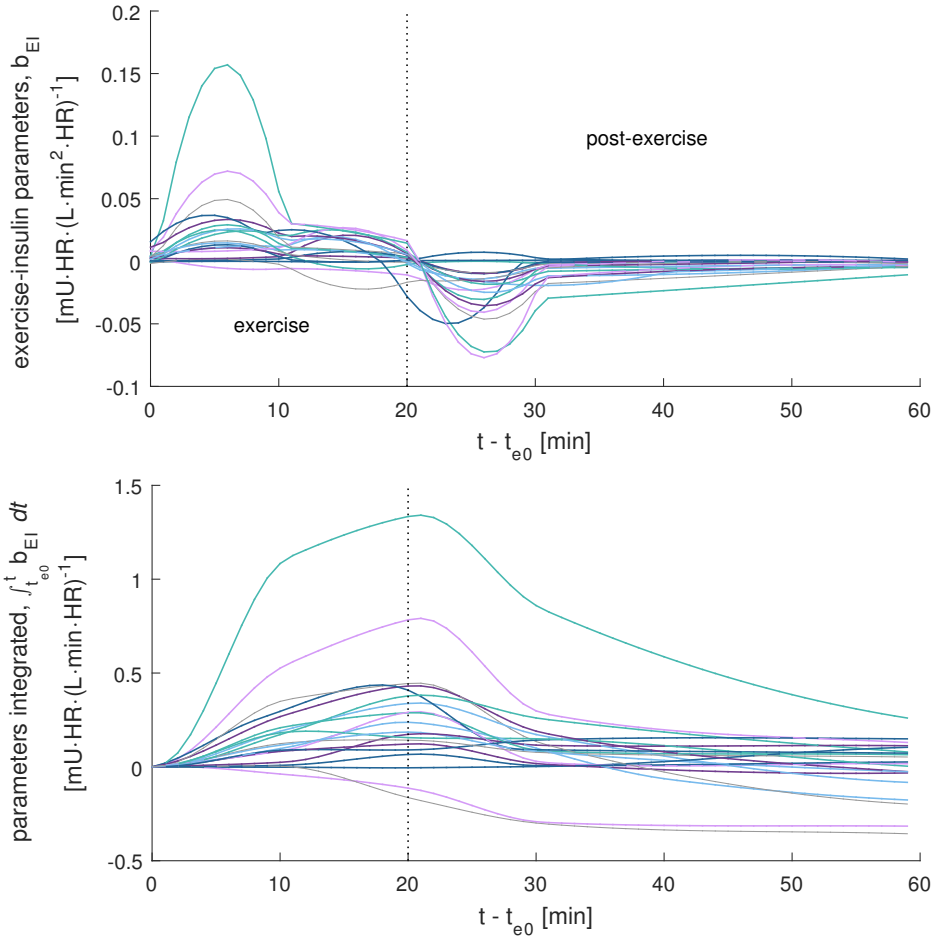

Figure 7.1: Exercise-insulin cross-correlative coefficients (top), and integrated (bottom)

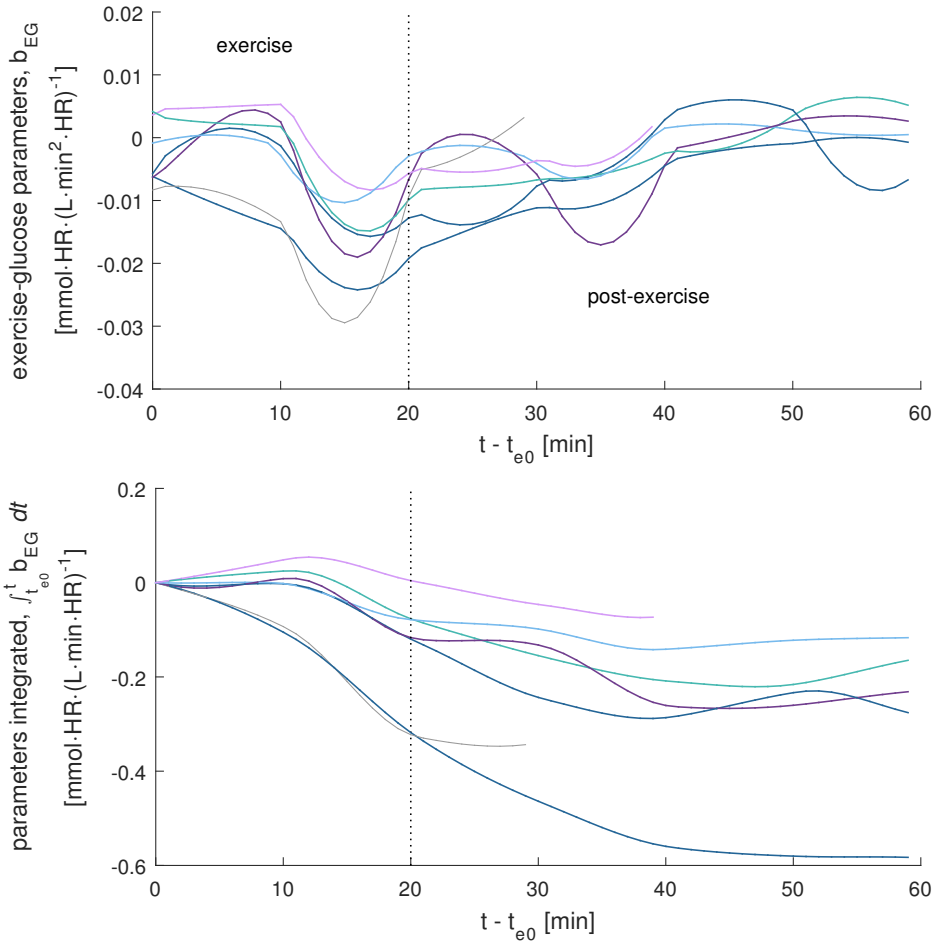

Figure 7.2: Exercise-glucose cross-correlative coefficients (top), and integrated (bottom)

Table 7.1: Median (Q_2), lower (Q_1) and upper (Q_3) quartiles for remaining parameters in both insulin and glucose models

parameter	description	Q_2	(Q_1, Q_3)
a_I	AC insulin term	0.994	(0.990,0.997)
c_I	insulin offset term	-0.0137	(-0.0997,0.0534)
a_G	AC glucose term	1.008	(0.995,1.013)
b_{IG}	insulin-glucose CC glucose term	-3.99×10^{-4}	$(-4.51, 0.60) \times 10^{-4}$
c_G	glucose offset term	-0.0611	(-0.0775,-0.0284)

Table 7.1.

7.4 Discussion

The present work applied NARX to a biological application with unequal input and output sampling rates. Interpolation of data allowed the NARX model to function on an appropriate time-scale. Exercise CC coefficients across the subjects showed consistent patterns. This consistency in outcomes across the heterogeneous cohort indicates the NARX approach was valid and valuable. The variability in magnitude of the CC profiles indicates the level of intra-subject variability.

The CC coefficients represent the instantaneous impact of exercise on insulin or glucose over time. Thus, the integrated $\mathbf{b}_{EI}$ profile is the exercise-mediated excursion of pump-delivered IAsp, as it appeared in the plasma. Insulin concentration generally increased during exercise, returning to normal afterwards. Thus the net effect of exercise on insulin appearance generally tends towards zero. This is expected due to the unchanged rate of insulin delivery to the subcutis. Increased blood flow is likely to raise the rate of SC absorption during exercise Kang et al. (1991). Temporarily lowered SC insulin levels would then potentially decrease the post-exercise appearance rate. If plasma or interstitial clearance rates were raised due to exercise, a net negative effect would be expected. This factor may have contributed to the few datasets tending toward net negative values.

Integrated $\mathbf{b}_{EG}$ shows an exercise-mediated deficit in glucose. The

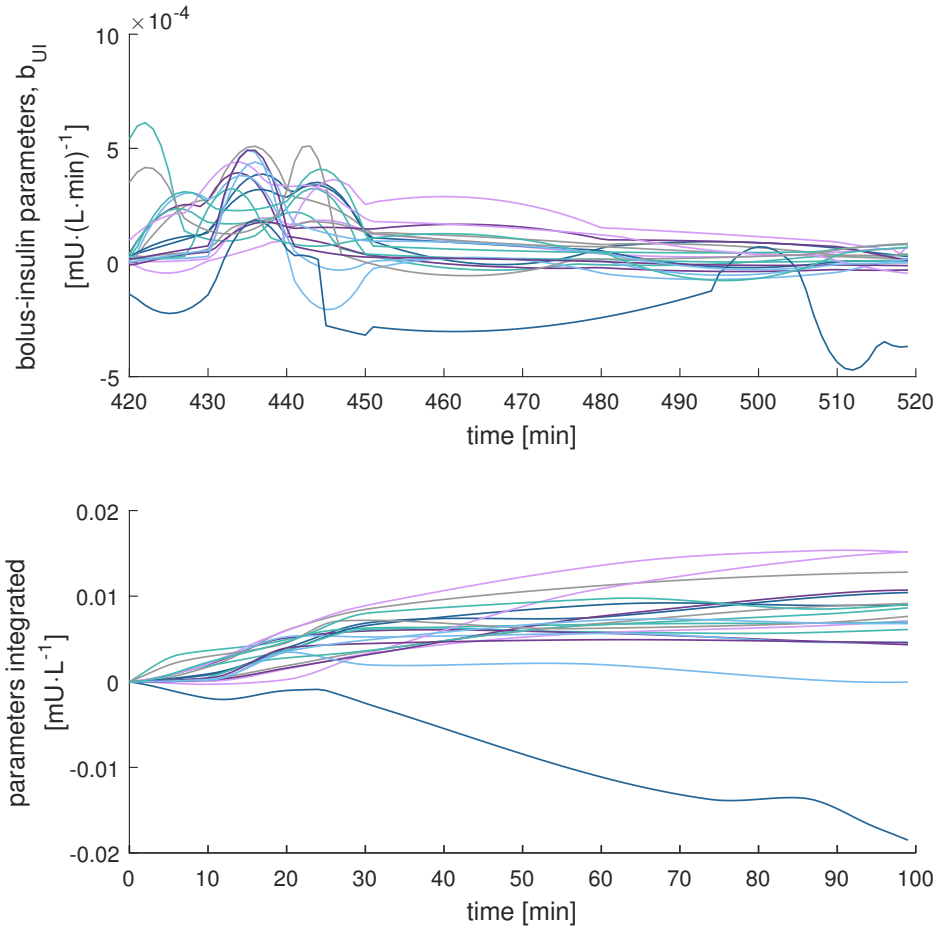

Figure 7.3: SC-plasma insulin cross-correlative coefficients (top), and integrated (bottom)

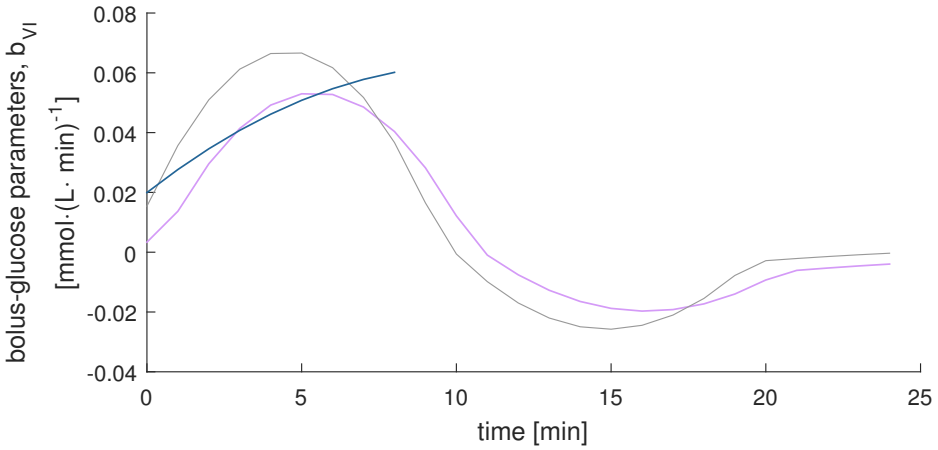

Figure 7.4: Intravenous-glucose cross-correlative coefficients for the few relevant datasets that used intravenous glucose.

magnitude of glucose deficit generally increased with exercise duration. However, this effect would likely plateau for some time during extended exercise periods, but would be dependent on factors such as the availability of muscular and hepatic glycogen stores (Yardley et al., 2013). Glucose deficit continued into the post-exercise period, which may be partly due to refuelling of depleted muscle glycogen.

NARX modelling was an effective approach for this type of data. In particular, the T1DM cohort lacks of endogenous insulin, thus negating the need for more complex deconvolution. The CC terms used to investigate the influence of exercise on plasma insulin yielded particular shapes that were not necessarily intuitive. Since NARX is largely data-driven, it is an operator independent approach that allowed these trajectories to be discovered. This method is in contrast to typical approaches which often compare and fit a hypothesised model. Therefore, such an approach may have not as effectively found or utilised the remarkably consistent shapes discovered by NARX.

The other parameters in the NARX models were not particularly useful and did not take on expected values. For example, the a_I term is related to the combined hepatic and renal insulin clearance (n_T) in a form that could be

approximately modelled by $n_T = 1 - a_I$. This relationship would provide a median n_T of 0.006 min^{-1} based on the results as opposed to the expected value on the order of 0.1 min^{-1}. Furthermore, many of the a_G parameter outcomes exceed the value of 1, identifying a self-dependent growth in glucose concentration rather than the decay seen physiologically. Likewise, results for the b_{IG} term which could be related to insulin sensitivity by $SI = -b_{IG}$ was identified in the right order of magnitude but sometimes positive, indicating insulin acting to increase rather than decrease glucose concentration in those cases.

These inconsistencies and discrepancies in the other NARX parameters is the result of trade-off between parameters and is due to practical non-identifiability. In data not shown plasma insulin simulated using Equations (9.2) and (9.3) also failed to get expected parameters from the NARX algorithm, and a_I was particularly sensitive to the rate of SC delivery. However, *a priori* knowledge of physiology implies that insulin clearance should be quite independent of SC delivery. In a typical physiological model, trade-off would be minimised by assigning *a priori* values to many parameters based on population averages from other clinical or modelling studies. In this case, the clear consistency and observability of the effect of exercise is not discounted by these other parameter outcomes. However, the limitation highlights NARX efficacy as an interim modelling method rather than a final representation of physiology.

A notable limitation to the method was the need for output interpolation. Figure 7.1 and Figure 7.2 (also 7.3 and 7.4) indicate nodes in the CC parameter trajectories at the sample times for insulin and glucose measurements. These nodes are an artefact of the interpolation, due to the presence of noise in the data and how that influenced the estimation of values by the Hermite cubic polynomials. The broad trends in the profiles are valid but the applicability of the higher resolution dynamics of the trajectory are reduced due to these artefacts.

Another limitation to the method was the use of an impulse function in

place of the step function that describes the period of exercise. This was a necessary manipulation of the data to observe the effect of exercise. Otherwise, the difference between the effects of starting, continuing, finishing and being finished with exercise would have confounded the NARX parameters. Impulse-based results are very useful anecdotally, but require validation in different exercise durations to establish robustness.

This analysis was intended to act as a basis for further work. The use of uniquely data-driven shape information and interpretation of physiological processes involved should aid development of robust, differential models. Any advances in modelling everyday events such as exercise will enhance analysis and control of glycaemia in T1DM, improving the quality of life of these individuals.

7.5 Summary

In subjects with T1DM, plasma appearance from SC IAsp increased during exercise. This observation was likely due to heightened blood flow quickening absorption from the subcutis. Following exercise, the plasma appearance temporarily decreased, generally resulting in a near net-zero effect overall. Lowered SC concentrations from exercise would slow absorption afterwards once blood flow was normalised, explaining the decreased appearance rate.

The subjects experienced a net-negative effect on plasma glucose due to exercise, consistent with the observed tendency for exercising outpatients with diabetes to become hypoglycaemic. The greatest rate of glucose deficit was generally near the end of exercise, tending back toward zero in the post-exercise period.

NARX modelling promotes data-driven outcomes, meaning that it allows the data to drive the behaviours defined by the model. In contrast, traditional modelling fits a completely *a priori* model to the data. In this case, interpolated input data had to be used with the NARX model. This

step resulted in some bumpy regions appearing in the results that are not expected to be real phenomena. This outcome limits the applicability of exact shapes discovered. However, the general form of the shapes are valuable, especially for further research and model development.

Chapter VIII

Basis modelling of exercise

This chapter details a differential model developed for the effect of exercise on plasma insulin and glucose concentrations, respectively. The models build on the work of the previous chapter that used data-driven techniques to observe the effect exercise. These differential models are evaluated for performance on the available data.

8.1 Motivation

In the previous chapter, an autoregressive modelling approach was used to observe the effect that exercise had on the plasma concentration of exogenous insulin administered in the subcutaneous tissue of the subjects with T1DM. It was found that exercise was associated with an increase in plasma insulin concentration that decreased again after exercise for a net-zero effect overall. The observed behaviour was thought to be a result of increased mobilisation from the subcutis due to increased blood flow and agitation, followed by a relative deficit in SC concentration that slows plasma uptake in the post-exercise period. This observation is in contrast to the behaviour of endogenous insulin in healthy individuals that is down-regulated during exercise to promote additional EGP (Yardley et al., 2013; Sonnenberg et al., 1990).

The effect of exercise on glucose concentration was also observed with NARX. It was found that exercise increased the rate of glucose disposal during exercise. The disposal rate returned to zero after exercise but not immediately. This increased glucose disposal caused a net reduction in glucose due to exercise, as is expected with the increased peripheral glucose demand for energy.

The NARX model outcomes were useful for deconvoluting and therefore observing the consistent patterns across the whole cohort. While the outcomes of the NARX provided these indicative patterns they fail to provide a model with meaningful parameters. Furthermore, the data required interpolation to be compatible with NARX, introducing artefacts not present in the data itself. Additionally, conversion of exercise input information from step to impulse function was required for observing the effect but would not therefore be robust to differing exercise durations. Differential models are much more robust to these concerns. The current chapter presents the next stage of exercise-insulin and exercise-glucose modelling using differential equations with basis functions.

It can be anticipated that in an outpatient environment, plasma insulin will not be measured at all. Therefore, it is important when developing a model for this context to avoid unnecessary complexity. Parameters governing this indirectly observed compartment will not be very practically identifiable during optimisation. Hence a simplistic insulin model is used in this work. There is no modelling of an interstitial compartment or nonlinear saturable hepatic insulin clearance. The exercise itself is modelled using basis functions for both glucose and insulin, that can be summed together in their effect for simplicity and robustness.

8.2 Methods

8.2.1 Data

Nineteen out of 24 datasets described in Chapter 5 were used for the present work. Four datasets were excluded due to the absence of exercise in the trial schedule. One further dataset was excluded from insulin modelling due to the absence of insulin boluses. In the remaining trials, all subjects ran on a treadmill for approximately 20 minutes while aiming to maintain a heart rate (HR^*) prescribed for either a mild or moderate exercise. Basal insulin was administered by pump as per each subject's normal daily pump settings, and small or large boluses were administered with and/or without food as

per the specific trial schedule.

8.2.2 Model and simulation

The insulin system was modelled with a single plasma compartment (I) with linear clearance. Inputs to the insulin model include the appearance of insulin from SC delivery (U_S) and the influence of exercise (E_I). This plasma compartment is modelled as a function of time (t, minute resolution) with the ordinary differential equation described:

$$\dot{I}(t) = \frac{U_S(t)}{V_I} + \epsilon_I E_I(t) - n_T I(t) \tag{8.1}$$

where V_I is the plasma insulin distribution volume, n_T is the total linear insulin clearance rate, and ϵ_I is the magnitude of exercise effect on insulin. $I(t)$ was calculated with the analytical solution of Equation (8.1) using cumulative trapezoidal integration.

Each measure of insulin administered subcutaneously by the pump appears as an equimolar curve in U_S over the following minutes. The curve shape is described by the basis function array ($\mathbf{f_U}$), based on SC insulin appearance models by Wong et al. (2008a).

$$\mathbf{f_U} = \mathbf{t}{k_u}^2 \mathrm{e}^{-k_u \mathbf{t}} \tag{8.2}$$

$$\mathbf{t} = [0, 1, 2, \cdots, 600] \text{ minutes} \tag{8.3}$$

where k_u is the SC rate parameter. To simulate the accumulative effect of continuous SC infusion, each time point for SC insulin appearance was therefore calculated with the dot product:

$$U_S(t) = \mathbf{f_U} \cdot [U_X(t), U_X(t-1), U_X(t-2), \cdots, U_X(t-600)] \tag{8.4}$$

where U_X terms indicate the pump input. For indices less than zero (i.e. before the experiment time began), information was used from pump settings and experimental notes of early morning boluses.

Like SC insulin, a sum of basis functions was used for the effect of exercise. The functional array for exercise ($\mathbf{f_{EI}}$) is an impulse followed by an equal area subtraction curve (Figure 8.1a), based on the results of Chapter 7.

$$\mathbf{f_{EI}} = [1, -\mathbf{t}{k_{eI}}^2 e^{-k_{eI}\mathbf{t}}] = [1, 0, -({k_{eI}}^2 e^{-k_{eI}}), \cdots, -(600{k_{eI}}^2 e^{-600k_{eI}})] \quad (8.5)$$

where k_{eI} is the exercise rate parameter in the insulin model. Thus individual time points in the insulin exercise effect array ($\mathbf{E_I}$) are therefore calculated:

$$E_I(t) = \mathbf{f_{EI}} \cdot [HR^*(t), HR^*(t-1), HR^*(t-2), \cdots, HR^*(t-601)] \quad (8.6)$$

where HR^* is target heart rate. An example of the exercise function and its integrated form, to represent actual plasma insulin deviation, are seen in Figure 8.1b-c.

The glucose system , based on Mansell et al. (2015d) was modelled with a

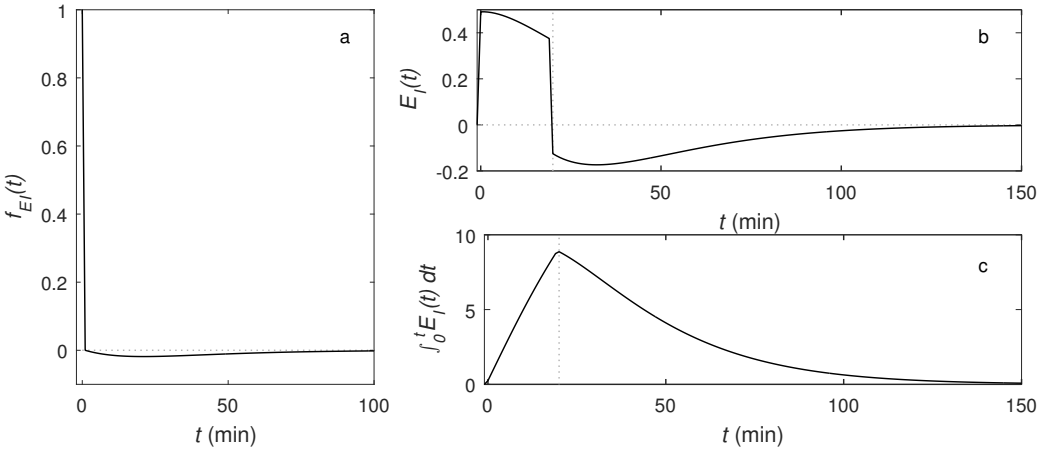

Figure 8.1: An indicative demonstration of the modelled effect of exercise on insulin, showing (a) the basis function, (b) the exercise effect function for 20 minutes of exercise (arbitrarily at $HR^* = HR_{max}$), and (c) the integrated exercise effect function.

single glucose compartment (G) with both insulin-dependent and insulin-independent glucose disposal. Inputs include glucose appearance from ingested food (P_S) and intravenous bolus (V). The exercise function

(E_G) also impacts directly on the glucose compartment.

$$\dot{G}(t) = -p_G(G - G_0) - SI(GI - G_0 I_0) + \frac{P_S(t) + V(t)}{V_G} + \epsilon_G E_G(t) \quad (8.7)$$

where SI is the insulin sensitivity, p_G is the hepatic glucose balance, G_0 is basal plasma glucose, I_0 is basal plasma insulin, V_G is the volume of glucose distribution and ϵ_G is the magnitude of the exercise effect on glucose.

Each measure of carbohydrate ingested appears as an equimolar curve in the $P_S(t)$ function, based on the Mansell et al. model. This curve contains some fast appearing glucose at a fixed ratio to the rest of the glucose. This was achieved through the following basis function array:

$$\mathbf{f_{P,m}} = 0.9\mathbf{t}{k_{p,m}}^2 \mathrm{e}^{-k_{p,m}\mathbf{t}} + 0.1\mathbf{t}(0.07^2)\mathrm{e}^{-0.07\mathbf{t}} \quad (8.8)$$

where $k_{p,m}$ is the glucose appearance rate parameter, $m = 1, 2$ denoting separate parameters and therefore basis functions for the meal (1) and the snack (2). This difference in parameter accounts for the differing glycaemic loads. The basis function is pictured in Figure 8.2a. This basis function is used to calculate the glucose appearance function at each time point, according to:

$$P_S(t) = \sum_{m=1}^{2} \mathbf{f_{P,m}} \cdot [P_{X,m}(t), P_{X,m}(t-1), P_{X,m}(t-2), \cdots, P_{X,m}(t-600)] \quad (8.9)$$

where $P_{X,1}$ is the carbohydrate input function for the meal and $P_{X,2}$ for the snack.

As with the insulin model, the effect of exercise on glucose was modelled by using a basis function $\mathbf{f_{EG}}$ based on the results in Chapter 7. This

functional array is modelled:

$$\mathbf{f_{EG}} = -\mathbf{t}{k_{eG}}^2 \mathrm{e}^{-k_{eG}\mathbf{t}} \tag{8.10}$$

$$\tag{8.11}$$

where k_{eG} is the exercise rate parameter in the glucose model. Thus individual time points in the glucose exercise effect array ($\mathbf{E_G}$) are therefore calculated:

$$E_G(t) = \mathbf{f_{EG}} \cdot [HR^*(t), HR^*(t-1), HR^*(t-2), \cdots, HR^*(t-600)] \tag{8.12}$$

An example of the exercise function and its integrated form, to represent actual plasma glucose deviation due to the muscular demand for glucose, are seen in Figure 8.2b-c.

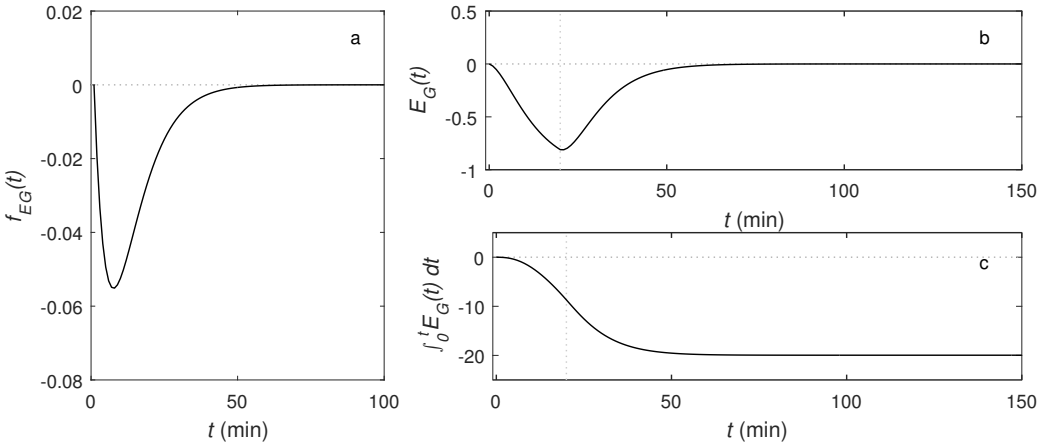

Figure 8.2: A demonstration of the modelled effect of exercise on glucose, showing (a) the basis function, (b) the exercise effect function for 20 minutes of exercise (arbitrarily at $HR^* = HR_{max}$), and (c) the integrated exercise effect function.

8.2.3 Parameter identification

The insulin model was fitted to individual datasets by identifying variables in the parameter set $\mathbf{x}_I = [n_T, k_u, V_I, k_{eI}, \epsilon_I]^{\mathrm{T}}$. An alternative insulin model

was also fit to the datasets that excluded the effect of exercise, i.e. $\epsilon_I = k_{eI} = 0$, ($\mathbf{x}_I = [n_T, k_u, V_I]^{\mathrm{T}}$). These two modelling cases are henceforth referred to as the exercise insulin model and no-exercise insulin model, respectively.

The glucose model was also fitted to datasets and the identified variables were those in the parameter set $\mathbf{x}_G = [SI, k_{p,1}, k_{p,2}, \epsilon_G]^{\mathrm{T}}$. If no snack was consumed, $k_{p,2}$ was set to zeros and omitted from the parameter set. Like insulin, a no-exercise glucose model was also fit to the datasets, i.e. $\epsilon_E = k_{eE} = 0$, ($\mathbf{x}_G = [SI, k_{p,1}, k_{p,2}]^{\mathrm{T}}$). In the no-exercise and exercise glucose models, the following *a priori* assumptions were made for other parameters: $p_G = 0.004$, $V_G = 16.7$L, $k_{eG} = 0.15\mathrm{min}^{-1}$, $G_0 = 4.5$mmol/L, $I_0 = \min([10, \min(I(t))])$mU/L (Mansell et al., 2015d; Lin et al., 2011). The $I(t)$ function for the glucose model was a Hermite cubic polynomial interpolation of the data, and $V(t)$ was simply taken as the data input for IV glucose.

Optimally fitted model parameters ($\mathbf{x}_{opt}$) were estimated by solving the least squares solution to the residual error in plasma insulin and plasma glucose for the respective models. The optimisation was undertaken with variants of the Levenberg-Marquardt-like gradient descent algorithm (Section 3.2.2.2). For the insulin model, the damping factor (λ) was initially, $\lambda_0 = 10^{-4}$ but $\lambda_i = 10\lambda_{i-1}$ if $||\mathbf{\Psi}_i|| > ||\mathbf{\Psi_{i-1}}||$, otherwise $\lambda_i = \max[0.9\lambda_{i-1}, 10^{-4}]$. If the parameter set yielded any NaN results, initial $\mathbf{x}$ was reinstated with $\lambda_i = 10\lambda_{i-1}$. For glucose, λ was simply kept at 0.1.

Starting parameter values were $\mathbf{x}_{I0} = [0.01, 0.05, 0.05, 0.05, 0.5, 0.05]^{\mathrm{T}}$ and $\mathbf{x}_{G0} = [0.0003, 0.02, 0.05, 0.1]^{\mathrm{T}}$, and perturbations were $\Delta\mathbf{x}_I = [10^{-5}, 10^{-5}, 10^{-5}, 10^{-5}, 10^{-6}]^{\mathrm{T}}$ and $\mathbf{x}_{G0} \times 10^{-4}$. A maximum of 250 iterations were allowed to reach the convergence criterion:

$$\frac{||\mathbf{x}_i - \mathbf{x}_{i-1}||}{||\mathbf{x}_i||} < 10^{-5} \tag{8.13}$$

Due to the poor practical identifiability of the k_{eI} parameter, it was identified in the exercise model using a hierarchical identification method (Schranz et al., 2011). In particular, k_{eI} was excluded from initial identification, fixed at 0.05, until the convergence criterion was first reached with the remaining parameter set (Schranz et al., 2011). Convergence of the full parameter set was continued. In this second stage, k_{eI} was bounded $0.01 \leq k_{eI} \leq 0.1$ and if instability repeatedly occurred in the parameter set (i.e. NaN results more than three times) k_{eI} was once again fixed to 0.05. This allowed most datasets to benefit from an optimised k_{eI} parameter but recognised the limitations inherent for some datasets.

8.2.4 Model performance analysis

R^2 was the primary goodness of fit measurement for each dataset. For both exercise and no-exercise models. R^2 was evaluated over entire experimental time, and separately for the two hour peri-exercise period ($t - t_{e0} \leq 2$ hours where t_{e0} indicates time of exercise commencement). Median, upper and lower quartiles for these results across the datasets are presented. Additionally, a collation of peri-exercise residual error profiles ($\Psi(t - t_{e0})$) for all datasets are presented for each of the exercise and no-exercise models.

A parameterisation analysis was also carried out. The CDF of peri-exercise residual errors in all datasets was computed for both the exercise and no-exercise models. These residual CDFs were compared against a CDF of expected measurement noise. Published intra-assay variance data at different insulin concentrations Petersen et al. (2010) was used to simulate expected measurement error. An over-parameterised model would have a residual CDF steeper than measurement noise, indicating that features caused by noise are modelled as if they were real phenomena. Thus, residual CDFs of an ideally parameterised model would be slightly shallower than that of measurement noise, and with an unbiased halfway crossover at $\Psi = 0$.

8.2.5 Model result interpretation

Mean and lower, median and upper quartile statistical outcomes for the identified exercise-related (k_{eI}, ϵ_I and ϵ_G) parameters were calculated. Additionally, correlations between the magnitude of exercise-mediated insulin excursion (ϵ_I) and other known variables across the cohort were determined. As part of this investigation, the relationship between ϵ_I and plasma insulin at the start of exercise I_{e0} was studied by calculating the correlation coefficient (R) and using variance analysis (ANOVA).

Since outcomes from two datasets were excluded as outliers when correlating ϵ_I and I_{e0}, a separate analysis was carried out to justify this decision. This analysis was similar to the concepts presented in the so-called bootlier (bootstrap-based outlier detection) plots of Singh and Xie (2003) which show that sampling from distributions containing outliers produces multimodal histograms. Ten thousand bootstrap iterations were carried out in which a randomly selected $n^* = 14$ subset from the original $n = 19$ datasets was chosen, and R between ϵ_I and I_{e0} calculated. This process was repeated three more times, still with $n^* = 14$ but out of a dataset pool excluding the two designated outliers, then with a pool excluding two other points that could otherwise be considered outlying if the designated outliers were not, then excluding all four of these points. This particular bootlier analysis variation was developed to determine whether the two designated outliers contributed disproportionately to the correlation outcomes compared to other datasets, and were therefore justifiably outlying.

8.3 Results

8.3.1 Insulin model

Figure 8.3 shows typical insulin model fitting results for two datasets. The exercise and no-exercise insulin models generally exhibited similar performance for SC insulin appearance. The exercise-model captured the increase in insulin during exercise and subsequent decrease after exercise

observed in the data. Conversely, the no-exercise model was not capable of capturing this excursion.

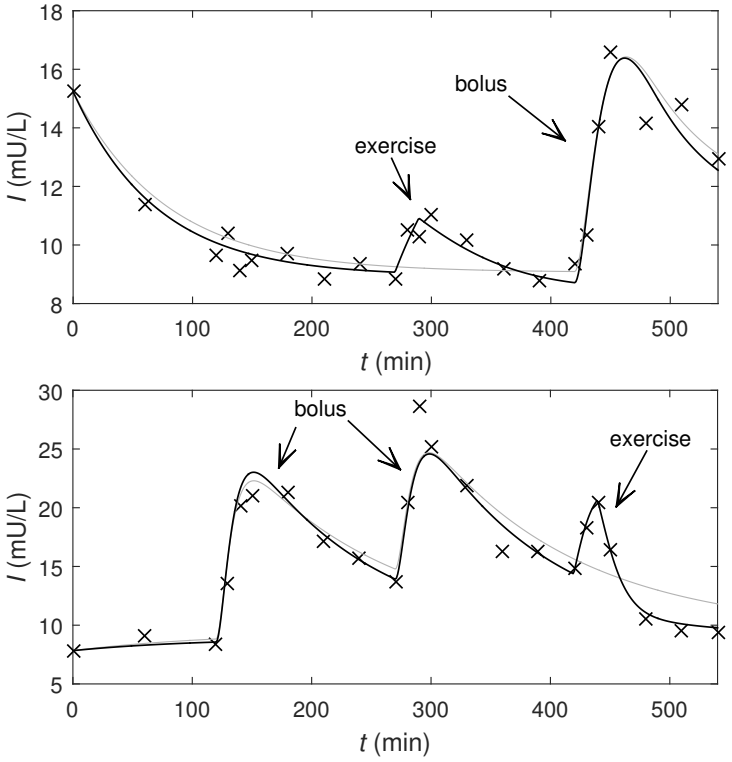

Figure 8.3: A typical fitted result for two separate datasets showing the data (×), modelled without exercise (grey) and modelled with exercise (black).

Goodness of fit, as evaluated by R^2, was reasonably good for both insulin models when evaluated over the full experimental period (Table 8.1). However, a noticeable improvement (12%) in median fit was achieved using the exercise model compared to the no-exercise model. By comparison, peri-exercise fit was very poor for the no exercise model ($R^2 = 0.31$) with a lower quartile R^2 less than zero. In this two hour period, modelling exercise substantially improved the fit.

The no-exercise insulin model shows a distinct pattern in the peri-exercise residual trajectories for the cohort (Figure 8.4a) with large positive residual

Table 8.1: Median, lower (Q_1) and upper (Q_3) quartiles of R^2 values in the insulin model variations, considering both the full experimental period and just the 2 hours after exercise commenced.

	full experiment		peri-exercise	
	R^2	(Q_1, Q_3)	R^2	(Q_1, Q_3)
modelled	0.91	(0.88,0.95)	0.86	(0.80,0.94)
unmodelled	0.81	(0.72,0.89)	0.41	(-0.13,0.57)

error in the first hour and smaller but negative residual error in the second hour. The exercise model was generally successful in attenuating both positive and negative residual error biases (Figure 8.4b), maintaining an approximately zero median residual error. Figure 8.4c shows that the no-exercise model has the shallowest rise in CDF and is biased toward positive residual errors. The exercise model CDF is much closer to the estimated measurement noise CDF but still shallower in rise. Unlike the no-exercise model CDF, the exercise model CDF has no apparent bias.

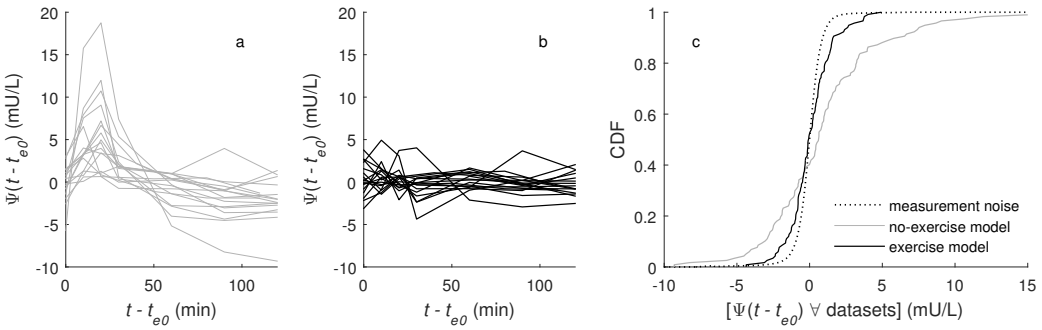

Figure 8.4: Analysis of peri-exercise residuals: (a) residual profiles for all datasets using the no-exercise insulin model; (b) residual profiles using the insulin exercise model; (c) CDFs for all-dataset collations of peri-exercise residuals, compared to distribution for expected measurement error.

Mean identified ϵ_I was 1.04 and the quartiles were 0.35, 0.78 and 1.36. The parameter k_{eI} was fixed to 0.05 for 9 out of 19 datasets based on the

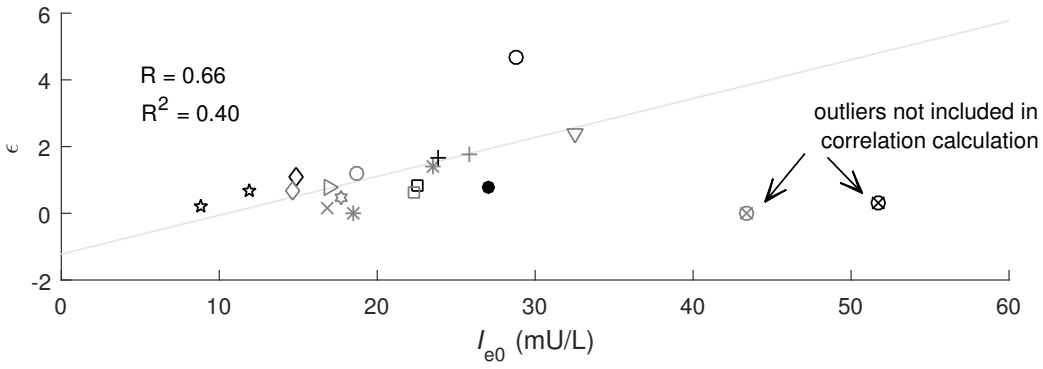

Figure 8.5: Plasma insulin at exercise commencement compared to exercise-induced excursion magnitude with linear trend. Each different marker style denotes a different patient. Marker colour denotes mild (grey) and moderate (black) levels of exercise.

algorithm in the methodology. Mean k_{eI} was 0.0496 for all datasets, and 0.0492 for datasets excluding those with fixed k_{eI}. Quartiles for k_{eI} were 0.041, 0.050 and 0.052 for all datasets, and 0.016, 0.045, 0.070 excluding the fixed case.

No significant relationships were found between ϵ_I and a range of population variables, with one exception: plasma insulin concentration immediately prior to exercise (I_{e0}). An appreciable correlation between the two variables was found (with outliers removed), giving an R value of 0.66 and corrected R^2 of 0.40. ANOVA calculated a p-value of 0.004 for the relationship compared to a constant ϵ_I. Figure 8.5 shows that all intra-patient pairs of datasets exhibited exclusively positive correlation between I_{e0} and ϵ_I.

The bootlier plots (Figure 8.6) show that when using the full dataset pool for sampling bootstrap populations (left) most R values fall into one of two bands. Both bands have poor correlation, one centred around a mean value of $\bar{R} = 0.25$ and the other $\bar{R} = 0.03$. A small band of well correlated outcomes is also present around $\bar{R} = 0.68$. Removing the two outliers at $I_{e0} = 43$ and $I_{e0} = 52$ mU/L from the available pool of datasets yields a

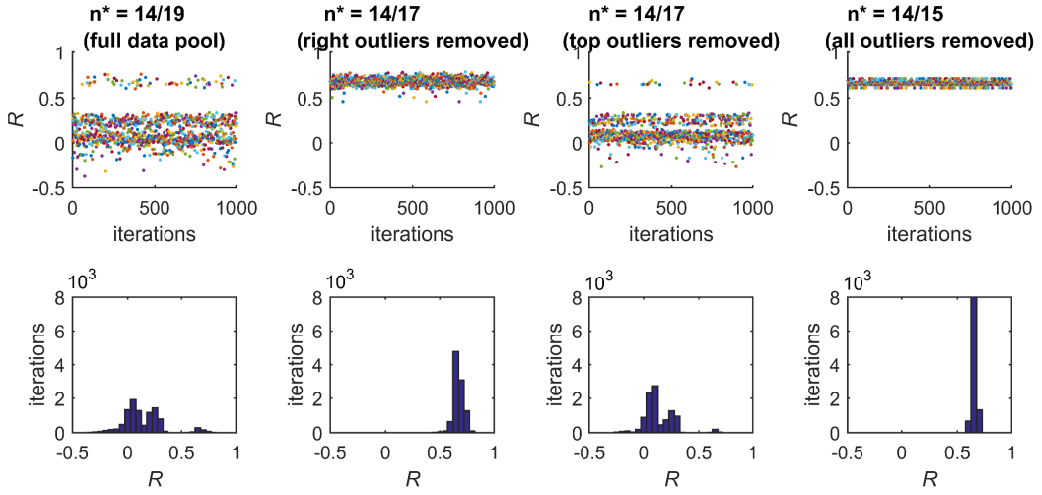

Figure 8.6: Distributions of correlation outcomes between I_{e0} and ϵ_I for same-sized subsets of the datasets. The left two cases exhibit the effect of removing the designated right-hand outliers from the available pool of datasets. The right two cases again exhibit this effect but with another two possible datasets removed that could be considered outlying if the righthand outliers were not. R at the first 1000 bootstrap iterations are plotted (top) and histograms for outcomes of all iterations (bottom).

single well-correlated band, $\bar{R} = 0.67$. Further removing the two other possible outlying points at $I_{e0} = 29$ and $I_{e0} = 33$ mU/L yields similar results to the initial analysis but with slightly tighter distributions. The correlation bands were located at $\bar{R} = 0.66$, $\bar{R} = 0.25$ and $\bar{R} = 0.06$ for a pool just excluding these two possible outliers. Excluding all four potential outliers, both designated and possible, yields a single band of well-correlated outcomes at $\bar{R} = 0.66$. Since the analysis wherein the two high I_{e0} outliers are removed was the only trial to achieve a consistent correlation band, the theory of Singh and Xie (2003) recommends that these points should be declared outliers.

8.3.2 Glucose model

Figure 8.7 gives two examples of the glucose model performing well with the inclusion of the exercise basis. One of the examples shows quite a large

Table 8.2: Median, lower (Q_1) and upper (Q_3) quartiles of R^2 values in the glucose model variations, considering both the full experimental period and just the 2 hours after exercise commenced.

	full experiment		peri-exercise	
	R^2	(Q_1, Q_3)	R^2	(Q_1, Q_3)
modelled	0.97	(0.93,0.99)	0.50	(0.17,0.90)
unmodelled	0.93	(0.83,0.98)	-0.12	(-1.11,0.66)

exercise-mediated excursion while the other has only a small change. In the rest of the cohort, some datasets showed small or even negligible changes due to exercise while other patients were highly effected. Median ϵ_G was 0.33 with lower and upper quartiles of 0.12 and 0.63 respectively. Figure 8.8 gives two examples of the glucose model performing less well. One example demonstrates an overly magnified exercise excursion immediately next to an ill-fitted intravenous glucose bolus. The other shows some unmodelled effects from the ingested meal.

The no-exercise glucose model has a median R^2 of 0.93 over the entire experimental period (Table 8.2) and the exercise glucose model improves this to 0.97. These goodness of fit measurements are higher and less variable than for the insulin model but the R^2 values have not been adjusted for the relatively higher sampling frequency. The improvement in the peri-exercise period from modelling exercise was comparable to insulin but the fit achieved was not as good overall, with a median R^2 of 0.50.

There were some particular outlying residuals that remained even after exercise was modelled (Figure 8.9a-b,d-e). It should be noted that unlike most datasets, these sets contained IV boluses during the experimental time. Several datasets experienced a large improvement in model residual with exercise modelled but many which had smaller residuals to begin with did not experience much improvement. Over the dataset collation, the peri-exercise residual distribution was significantly positively biased when exercise was not modelled (Figure 8.9c). When exercise was modelled this

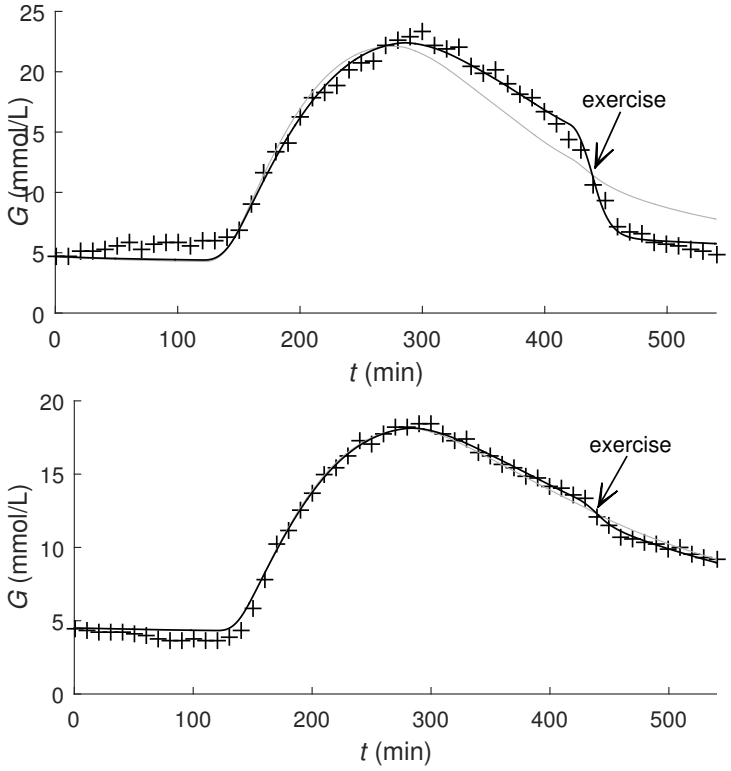

Figure 8.7: Typical good fitting results for two separate glucose datasets showing the data (+), modelled without exercise (grey) and modelled with exercise (black).

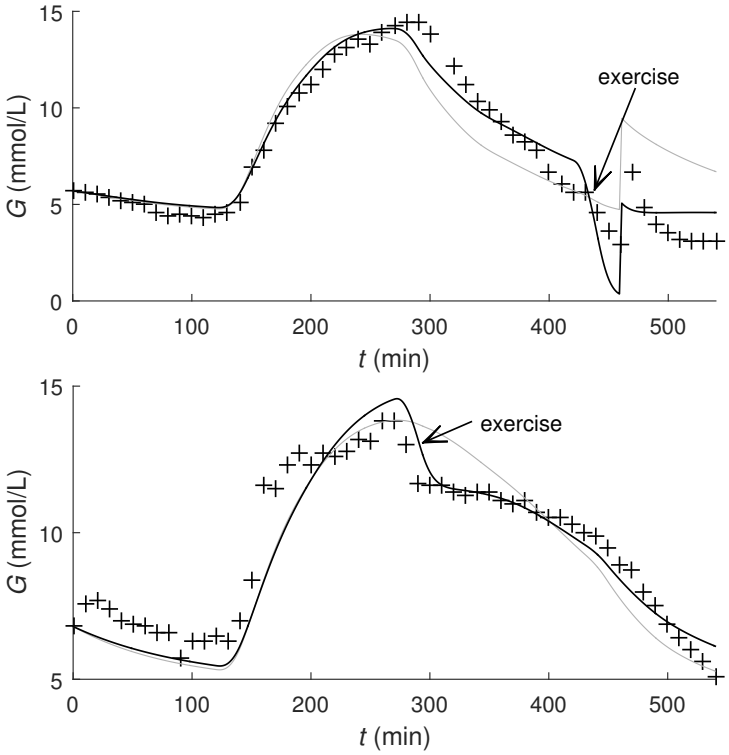

Figure 8.8: Typical poor fitting results for two separate glucose datasets showing the data (+), modelled without exercise (grey) and modelled with exercise (black).

distribution was very close to the expected measurement noise distribution. Over the whole experimental time, modelling exercise brought the distribution of residuals closer to that of the measurement noise, but still shallower (Figure 8.9f).

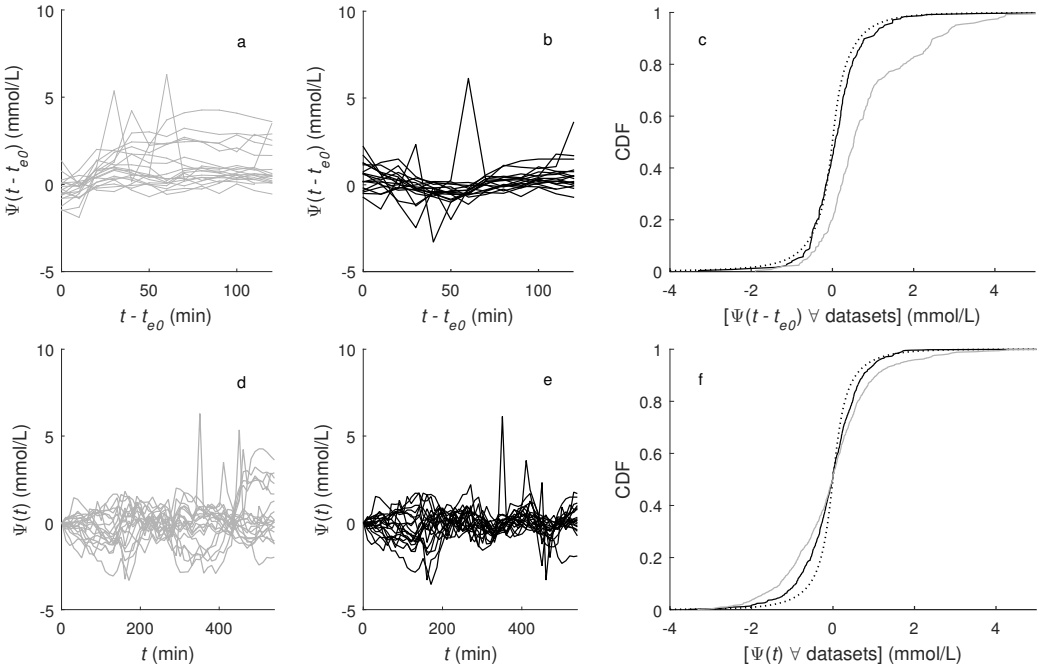

Figure 8.9: Analysis of peri-exercise residuals: (a) residual profiles for all datasets using the no-exercise glucose model; (b) residual profiles using the glucose exercise model; (c) CDFs for all-dataset collations of peri-exercise residuals, compared to distribution for expected measurement error. Plots (d-f) are equivalent to (a-c) but for the full experimental time.

8.4 Discussion

The mathematical model for the effect of exercise on plasma insulin concentration was effective in the cohort of subjects with T1DM treated by SC pump. Table 8.1 demonstrates that the exercise-model improved the goodness of fit in insulin from $R^2 = 0.81$ to 0.91 over the full experimental time in the median case. Focusing on the peri-exercise period specifically, two hours from the start of exercise, goodness of fit improved substantially

by modelling exercise, from R^2 = 0.41 to 0.86. Modelling the effect of exercise on plasma glucose concentration also improved fit with peri-exercise R^2 increasing from -0.02 to 0.50. Full dataset R^2 increased from 0.93 to 0.97 when the exercise terms were used.

In addition to the R^2 metric, the residual collation in Figure 8.4a-b shows that residuals for the no-exercise insulin model have a distinct positive then negative trajectory. In contrast, the exercise model shows little positive or negative bias, as confirmed by the peri-exercise residual CDF of Figure 8.4c. Furthermore, this CDF is slightly shallower than that expected from noise, indicating that the model is not over-parameterised. Over-parameterised models can adhere to the data closer than the measured accuracy should allow. In these cases, the model is capturing effects that are dependent on measurement noise and have no relevance to the underlying behaviour. These outcomes of good fit, no bias and appropriate parameterisation demonstrate the efficacy of the exercise basis function model as an addition to the basic insulin model.

The glucose model was not as effective as the insulin model with some large excursions in the model residual, despite the improvements. This appeared to be largely due to limitations in the general form of the glucose model other than with the specific exercise basis. In particular, the observed effect of the IV glucose was inconsistent with the modelled effect, causing trade-off with exercise magnitude in some datasets. This physiological observation is likely due to an acceleration of glucose disposal from plasma in response to IV glucose bolus, unaccounted for by the model. Additionally, the glucose appearance basis from the ingested meal was not effective for some datasets. In the peri-exercise period, the residual distribution analysis indicates that the model may be close to over-parameterisation, which may be consistent with some observations of trade-off between behaviours.

The structure of the basis models was simple and easy to apply to existing models. The equitable plus and minus portions of the insulin basis function

reflect well the fact that there is no expected change in the insulin entering the system via the SC pump or leaving the system (assuming that clearance rates are unchanged). For glucose, an increasing but saturated rate of glucose disposal in response to exercise seemed a reasonable approximation of physiological processes. In the post-exercise period, this rate took time to return to zero, consistent with observation of continued muscular uptake to refuel glycogen stores. The ability to sum the basis functions together makes it robust to variable exercise duration. However, the models should be validated on longer exercise periods to check that no additional physiological effects are influenced by exercise duration.

The intra-subject magnitude of the exercise effect on insulin was not always consistent. This motivated further investigation into what influenced the magnitude (ϵ_I). Figure 8.4 shows positive correlation between the plasma insulin concentration immediately prior to exercise (I_{e0}) and ϵ_I when excluding two particular outliers (R = 0.66, p = 0.004). A suggested reason for the correlation is that high plasma insulin indicates a high SC concentration that is more responsive to exercise-induced agitation and high blood flow. It should be noted that a dataset excluded for the absence of SC boluses also showed negligible changes in the peri-exercise period. This observation further supports the notion that SC concentration, and the effect of boluses in particular, affects exercise-induced plasma insulin excursions.

The outlier exclusion in the I_{e0} to ϵ_I correlation is supported by the evidence in the bootlier analysis of Figure 8.6. The literature notes that outlying data tends to create multi-modal distributions when performing bootstrapping analyses (Singh and Xie, 2003), which is observed in the lefthand plots of the figure. Removing the two outliers removes the multi-modal distributions, leaving only the higher correlation outcomes. To further the validity of this bootlier analysis, the same procedure was carried out with two other potential outlier data points. Removing these datasets did not alter the outcomes sufficiently to define these points as outliers. While this validates the $\bar{R} = 0.66$ correlation, the consistency of results

shows that the core datasets do produce a strong correlation. It should be noted that even in the outliers, all intra-subject dataset pairs had positive I_{e0} to ϵ_I correlations.

The Levenberg-Marquardt variant was generally successful in optimising parameters in the insulin and glucose models, evidenced by the achieved goodness of fit (Table 8.1 and 8.2). The particular method of fixing and then allowing k_e to be optimised under certain conditions allowed the best compromise between identification stability and fit for insulin. The k_e exhibited behaviours often associated with lower practical identifiability, especially in some datasets. When identified, k_e had a median value of 0.045 with lower and upper quartiles of 0.016 and 0.070. These outcomes support the *a priori* value of 0.050 that was used for the remaining datasets.

The combination of R^2, residual trajectory bias analysis and residual CDF analysis provide a clearer overall picture of model performance than just R^2 alone. Models must have a good compromise between fitting ability and practical identifiability. If effects are modelled beyond their ability to be observed in the available data (i.e. the signal-to-noise-ratio is too low) then the model outcomes are useless, or worse, misleading. This is especially true if there is no recognition of the limitations in the unique observability of features, since the realistic expectations of the model and data can be lost amongst the mathematics (Docherty et al., 2011; Raue et al., 2009; Saccomani, 2013).

If the present insulin model were to be used in an outpatient setting, all parameters relating to exercise would have to be *a priori* since the plasma insulin compartment is not observed directly. Hence, the importance of uncovering causative mechanisms that could inform *a priori* parameter estimates. Though the glucose model could be made significantly more complex to achieve an improved fit, such a directive would need to be balanced by recognition of the limitations of outpatient data.

The correlation of plasma insulin concentration and exercise excursion magnitude relied on the exclusion of two outliers, which were from the same subject. The bootlier analysis justified this exclusion, but at the risk of seeming like a manufactured outcome, appropriate caution should accompany the $\bar{R} = 0.66$ correlation. The correlation should be seen as suggestive rather than definite, and certainly not causative. However, the correlation does prompt interest for further investigation. In particular, if a correlation were established, a single plasma insulin measure could be used to provide a patient-specific *a priori* estimate of ϵ_I.

In future, the insulin model would benefit from well-informed parameter estimates for ϵ in particular. Hence, further work could be carried out to link SC properties to the exercise effect. Additionally, successfully modelling the effect of exercise on insulin is only a precursor to successfully modelling the overall effect of exercise on glucose, which is significantly more complex. This was shown in the increased number of behaviours, species and parameters used in the glucose model, yet still inviting room for an improvement in fitting accuracy. Whether the glucose model were improved or not, both models should be tested with longer durations of exercise to see if the physiological principles determined in this analysis can be extrapolated beyond 20 minutes of exercise.

8.5 Summary

This chapter introduces an effective basis model for the effect of exercise on subcutaneously administered IAsp in individuals with T1DM. The exercise model fits well with the data, with $R^2 = 0.86$ around the exercise period compared to $R^2 = 0.41$ when exercise is not modelled. Analysis of the model residuals around this period collated across all datasets indicate that the exercise model is not biased and is appropriately parameterised. Additionally, another basis model was developed for the effect of exercise on glucose. This model performed adequately, improving fit proximal to the exercise period from $R^2 = -0.02$ to $R^2 = 0.50$ but other aspects of the glucose model limited the overall performance.

The identified magnitude of exercise-mediated excursion in plasma insulin appeared to be correlated to the concentration of plasma insulin immediately prior to exercise. This was suspected to be due to higher SC concentrations resulting in both higher plasma insulin and higher responsiveness to exercise-induced agitation and high blood flow. These correlations are strong for most datasets ($R = 0.66$) but tentative due to the need for excluding two datasets from the correlation.

Part III

Identifiability and model recovery

Chapter IX

Identifying secondary effects in increasing data

This chapter details an *in silico* analysis proving the potential for identifying everyday life (or secondary) effects on glycaemia in sparse, outpatient diary data. Monte Carlo analyses are used to compare identified model parameters to those in the underlying virtual patient for increasingly large datasets. The content of this chapter was published as an article in the Journal of Mathematical Biosciences (Mansell et al., 2015d), and a simplified version of the research presented at the 15th Annual Diabetes Technology Meeting (Mansell et al., 2015a). Note that this work preceded the model-building of previous chapters. Hence, the model used in this and the subsequent chapter does not include the updated features.

9.1 Motivation

There is significant potential benefit in developing effective glycaemic control mechanisms for individuals with T1DM similar to those used for the critically ill (Chase et al., 2011; Plank et al., 2006). However, there are many social and psychological factors that confound the type of regimented glycaemic control used successfully in the critically ill who are typically sedated. In particular, some social situations induce over consumption. Furthermore, stress, anxiety and frustration can affect glycaemic behaviour and occur intermittently. Stress and related factors can be caused by self-monitored blood glucose, regimented lifestyles, and unpredictable glycaemic variability (Rubin and Peyrot, 2001). Thus, a further, necessary goal of glycaemic control algorithms for outpatients should be mitigating the psychological impact of the control algorithm itself by allowing greater flexibility in daily activities.

There are many secondary effects that influence glycaemic control. It is

well established that emotional (as well as medical) stress results in hyperglycaemia in individuals with T1DM (Surwit et al., 1992; Lloyd et al., 1999). This hyperglycaemia is due to insulin resistance caused by the endogenous release of corticosteroids and catecholamines (Ward et al., 2011). Sleep deprivation is also responsible for changes in insulin sensitivity without significant changes in cortisol levels (González-Ortiz et al., 2000). In contrast, moderate-intensity (aerobic) exercise can lower blood glucose significantly, and eventually causes hypoglycaemia if care is not altered (Sonnenberg et al., 1990; Yardley et al., 2013). These factors provide challenges for self-managed glycaemic regulation. Furthermore, they are capable of confounding model-based control algorithms due to the lack of quantitative evidence or direct identification of their effect on glycaemia.

The use of physiological modelling has emerged in the field of glycaemic control for the critically ill (Pappada et al., 2013; Pielmeier et al., 2010; Chase et al., 2011). Inter- and intra- patient variability provides challenges to maintaining glycaemic control for individual patients. Thus, these modelling methods identify a number of patient-specific parameters as well as using *a priori* population-average parameters (Chase et al., 2011). Recent developments have also been made in the field of automated treatments for outpatients with T1DM that are using CGMs (Hovorka et al., 2013; Bequette, 2012; Cobelli et al., 2011). Some of these developments also include compensation for stress hyperglycaemia (Ward et al., 2011). However, this type of treatment is still experimental and has high cost and complexity (Khovanova et al., 2013; Bequette, 2012). Hence, it may be more practical to improve upon conventional approaches such as self-monitored glucose with multiple daily insulin injections (Wong et al., 2008c, 2009). Knowledge of relevant patient-specific parameters would benefit model-based therapy support for insulin dosing information.

Sparse, irregular data provides challenges in uncovering clear trends. Thus the purpose of this research was to test parameter estimation in such data, identifying some of the key patient-specific secondary effects on glycaemic dynamics: stress, fatigue and exercise. The data was generated *in silico*

with efforts to mimic self-reported, diary-style data with simulated self-monitored glucose measurement and omission errors. The results obtained from parameter identification were assessed in accumulating data-sets over a Monte Carlo (MC) population. Finally, the methods were tested for their ability to handle long-term changes in insulin sensitivity (SI) that occur due to changes in a patient's metabolism (Mayer-Davis et al., 1998; Abate et al., 1995; Wu, 2005).

9.2 Methods

9.2.1 The virtual patient

To test the estimation of factors affecting glycaemic dynamics, a virtual patient with T1DM was simulated *in silico*. The patient ingested regular meals and the occasional snack. They took insulin boluses with meals as well as a constant insulin infusion to mimic slow acting insulin. The virtual patient also participated in moderate exercise several times a week and experienced days of stress or fatigue several times per month.

The model used to simulate the glycaemic dynamics of the *in silico* patient is a variation of the clinically validated DISST model (Lotz et al., 2010). The adaptations include a nutrition model (Wong et al., 2008c, 2009; Lin et al., 2011) and effects of exercise, stress, fatigue and SI drift. The model consists of *a priori* parameters (definitions in Table 9.1), time-dependent inputs (definitions in Table 9.2) and identified variables (Table 9.1). A flowchart showing the order of dependent species in the model can be seen in Figure 9.2.

First, subcutaneous insulin concentration (U_S) was modelled as a kinetic delay from regular bolus doses and a basal infusion (U_X):

$$\dot{U}_S(t) = U_X(t) - k_X U_S(t) \tag{9.1}$$

Interstitial insulin concentration (Q) was modelled as being co-dependent with plasma insulin (I) which is a function of U_S:

$$\dot{I}(t) = -(n_T + n_I)I(t) + n_I Q(t) + \frac{k_X U_S(t)}{V_p} \tag{9.2}$$

$$\dot{Q}(t) = -(n_I + n_C)Q(t) + n_I I(t) \tag{9.3}$$

A linear model was used to predict gut glucose (P_S). The gut glucose model included regular meals of varying glucose content (P_X) and randomly timed snacks (P_C)(Wong et al., 2008c, 2009; Lin et al., 2011):

$$\dot{P}_S(t) = \frac{P_X(t) + P_C(t)}{V_G} - k_1 P_S(t) \tag{9.4}$$

Circadian rhythms are known to influence insulin sensitivity but there are conflicting reports on the nature and shape (Van Cauter et al., 1997; Carroll and Nestel, 1973; Sensi and Capani, 1976). In absence of consensus in reported profile, SI was modelled in Equation (9.5) with overlapping triangular basis functions (g_{1-3}). These functions produce daily rhythms with morning, midday and afternoon peaks, SI_{1-3}. The bases and resulting SI profile are pictured in Figure 9.1. Additionally, SI is influenced by the presence of stress (σ), fatigue (φ) and long-term drift:

$$SI(t) = \left(SI_1 g_1(t) + SI_2 g_2(t) + SI_3 g_3(t)\right)\left(1 - \sigma(t) - \varphi(t)\right)\left(1 + \frac{D(\%)t}{100(\%)t_y}\right) \tag{9.5}$$

where D(%) is the yearly percentage increase in insulin sensitivity (defined in the analysis methodology, Section 2.5) and t_y is 525600 minutes per year. The modelled species Q, P_S and SI were introduced into the blood glucose model (G), along with the effect of exercise (ε) (Yardley et al., 2013):

$$\dot{G}(t) = -p_G\left(G(t) - G_0 + \varepsilon(t)\right) - SI(t)\left(G(t)Q(t) - G_0 Q_0\right) + k_2 P_S(t) \tag{9.6}$$

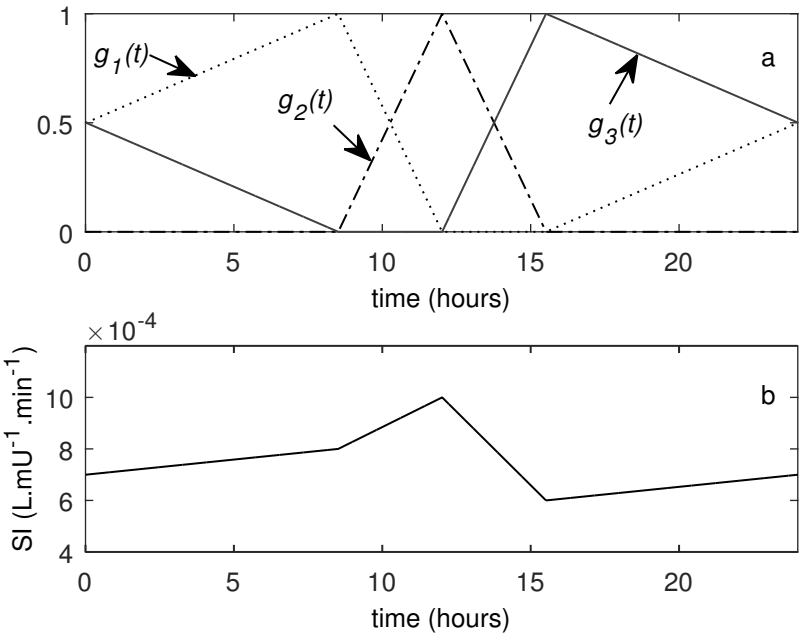

Figure 9.1: The shape of the daily basis functions g_{1-3} (a) and resulting SI profile determined by Equation (9.5) (b) with time measured from 12am midnight

Stress, fatigue and exercise contributions were the product of a peak value and a time-dependent function:

$$\varepsilon(t) = \varepsilon_{max} f_{\varepsilon}(t) \tag{9.7}$$

$$\sigma(t) = \sigma_{max} f_{\sigma}(t) \tag{9.8}$$

$$\varphi(t) = \varphi_{max} f_{\varphi}(t) \tag{9.9}$$

where the functions f_i define when each of the effects occurs and the intensity, $f_i \in \{0, 0.5, 0.6, 0.7, 0.8, 0.9, 1\}$. Thus, the max values indicate the maximal contributions possible from each of the effects.

9.2.2 Simulation

The model was simulated for either one or two years with time-varying species using one minute resolution. Analytical solutions to the model equations were used for the simulation. MATLAB's symbolic differential equation solver

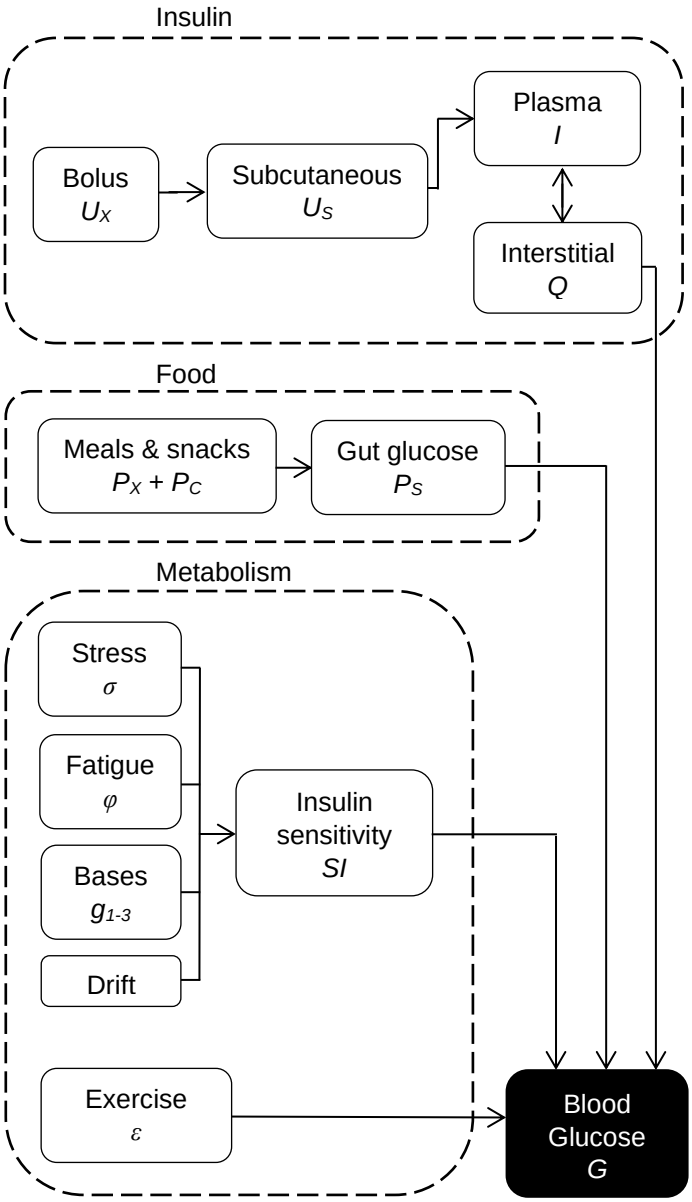

Figure 9.2: The flow of dependency in the model, also indicating the order in which the species needed to be simulated

Table 9.1: Parameter constants used to simulate the virtual patient glycaemic profiles in the model. The * indicates parameters which were identified as variables from virtual data

Parameter	Description	Value	Unit
n_I	Plasma to interstitium transport rate	0.02	min^{-1}
n_T	Plasma insulin clearance rate	0.1	min^{-1}
n_C	Cell metabolism of insulin	0.02	min^{-1}
V_p	Volume of distribution of plasma insulin	4.3	L
p_G	Glucose dependent balance	0.004	min^{-1}
V_G	Glucose distribution volume	12.4	L
k_1	Stomach to gut glucose transfer rate	0.05	min^{-1}
k_2	Rate of glucose absorption from gut	0.008	min^{-1}
k_X	Rate of insulin injection site dispersal	0.01	min^{-1}
${G_0}^*$	Basal glucose concentration	4.5	$\text{mmol} \cdot \text{L}^{-1}$
Q_0	Basal interstitial insulin concentration	4.23	$mU \cdot L^{-1}$
${\varepsilon_{max}}^*$	Exercise coefficient	6.5	$\text{mmol} \cdot \text{L}^{-1}$
${\sigma_{max}}^*$	Stress coefficient	0.3	
${\varphi_{max}}^*$	Fatigue coefficient	0.1	
${SI_1}^*$	Morning (8.30am) SI peak	0.8×10^{-3}	$\text{L} \cdot \text{mU}^{-1} \cdot \text{min}^{-1}$
${SI_2}^*$	Midday (12pm) SI peak	1.0×10^{-3}	$\text{L} \cdot \text{mU}^{-1} \cdot \text{min}^{-1}$
${SI_1}^*$	Afternoon (3.30pm) SI peak	0.6×10^{-3}	$\text{L} \cdot \text{mU}^{-1} \cdot \text{min}^{-1}$

was used to find the analytical solution to the more complex interdependent species of Equations (9.2) and (9.3). The full set of analytical solutions for the virtual patient follow. Glucose absorbed from the stomach was simulated with:

$$P_S(t) = e^{-k_1 t}\left(P_{S,0} + \int_0^t e^{k_1 t}\left(P_X(t) + P_C(t)\right)dt\right) \tag{9.10}$$

The SC insulin solution is described:

$$U_S(t) = e^{-k_X t}\left(\frac{U_{X,0}}{k_X} + \int_0^t e^{k_X t} U_X(t) dt\right) \tag{9.11}$$

$$\tag{9.12}$$

The interstitial insulin solution is described:

$$Q(t) = e^{-0.5(\rho_1+\rho_2)t}e^{-0.5(\rho_1-\rho_2)t}(q_1 + q_2) \tag{9.13}$$

$$q_1 = e^{0.5(\rho_1+\rho_2)t}\left(5.896 + \int_0^t \frac{n_I e^{0.5(\rho_1-\rho_2)t}k_X U_S(t)}{V_P\rho_2}dt\right) \tag{9.14}$$

$$q_2 = e^{0.5(\rho_1-\rho_2)t}\left(-1.668 + \int_0^t -\frac{n_I e^{0.5(\rho_1+\rho_2)t}k_X U_S(t)}{V_P\rho_2}dt\right) \tag{9.15}$$

$$\rho_1 = n_C + 2n_I + n_T \tag{9.16}$$

$$\rho_2 = \sqrt{n_C^2 - 2n_C n_T + 4n_I^2 + n_T^2} \tag{9.17}$$

The solution to the blood glucose model is given as:

$$G(t) = e^{-\gamma}\left(G_0 + \int_0^t e^{\gamma}\left(p_G(G_0 - \varepsilon(t)) + SI(t)G_0Q_0 + k_2P_S(t)\right)dt\right) \tag{9.18}$$

$$\gamma = \int_0^t p_G + SI(t)Q(t)dt \tag{9.19}$$

All integrals were calculated with trapezoidal numerical integration. Numerical instabilities meant that simulations had to be undertaken in sections of seven days at a time and concatenated.

Each run within the MC analyses generated a patient using the same Table 9.1 parameter values, but with variation in certain input vectors ($\mathbf{P_X}$, $\mathbf{P_C}$, $\mathbf{f}_\varepsilon$, $\mathbf{f}_\sigma$, $\mathbf{f}_\varphi$). $\mathbf{P_X}$ took on random values between 72-90 grams of carbohydrate at mealtimes, which corresponds to 400-500 mmol of glucose. $\mathbf{P_C}$ was 30 grams carbohydrate (160 mmol glucose) at 52 random times throughout a year. The $\mathbf{f}_\sigma$ vector contained three random full-day occurrences per 28 days while $\mathbf{f}_\varphi$ was given five days. Occurrences in $\mathbf{f}_\varepsilon$ were two hours in the morning for three randomly chosen days a week. For each occurrence of these secondary effects, an intensity of 50-100% was assigned.

Table 9.2: Time-dependent vector inputs for used to simulate the virtual patient, noting that the simulation uses 1 minute resolution

Vector	Description	Value	Unit
$\mathbf{P_X}$	meals	$\begin{cases} [400, 500] & \text{at } 0800, 1200 \text{ and } 1900 \text{ hrs daily} \\ 0 & \text{otherwise} \end{cases}$	mmol
$\mathbf{P_C}$	snacks	$\begin{cases} 160 & \text{at 52 random } t \text{ per year} \\ 0 & \text{otherwise} \end{cases}$	mmol
$\mathbf{U_X}$	insulin doses	$\begin{cases} 1000 & \text{with meals} \\ 4 & \text{otherwise} \end{cases}$	mU
$\mathbf{f}_\varepsilon$	exercise	$\begin{cases} \in [0.5, 0.6, ..., 1.0] & \text{at 1830 to 1030 hrs, 3 days/week} \\ 0 & \text{otherwise} \end{cases}$	
$\mathbf{f}_\sigma$	stress	$\begin{cases} \in [0.5, 0.6, ..., 1.0] & \text{3 days per 4 weeks} \\ 0 & \text{otherwise} \end{cases}$	
$\mathbf{f}_\varphi$	fatigue	$\begin{cases} \in [0.5, 0.6, ..., 1.0] & \text{5 days per 4 weeks} \\ 0 & \text{otherwise} \end{cases}$	
$\mathbf{g_1}$	morning SI basis	$\begin{cases} 0 & \text{1200 to 1530 hours} \\ 1 & \text{0830 hours} \\ 0 < g_1 < 1 & \text{otherwise}^* \end{cases}$	
$\mathbf{g_2}$	midday SI basis	$\begin{cases} 0 & \text{1530 to 0830 hours} \\ 1 & \text{1200 hours} \\ 0 < g_2 < 1 & \text{otherwise}^* \end{cases}$	
$\mathbf{g_3}$	afternoon SI basis	$\begin{cases} 0 & \text{0830 to 1200 hours} \\ 1 & \text{1530 hours} \\ 0 < g_3 < 1 & \text{otherwise}^* \end{cases}$	

*triangular basis function forms are pictured in Figure 9.1

9.2.3 Data acquisition

Diary-like data was sampled' from the glucose simulation to mimic daily finger-prick measurements. Meal carbohydrate estimates, insulin doses, as well as instances and intensity of exercises, stress and fatigue were also recorded.

Blood glucose measurements were sampled randomly from G at 6 non-adjacent times per day between the hours of 6am and 12 midnight. This random distribution yields a more conservative approach than if sampling was limited to around mealtimes. In particular, mealtime sampling would capture dynamic responses to meal perturbations and thus would maximise practical identifiability of metabolic parameters (Docherty et al., 2011). The sampling frequency could also be considered a conservative estimate for fastidious individuals with poor blood glucose control.

There is significant measurement error and variation associated with blood glucose measurements (Freckmann et al., 2013). To mimic this error, 10% normally distributed noise was applied to the blood glucose data. Misrepresentation and error are also common in a patient's carbohydrate estimates (Wong et al., 2009). Thus, the acquired data neglected the snacks (P_C) and 10% uniformly distributed noise was applied to P_X. Hence, P_S calculated during parameter identification was different from that of the true simulated patient. The Q, f_ε, f_σ and f_φ vector profiles used in parameter identification were equal to those used to simulate the virtual patient.

9.3 Parameter identification

The identification set included circadian SI parameters, basal blood glucose and parameters for exercise, stress and fatigue: $\mathbf{x} = [SI_1, SI_2, SI_3, G_0, \varepsilon_{max}, \sigma_{max}, \varphi_{max}]^{\mathrm{T}}$. The Gauss-Newton method for gradient descent was used to minimise the least-squares residual between the data and a forward simulation of G using the current parameter

estimates, $\mathbf{x}_i$. This residual is given by:

$$\mathbf{\Psi}_i = \mathbf{G}_i(t_S) - \mathbf{G_S} \tag{9.20}$$

where $\mathbf{G_S}$ is the sampled data and $\mathbf{G}_i(t_S)$ is the modelled blood glucose at the sample times (t_S) for the present iteration (i). S denotes the samples $1 \dots n$, where n is the number of samples.

The first iteration parameter set was defined as $\mathbf{x}_0 = [10^{-3}, 10^{-3}, 10^{-3}, G(t_0), 10, 0.1, 0.1]$. Iterations continued until the tolerance criteria were satisfied: $||\mathbf{x}_{i+1} - \mathbf{x}_i||_2 < 10^{-8}$ and $i > 10$.

9.4 Analysis methodology

A two-part Monte Carlo approach was used to evaluate the estimation of the behaviours present in the simulation. To investigate the convergence of parameter values in increasing data, identification was conducted in data subsets of one week up to one year. To capture long-term drift in SI, Part II identifies parameters in 90 day data subsets whose start dates shift by ten days at a time, for a total of two years. Figure 9.3 shows a flowchart of the Monte Carlo analytical process for both parts.

All analyses were undertaken on a 64-bit Intel® Core™ i7-2600 (3.4 GHz) CPU personal computer with 32GB of RAM using MATLAB (2013b Version 8.2.0.701).

9.4.1 Part I

Data was sampled from a one year simulation of glucose that contained no long-term drift in SI ($D(\%) = 0$). The parameter set $\mathbf{x}$ was identified for increasing subsets of this data (G_S) for 7, 14, 21, 35, 56, 91, 147, 238 and 365 days.

When a data subset did not contain any randomly generated days of stress or fatigue, σ_{max} and φ_{max} were set to zero and excluded from identification.

When both stress and fatigue effects occurred concurrently and thus yielded a structurally non-identifiable system, both parameters were excluded from identification, as their effects can only be quantified when there are separate instances recorded (Docherty et al., 2011; Bellu et al., 2007).

The parameter set $\mathbf{x}$ was identified in 2000 simulations of the patient for each data set length (n). The CV, mean, and 95% confidence interval (CI) were calculated for each data size (n) for each parameter. The CV values for each parameter ($\mathrm{CV_x}$) were related to the length of the data subset set via the function:

$$\mathrm{CV_x}(n) = \frac{y_1}{\sqrt{\frac{n}{6} + y_2}} \tag{9.21}$$

where y_1 denotes the magnitude of the CV and y_2 allows an offset to account for when effects are not present in early data.

9.4.2 Part II

Part II measured the ability of the identification method to accurately capture all parameters in data that contained insulin sensitivity drift over a 2 year data collection period. In this analysis, SI was set to increase linearly by 10% during the first year ($D(\%) = 10$), then decline by 20% in the second year ($D(\%) = -20$). Neither the magnitude nor shape of SI drift were treated as *a priori*. Thus, the drift could not be identified directly. Instead, the analysis used subsets of data that shifted through time to capture all identified parameters in a moving average.

A 90 day data subset was taken starting each successive 10 days until the full 730 days was used. This process was repeated for 2000 virtual patient simulations, with mean and 95% CI calculated for each data subset across the simulations.

To attenuate apparent periodicity in the drift patterns, the parameter identification method was adjusted to penalise $SI_1 - SI_3$ values that

strayed too far from values obtained in the previous data subset. This attenuation was achieved by modifying Equation (9.20) to include additional penalty function terms in the objective function:

$$\boldsymbol{\Psi}_{w,i} = \begin{bmatrix} G_i(t_1) - G_1 \\ G_i(t_2) - G_2 \\ \vdots \\ G_i(t_n) - G_n \\ \alpha(SI_{1,i} - SI_{1,w-1}) \\ \alpha(SI_{2,i} - SI_{2,w-1}) \\ \alpha(SI_{3,i} - SI_{3,w-1}) \end{bmatrix} \tag{9.22}$$

where i is the present iteration of identification in a 90 day data subset (w) and $G_{1\ldots n}$ is the data contained within that subset. α is a factor that determines the magnitude of penalisation of changes in insulin sensitivity across subsets. The ability to capture long-term drift in SI was compared with $\alpha = 0$, 2×10^4 and 4×10^4; where the 10^4 converts SI to values to between 1 and 10, thus, comparable in scale to the $G(t)$ values.

Singular values of ε_{max}, σ_{max} and φ_{max} for the full two year period were found using an average over every 90 day data subset. This was carried out for $\alpha = 2 \times 10^4$ only. These values were analysed across the population for mean, 95% CI and CV.

9.5 Results

9.5.1 Part I

Figure 9.4 shows that the CV in each parameter converged with increasing days of data. The function of Equation (9.21) was fitted to the parameter CV values, and values for $y_{1,2}$ and R^2 are presented in Table 9.3. G_0 had the lowest variation coefficients of all the identified parameters while ε_{max} had the greatest, followed by φ_{max} and σ_{max}. R^2 was over 99.9% for all parameters thus indicating strong adherence to the $1/\sqrt{n}$ rule (Whitley and

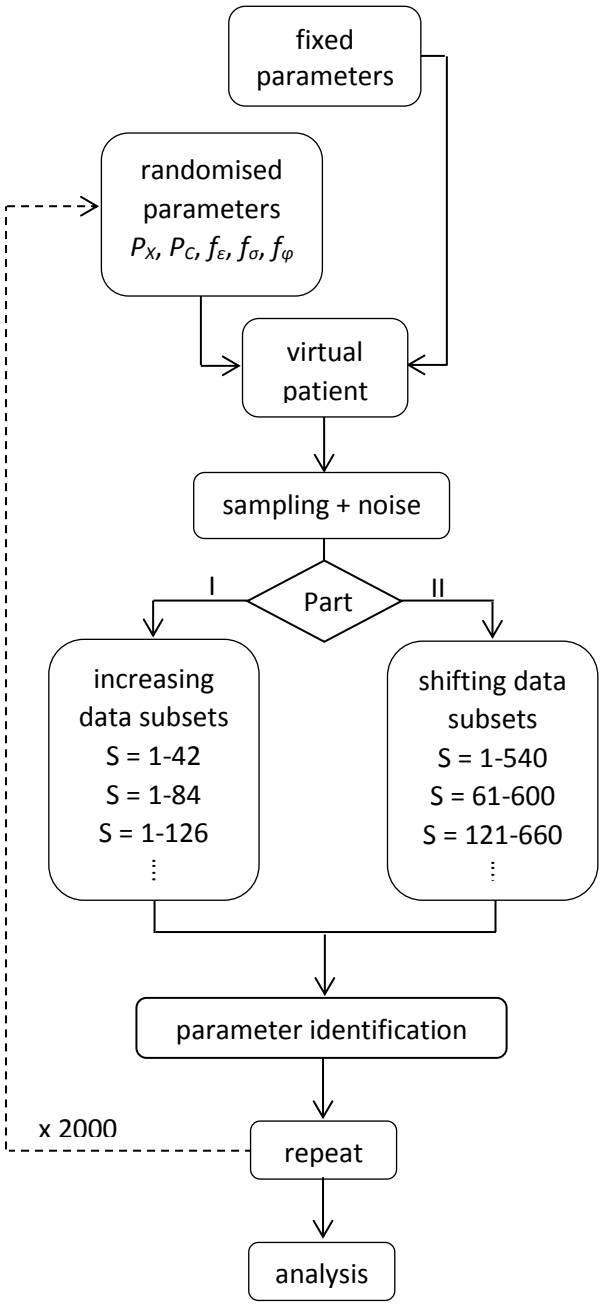

Figure 9.3: The Monte Carlo analysis, showing the distinction between Parts I and II for data subset selection. Note that the actual data is not interchanged between the two parts, since Part II contains long-term drift in SI while Part I does not

Table 9.3: Trend-line parameters for $CV_x(n)$ and the R^2 value

Parameter	y_1	y_2	R^2
SI_1	0.531	-1.537	1.000
SI_2	0.677	-1.029	1.000
SI_3	0.498	-0.814	1.000
G_0	0.116	-0.317	0.999
ε_{max}	0.921	-6.906	1.000
σ_{max}	1.854	-9.730	1.000
φ_{max}	4.746	-7.998	1.000

Ball, 2002). The higher y_2 values for the secondary effects implied greater offsets with respect to days. Figure 9.5 shows that the precision of each parameter improved with increasing days of data although some small biases were observed. The biases were relatively small by day 385 (SI_1, 0.9%; SI_2, 0.9%; SI_3, 0.6%; G_0, 0.9%; ε_{max}, 0.04%; , σ_{max}, 0.2%; φ_{max}, 0.2%). To evaluate convergence, CV was evaluated for repeat sets of size 1950, 1951, 1952, ..., 2000 repeats. These values were within 0.5% of the 2000 repeat CV for every parameter, indicating that the Monte Carlo simulation cohort had converged suitably.

9.5.2 Part II

Figure 9.6 shows that the long-term drift in insulin sensitivity was readily captured over the data sets tested, but lagged the true drift. Furthermore, the drift in insulin sensitivity caused some drift to occur in the secondary effect parameters (ε_{max}, φ_{max} and σ_{max}) that was not present in the underlying behaviour of the virtual patient. Figure 9.7 shows that increasing the α value smoothed out the oscillating patterns in insulin sensitivity, but Figure 9.6 shows that higher α values caused greater variation in other parameters and increased the lag in the mean identified SI profile.

Values for ε_{max}, φ_{max} and σ_{max} obtained with $\alpha = 2 \times 10^4$, yielded relatively small 95% confidence intervals and all biases were below 1% (Table 9.4). Figure 9.7 shows a typical example of the effect of α on drift

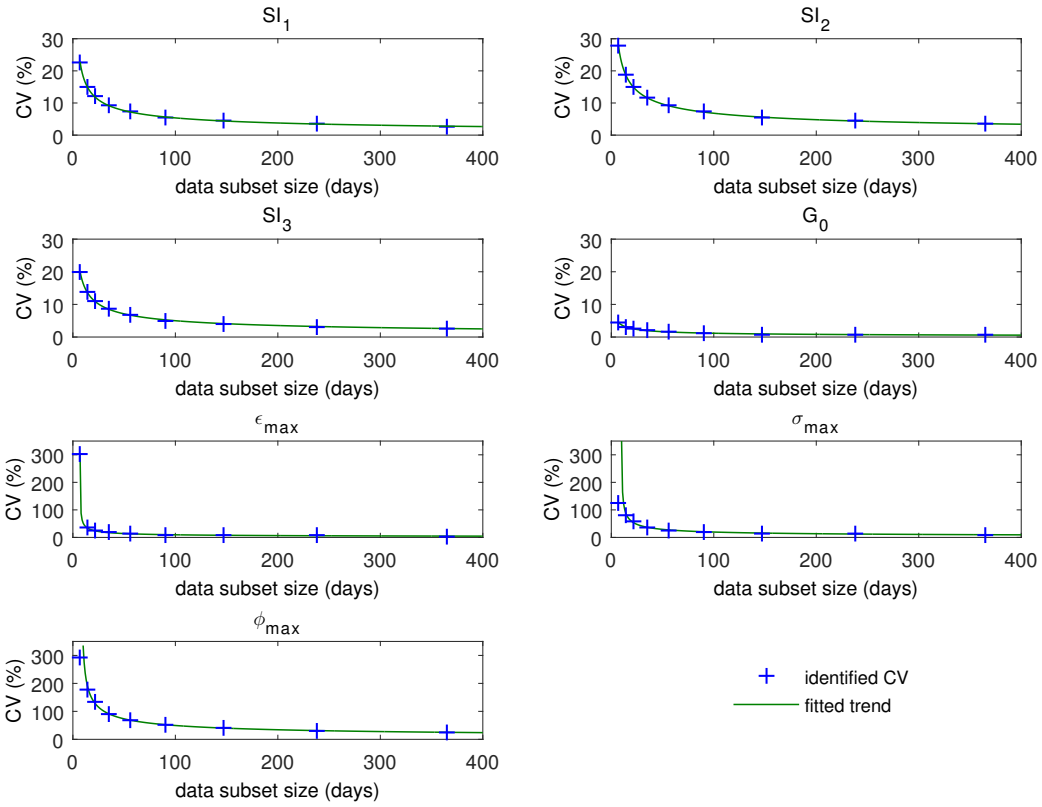

Figure 9.4: CVx(n) for each identified parameter over 2000 repeats for each data subset length fitted with the trend-lines of 9.21. Note the different magnitude of the secondary effect parameters

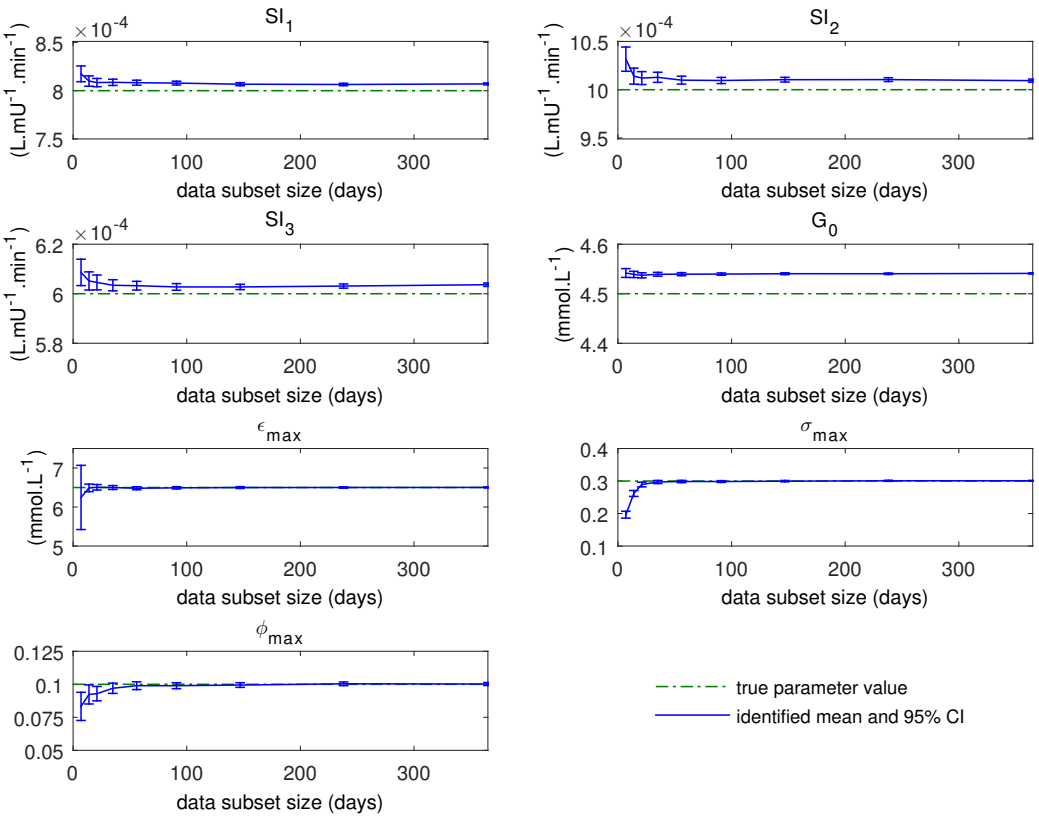

Figure 9.5: Convergence of identified parameter values compared to true values as days of data increased for 2000 repeats

Table 9.4: Average of secondary effects over every 90 day data subset for $\alpha = 2 \times 10^4$ with 2000 repeats

Parameter	True value	Mean	95%CI	Relative bias	CV
ε_{max}	6.5	6.44	(6.43,6.45)	-0.9%	3.7%
σ_{max}	0.3	0.299	(0.298,0.300)	-0.2%	7.6%
φ_{max}	0.1	0.0995	(0.0986,0.1004)	-0.5%	19.6%

patterns in daily SI mean for an individual simulation and identification process. Greater values of α attenuated the random drift in SI, allowing the method to better emulate the original drift pattern.

Using Equation (9.21) and the parameters in Table 9.3, the variation coefficient in the secondary effects for Part II was compared with Part I for $\alpha = 2 \times 10^4$. To achieve the same variation coefficient as that of 100 days with no drift effects, it would require 118, 120 and 123 days of data with drift present for the ε_{max}, σ_{max} and φ_{max} parameters, respectively.

A single 91 day period required an average of 3.4 seconds of computational time and one 730-day, 65-data subset repeat of the drift analysis required an average of 578 seconds.

9.6 Discussion

The accuracy of the model parameters for the individual virtual patients and the precision of model parameters of the *in silico* cohort increased in accuracy as more data accumulated. Some small bias ($< 1\%$) occurred in each parameter across the virtual cohort by day 385 (Figure 9.5). These small biases were due to the log-normal parameter distributions that result from identifying the effects from 1st order models in data that have normally distributed measurement error. In accordance with expectations, the CV_X values reduced in proportion to $1/\sqrt{n}$ (9.4) (Whitley and Ball, 2002) with R^2 values all exceeding 99.9%. As sparse measurement data accumulates, failure to adhere to $1/sqrtn$ would imply instability during parameter identification or significant parameter trade-off. The strong

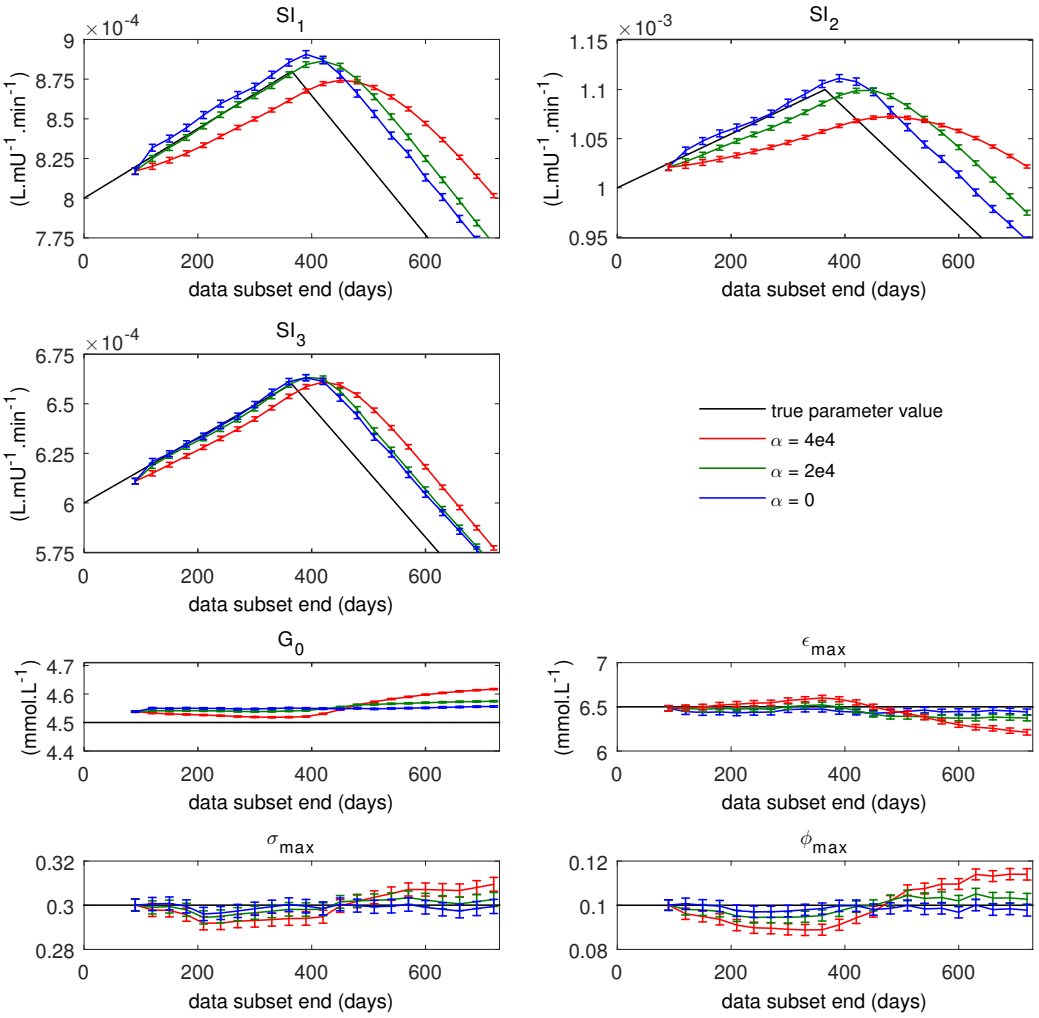

Figure 9.6: The effect of increasing α on parameter identification of 90 day periods when long-term drift is present for 2000 repeats (showing every 3rd point for clarity)

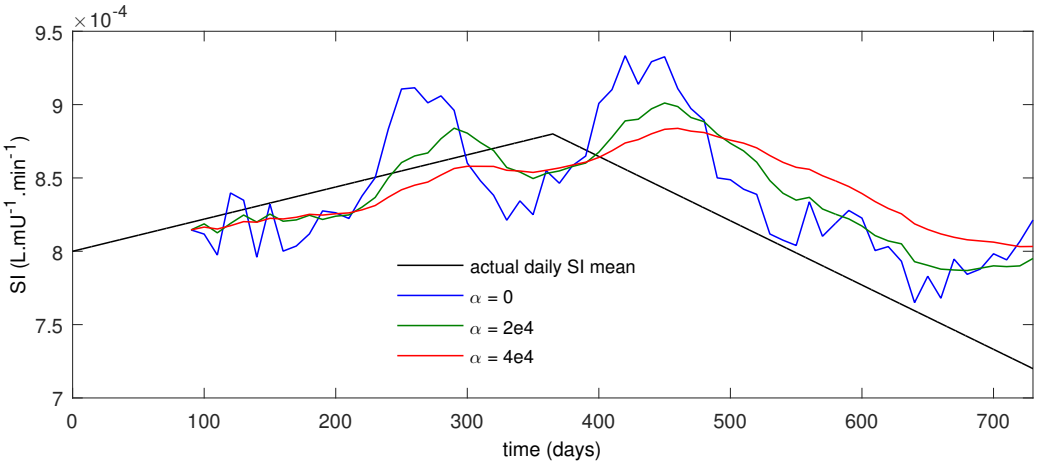

Figure 9.7: An example of a typical run showing identification of the mean of SI_{1-3} at the end of each 90 day data subset for increasing values of α

correlation to the trend in the results validates the identification method as well as the robustness of the parameters.

Identifying y_2 in Equation (9.21) was necessary as the randomised occurrences of some parameters meant that some identification sets did not have any stress or fatigue in the early stages. Both σ_{max} and φ_{max} are on 28 day alternations and therefore appeared anywhere between 0 and 3 times in the first 7, 14 and 21 days. These three data subset lengths were therefore excluded from trend-fitting for σ_{max} and φ_{max} because these data subsets are shorter than might be used in practice and it was more useful to capture the long-term trends than initial transience. Overall, the results indicate that noise in blood glucose and food intake, in addition to instances of unreported food intake, can be overcome by an accumulation of data and robust parameter identification, even in the presence of sparse, irregular data.

It is well established that insulin sensitivity undergoes long-term drift due to changes in a patient's metabolism (Abate et al., 1995; Mayer-Davis et al., 1998; Wu, 2005). For that reason, it would be misguided to identify single values of SI_{1-3} for periods that are longer than a few months. Insulin

sensitivity can increase or decrease at any time and while it is likely to drift in a steady manner, it was important that the identification method did not make any assumptions of the drift profile. Using consecutive data subsets to observe the drift pattern fulfilled this requirement, but caused some lag in identification. While the modelling approach used in Part II of this analysis yielded transient parameter values, it was effectively a traditional constant parameter approach. In particular, constant values for each of the SI and secondary effect parameters were determined for a particular 90 day window. The outcomes of Part I implied reasonably robust parameter values could be obtained in 90 days of data. Part II showed that it is possible to identify parameters that influence glycaemia in the presence of SI drift that would inevitably occur in free-living individuals.

The Monte Carlo simulation implied that drift in insulin sensitivity was easily inferred, but that this identification also lagged the underlying true behaviour. This lag should be expected due to the need to accumulate enough sparse, irregular data to identify the trend. While Figure 9.6 appears to show no advantage and increased lag due to the penalisation of changes in SI, Figure 9.7 shows the need for this parameter to limit the systematic oscillation in measured insulin sensitivity and allowing for more practical inference of the underlying trends. The optimal α out of the few examined was 2×10^4 because it attenuated much of the noise, but did not flatten the SI trends excessively. Further refinement of the α value is necessary prior to further implementation of the method.

The secondary effects (ε_{max}, σ_{max} and φ_{max}) remained identifiable in the presence of SI drift. Table 9.4 shows high precision (CV$<$ 20%) and small biases ($<$ 1%). Note that the secondary parameters were effectively identified over the whole period and thus built up precision due to the number of data points available. The validity of this assumption relies on the consistency of secondary effects on glycaemia, which has not been investigated.

To assess the robustness of the secondary parameters to drift, an analysis

was undertaken to estimate how many days of data with SI drift would be needed to match 100 days of data without drift. The PART I CV_X values for the secondary parameters were similar to the PART II CV_X values for the equivalent number of days. In particular, the CV values after 100 days without drift was equivalent to the CV of 118-123 days with drift. This outcome indicates a high level of robustness that allows the methods to capitalise on the majority of the information collected over 2 years, despite the presence of drift.

While using virtual patients limits the explicit clinical relevance of the outcomes of this study in real patients, it was sensible to carry out this stage of the investigation *in silico*. The advantages of an initial *in silico* study are the ability to control exactly what the model entails and compare the identified parameters to true values. This method also facilitated effective statistical analysis through repeated generation of the model. Hence, any outcomes were a factor of the input data that were controllable and thus it was possible to determine the robustness of the mathematics in the presence of noise and a known level of confounding behaviour. *In vivo*, the level of confounding behaviour would not be known, and thus the origin of parameter variance would remain ambiguous.

In the simulated model, basis function shapes perfectly matched the input model shapes. However, in real data, basis functions will give the identification scheme some freedom to emulate the circadian rhythm, but cannot be any more than an approximation to the true shape that is currently unknown. Likewise in the model, perfect interstitial insulin profiles were used during identification, but diary data will not contain measurements of insulin but will have dose descriptions instead. Hence, insulin pharmacokinetics will need to be estimated using currently available models. While there is general knowledge available of the pharmacokinetics of different insulin products, the patient- and dose- specific behaviour is much more variable and unknown (Wong et al., 2008a,b). Regardless, this computational study proves the concepts to justify focused clinical trials where these profiles can be optimised.

There are likely to be many confounding effects for a real system that cannot be directly accounted for, such as low patient compliance, errors in insulin dosing or dose recording, and errors in meal records. Thus, the *in silico* analysis mimicked this type of behaviour by including an unrecorded snack intake, the effect of which was still favourably offset by the $1/\sqrt{n}$ convergence rate of the parameter values. However, if similar un-modelled effects are substantial and frequent, the quality of results would deteriorate. In reality, the group that may gain advantage from this type of model based glycaemic regulation is a subgroup of people with T1DM who are willing to undergo relatively stricter control regimens and are more meticulous at diary recording. In particular, the diary data taken by such individuals must include information on exercise, stress and fatigue. However, new software and technology can ease and improve this process by augmenting and even replacing traditional diary-taking methods.

The glycaemic model used was relatively simple but allowed the key governing dynamics to be captured. There are a few quantitative models of the impact of exercise on metabolism in diabetes (Dalla Man et al., 2009; Roy and Parker, 2007; Breton, 2008), but none that examine a wider range of secondary influences on glycaemic behaviour. The evidence suggests that moderate-intensity exercise causes non-insulin mediated glucose uptake (Yardley et al., 2013) and thus the linear glucose depletion model used in this analysis represents a valid estimate for the true dynamics. Likewise, with stress and sleep-deprivation, both are known to reduce insulin sensitivity (Rizza et al., 1982; Räikkönen et al., 1996; González-Ortiz et al., 2000), but the specific dynamics are unknown. In particular, it is unknown whether the conditions interact additively or multiplicatively and how the physiological strength of the conditions increases with perceived intensity. The chosen model used additive stress and fatigue effects that increased in strength linearly with perceived intensity. All approximations served to validate the identification methods used and were thus acceptable at this stage in the research process. Due to the large number of assumptions made *in silico*, observational tests must be undertaken *in vivo* to validate

and improve this model.

A single 91 day data subset required 3.4 seconds to identify all parameters using the Gauss-Newton approach, and thus could be used in real time control. The full 730 day analysis required 578 seconds and would be cumbersome in real-time control. Ideally, secondary effects would only need to be identified once and could be used in concert with recent insulin sensitivity values, thus speeding up the process. Equally, a faster code than MATLAB could speed up this computation by 10-100×.

Inference of long-term drift in SI was enhanced by the penalisation of changes in SI across data subsets. In some cases, the random oscillations in SI drift patterns created some difficulty in establishing the underlying trends for individual runs. The penalisation process succeeded in reducing the oscillations. However it is also anticipated that changes in SI could be steeper than in this simulation. Studies have reported an average drop in insulin sensitivity of 50% for pubescent individuals (Hannon et al., 2006), and a 34% average drop over 3.3 years in pre-diabetics (Aizawa et al., 2014). Another study reports a 50% drop in insulin resistance (inversely related to SI) after 6 months dieting in obese individuals (Montastier et al., 2014). There are also significant changes in SI during pregnancy (Cousins, 1991) and even changes correlated to intake of certain spices (Kouzi et al., 2015). With larger changes compared to the impact of noise, the SI drift would be easier to discern.

Identification restrictions sometimes applied when fatigue and stress occurred concurrently such to create a non-identifiable problem in time periods of less than 4 weeks. Non-identifiability existed when σ_{max} and φ_{max} occurred concurrently. However, cases of non-identifiability ceased to occur for larger time periods due to the difference in timing of stressful and fatigued days. However, in an organic system there is very likely to be crossover between fatigue and stress, thus generating the need for a robust algorithm in real world application. While computational parameter identification will remain stable so long as there is at least some distinction

between periods of stress and fatigue, the validity of the results will be inclined to decrease with greater degrees of crossover.

While it is common knowledge that emotional stress causes hyperglycaemia (Surwit et al., 1992; Lloyd et al., 1999), parameter identification and control in this area has not effectively been attempted in outpatients and not in a self-reported data style presented in this research (Ward et al., 2011). Some people living with T1DM find continuous control of blood glucose arduous. This research is less aimed at meticulous persons who test often and maintain good control, either reactionary or proactive, but at those who consistently struggle to avoid hypo- and hyper- glycaemia and who are willing to adhere to dietary regimes and control protocols. For these people, secondary effects such as stress and exercise may play a huge role and to be able to quantify the strength of each secondary effect to even some degree of accuracy has real potential to improve their quality and length of life for this subgroup.

This analysis only considered a few of the many factors that are known to affect glycaemia. However, the methods developed in this chapter could be used to incorporate a larger number of additional secondary effects. For example, menstrual cycles affect blood glucose levels in women with diabetes (Lunt and Brown, 1996; Ramalho et al., 2009), and depression has an equivalent effect to that of stress (Nathan et al., 1981; Lustman et al., 2000) and other not yet investigated effects could also be tested.

9.7 Summary

This study presented and tested the robustness of a method to identify parameters for insulin sensitivity, exercise, stress and fatigue in the presence of sparse, irregular data that is noisy and includes errors of omission and accuracy typical of self-managed blood glucose diary data. It showed that sparse, irregular and noisy data could be overcome as such data accumulated to provide a clearer picture of patient status. Part I of this analysis showed that the reduction in CV for parameters in increasing

data was in accordance with the rule $1/\sqrt{n}$ and thus provided evidence that measurement error and other sources of noise cannot obscure the estimation of key glycaemic factors. Part II allowed for identification of secondary effects over longer time periods by capturing an anticipated long term drift in SI. Based on the results presented, the methods developed appear capable of measuring secondary effects in glycaemic control in patients living with T1DM. However, an *in vivo* observational trial should be undertaken to validate these findings with the ultimate purpose of providing tools to improve glycaemic control and quality of life of individuals that have T1DM.

Chapter X

Low road: a-posteriori identifiability

This chapter presents an evaluation of the practical identifiability of patient-specific parameters identified in sparse diary data from the virtual patient in the previous chapter. This work was published as a conference paper and presented at the 2015 World Congress for the International Federation of Automatic Control (Mansell et al., 2015b). The 'Low road' refers to the method being numerical rather than purely analytical, which by comparison would be substantially more difficult to derive.

10.1 Motivation

In the previous chapter seven glycaemic parameters were identified in sparse blood glucose data from a virtual patient. The results of the Monte Carlo analyses proved the parameters were all observable, and that measurement noise and un-modelled effects could be overcome as data size increased, with CV across the population reducing in proportion to $1/\sqrt{(n)}$ and only small ($< 1\%$) biases resulting after one year. To observe long-term drift in SI, a 90 day data window was progressed along a 2 year period to identify parameters in a moving average. Information for stress, fatigue and exercise parameters were still able to be captured with biases remaining less than 1% and CV being approximately equivalent to drift-free outcomes.

Practical non-identifiability occurs when experimental data is of insufficient quality or quantity compared to the size of a model Raue et al. (2009); Docherty et al. (2011) as explained in Section 3.3.2. This chapter investigates identifiability in the six most variable parameters from the original seven-parameter model. Specifically, the aim is to determine the data quantity required to support all six parameters without encountering such parameter interference.

10.2 Methods

All computation was carried out in MATLAB R2014a. The virtual patient in this chapter was modelled and simulated the same as that of Section 9.2.1.

10.2.1 Parameter identification

Like the previous chapter, the Gauss-Newton method of gradient descent was used to identify the least squares solution of variable set $\mathbf{x}$ by minimising the residual error between the sampled and forward-simulated blood glucose (Equation (9.20)) over several iterations. This time, however, parameters of interest were subsets of those in the set:

$$\mathbf{x} = [SI_1, SI_2, SI_3, \varepsilon_{max}, \sigma_{max}, \varphi_{max}]^{\mathrm{T}} \tag{10.1}$$

where between 2 and all 6 of these parameters were identified as variables when required. Variables were initially set to relevant subsets of $x_0 = [10^{-3}, 10^{-3}, 10^{-3}, 1, 0.1, 0.1]^{\mathrm{T}}$ and Gauss-Newton iterations were continued until the tolerance criteria $\left|\left|\frac{x_{i-1}-x_i}{x_0}\right|\right|_2 < 10^{-4}$ yielded approximately 4 significant figures of convergence precision on parameter estimates.

10.2.2 Structural identifiability and stability checks

When instances of exercise, stress or fatigue were not present in an identified period of time, ε_{max}, σ_{max} and φ_{max} were set to zero and excluded from identification. When both stress and fatigue effects occurred concurrently yielding a structurally non-identifiable system, both parameters were excluded, as their effects can only be quantified when there are distinguishable instances (Docherty et al., 2011; Bellu et al., 2007).

For occasional instances in small sets of data where noise and un-modelled effects rendered Gauss-Newton identification unstable (when singular matrix occurred or $i > 30$), latter variables were removed from the process every 20 iterations until successful identification occurred.

10.2.3 Error analysis proof of concept

The broad concept behind this method of evaluating practical identifiability begins by considering the error between simulated and identified values in parameters for an increasing dataset size, similar to the previous chapter (Mansell et al., 2015d). However, to evaluate whether or not to identify a new, previously *a priori* parameter without reducing practical identifiability, the error in the original identified variables is considered both with and without the new parameter identified in increasing dataset size. A new specification, the norm error, was created to singularly quantify the effect of the introduced parameter on the full set of previously identified variables.

Forty days of data was simulated, and this data was broken up into subsets of 0-1, 0-2, 0-3, to 0-40 days. Initially only SI_{1-2} was identified with incorrect '*a priori*' values set for the remaining parameters: $SI_3 = 0.4 \times 10^{-3}$, $\varepsilon_{max} = \sigma_{max} = \varphi_{max} = 0$. Then SI_3 was also included as an identified variable. Figure 10.1 shows the SI parameter estimates when identifying two versus three variables for a particular virtual patient, to demonstrate the error analysis concept. Note that the 3-variable set yielded larger error in SI_2 for days 1-10 compared to the 2-variable set. This shows the trade-off that SI_3 causes in SI_2 for small datasets.

The combined specification of norm error for the 2-variable subset $\mathbf{x} = [SI_1, SI_2]$ was calculated as:

$$e = \left|\left| \frac{\mathbf{x} - \mathbf{x}_{true}}{\mathbf{x}_{true}} \right|\right|_2 \tag{10.2}$$

where $\mathbf{x}_{true}$ is the original model input. Norm error was calculated for these two variables both for 2-variable and 3-variable identification. Figure 10.2 shows how e changes for the increasing dataset sizes. After approximately 23 days of data, the combined norm-error for SI_{1-2} is reduced with the introduction of SI_3 into the variable set.

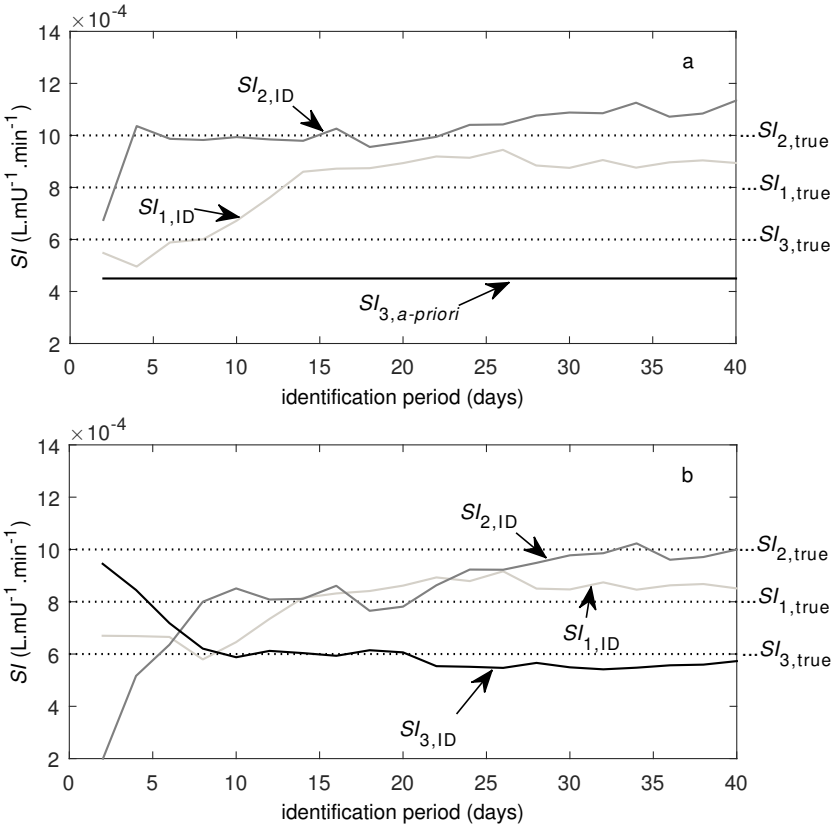

Figure 10.1: Identification for a data set with 2 variables plus one *a priori* parameter (a) and all 3 as variables (b).

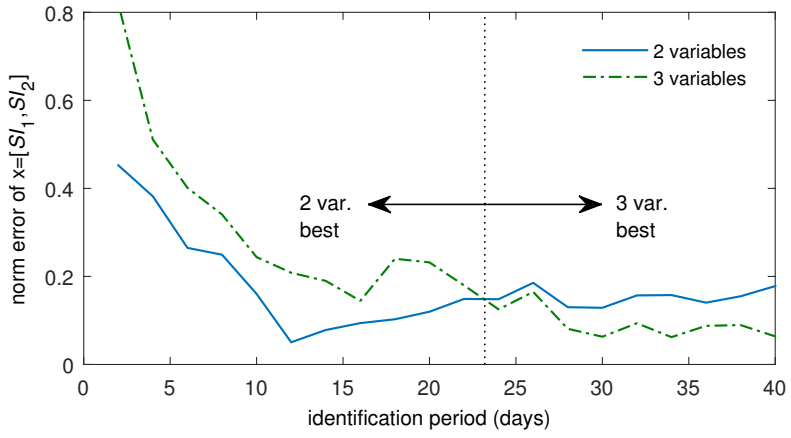

Figure 10.2: Norm-error of SI_{1-2} for 2 and 3 variable identification sets. Prior to 23 days the least error is achieved by treating SI_3 as *a priori*, afterwards it is better identified as a variable.

10.2.4 Monte Carlo analysis

A more thorough error analysis was carried in a Monte Carlo population of virtual patients, investigating the effect of each new parameter addition: SI_3, ε_{max}, σ_{max}, and φ_{max}.

This time, 89 days of data was simulated for 1000 patients. These datasets were broken into subsets from zero to [2, 3, 5, 8, 13, 21, 34, 55, 89] days. SI_{1-2} were identified for all data subsets for all patients. SI_3, ε_{max}, σ_{max}, and φ_{max} were all added to the variable set one at a time, with new identification occurring at each addition. Norm-error was calculated for variable subsets $\mathbf{x}_{1-2}$ for all results, $\mathbf{x}_{1-3}$ when 3 or more variables were identified, and so on up to norm-error of $\mathbf{x}_{1-5}$ for 5 and 6 variable cases. The specific day when an increase in the number of variables yielded improved precision in each previous variable subset were located for the population mean.

To quantify the effects of variability on the population outcomes, the 89 day subset was used to calculate mean reduction in norm-error for each variable subset from $\mathbf{x}_{1-2}$ to $\mathbf{x}_{1-5}$ for each variable introduction. This reduction in norm-error was defined as:

$$1 - \frac{\bar{e}_{new}}{\bar{e}_{old}} \tag{10.3}$$

The fraction of non-improved cases was also calculated.

10.3 Results

Figure 10.3 is the population equivalent of Figure 10.2, extended to show the effect of further parameter introductions on SI_{1-2}. For the Monte Carlo population mean, the point at which a 3-variable set favoured the precision of SI_{1-2} was at four days. Introducing ε_{max}, σ_{max}, and φ_{max} as variables reduced the SI_{1-2} norm-error at three, nine and 34 days, respectively.

Further consideration was taken into to the norm-error of variable sets

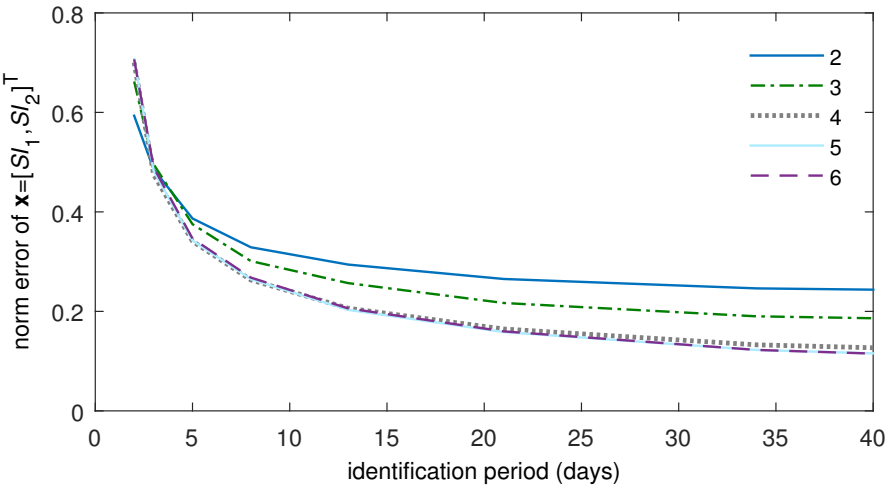

Figure 10.3: Norm error of SI_{1-2} as 2-6 variables are identified over a population. Reduced error for variable introductions 3-6 occurs at 4, 3, 9 and 34 days.

greater than just SI_{1-2}. Table 10.1 shows that for the population mean, crossover days for beneficially introducing certain parameters into the variable set were comparable across all norm-error sets (e.g. ε_{max} improves norm-error of both SI_{1-2} and SI_{1-3} after 3 days). Additionally, the crossover days generally increased for subsequent variable additions (e.g. the 5th parameter, σ_{max}, can be introduced as a variable on average 3 days after the 4th parameter, ε_{max}).

Table 10.1: Mean day for an introduced parameter to improve precision in other variable sets.

parameter	variable subset evaluated				
introduced	$\mathbf{x}_{1-2}$	$\mathbf{x}_{1-3}$	$\mathbf{x}_{1-4}$	$\mathbf{x}_{1-5}$	average
$x_3 = SI_3$	4				4
$x_4 = \varepsilon_{max}$	3	3			3
$x_5 = \sigma_{max}$	9	5	5		6
$x_6 = \varphi_{max}$	34	27	27	26	29

Table 10.2 gives statistics for the degree of norm-error improvement after 89 days for each increase in variable number. Identifying SI_3 reduced

norm-error in SI_{1-2} by 29% on average, only failing to improve the error in 1% of cases. Introducing the exercise parameter, ε_{max}, produced greater mean error reductions (28 and 41% for SI_{1-2} and SI_{1-3}), but also had a greater no-benefit rate of 6-18%. Introducing stress, σ_{max}, and fatigue, φ_{max}, as variables had less benefit in error reduction, especially for φ_{max}, where mean reductions ranged from an increase in error of 6% to a reduction of 6% and no-benefit rates were 28-40%.

Table 10.2: Population variability statistics for 89 days of data with mean reduction in norm-error for parameter sets as subsequent parameters were introduced and the no-benefit rate where precision was not improved.

parameter introduced	statistic	variable subset evaluated			
		$\mathbf{x}_{1-2}$	$\mathbf{x}_{1-3}$	$\mathbf{x}_{1-4}$	$\mathbf{x}_{1-5}$
$x_3 = SI_3$	reduction	29%			
	no-benefit	1.3%			
$x_4 = \varepsilon_{max}$	reduction	28%	41%		
	no-benefit	18%	6.2%		
$x_5 = \sigma_{max}$	reduction	9.0%	23%	16%	
	no-benefit	20%	8.6%	16%	
$x_6 = \varphi_{max}$	reduction	-6.2%	6.2%	3.7%	2.6%
	no-benefit	40%	28%	34%	36%

10.4 Discussion

Introducing a new parameter into the identified set of variables can reduce the error of the original variables due to the ability of the introduced parameter to assume a value that has less associated error than an *a priori* estimate. In the example virtual patient, a comparison of Figure 10.1a and 10.1b shows that by the end of 40 days, the error in SI_{1-3} was less when SI_3 was identified as a variable, rather than taken as an incorrect *a priori* parameter. However, too little data results negates this beneficial effect. Figure 10.1b shows that identifying SI_3 introduced large error in SI_2 for small n. This outcome demonstrates that, at first, the data was not sufficient to support all the variables with any degree of accuracy, and reduced practical identifiability resulted in variable interference (Raue

et al., 2009; Docherty et al., 2011).

SI_{1-3} are equivalent parameters that peak at different times of the day. Hence the times at which data points were taken would influence accuracy in SI_{1-3} estimates. For example, if data points have largely been sampled in the morning, then the effect of the afternoon SI is not easily distinguishable, and the resulting error may propagate particularly strongly into the midday SI, as was the likely case in Figure 10.1b. As more data accumulated, with more random additions inevitably occurring in the afternoon, the afternoon SI began to achieve accuracy and all variables were benefited. This illustrates the concept of the contribution of data to practical identifiability.

While mean population results appear to clearly indicate when parameters should be introduced as variables (Figure 10.3), the trends fail to capture variability effects and thus represent an ideal case rather than average. In particular the population value averages out y-dimensional error in Figure 10.3 but thus misrepresents the x-dimensional location of mean crossover day, the sought after property. In fact, for individual sets of data there were frequently multiple crossovers points or none at all in the first 89 days. This reality cannot be captured by the mean, thus the statistical data of Table 10.2 was calculated.

Based on results for variability effects, SI_3 appears beneficial to introduce by day 89 since it reduced norm-error of SI_{1-2} in 99% of cases. Since the appearance of SI_3 was daily, its accuracy weighed heavily on the outcomes of other variables. Comparatively, stress occurred much less frequently and had lower gains for greater risk (no-benefit rate 9-20%). Exercise, ε_{max}, also appears to introduce large benefits (28-41%) but also represents a moderate no-benefit rate (6-18%). Since the model includes frequent exercise at the same time of day, not identifying ε_{max} is likely to skew at least one SI peak value, thus the risk from including the parameter in the model could be deemed acceptable.
Like stress, fatigue was relatively infrequent. Thus, many more days of data

were required to achieve accuracy and minimise interference with other variables. This can be seen in the higher no-benefit rates (28-40%) and lower gains (-6% to 6% error reduction). This indicates that both the σ_{max} and φ_{max} parameters should not be identified due to their tendency for error propagation in other parameters.

Of course, while introducing some parameters is likely to increase error in other parameters, this detriment must be weighed against the benefit identifying the new parameter itself. A small error increase could be an acceptable price for the advantageous information. However, a best case for all parameters could be achieved by identifying a base parameter set of regular and highly identifiable parameters, then fixing some or all of these parameters while performing a second identification round to ascertain the less frequent parameters.

An *in silico* analysis was the best platform for investigating the research presented in this paper since true parameter values are non-existent in real data. Therapeutic glycaemic modelling can be difficult due to the presence of measurement noise, un-modelled effects and sometimes practical non-identifiability. It has been shown that much of these effects can be accounted for in a stable manner through the timely addition of new parameters into the identified set of variables. It remains unknown how real data would respond to equivalent parameter introductions. However, the concepts explored in this chapter are foundational to development and and testing the efficacy of other analysis methods independent of error and perhaps instead evaluating properties such as variability in specific datasets.

There are many factors that can significantly affect the glycaemic dynamics of people with diabetes, not limited to those modelled in this report. The ability to identify a large number of such parameters in one set of data would be valuable. However, if certain parameters are introduced too soon during data accumulation, they can seriously reduce the precision of the other parameter estimates. If introduced too late, then un-modelled behaviour, or grey' noise, is the limiting factor on the precision of identified

variables. Hence the importance of this type of identifiability analysis.

10.5 Summary

Identification of increasing numbers of parameters generally improves error in the parameter group by capturing otherwise un-modelled effects. However insufficient data can reduce practical identifiability, increasing parameter interference and error. The point at which data does become sufficient was diagnosed through analysis of error in equivalent variable sets before and after parameter introduction.

Specific to this model and analysis, the two parameters SI_3 and ε_{max} appear reasonably beneficial to introduce after 89 days, while σ_{max} and φ_{max} may be better excluded until the other parameters can be well established and fixed.

Error-based analysis was ideal for exploring the effect of practical identifiability on the model, but will ultimately be ineffective for *in vivo* data, requiring improved methods. Identifying large numbers of parameters with known confidence would be useful in diabetes. Greater knowledge of secondary glycaemic factors, could achieve improved glycaemic control with greater lifestyle flexibility.

Chapter XI

High road: a priori identifiability

The content of this chapter is a more theoretical vein of research, developing an *a priori* practical identifiability evaluation method. This work was published as a conference paper and presented at the 2015 World Congress for the International Federation of Automatic Control (Mansell et al., 2015c) with a small investigation on additive noise included as further work. The 'High road' refers to the development of a more pure analytical method. Analytical methods are often more complicated to ascertain than their numerical counterparts.

11.1 Motivation

Physiological modelling is becoming a standard approach to investigating complex biological systems to recover parameter values that cannot be directly measured (Saccomani, 2013). Nonetheless, outcomes of such parameter identification should not necessarily be accepted without evaluation of the credibility of the results and models. Structural identifiability is a discernible binary model property that states that under ideal data conditions the unknown parameters can be uniquely and exactly recovered from input-output relationships (Bellu et al., 2007). However, affirmation of structural identifiability is not in itself sufficient to ensure precision in identifying true parameter values.

In recent years, analysis methods have emerged to detect and evaluate practical rather than structural non-identifiability. These methods determine when the data quantity and quality is insufficient for the size of a model, resulting in mutual interference of two or more parameters (Docherty et al., 2011; Raue et al., 2009; Saccomani, 2013). The result of such interference is increased parameter variability and bias with no clear

cause. Thus, practical identifiability analyses are greatly beneficial when designing and utilising models identified from noisy data, since they can diagnose problems that structural identifiability analyses cannot (Docherty et al., 2011).

This chapter presents preliminary research into a new method of practical identifiability analysis that aims to link properties of a model, data size and measurement error to variance in results expected from a population of data. Information about population variance can be captured by a Principal Component Analysis (PCA), which is a multivariate analysis that reduces data variability to a new set of variables calculated from an eigen-decomposition problem (Jolliffe, 1986). Thus, MC simulations were carried out *in silico* to find the connections from *a priori* model and data information to PCA outcomes.

11.2 Methods

11.2.1 The model

To prevent complex effects from obscuring underlying behaviours, a simple model was used as a precursor to larger physiological models. The output, $b(t)$, for discrete time steps, $t = (1, t_n)$, was produced from the superposition of step and ramp functions (pictured Figure 11.1):

$$b(t) = \alpha \mathrm{H}(t - t_{n/2}) + \frac{\beta t}{n} \tag{11.1}$$

where n is the number of discrete time steps, H is the Heavyside function that forms a binary step, $t_{n/2}$ is rounded up to the nearest integer, and α and β are constant parameters equal to 1 unless stated otherwise.

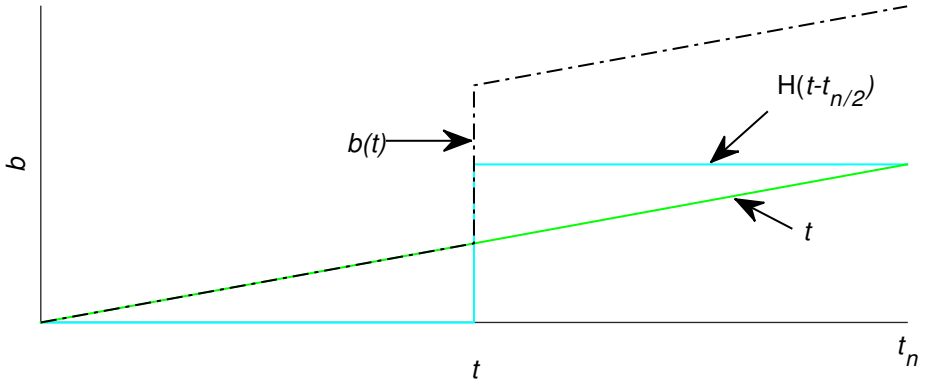

Figure 11.1: A graphical representation of the model

11.2.2 Parameter identification

Linear regression of the model for discrete output data gives:

$$\mathbf{Ax} = \mathbf{b} \tag{11.2}$$

$$\mathbf{A} = \begin{bmatrix} 0 & \frac{1}{n} \\ 0 & \frac{2}{n} \\ \vdots & \vdots \\ 0 & \frac{t_{n/2-1}}{n} \\ 1 & \frac{t_{n/2}}{n} \\ 1 & \frac{t_{n/2+1}}{n} \\ \vdots & \vdots \\ 1 & \frac{t_n}{n} \end{bmatrix}, \mathbf{x} = \begin{bmatrix} \alpha \\ \beta \end{bmatrix}, \text{and } \mathbf{b} = \begin{bmatrix} b_1 \\ b_2 \\ \vdots \\ b_{n/2-1} \\ b_{n/2} \\ b_{n/2+1} \\ \vdots \\ b_n \end{bmatrix} \tag{11.3}$$

(11.4)

Random multiplicative white noise was introduced to $\mathbf{b}$ to create an imperfect data set ($\hat{\mathbf{b}}$):

$$\hat{\mathbf{b}} = \mathbf{b} \odot (\mathbf{1} + \mathbf{e}) \text{ for } \mathbf{e} \subset \mathbb{N}(\mathbf{0}, \sigma^{\mathbf{2}}) \tag{11.5}$$

where the $\odot$ symbol indicates element-wise vector multiplication.

The least-squares solution ($\hat{\mathbf{x}}$) of the variables for α and β to the noisy data

Table 11.1: Variable definitions for Monte Carlo simulation schemes, where n = data size, $\mathbf{x}$ is the true solution to the parameters, σ = output error standard deviation, and γ is an arbitrary variable.

scheme	constants	variables
1a	$n = 10$,$\mathbf{x} = [1, 1]^{\mathrm{T}}$,$\sigma = 0.1$	none
1a	$n = 10$,$\mathbf{x} = [1, 1]^{\mathrm{T}}$,$\sigma = 0.2$	none
1a	$n = 50$,$\mathbf{x} = [1, 1]^{\mathrm{T}}$,$\sigma = 0.1$	none
2	$n = 10$,$\mathbf{x} = [1, 1]^{\mathrm{T}}$	$\sigma = 0, 0.1, 0.2, \ldots, 1$
3a	$n = 10$,$\sigma = 0.1$	$x = [1, \gamma]^{\mathrm{T}}, \gamma = 4, 8, \ldots, 100$
3b	$n = 10$,$\sigma = 0.1$	$x = [\gamma, \gamma]^{\mathrm{T}}, \gamma = 4, 8, \ldots, 100$
3c	$n = 10$,$\sigma = 0.1$	$x = [1, \gamma^{1.5}]^{\mathrm{T}}, \gamma = 4, 8, \ldots, 100$
4	$\sigma = 0.1$,$\mathbf{x} = [1, 1]^{\mathrm{T}}$	$n = 4, 8, \ldots, 100$

set was calculated as:

$$\hat{\mathbf{x}} = (\mathbf{A}^{\mathrm{T}}\mathbf{A})^{-1}\mathbf{A}^{\mathrm{T}}\hat{\mathbf{b}} \tag{11.6}$$

11.2.3 Monte Carlo simulation and variables

Parameter outcomes from multiple data sets 1 through r, each with random multiplicative white noise of variance σ^2, were stored in a matrix:

$$\mathbf{X} = [\hat{\mathbf{x}}_1\ \hat{\mathbf{x}}_2 \cdots \hat{\mathbf{x}}_r]^{\mathrm{T}} \tag{11.7}$$

This process was carried out using 10^6 repeats for each combination of noise variance (σ^2), true parameter values ($\mathbf{x}$), and data length (n). Several testing schemes, described in Table 11.1, were investigated. Schemes 1a-c used single combinations of these properties while schemes 2-4 used variable inputs over a range in order to capture trends.

11.2.4 Analysis

For schemes 1a-c, two dimensional objective surfaces were created over a range of α and β of -0.5 to 2.5 by taking the norm of residual error between the output created by these combinations of $\mathbf{x}$ and that of true output ($\mathbf{b}$):

$$\psi(\mathrm{x}_1, \mathrm{x}_2) = ||\mathbf{A}\mathbf{x} - \mathbf{b}||_2 \tag{11.8}$$

Correlation between the matrix equation and resulting MC scatter was sought by carrying out eigen-decomposition on the 2×2 $\mathbf{A}^{\mathrm{T}}\mathbf{A}$ matrix, and comparing it to outcomes of the PCA on the $\mathbf{X}$ matrix. PCA first involves calculation of a mean-centred matrix ($\bar{\mathbf{X}}$) that contains both columns of $\mathbf{X}$ in Equation 5 with their mean value subtracted. This is followed by an eigen-decomposition of the covariance matrix ($\mathbf{C}$), defined:

$$\mathbf{C} = \frac{1}{r-1}\bar{\mathbf{X}}^{\mathrm{T}}\bar{\mathbf{X}} \tag{11.9}$$

Both PCA and $\mathbf{A}^{\mathrm{T}}\mathbf{A}$ eigenvectors were compared and eigenvalue trends correlated to other independent variables.

11.2.5 Additive noise model validation

The majority of modelling and analysis for this investigation utilises multiplicative white noise. Multiplying the noise significantly complicates the relationship between *a priori* information and PCA outcomes compared to adding white noise. For additive noise, the relationship can be modelled:

$$\lambda_{PCA} = \frac{\sigma^2}{\lambda_{\mathbf{A}^{\mathrm{T}}\mathbf{A}}} \tag{11.10}$$

To validate this eigenvalue relationship on the step-ramp model, PCA outcomes were compared to the *a priori* modelled PCA eigenvalues from Equation (11.10) for a 10^6 Monte Carlo population with additive noise. For this population, $\alpha = \beta = 1$ was assigned, although another arbitrary parameter combination was also tested. A range of n from 2 to 100 was used.

11.3 Results

All analysis were carried out using MATLAB R2014a. Eigen-decomposition analysis showed that the $\mathbf{A}^{\mathrm{T}}\mathbf{A}$ eigenvectors were parallel with the principal components of the parameter distribution from the MC analysis of scheme 1a, Figure 11.2. PCA produced the greatest eigenvalue in the direction of greatest spread, while the smallest eigenvalue of $\mathbf{A}^{\mathrm{T}}\mathbf{A}$ was in this direction.

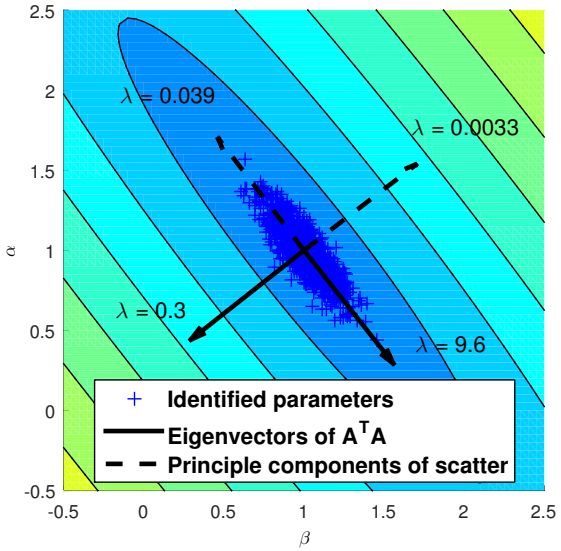

Figure 11.2: A comparison of $\mathbf{A}^{\mathrm{T}}\mathbf{A}$ eigenvectors and principal components of parameter identification scatter, pictured on an error objective surface. $\sigma = 0.1$, $n = 10$.

Doubling the standard deviation of noise in the output data (scheme 1b) did not affect the eigenvector direction but created a larger distribution of parameters, as seen in Figure 11.3. The change in output noise did not affect the $\mathbf{A}^{\mathrm{T}}\mathbf{A}$ eigenvalues but PCA eigenvalues were both quadrupled in value.

Increasing the data quantity by 5 times (scheme 1c) reduced the parameter spread to a comparable width of scheme 1a although the output noise was still that of scheme 1b. In this case, increased steepness in the objective surface was accompanied by greater $\mathbf{A}^{\mathrm{T}}\mathbf{A}$ eigenvalues, 533% and 435% of their scheme 1a-b values, and decreased PCA eigenvalues, at 13% and 23% of their scheme 1b values, respectively. There was also a reduced eccentricity of the elliptical contours in the objective surface and an alteration in both the eigenvalue ratios (λ_1/λ_2), increasing for $\mathbf{A}^{\mathrm{T}}\mathbf{A}$ and decreasing for PCA, which in both cases corresponded to a reduced difference between λ_1 and λ_2.

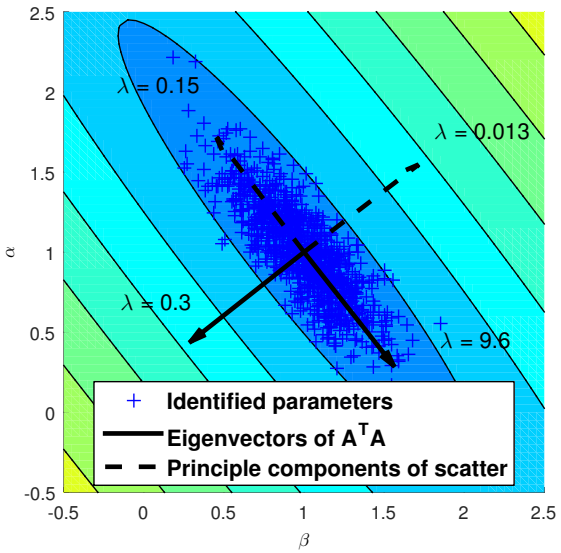

Figure 11.3: A comparison of $\mathbf{A}^{\mathrm{T}}\mathbf{A}$ and PCA eigenvectors with double the noise from Figure 11.2. $\sigma = 0.2$, $n = 10$.

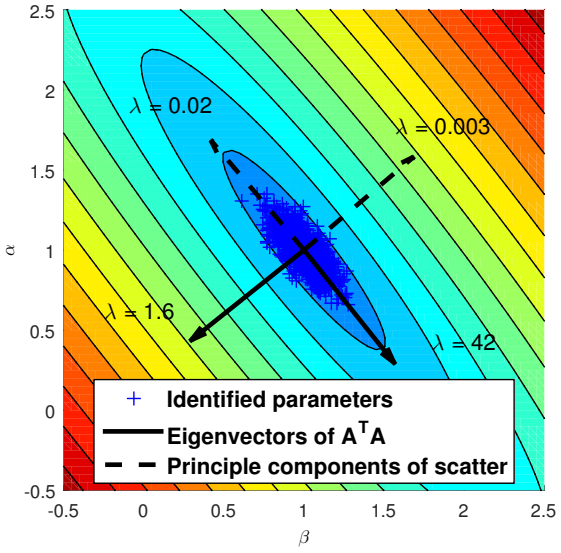

Figure 11.4: A comparison of $\mathbf{A}^{\mathrm{T}}\mathbf{A}$ and PCA eigenvectors now with five times the data points compared to Figure 11.3. $\sigma = 0.2$, $n = 50$.

Scheme 2 investigated the effects of changing the relative contribution of model parameters ($\mathbf{x}$) when $\mathbf{A}$ and therefore the $\mathbf{A}^{\mathrm{T}}\mathbf{A}$ eigenvalues were unaffected. The results gave a strong linear correlation between PCA eigenvalues and noise variance (R^2 = 1.0000 for λ_{1-2}), with the full relationships listed in Table 11.3. The eigenvalues had zero-value for zero noise and the ratio between eigenvalues, λ_1/λ_2, was consistent at approximately 11.8 through all noise values.

Like the effect of noise, changes to the parameter values in $\mathbf{x}$ influenced PCA and also had no effect on the properties of $\mathbf{A}^{\mathrm{T}}\mathbf{A}$. Scheme 3a and 3b both resulted in strong linear correlation between the eigenvalues of the PCA and the square of the variable γ (relationships listed in Table 11.3, R^2 = 1.0000). However, eigenvalues λ_{1-2} for scheme 3b were approximately 4-5 times greater than those of 3a. In scheme 3c, where one parameter was equal to $\gamma^{1.5}$, the PCA eigenvalues were now proportional to γ^3 (Table 11.3, R^2 = 1.000). The ratio PCA eigenvalues fitted well with a two-term power model: $\lambda_1/\lambda_2 = a\gamma^b + c$ for both schemes 3a and 3c while 3b showed no changes in the ratio, seen in C11.5. Table 11.2 gives the value of these power model parameters and the R^2 values.

The results of scheme 4 showed that the $\mathbf{A}^{\mathrm{T}}\mathbf{A}$ eigenvalues were linearly proportional to data size while the PCA eigenvalues were inversely so (Table 11.3, R^2 = 1.000). Ratios of λ_1/λ_2 were affected by data size in both cases. A two-term power model was fitted to this trend, Figures 11.6-11.7 (PCA R^2 = 1.0000, $\mathbf{A}^{\mathrm{T}}\mathbf{A}$ R^2 = 0.997). However, the residual error (not shown), particularly for $\mathbf{A}^{\mathrm{T}}\mathbf{A}$ data, reveals behaviour uncaptured by these models.

Figure 11.8 shows the performance of this model for a range of n in 10^6 repeats of a Monte Carlo simulation. The *a priori* model appears to fit well with the PCA outcomes and the residual shows no systemic bias. Equivalent outcomes occurred with arbitrary choices of $\mathbf{x}$ (data not shown).

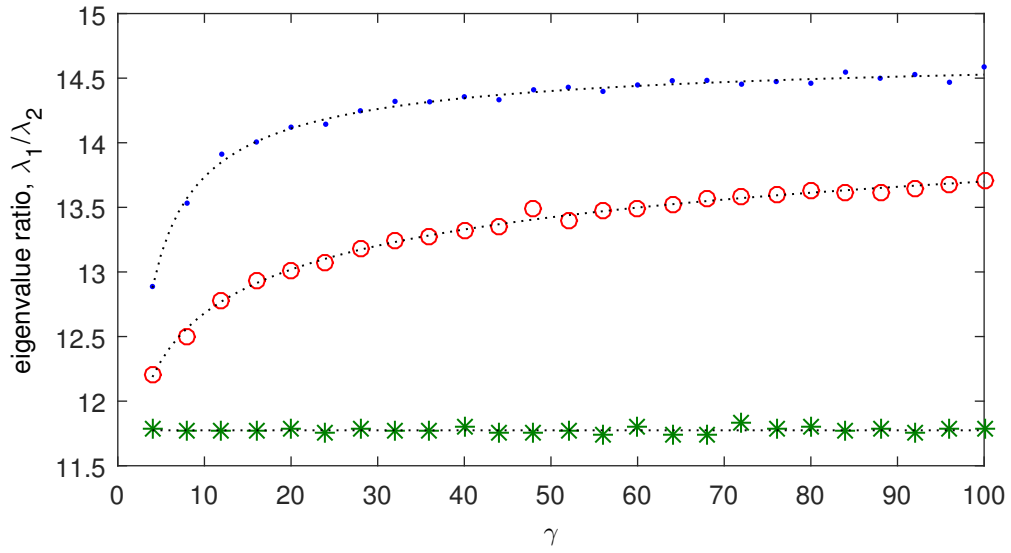

Figure 11.5: Results for PCA eigenvalue ratio compared with changes in γ, which influences $\mathbf{x}$. Schemes 3a and 3c are fitted to two-term power models while 3b is fitted to a horizontal function.

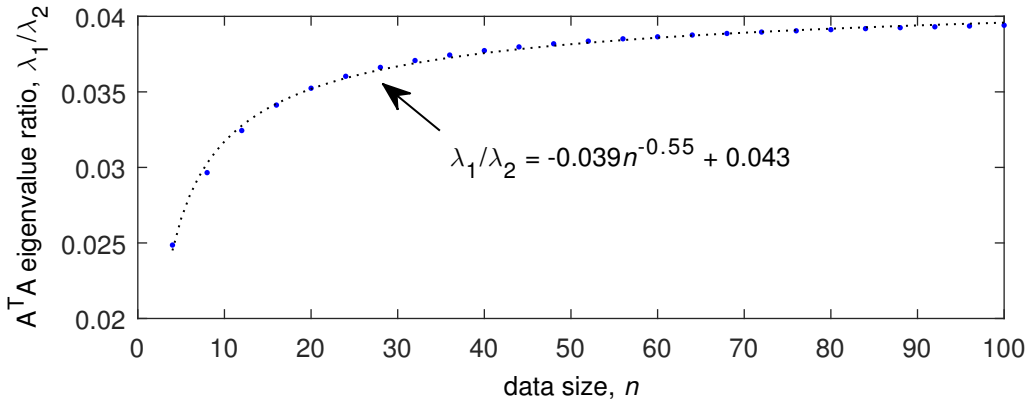

Figure 11.6: Results for PCA eigenvalue ratio against n.

Table 11.2: Model fits for eigenvalue ratio compared to the variable γ for two schemes where $\mathbf{x} = f(\gamma)$.

model	scheme	a	b	c	R^2
$\frac{\lambda_1}{\lambda_2} = a\gamma^b + c$	3a	-4.74	-0.674	14.7	0.993
	3b	0	-	11.8	-
	3c	-5.46	-0.124	16.8	0.994

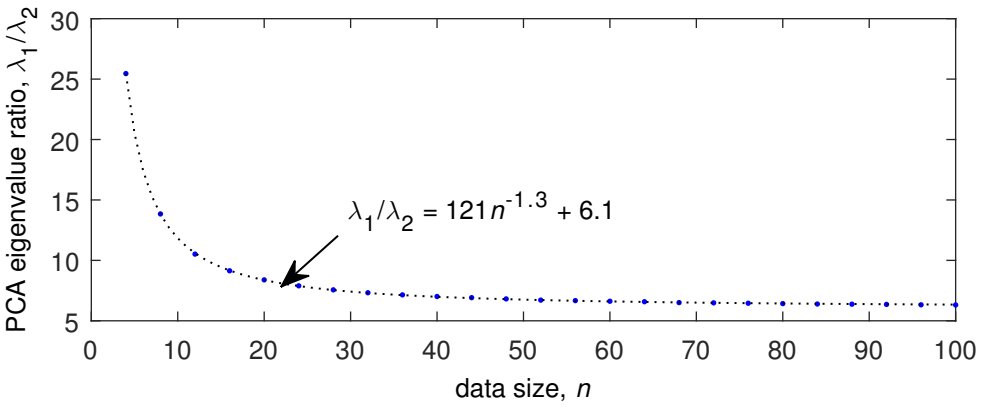

Figure 11.7: Results for $\mathbf{A}^{\mathrm{T}}\mathbf{A}$ eigenvalue ratio against n.

Table 11.3: Relationships found between model and data variables against the eigenvalues of PCA and $\mathbf{A}^{\mathrm{T}}\mathbf{A}$ eigenvalues against variables for schemes 2-4.

scheme	PCA relations	$\mathbf{A}^{\mathrm{T}}\mathbf{A}$ relations
2	$\lambda_1 = 3.88\sigma^2$ $\lambda_2 = 0.33\sigma^2$	$\lambda_1 = 0.30$ $\lambda_2 = 9.6$
3a	$\lambda_1 = 0.0090\gamma^2 + 0.35$ $\lambda_2 = 0.00062\gamma^2 + 0.035$	$\lambda_1 = 0.30$ $\lambda_2 = 9.6$
3b	$\lambda_1 = 0.039\gamma^2 - 0.041$ $\lambda_2 = 0.0033\gamma^2 + 0.0017$	$\lambda_1 = 0.30$ $\lambda_2 = 9.6$
3c	$\lambda_1 = 0.011\gamma^3 + 65$ $\lambda_2 = 0.00079\gamma^3 + 6.0$	$\lambda_1 = 0.30$ $\lambda_2 = 9.6$
4	$\lambda_1 = (4.4n - 19)^{-1}$ $\lambda_2 = (26n - 41)^{-1}$	$\lambda_1 = 0.032n - 0.027$ $\lambda_2 = 0.80n + 1.5$

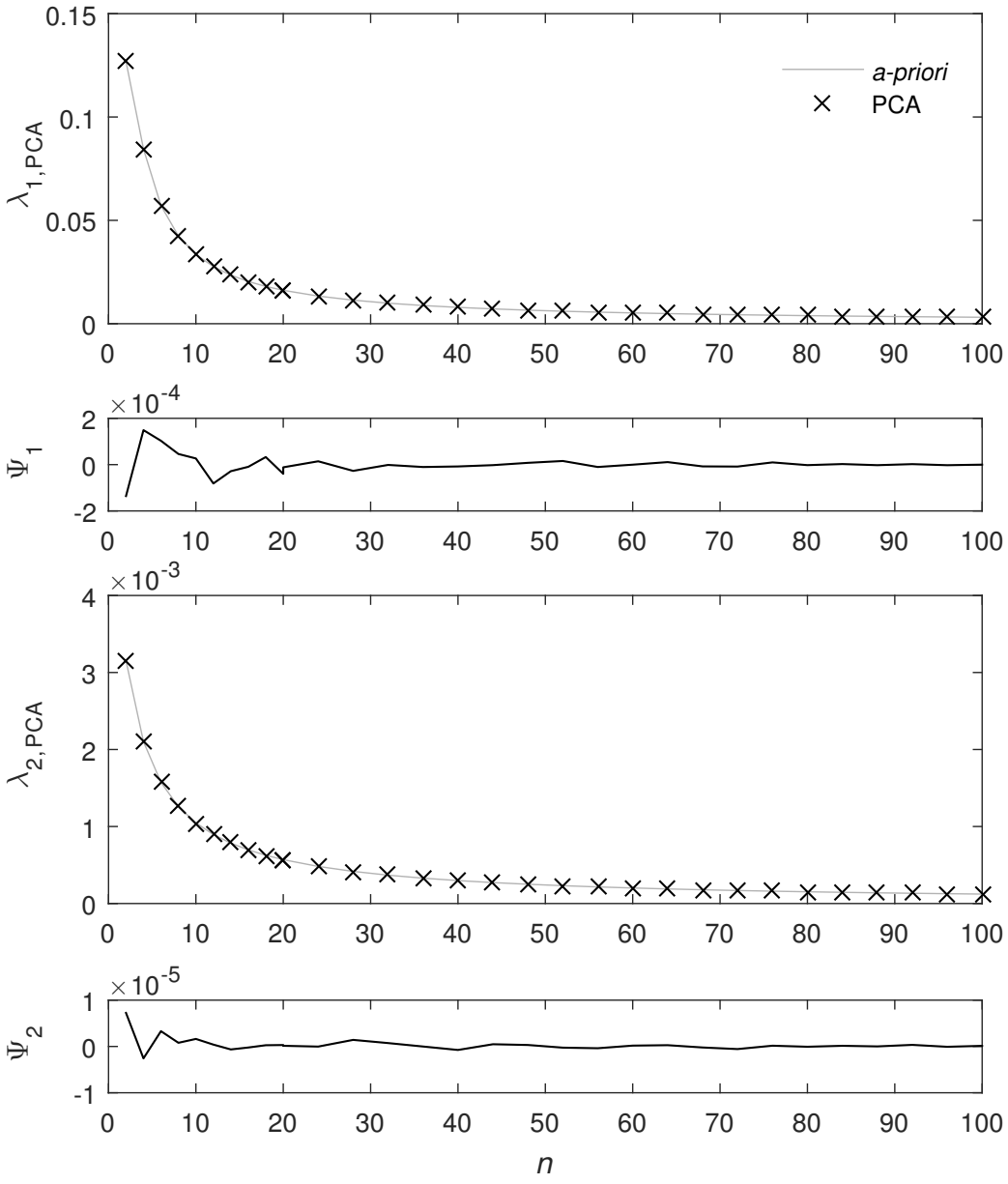

Figure 11.8: PCA eigenvalue outcomes for parameters identified in datasets of increasing size, alongside the *a priori* PCA eigenvalue model from Equation (11.10). Note the differing scales in the plots, especially for residual error (Ψ) which is relatively small compared to the respective eigenvalues.

11.4 Discussion

The relationships between eigenvectors of the model equation matrix ($\mathbf{A}^{\mathrm{T}}\mathbf{A}$) and Monte Carlo parameter spread shown in Figures 11.2-11.4, show deterministic behaviour that could contribute to advances in *a priori* model identifiability analyses. Should all the factors determining PCA eigenvalues be ascertained in a usable and broadly applicable manner, then there is potential to estimate wider outcomes of a population of data when only a single set is processed, as in some cases with real data. Several linearised relationships have been discerned for a simple model ($\mathrm{R}^2 = 1$).

Principal component information could be further processed into useful statistical measures such as variance or confidence limits on identified parameters *a priori*. For physiological models and analysis, these, in turn, could be used to evaluate the certainty of outcomes for diagnosis or control, or the degree of practical identifiability of model parameters with assumed data. Infinite confidence intervals indicate practical non-identifiability (Raue et al., 2009) and since identifiability is a continuous artefact (Docherty et al., 2011), smaller finite intervals could be useful in evaluating whether the degree of identifiability is acceptable, subject to the needs of the research or application. Where multiple models of a system are available, the practical identifiability of each could be compared to determine the best model for the data.

It is a useful outcome that the effect of noise in the output data on the resulting data spread was linearly correlated with noise variance by the relationship: $\lambda_{PCA} \propto \sigma^2$ with no changes to the ratio between eigenvalues. This result makes intuitive sense since noise drives the spread of identified parameters. With no noise, the true parameters would be identified and the spread would be zero in all directions, even for a practically non-identifiable, but structurally identifiable model. This relationship is likely applicable over a range of models where noise is confined to output data and is zero-mean.

The results clearly indicate a relationship between the PCA eigenvalues and the value of $\mathbf{x}$. This outcome was expected since the identified parameter set, $\hat{\mathbf{x}}$, is dependent on the noisy $\hat{\mathbf{b}}$ vector, defined Equation 3, which can also be defined as a function of the original parameter set:

$$\hat{\mathbf{b}} = \mathbf{E}\mathbf{b} = \mathbf{E}\mathbf{A}\mathbf{x} \tag{11.11}$$

where $\mathbf{E}$ is a diagonal matrix of $(1 + \mathbf{e})$. Thus substitution into Equation 4 yields an identified parameter definition of:

$$\hat{\mathbf{x}} = (\mathbf{A}^{\mathrm{T}}\mathbf{A})^{-1}\mathbf{A}^{\mathrm{T}}\mathbf{E}\mathbf{A}\mathbf{x} \tag{11.12}$$

The parameters $\mathbf{x}$ are further propagated into the data storage matrix, $\mathbf{X}$, and into the covariance matrix, $\mathbf{C}$, before eigen-decomposition where the eigenvalues for a 2×2 matrix can be calculated with:

$$\lambda = \frac{T_r}{2} \pm \sqrt{\frac{{T_r}^2}{4} - D} \tag{11.13}$$

where T_r and D are the trace and determinant of the matrix respectively. The calculation of these eigenvalues therefore appears to be deterministic, especially since it has already been shown that the effect of the noise can be described purely by the variance. Given the convolution involved in the substitution of full definitions of $\hat{\mathbf{x}}$ into the PCA eigenvalue equation, results drawn instead from MC simulations were highly valuable.

The evidence in Table 11.3 suggests that the eigenvalues are scaled by the dot product of $\mathbf{x}$ with itself, which is the sum of squared parameters:

$$\lambda_{PCA} \propto \mathbf{x} \cdot \mathbf{x} = \sum {\mathrm{x}_i}^2 \tag{11.14}$$

Both eigenvalues in each case are affected in the same manner proportionally and the order of that proportionality is the square of the highest order by which an $\mathbf{x}$ parameter changes. When one or both parameters was equal to γ then λ_{PCA} were strongly proportional to γ^2, though with greater magnitude for scheme 3b than 3a which shows an

accumulative effect of changes in the two parameters. Further, when one parameter was equal to $\gamma^{1.5}$ then λ_{PCA} were strongly proportionality to γ^3. In addition to this relationship, changing x-parameters altered eigenvalue ratios but only when parameters were affected to different orders than each other, otherwise the ratio was constant, as with scheme 3b when $\mathbf{x} = [\gamma, \gamma]^{\mathrm{T}}$. For cases 3a and 3c, the eigenvalue ratio changes fitted well with two-term power models where the exponent term on γ was between -1 and 0 in both cases. This outcome indicates that the eigenvalue ratio is related to the relative difference in appearance or in this case magnitude of the two species in the model: the step and ramp.

The relationships of $\mathbf{A}^{\mathrm{T}}\mathbf{A}$ and PCA eigenvalues to n and $n-1$ respectively for the step-ramp model (Table 11.3) highlights the inverse nature of the two. The PCA eigenvalues describe the level of spread in the direction of the principal components while the $\mathbf{A}^{\mathrm{T}}\mathbf{A}$ eigenvalues could be described as evaluating the steepness of the objective surface in the principal directions of the surface geometry. As the quantity of data increases, the steepness of the objective surface increases, confining the MC spread to a smaller area. There was also an n-dependence for both $\mathbf{A}^{\mathrm{T}}\mathbf{A}$ and PCA eigenvalue ratios, λ_1/λ_2, the latter of which fitted well to a two-term power model (Figure 11.6) where the exponent of n was -1.32. Similar to the case with the changing parameter values, the ratio change may be related to the relative changes in magnitude of the step and ramp as they appear in the matrix. For this model, as n increases, the norm of each column in $\mathbf{A}$ increases but at different rates due to the different forms of the species.

There are several limitations to this first analysis based on our findings. The foremost limitation is its restriction to systems with separable parameters where a matrix equation $\mathbf{Ax} = \mathbf{b}$ can be defined. There may also be issues with parameter models that yield non-elliptical objective surfaces, as they are poorly described by PCA. This issue could, in some cases, be remedied by identifying related parameters and inferring the desired parameter, for example identifying and evaluating $1/x_i$ instead of x_i. Another small limitation is that true noise variance may not be be

known in real data, though an estimate would likely be sufficient in most cases. Since PCA eigenvalues are dependent on $\mathbf{x}$, systems with low levels of practical identifiability and subsequent reduced accuracy in $\hat{\mathbf{x}}$ will likely influence how the identifiability of the system is perceived by the analysis. Model systems with $\mathbf{A} = f(\mathbf{x})$ have been shown in unpublished results to introduce much larger error than could be accounted for by this analysis.

Using a simple model was extremely useful for discerning some of the relationships between $\mathbf{A}^{\mathrm{T}}\mathbf{A}$ and PCA, all of which could contribute in some way to fundamental relations for more complex biological models. Ultimately, PCA eigenvalues could be robustly calculated with $\mathbf{A}^{\mathrm{T}}\mathbf{A}$, circumventing the need for population-wide data. There is still a missing link between changes in the properties of the $\mathbf{A}$ matrix and the resultant scaling of the eigenvalues and the altered eigenvalue ratio. All relationships must be found for the simple case prior to a deterministic approach for all models can be developed. Furthermore, direct links between PCA and parameter confidence estimates require research, though there appears to be deterministic relationships between the two.

Though the deterministic relationship is not yet fully defined for multiplicative white noise, additive white noise yields a much simpler relationship, described in Equation (11.10) where the variance in the scatter is inverse to the model eigenvalues, further scaled by the noise variance. It is clear that this eigenvalue model is valid for the step-ramp model (Figure 11.8) and is valid for arbitrary n and $\mathbf{x}$. The relationship may indeed be more widely applicable to other similarly simple models and perhaps even more complex models with linearly separable variables. The implication is that for such models, assuming additive white noise, it is easy to estimate the variation in population outcomes based on only the model, some data, and an estimate of the noise variance.

The simplicity of the additive model, while encouraging, is not directly applicable in the context of physiological modelling. In particular, blood glucose measurements generally have multiplicative error as opposed to

additive or mixed (Werner et al., 1978). In some situations, the magnitude of a measured species compared to its variation might allow for an additive noise approximation to be valid. However, this is not the case for blood glucose, especially in individuals with diabetes, since glucose can easily vary between 4 and 20 mmol/L. Nevertheless, the additive noise model will be useful as a reference for further work in defining the eigenvalue relationship with multiplicative noise.

Models can be used to measure, diagnose and predict the behaviour of many phenomenon. However, even well justified model formulations can cause failure of model-based analyses. Structural non-identifiability occurs when multiple model parameters trade off to describe the same behaviour. While some methods for determining model structural identifiability have been in existence for many decades (Pohjanpalo, 1978; Bellman and Åström, 1970; Ritt, 1950), there remains a consistent stream of research in this field (Audoly et al., 1998, 2001; Bellu et al., 2007).

This research is driven, in part, by the ambiguous identifiability of a particular model of glycaemic dynamics (Bergman et al., 1979; Cobelli et al., 1998; Pillonetto et al., 2002, 2003). More recently it has been discovered that the cause of this failure was practical rather than structural identifiability (Docherty et al., 2011). The Docherty et al. approach to practical identifiability analysis was descriptive rather than predictive but the relationships found, and deterministic nature of the MC analyses implies that the concept could become a predictive *a priori* practical non-identifiability analysis.

11.5 Summary

There are deterministic links between properties of the step-ramp model equation, data size and measurement noise to the resulting principal component analysis of a Monte Carlo simulation. Eigenvectors for $\mathbf{A}^{\mathrm{T}}\mathbf{A}$ and PCA line up directly and the eigenvalues are inversely related. $\mathbf{A}^{\mathrm{T}}\mathbf{A}$ eigenvalues describe magnitude of steepness in the objective error surface,

increasing linearly with data size for the model, and PCA eigenvalues describe the magnitude of spread from a population of data, with an inverse relationship to data size. Noise in output data increased PCA eigenvalues in proportion to noise variance. Principal component eigenvalues also appear to be a scaled dot product of the parameter set, $\mathbf{x} \cdot \mathbf{x}$, and differing orders of change between parameters alters eigenvalue ratio, likely due to different comparative magnitudes of the step and ramp in the model. Data size also produced eigenvalue ratio changes, but in both PCA and $\mathbf{A}^{\mathrm{T}}\mathbf{A}$, likely also related to comparative step-ramp magnitude.

Most but not all factors for direct PCA eigenvalue calculation have been ascertained for the simple step-ramp model. However, using additive rather than multiplicative noise yields a simple and deterministic relationship, though this has limited usefulness compared to multiplicative noise. Future research will include aims to find the missing links to multiplicative noise, as well as to research more complex biological models, and interval estimation on the basis of PCA. Confidence intervals estimated for a single parameter identification outcome, as opposed to a whole population, would be useful where little information is available. The level of confidence in parameters for diagnosis and control would be useful, along with the ability to evaluate the practical identifiability of a model and, where applicable, choose the best model for a set of data.

Chapter XII

Noise and gestational diabetes diagnosis

This chapter presents an *in silico* analysis exploring the extent that pre-analytical glucose decay in clinical OGTTs results in underdiagnosis of gestational diabetes. This work was done in collaboration with the Canterbury District Health Board who kindly provided de-identified OGTT data for a local population of pregnant women. The content of this chapter has been published in the Journal of Clinical Biochemistry (Mansell et al., 2017a)

12.1 Motivation

The two-hour OGTT is a standard method for clinical diagnosis of gestational diabetes (GDM). During the procedure, the fasted patient ingests a 75g oral glucose load. Venous blood samples are taken immediately before ingestion, at one hour after ingestion and two hours afterwards. These samples are assayed for blood glucose concentration and the values are then compared to diagnostic criteria for GDM. While many diagnostic levels exist, a commonly used criteria for GDM was defined by the International Association of Diabetes and Pregnancy Study Group (IADPSG). The IADPSG recommends diagnoses of GDM when any one of the thresholds are exceeded: fasting glucose $\geq$ 5.1 mmol/L; one-hour glucose $\geq$ 10.0 mmol/L; or two-hour glucose $\geq$ 8.5 mmol/L (Duran et al., 2014).

In typical clinical practice, tubes containing blood samples are treated with sodium-fluoride in order to preserve glucose concentration until laboratory analysis can take place. However, research has suggested that GDM is systematically underdiagnosed as the use of fluoride tubes to store blood prior to assays leads to significantly lower readings than gold standard

methods (Daly et al., 2016; Carey et al., 2016; Uchida et al., 1988). In particular, Uchida et al. (1988) found that fluoride tubes attenuate glucose decay but a minor reduction in serum glucose still occurs. This decay was on the order of 8% glucose and plateaued after approximately two hours at room temperature. Hence, the measurable glucose levels from samples stored in fluoride tubes reduces over the time between the sampling time and the laboratory process time. Since fasting, one-hour and two-hour samples tend to be batched and processed together, there is differing measured glucose bias in the three samples (Carey et al., 2016; Daly et al., 2016).

This investigation determines the likelihood of misdiagnosis of GDM in the presence of fluoride-induced bias in glucose measurement. Understanding the limitations of a diagnostic test is critical to applying it effectively and thus providing the best possible healthcare.

12.2 Methods

12.2.1 Cohort simulation

12.2.1.1 Virtual cohort

A cohort of 1 million virtual test subjects was simulated using glucose distributions that were summarised in a prior study by Hypoglycaemia and Adverse Pregnancy Outcomes (HAPO) (The HAPO Study Cooperative Research Group, 2008). Fasting (G_0), one hour (G_1) and two hour (G_2) glucose values were drawn from the distributions described by the following equations and pictured in Figure 1:

$$G_0 = 3.9 + \mathrm{e}^{\mathbb{N}(-0.8,0.6)} \tag{12.1}$$

$$G_1 = 2.1G_0 + \mathbb{N}(-1.9, 1.5) \tag{12.2}$$

$$G_2 = 0.2G_0 + 0.52G_1 - 2.3 + \mathrm{e}^{\mathbb{N}(1.3,0.24)} \tag{12.3}$$

where $\mathbb{N}(\mu, \sigma)$ is a normal distribution with a mean of μ and a standard deviation of σ.

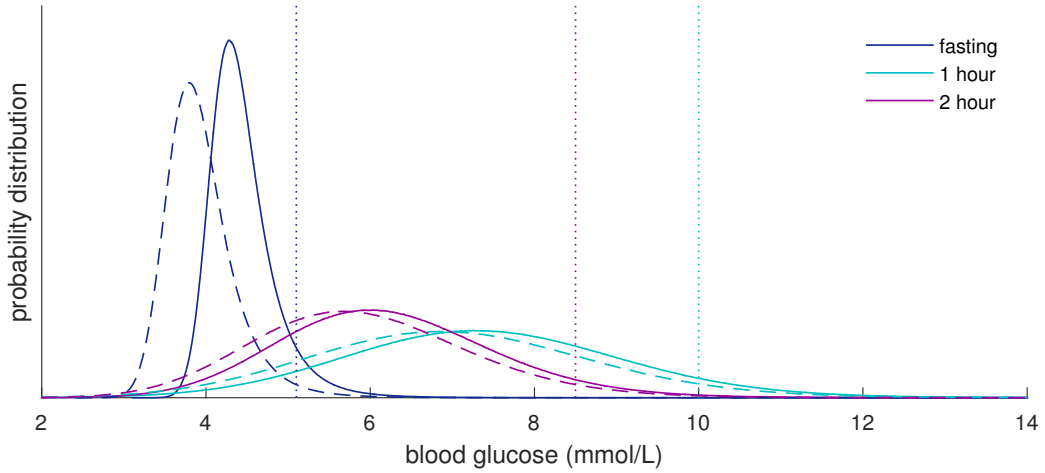

Figure 12.1: The probability distributions for fasting, 1 and 2 hour glucose in the simulated cohort. Solid lines indicate gold standard; dashed lines indicate fluoride tubes; dotted lines show the diagnostic thresholds.

These distributions were designed to create plausible OGTT results within ±2% of reported target values for mean ($G_0 = 4.5$ mmol/L, $G_1 = 7.4$ mmol/L, $G_2 = 6.2$ mmol/L), inter-sample correlation ($R_{0-1} = 0.38$, $R_{0-2} = 0.30$, $R_{1-2} = 0.68$) and standard deviations (0.4, 1.7, 1.3 mmol/L) based on the large ($n > 23,000$) HAPO study (The HAPO Study Cooperative Research Group, 2008).

Published intra-individual CV on glucose measurement reported by the HAPO study was 4.4% (Nesbitt et al., 2006). Hence, to mimic results from the gold standard (GS) glucose analysis methods used by HAPO, the simulated glucose values were multiplied by a normal distribution of values, $G_{h,GS} = G_h\mathbb{N}(1, 0.044)$ for $h = 0, 1$ and 2 hours.

Both Daly et al. (2016) and Carey et al. (2016) demonstrated differences in glucose results associated with using test tube preservatives with typical batching processes compared to research-grade methods equivalent to the gold standard methods utilised in HAPO. In the larger of the two studies by Daly et al., the mean error between fluoride tubes and the gold standard

method were -0.5, -0.4, and -0.2 mmol/L for G_0, G_1 and G_2 respectively. In the Carey et al. data, the standard deviations in the errors between fluoride and gold standard were approximately 4% of the mean measured fluoride-tube value. Hence, fluoride-tube glucose outcomes ($G_{0-2,F}$) were created with the following equations:

$$G_{0,F} = (G_{0,GS} - 0.5)\mathbb{N}(1, 0.04) \tag{12.4}$$

$$G_{1,F} = (G_{1,GS} - 0.4)\mathbb{N}(1, 0.04) \tag{12.5}$$

$$G_{2,F} = (G_{2,GS} - 0.2)\mathbb{N}(1, 0.04) \tag{12.6}$$

12.2.1.2 Real-virtual hybrid cohort

A hybrid cohort was created with real fluoride-tube glucose assays from pregnant women in New Zealand ($n = 1305$) that were used to simulate corresponding gold-standard data. The HAPO population on which the fully virtual cohort are based were randomly selected and thus representative of a typical population of pregnant women. In contrast, this cohort represents a population more typically administered this OGTT in a clinical context, who have first screened positive in the one-hour 50g OGTT. The typical New Zealand diagnostic criteria requires one glucose threshold to be exceeded out of $G_0 \geq 5.5$ and $G_2 \geq 9.0$ mmol/L.

The gold standard simulated values were created with the following equations, and both the real and simulated cohorts are pictured in Figure 12.2.

$$G_{0,GS} = G_{0,F}\mathbb{N}(1, 0.04\sqrt{2}) + 0.5 \tag{12.7}$$

$$G_{2,GS} = G_{2,F}\mathbb{N}(1, 0.04\sqrt{2}) + 0.2 \tag{12.8}$$

12.2.2 Analysis

The fluoride and true simulated OGTT results were evaluated against the IGADSG diagnosis criteria (Duran et al., 2014). By this criteria, patients

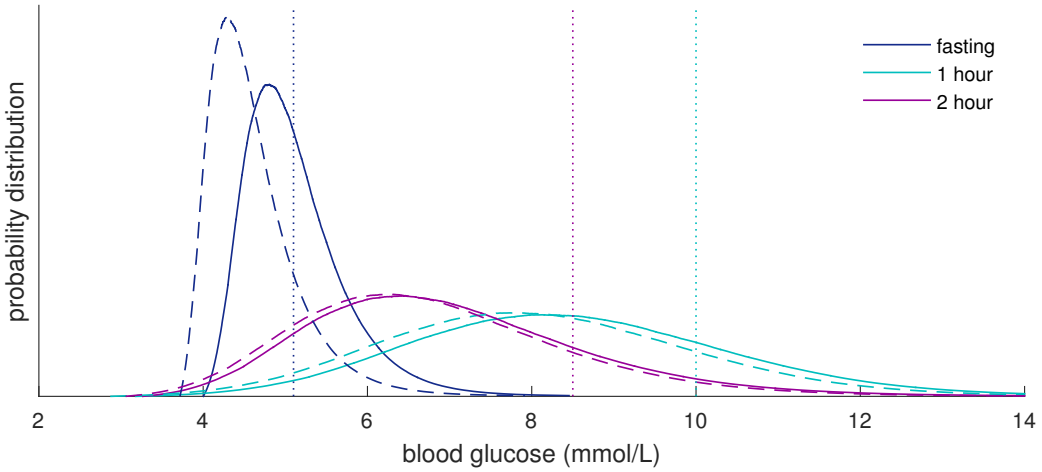

Figure 12.2: The $n = 1305$ cohort for fasting and two hour glucose. Dashed lines are real fluoride-preserved data; solid lines are the simulated gold standard cohort; dotted lines show the diagnostic threshold.

must exceed just one of the three glucose thresholds for a positive diagnosis. The thresholds are $G_0 \geq 5.1$,$G_1 \geq 10.0$,$G_2 \geq 8.5$ mmol/L. A confusion matrix was created to calculate the rate of true positive (TP), true negative (TN), false positive (FP) and false negative (FN) diagnostic outcomes using the fluoride tubes compared to gold standard methods. These rates were used to calculate the sensitivity ($\frac{\text{TP}}{\text{TP+FN}}$) and specificity ($\frac{\text{TN}}{\text{TN+FP}}$) of glucose measurements that were stored in fluoride tubes with respect to findings of the gold standard tubes.

Fluoride and gold standard outcomes were compared for each of fasting, one-hour and two-hour glucose with respect to the IGADSG thresholds on scatter plots. Receiver operating characteristic (ROC) curves were also created for fluoride against gold standard. To determine the glucose thresholds from fluoride tubes that match gold standard diagnostics, the optimal sensitivity and specificity obtainable from the fluoride tubes was determined. This optimal point was defined as the point closest to 100% sensitivity and specificity (the point closest to the top-left of the ROC curves), i.e. when $\min\left(|||[1-\text{sensitivity}, 1-\text{specificity}]||_2\right)$ is true.

All computational analysis were carried out in MATLAB R2015a on a 64-bit Intel® Core™ i7-4770 CPU @ 3.40GHz with 16.0 GB of RAM.

12.3 Results

Based on the OGTT results with the gold standard methods, 14% of the cohort met the requirements for a diagnosis of GDM (Table 12.1). Under two thirds of these individuals were also identified by the fluoride-tube OGTT. Hence the sensitivity was calculated as 57.5%. There were very few individuals (0.3%) diagnosed with GDM based on fluoride tubes who were not diagnosed with gold standard methods. Hence, the specificity was near 100%.

Figure 12.3 shows that fasting glucose has the lowest sensitivity with many FN outcomes (pink quadrant). One and two hour glucose have similar ROC curves, with reasonably high sensitivity. In contrast, the fasting glucose stored in the fluoride tube yielded poor sensitivity. table 12.2 shows that the fluoride-tube glucose thresholds with the optimum combination of sensitivity and specificity are 4.4, 9.2 and 7.9 mmol/L for G_{0-2} respectively.

The results for the hybrid cohort with NZ diagnostic criteria are very similar to those of the large *in silico* population with the IADPSG diagnostic criteria. The sensitivity of the test was 48.4% (Table 12.3), indicating approximately half of diagnosable patients were overlooked. Fasting glucose had very low sensitivity with many false negative outcomes, more so than two-hour glucose. Optimum glucose thresholds to achieve diagnostic equivalence were 4.8 and 8.5 mmol/L for and respectively (Table 12.4).

12.4 Discussion

The use of *in silico* modelling was effective in estimating and visualising the effect of glucose decay in fluoride tubes on clinical diagnosis outcomes on a large population of individuals. The results demonstrated that the typical

Table 12.1: The confusion matrix for the overall diagnostic outcomes, and each sample time, of fluoride-tube OGTT compared to OGTT with gold standard tube treatment in the virtual cohort. Note: contrary to typical confusion matrices, the orientation of the different boxes to gain consistency with Figure 12.3.

	OVERALL		G_0	
	Gold -ve	Gold +ve	Gold -ve	Gold +ve
Fluoride +ve	FP 0.3%	TP 7.8%	FP 0.0%	TP 1.8%
Fluoride -ve	TN 86.2%	FN 5.8%	TN 93.9%	FN 4.3%
	Specificity 99.6%	Sensitivity 57.5%	Specificity 100%	Sensitivity 29.4%

	G_1		G_2	
	Gold -ve	Gold +ve	Gold -ve	Gold +ve
Fluoride +ve	FP 0.2%	TP 4.5%	FP 0.2%	TP 3.5%
Fluoride -ve	TN 93.0%	FN 2.3%	TN 94.7%	FN 1.6%
	Specificity 99.8%	Sensitivity 66.3%	Specificity 99.8%	Sensitivity 68.6%

Table 12.2: Diagnostic characteristics at the point on the ROC curve closest to the top left corner for each sample time in the virtual cohort.

sample time	original sensitivity	original specificity	c-ROC	new threshold (mmol/L)	optimal sensitivity	optimal specificity
0 hour	29.4%	100%	0.990	4.4	95.5%	94.5%
1 hour	66.3%	99.8%	0.994	9.2	96.5%	96.3%
2 hour	68.6%	99.8%	0.995	7.9	97.0%	96.8%

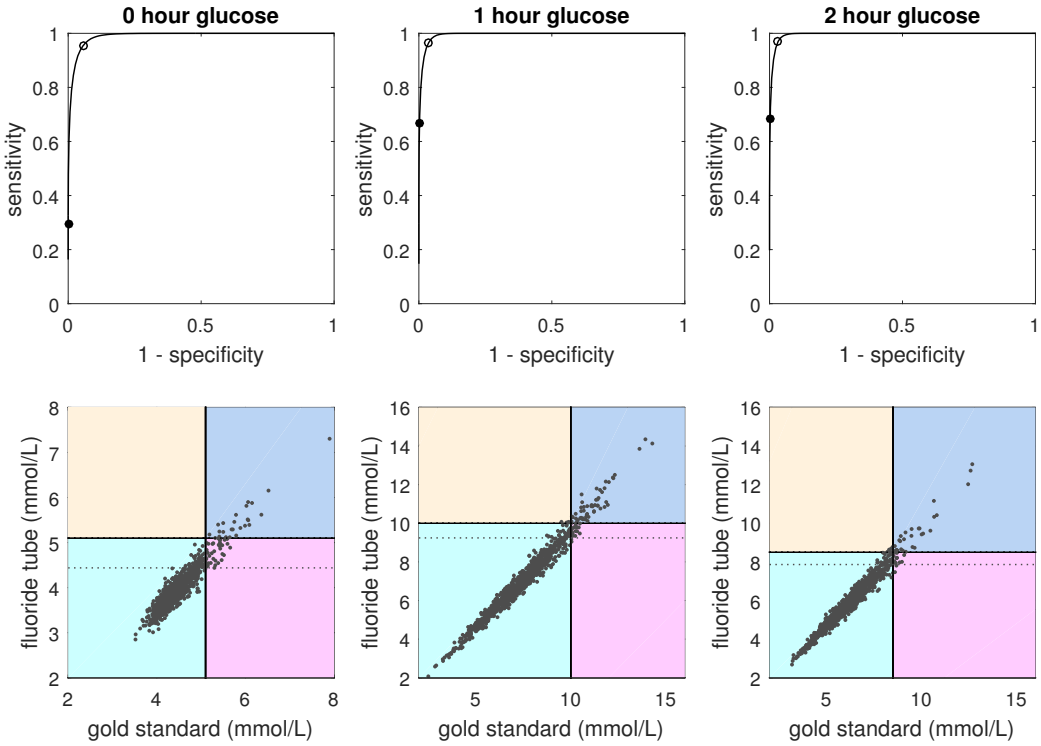

Figure 12.3: ROC curves for fluoride tubes vs gold standard in the virtual cohort, with the point of diagnostic threshold marked •, and optimal threshold marked ∘ (top row). Scatter plots of fluoride tubes vs gold standard glucose for a representative cohort of 1000, with the optimal threshold shown by the dotted line (bottom row).

Table 12.3: The confusion matrix for the diagnostic outcomes of fluoride-tube OGTT compared to OGTT with gold standard tube treatment for the hybrid $n = 1305$ cohort. Note: contrary to typical confusion matrices, the orientation of the different boxes to gain consistency with Figure 12.4.

	OVERALL		G_0		G_2	
	Gold -ve	Gold +ve	Gold -ve	Gold +ve	Gold -ve	Gold +ve
Fluoride +ve	FP 7	TP 171	FP 2	TP 78	FP 9	TP 113
Fluoride -ve	TN 945	FN 182	TN 1033	FN 192	TN 1152	FN 31
	Specificity 99.3%	Sensitivity 48.4%	Specificity 99.8%	Sensitivity 28.9%	Specificity 99.2%	Sensitivity 78.5%

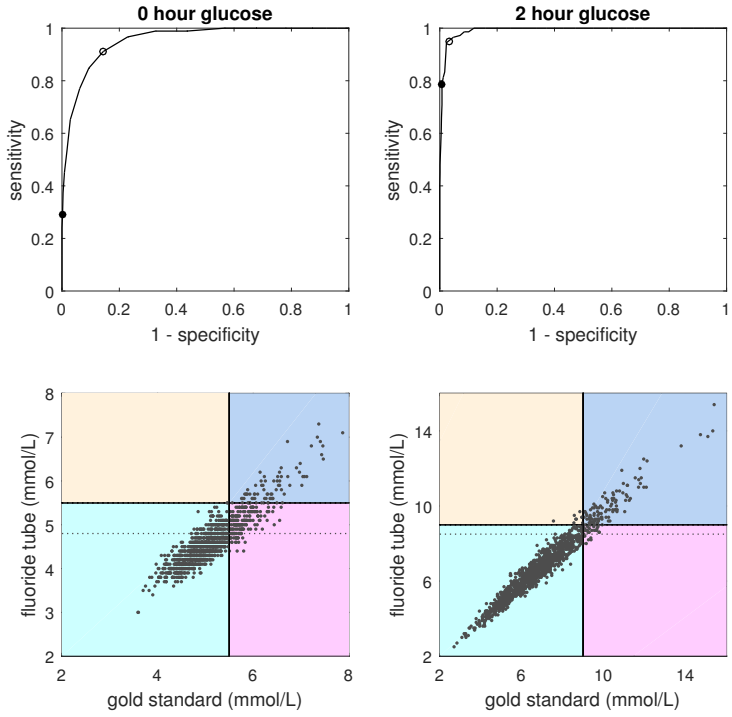

Figure 12.4: ROC curves for fluoride tubes vs gold standard in the hybrid $n = 1305$ cohort, with the point of diagnostic threshold marked $\bullet$, and optimal threshold marked $\circ$ (top row). Scatter plots of fluoride tubes vs gold standard glucose for a representative cohort of 1000, with the optimal threshold shown by the dotted line (bottom row).

Table 12.4: Diagnostic characteristics at the point on the ROC curve closest to the top left corner for each sample time in the hybrid cohort.

sample time	original sensitivity	original specificity	c-ROC	new threshold mmol/L	optimal sensitivity	optimal specificity
0 hour	28.9%	99.8%	0.954	4.8	91.1%	85.6%
2 hour	78.5%	99.2%	0.992	8.5	95.1%	96.9%

clinical procedure of batching blood samples in fluoride-preserved tubes had a noticeable effect on diagnosis outcomes *in silico*. Table 12.1shows that in the virtual cohort over a third of samples that led to a positive diagnosis with the gold standard methods were not diagnosed when fluoride tubes were used. This false negative rate was even greater (over half) in the hybrid cohort of local pregnant women. Low sensitivity is a clinically relevant outcome as false negatives will lead to a lack of medical intervention for at-risk individuals.

Figure 12.3 shows that fasting glucose had a particularly low sensitivity. In batched samples, fasting glucose has the longest wait before processing and thus the greatest extent of glucose decay. One-hour glucose was less susceptible to glucose decay than two-hour glucose due to the overall higher glucose values and the absolute, rather than proportional decay, caused by the fluoride tubes. However, the selection of an absolute decay of glucose in this simulation is justified by the fact that the decay in both Daly et al. (2016) and Carey et al. (2016) populations appeared to depend only on time in the sense of strictly increasing population error for earlier samples, i.e. 0.5, 0.4 and 0.2 mmol/L for (Daly et al., 2016). This does not rule out a dependency of glucose decay on nominal glucose concentration, but the assumption is valid in the absence of more direct evidence.

Table 12.2 suggests that optimal diagnosis rates in the virtual cohort with fluoride tubes are achieved with glucose thresholds at 4.4, 9.2 and 7.9 mmol/L rather than 5.1, 10 and 8.5 mmol/L. The difference in threshold values is remarkable, especially for fasting glucose since 4.4 mmol/L is considered a healthy fasting concentration. However, a batched fluoride-tube fasting glucose of 4.4 mmol/L implies much higher actual fasting glucose. Additionally, it must be accepted that a shift in diagnostic threshold towards markedly improved sensitivity trades off with a small increase in specificity. Table 12.2 shows that rates of specificity remain above 94% when the optimal threshold increases sensitivity to $> 95\%$. An equivalent outcome was found in the hybrid cohort with the optimal fasting threshold at 4.8 from 5.5 mmol/L and two hour at 8.5 from 9.0 mmol/L.

The simulated populations were successfully created with similar characteristics to those published for the large HAPO cohort. Laboratory process effects were implemented in the data. Reported intra-individual variation on glucose assay by the gold standard method was applied (Nesbitt et al., 2006). The effect of glucose decay in fluoride tubes when the three blood samples are batched together and processed at once was also easily applied (Carey et al., 2016). Using a large virtual population of 1 million mitigated the influence of discrete patient numbers influencing the false-positive and false-negative rates at the diagnosis thresholds.

The disadvantage of using the published summary of the HAPO cohort characteristics is that mean, standard deviation and correlation does not fully describe the shape of non-normal distributions. This means that there is a great range of possible variations, especially in the shape and size of the tails. In particular, many different distribution shapes meet the listed criteria. Since the nature of the tail distributions is most critical in diagnostic outcomes, the exact applicability of these *in silico* analyses is limited by the uncertainty of the true shapes (Figure 12.3). However, the use of log-normal distributions for these distributions has been found in a number of studies (Peplies et al., 2014; Kirchsteiger et al., 2015; Kovatchev et al., 1997).

The hybrid cohort demonstrated similar outcomes to the fully virtual cohort. This equivalence in outcomes is largely due to the replication of simulation strategy, despite the underlying real cohort. However, since the literature provides good evidence for the effect of batched fluoride samples (Carey et al., 2016; Daly et al., 2016), this analysis is equally valid. Moreover, the hybrid cohort overcomes some of the limitations of unknown distribution shapes in the HAPO populations. Additionally, the extension to a more realistic clinical cohort is useful, compared to HAPO which was intentionally more inclusive in its selection criteria for other research purposes.

The present analysis builds on the work of the small *in vivo* study by Carey et al. (2016) which directly compared glucose assay outcomes with fluoride-tube batching to the gold standard methods used in HAPO. This *in silico* study demonstrates on a larger scale the potential for this current common practice to have a clinically relevant diagnostic impact on the OGTTs of pregnant women. While the findings of this study strongly imply that there is a lack of sensitivity when fluoride tubes are used for diagnosis of GDM, further research in a prospective human study must be undertaken to confirm the findings and determine the relevant equivalent diagnostic thresholds.

12.5 Summary

Both the *in silico* and hybrid populations analysed in this chapter suggest that the typical practice of assaying batches of fluoride-preserved OGTT samples results in a markedly low diagnostic sensitivity compared to gold standard practices. In particular, fluoride-tube sensitivity with the 75g OGTT using the IADPSG criteria was 57.5% in the simulated cohort, indicating over a third of diagnosable patients would be overlooked. Similarly, the hybrid cohort had an overall diagnostic sensitivity of 48.4% with more than half of diagnosable patients overlooked.

The duration of glucose decay was most significant for a fasting samples, and thus noticeably reduced the apparent glucose concentration. Hence, optimum diagnosis rates would require lower glucose thresholds when using fluoride as a preservative compared to thresholds based on gold standard glucose assays. Likewise, but to a progressively lesser extent the one and two hour sample thresholds should be lower to gain diagnostic equivalence to gold standard samples.

Part IV

Conclusions and future work

Chapter XIII

Summary and concluding remarks

13.1 Summary

Type 1 diabetes is an autoimmune disease affecting an increasing number and proportion of people worldwide. The primary clinical characteristic of the disease is hyperglycaemia due to a lack of endogenously produced insulin. Autoimmune destruction of the insulin-producing β cells in the pancreas tends to be absolute, especially in younger individuals. Fortunately, the widespread availability of manufactured insulin provides viable treatment. However, insulin administration only mitigates some symptoms of diabetes and is not a cure for the disease. Presently T1DM is managed, not cured. Insulin treatment is daily and ongoing, and therefore burdensome for the individual. This is particularly due to the delicate balance required to treat hyperglycaemia but avoid hypoglycaemia.

The appropriate doses of insulin required to achieve euglycaemia are uncertain during the everyday life of some outpatients with diabetes. Hence, individuals are often not able to engage in the fullness of activities enjoyed by the healthy. For example, a strict routine for mealtimes can substantially improve glycaemic control, improving quality of life. However, the routine is kept at the expense of flexibility, which can negatively impact on social and psychological freedoms, thereby reducing the quality of life. This example demonstrates both the inherent difficulties of accounting for all influences on glucose metabolism in the everyday, as well as the need for treatment to be a good compromise between improving glycaemic control and decreasing the burden of the disease. Each of these factors contributes positively to the perceived quality of life.

Much of the current research in diabetes management is focused on achieving a successfully automated closed-loop control solution to diabetes, termed the artificial pancreas. This would be the most ideal treatment solution for individuals with T1DM since it could potentially achieve near normal glycaemia with minimal human input. An effective closed-loop controls system would negate some or much of the need for anticipating the effect of certain everyday factors, by observing and directly influencing the target species, blood glucose concentration, at a higher sampling frequency than for self-managed methods.

However, the yet unresolved problem for the artificial pancreas is the inability to obtain high enough quality glucose measurements at a high sampling frequency. Meters that use finger-pricking are reasonably reliable but require effort, pain and long term scarring. Hence, the maximum frequency of use is only a few times daily in self-managed individuals. Continuous glucose monitoring (CGM) systems are able to achieve high frequency data (typically every 5 minutes) but do not measure blood glucose directly, resulting in both delay and damping of observed dynamics. Additionally, CGMs are prone to unpredictable spikes and jumps in error, along with a steady error drift. These problems are ameliorated with frequent recalibration to finger-prick measurement (e.g. once daily) and recommendations to confirm some measurements (particularly hypoglycaemic) before adjusting treatment. Nevertheless, the performance of CGMs are at present insufficient to ensure safe and effective closed-loop control.

In contrast to a closed-loop control focus, the present work falls into the vein of research that aims to inform and improve self-managed blood glucose control. Glucose metabolism is complex, multifaceted, and subject to a wide range of influences arising in everyday life. Some factors have very minor and clinically insignificant effects while others can severely impact on glycaemic control, but these differentiations vary widely across individuals. Some patients are termed "brittle" by clinicians due to their

sensitivity to external factors and inability to achieve good glycaemic control despite rigorous effort. These individuals in particular would benefit from model-based decision support that is personalised and includes as many factors as are both relevant and observable. Even without model-based decision support, greater personalised knowledge of these factors would be beneficial.

Four major categories of everyday life factors have been studied in depth in the literature, presented in Chapter 4: nutrition, psychological effects, physical activity and metabolic rhythms. These areas were considered to encompass many factors that have recognised effects on glycaemia but lack consensus around modelling. This chapter collated and compared various models of these effects in outpatients to reduce undesirable systemic and non-random grey noise affecting model outcomes. The analysis considered how the measurement of such factors affect the model. However, with the right tools, data and models, it can be expected that observable signals from a variety of factors are separable and quantifiable.

Developing and selecting the right model is a major theme of the present work. Ultimately, personalisable models would need to be used with data from the outpatient environment to capture that glimpse of the everyday. However, the data used in the present work, described in Chapter 5, is an effective stepping stone toward such a goal. The data is of very high research quality but introduces some of the variability of the everyday in a prescribed manner, and in a heterogeneous cohort. The resulting richly descriptive and dynamic data has been ideal for developing an understanding of the physiological aspects of some of the effects being considered. The subsequent model development has thus been informed by the breadth and depth of the behaviour and the variability that can also be expected outpatients.

Models fully informed by the breadth and depth of information in the research data are also an intermediary stage. Indeed, the development of a subcutaneous model in Chapter 6 highlighted that even best choice of

model with respect to the research data was not that which contained the most detail that the data could afford. This work was valuable in part because of the lack of subcutaneous models specific to a continuous infusion of insulin aspart. Therefore, the model(s) developed fulfil a particular demand. But perhaps more valuable still was a demonstration of the rigorous analysis process for assessing relative model performance.

While some models appear to be designed with a poor understanding of some of the mathematical limitations in physiological modelling around the issue of robustness and practical non-identifiability, the subcutaneous model analyses of Chapter 6 made every effort to consider more than just model fitting ability. A model in itself may be pioneering in its physiological descriptiveness and accuracy. But if it cannot be used effectively in the context of its intended purpose due to insufficient data quality and quantity, then the descriptiveness and accuracy are wasted. Hence, it is not surprising that one of the much simpler subcutaneous insulin models was found to be best when considering these clinically relevant metrics. When poor understanding of this problem prevails, the confidence placed in the descriptiveness and accuracy (or a long legacy of use) can lead to poor or dangerous model interpretation for a clinical context. Hence, the methodology and outcomes of Chapter 6 are an important addition to the research field.

Development of a model for the effect of moderate aerobic exercise on insulin and glucose did not include the same level of rigorous analysis as the subcutaneous model. Nonetheless, a unique and perhaps novel approach was taken in this model development process. The use of autoregressive modelling to retrieve information on underlying behaviours (Chapter 7) is uncommon in itself. Usually, NARX models are used as a black box, where the correlative information is not sought after so much as the model's ability to make output predictions based on the same type of inputs as are encountered in the training stage. By uncovering the correlative information for exercise, the present method can instead be considered grey-box modelling, not being as physiologically rigorous in definition as

most differential glycaemic models, but not just about the inputs to outputs performance either. This method was an effective step in the development process as it allowed the data to inform the model more directly than if guess and check iterations were carried out.

Additionally, the exercise-effect behaviour uncovered was remarkably consistent across the heterogeneous cohort. Therefore, despite the limitations of NARX modelling, the results were interesting and persuasive at a descriptive level at least. To illustrate this, there was found to be contention in the literature over whether exercise influenced the concentration of exogenous insulin in the plasma positively, negatively, or not at all. The NARX analysis demonstrates that there was a positive effect during exercise and negative afterwards, for the type of exercise carried out and in the experimental conditions prescribed. Indeed, the further work in Chapter 8 showed that the magnitude of this excursion appears correlated to subcutaneous concentration, especially relating to insulin boluses. This observation would further explain the contention in the literature, since some experiments would inevitably aim to increase repeatability by removing insulin boluses. Evidently, such an experimental design would likely not see the same effect as observed amongst an everyday routine that contains boluses. This notion further highlights the value of NARX in being able to deconvolute the exercise effect from other dynamics.

Beyond the NARX and in anticipation of an outpatient context, the basis models presented in Chapter 8 were designed as a simplistic implementation of a model containing the effect of exercise. The underlying plasma insulin model neglects some known physiological features such as saturated clearance and interaction with interstitium. These simplifications were intentional since the sophisticated insulin pharmacokinetics are not likely to be observable in outpatients. Still, the model performed well as the exercise basis is an effective addition to the model. The basis function used in the model is easier to apply than attempting to alter subcutaneous uptake rates, which is the likely physiological mechanism. Correlation of the magnitude of the exercise-induced insulin excursion to prior insulin

concentration appears significant, though cautionary, but represents work towards a more extensively *a priori* insulin model, which would be most appropriate for outpatients given the limitations in observability.

A basis model was also created for the effect of exercise on glucose. The glucose model was also relatively simple, which noticeably limited its fitting performance, particularly due to unmodelled effects in the appearance of food and in the physiological responses to intravenous glucose bolus. However, the exercise basis itself performed well and improved the model fit. The model featured an increasing but saturated rate of glucose disposal as exercise was carried out in response to an increase in peripheral glucose demand. This exercise-induced glucose disposal remained post-exercise, possibly representing a refuelling of peripheral glycogen stores, but eventually returned to zero.

Chapter 9 demonstrates *in silico* that though the data quality expected from outpatients is poor, this limitation is overcome with time. As data accumulates, parameter estimates for everyday effects tend towards the true underlying value with minimal bias. This result emerged despite the various sources of error that were introduced, such as glucose measurement noise, unrecorded food intake and carbohydrate misestimation. Additionally, it was found that longer-term changes in insulin sensitivity could be accounted and compensated for, further increasing the viability of this type of data collection. This finding represents a pathway toward personalisable glycaemic models that can be fit to the individual, for the individual.

Further work was carried out in consideration of practical identifiability for model recovery in outpatient data. Chapter 10 presented an analysis for evaluating the value of identifying increasing parameter sets. The caution is that identifying too many parameters in insufficient data can result in substantial parameter trade-off, unknowingly introducing large errors. While the analysis in its current form only works *in silico* where the true parameter values are known, the results provide insight into the likely capabilities of the model and data. On the other hand, an analysis

developed from the initial work of Chapter 11 would be able to evaluate the likely confidence intervals of parameters with only the information expected from real data. However carried out, an analysis around the practical identifiability of the parameter estimates is crucial if the identified parameters are to be fed back into control strategies and systems.

Chapter 12 provides an interesting case-study of the influence of a particular form of grey-noise on clinical interpretation of diagnostic outcomes in gestational diabetes. This work is somewhat tangential to the main focus of the present work in T1DM. However, it is valuable to clinicians in highlighting the limitations of the typical laboratory processing techniques used, and the implication for getting appropriate treatment to those in need. Though some assumptions have been made in the simulation of test cohorts, the evidence of poor test sensitivity in typical practice is unambiguous. This outcome also generally highlights the possible effect of measurement noise on the observability of behaviours, particularly systemic grey-noise in small data quantities.

Overall, the present work takes great strides towards an improvement in glycaemic control for individuals with diabetes by modelling the effects of everyday life factors. There is a distinct value in modelling such factors, so long as the models are effective and robust. The ability to use models in an outpatient context would be beneficial for a large number of individuals, since there the unique effects of a unique set of everyday life factors would be observed. Hence, the models have been developed with consideration to the practical identifiability constraints of outpatient data. Furthermore, an *in silico* investigation of the efficacy of model recovery in outpatients shows positive preliminary results, and further work was carried out addressing identifiability analyses specifically. Ultimately, sound modelling of everyday life factors would improve the quality of life for sufferers of diabetes by improving control and decreasing the burden of disease management.

13.2 Concluding remarks

Three broad conclusions can be drawn from this work. The first is that the literature demonstrates numerous factors present in the outpatient environment that can noticeably affect glucose metabolism and thus glycaemic control. These factors include physical activity, psychological stress and depression, daily metabolic rhythms, menstrual cycles, food variability and so on. Furthermore, technologies are increasingly being developed to measure the presence or effect of some of these factors. Without accounting for these everyday life factors, model-based control techniques are limited in their effectiveness, reliability and safety. Hence there is a need to model such factors, specific to individual patients.

The second broad conclusion is the need to consider practical identifiability. This type of identifiability is as valid to ensure as the traditional structural identifiability, perhaps even more so given its subtler presentation. In practice this means that although everyday life effects for outpatients should be modelled, they can only be modelled to the degree of complexity allowed by the quality of information present. Patient-specific variables should be identified with sufficient confidence to ensure safety and effectiveness.

The final broad conclusion is that despite the challenges of outpatient data quality, it appears entirely possible to identify the patient-specific parameters sought, if enough data can be collected over a longer period of time. Preliminary computational simulations suggest that it is possible to identify everyday life factors and other metabolic variables modelled in a virtual patient, even with sparse data, noise and unmodelled effects. Since everyday life effects cannot all be controlled and simulated in the inpatient environment, it is hugely important that they can be measured in the outpatient environment.

Chapter XIV

Future work

The present work demonstrates the scientific foundation for advances in interventional treatment. However, further advances are necessary before such an intervention. With the current data, there is yet more model development and evaluation that could be carried out. A highly functional glucose model is the main goal as blood glucose is the target species for control and is readily measured in outpatients.

Glucose dynamics are considerably more complex than insulin due to the large variety of regulatory influences. Since several hormones other than insulin affect glycaemia, there is potential to improve understanding and physiological modelling of the dynamic effects of these hormones, and to generally improve the physiological accuracy of the glucose model as necessary. However, keeping in mind the substantial practical identifiability constraints of outpatient data, advancing the glucose model would likely need to be followed by wise simplifications. This may seem redundant, however not all simplifications or complications of modelled behaviour are beneficial. Like the process carried out with the subcutaneous insulin model, it would be beneficial to be able to model all reasonable behaviours and evaluate which simplifications of these behaviours will be the best compromise of fit, prediction ability and parameter robustness.

Some aspects of the glucose model will need improving, beyond what the current data can inform. This is particularly true for forms of exercise other than moderate aerobic exercise, or at greater durations (given the influence of glycogen depletion). Moreover, the medium term influence of physical activity on insulin sensitivity spanning multiple days needs some viable model pathways. Other everyday life effects such as stress will require some

model development as well. These model developments could be built on information from the literature and tested on outpatient data directly.

Additional *in silico* analysis of model recovery could be carried out. These would include updated versions of the models since the model recovery work pre-dated the model-building. On the other hand, the model recovery analysis was always intended as a proof of concept for the overall research goals. The concept appears to be proved well by the results. Additionally, preliminary *in vivo* testing of the models would be low cost and low risk. The data would be collected using a diary template distributed and recollected by a primary healthcare provider. No intervention would be carried out during this observations stage of the research. Only small numbers of patients would need to be recruited due to the individualised application of the work.

A rigorous testing of models in the outpatient data would then need to be carried out. This process would include evaluation of the robustness and reliability of all identified parameters. This stage of the research would be pivotal. Though all prior research has and would be valuable in some capacity, these tests would confirm whether the everyday effects considered are actually observable in the type of data collected. If not, then steps could be taken to improve the quality of the data for another next attempt. This could include an increase in the number of easily wearable sensors for heart rate, temperature, sympathetic nerve activity and so on. These would provide clearer input parameters for certain everyday effects and would improve model outcomes compared to subjective diary recordings.

Pending successful identification of everyday life effects, considerable *in silico* analysis would need to be carried out to evaluate whether interventional treatment could be safely and effectively implemented. Multiple control strategies would be tested with the information provided, and a suitable user interface would be required for the model-based insulin recommendations. These analyses would inform ethical applications for recruitment of patients to test interventions. Experimental design would

need to be rigorous to evaluate whether the intervention is successful. Crossover would be necessary to compare intervention periods versus non-intervention periods. A combination of metrics would be used for the evaluation including HbA1c measurement, number of hypoglycaemic events, percentage of blood glucose in the target band, and patient interviews. The patients would need to be well instructed, especially to check that intervention-recommended insulin doses are reasonable compared with their intuition and past experience.

The present scope of the future work ends at determining if patient trials were successful. If interventional treatment performs well enough, then the research could increase the scope to larger trials and ultimately implementation to unstudied individuals.

Bibliography

Abate, N., A. Garg, R. M. Peshock, J. Stray-Gundersen, and S. M. Grundy
1995. Relationships of generalized and regional adiposity to insulin sensitivity in men. *Journal of Clinical Investigation*, 96(1):88–98.

Abdulla, H., B. Phillips, K. Smith, D. Wilkinson, P. J. Atherton, and I. Idris
2014. Physiological mechanisms of action of incretin and insulin in regulating skeletal muscle metabolism. *Current Diabetes Reviews*, 10(5):327–335.

Ackerman, E., J. W. Rosevear, and W. F. McGuckin
1964. A mathematical model of the glucose-tolerance test. *Physics in Medicine and Biology*, 9(2):203.

Ahrén, B.
2013. Incretin dysfunction in type 2 diabetes: Clinical impact and future perspectives. *Diabetes and Metabolism*, 39(3):195–201.

Aizawa, T., K. Yamauchi, and M. Yamada
2014. Longitudinal changes in insulin sensitivity, insulin secretion, beta cell function and glucose effectiveness during development of non-diabetic hyperglycemia in a japanese population. *SpringerPlus*, 3(1):1–6.

Alsalim, W., B. Omar, G. Pacini, R. Bizzotto, A. Mari, and B. Ahrén
2015. Incretin and islet hormone responses to meals of increasing size in healthy subjects. *Journal of Clinical Endocrinology and Metabolism*, 100(2):561–568.

American Diabetes Association
2006. Diagnosis and classification of diabetes mellitus. *Diabetes care*, 29(1):S43–8.

Atkinson, M. A. and G. S. Eisenbarth
2001. Type 1 diabetes: new perspectives on disease pathogenesis and treatment. *The Lancet*, 358(9277):221 – 229.

Audoly, S., G. Bellu, L. D'Angio, M. P. Saccomani, and C. Cobelli
2001. Global identifiability of nonlinear models of biological systems. *Biomedical Engineering, IEEE Transactions on*, 48(1):55–65.

Audoly, S., L. D'Angio, M. P. Saccomani, and C. Cobelli
1998. Global identifiability of linear compartmental models-a computer algebra algorithm. *Biomedical Engineering, IEEE Transactions on*, 45(1):36–47.

Bassett D.R, J., B. E. Ainsworth, A. M. Swartz, S. J. Strath, W. L. O'Brien, and G. A. King
2000. Validity of four motion sensors in measuring moderate intensity physical activity. *Medicine and Science in Sports and Exercise*, 32(9 SUPPL.):S471–S480.

Bellman, R. and K. J. Åström
1970. On structural identifiability. *Mathematical Biosciences*, 7(34):329–339.

Bellu, G., M. P. Saccomani, S. Audoly, and L. DAngiò
2007. Daisy: A new software tool to test global identifiability of biological and physiological systems. *Computer Methods and Programs in Biomedicine*, 88(1):52–61.

Bequette, B. W.
2012. Challenges and recent progress in the development of a closed-loop artificial pancreas. *Annual Reviews in Control*, 36(2):255–266.

Bergman, R. N., Y. Z. Ider, C. R. Bowden, and C. Cobelli
1979. Quantitative estimation of insulin sensitivity. *American Journal of Physiology*, 236:E667–77.

Beutner, F., R. Ubrich, S. Zachariae, C. Engel, M. Sandri, A. Teren, and S. Gielen
2015. Validation of a brief step-test protocol for estimation of peak oxygen uptake. *European Journal of Preventive Cardiology*, 22(4):503–512.

Borghouts, L. B. and H. A. Keizer
2000. Exercise and insulin sensitivity: A review. *International Journal of Sports Medicine*, 21(1):1–12.

Bornhorst, G. M. and R. P. Singh
2014. Gastric digestion in vivo and in vitro: How the structural aspects of food influence the digestion process. *Annual Review of Food Science and Technology*, 5(1):111–132.

Brazeau, A.-S., R. Rabasa-Lhoret, I. Strychar, and H. Mircescu
2008. Barriers to physical activity among patients with type 1 diabetes. *Diabetes Care*, 31(11):2108–2109.

Brems, D. N., L. A. Alter, M. J. Beckage, R. E. Chance, R. D. DiMarchi, L. K. Green, H. B. Long, A. H. Pekar, J. E. Shields, and B. H. Frank
1992. Altering the association properties of insulin by amino acid replacement. *Protein Engineering*, 5(6):527–533.

Breton, M. D.
2008. Physical activity–the major unaccounted impediment to closed loop control. *Journal of Diabetes Science and Technology*, 2(1):169–174.

Campioni, M., G. Toffolo, R. Basu, R. A. Rizza, and C. Cobelli
2009. Minimal model assessment of hepatic insulin extraction during an oral test from standard insulin kinetic parameters. *American Journal of Physiology - Endocrinology and Metabolism*, 297(4):E941–E948.

Carey, R., M. Churcher, H. Heenan, R. Hughes, C. Florkowski, and H. Lunt
2016. Measurement of pregnancy ogtt plasma glucose: do citrate blood collection tubes lead to an over-diagnosis of gdm?

Carr, R. D., M. O. Larsen, M. S. Winzell, K. Jelic, O. Lindgren, C. F. Deacon, and B. Ahrén
2008. Incretin and islet hormonal responses to fat and protein ingestion in healthy men. *American Journal of Physiology - Endocrinology and Metabolism*, 295(4):E779–E784.

Carroll, K. F. and P. J. Nestel
1973. Diurnal variation in glucose tolerance and in insulin secretion in man. *Diabetes*, 22(5):333–348.

Carson, E. R. and C. Cobelli
2001. Modelling methodology for physiology and medicine. *Acad Press Series Biomed Eng*, xiv:421.

Cernea, S.
2011. The role of incretin therapy at different stages of diabetes. *Review of Diabetic Studies*, 8(3):311–326.

Chase, J., G. M. Shaw, X. W. Wong, T. Lotz, J. Lin, and C. E. Hann
2006. Model-based glycaemic control in critical care - a review of the state of the possible. *Biomed Signal Process Control*, 1(1):3 – 21.

Chase, J. G., A. Le Compte, J.-C. Preiser, G. Shaw, S. Penning, and T. Desaive
2011. Physiological modeling, tight glycemic control, and the icu clinician: what are models and how can they affect practice? *Annals of Intensive Care*, 1(11).

Chase, J. G., A. J. Le Compte, F. Suhaimi, G. M. Shaw, A. Lynn, J. Lin, C. G. Pretty, N. Razak, J. D. Parente, and C. E. Hann
2010. Tight glycemic control in critical care. the leading role of insulin sensitivity and patient variability: a review and model-based analysis. *Comput Methods Programs Biomed*.

Chase, J. G., G. Shaw, A. Le Compte, T. Lonergan, M. Willacy, X. W. Wong,

J. Lin, T. Lotz, D. Lee, and C. Hann
2008. Implementation and evaluation of the sprint protocol for tight glycaemic control in critically ill patients: a clinical practice change. *Crit Care*, 12(2):R49.

Chee, F., T. Fernando, A. Savkin, and V. Van Heeden
2003. Expert pid control system for blood glucose control in critically ill patients. *IEEE Transactions on Information Technology in Biomedicine*, 7(4):419–425.

Cherrington, A. D.
1999. Control of glucose uptake and release by the liver in vivo. *Diabetes*, 48(5):1198–214.

Choi, S., S. Kim, J. S. Yang, J. H. Lee, C. Joo, and H. I. Jung
2014. Real-time measurement of human salivary cortisol for the assessment of psychological stress using a smartphone. *Sensing and Bio-Sensing Research*, 2:8–11.

Clark, D. W. and T. V. Nowak
1994. Diabetic gastroparesis: What to do when gastric emptying is delayed. *Postgraduate Medicine*, 95(5):195–198+201.

Cobelli, C., F. Bettini, A. Caumo, and M. J. Quon
1998. Overestimation of minimal model glucose effectiveness in presence of insulin response is due to undermodeling. *American Journal of Physiology - Endocrinology and Metabolism*, 275(6 38-6):E1031–E1036.

Cobelli, C., A. Caumo, and M. Omenetto
1999. Minimal model sg overestimation and si underestimation: improved accuracy by a bayesian two-compartment model. *Am J Physiol*, 277(3 Pt 1):E481–488.

Cobelli, C., C. D. Man, G. Toffolo, R. Basu, A. Vella, and R. Rizza
2014. The oral minimal model method. *Diabetes*, 63(4):1203–1213.

Cobelli, C., E. Renard, and B. Kovatchev
2011. Artificial pancreas: Past, present, future. *Diabetes*, 60(11):2672–82.

Collins, P. J.
1991. Role of the proximal and distal stomach in mixed solid and liquid meal emptying. *Gut*, 32(6):615–619.

Cousins, L.
1991. Insulin sensitivity in pregnancy. *Diabetes*, 40(SUPPL. 2):39–43.

Cryer, P., S. Davis, and H. Shamoon
2003. Hypoglycemia in diabetes. *Diabetes Care*, 26(6):1902–1912. cited By 617.

Dai, J. S., J. Li, Z. K. Gu, and B. Sun
2008. Utility of pedometer to assess daily physical activity. *Journal of Clinical Rehabilitative Tissue Engineering Research*, 12(35):6883–6887.

Dalla Man, C., M. D. Breton, and C. Cobelli
2009. Physical activity into the meal glucose-insulin model of type 1 diabetes: in silico studies. *Journal of diabetes science and technology*, 3(1):56–67.

Dalla Man, C., M. Camilleri, and C. Cobelli
2006. A system model of oral glucose absorption: Validation on gold standard data. *IEEE Transactions on Biomedical Engineering*, 53(12):2472–2478.

Daly, N., I. Flynn, C. Carroll, M. Farren, A. McKeating, and M. J. Turner
2016. Impact of implementing preanalytical laboratory standards on the diagnosis of gestational diabetes mellitus: A prospective observational study. *Clin Chem*, 62(2):387–91.

De Boer, I. H., B. Kestenbaum, T. C. Rue, M. W. Steffes, P. A. Cleary, M. E.

Molitch, J. M. Lachin, N. S. Weiss, and J. D. Brunzell
2008. Insulin therapy, hyperglycemia, and hypertension in type 1 diabetes mellitus. *Archives of Internal Medicine*, 168(17):1867–1873.

De Santos Sierra, A., C. Sánchez Ávila, J. Guerra Casanova, and G. Bailador Del Pozo
2011. A stress-detection system based on physiological signals and fuzzy logic. *IEEE Transactions on Industrial Electronics*, 58(10):4857–4865.

Docherty, P. D., J. G. Chase, T. F. Lotz, and T. Desaive
2011. A graphical method for practical and informative identifiability analyses of physiological models: A case study of insulin kinetics and sensitivity. *BioMedical Engineering Online*, 10.

Douard, V. and R. P. Ferraris
2008. Regulation of the fructose transporter glut5 in health and disease. *American Journal of Physiology - Endocrinology and Metabolism*, 295(2):E227–E237.

Duran, A., S. Sáenz, M. J. Torrejón, E. Bordiú, L. del Valle, M. Galindo, N. Perez, M. A. Herraiz, N. Izquierdo, M. A. Rubio, I. Runkle, N. Pérez-Ferre, I. Cusihuallpa, S. Jiménez, N. García de la Torre, M. D. Fernández, C. Montañez, C. Familiar, and A. L. Calle-Pascual
2014. Introduction of iadpsg criteria for the screening and diagnosis of gestational diabetes mellitus results in improved pregnancy outcomes at a lower cost in a large cohort of pregnant women: The st. carlos gestational diabetes study. *Diabetes Care*, 37(9):2442–2450.

Duun-Henriksen, A. K., S. Schmidt, K. Nørgaard, and H. Madsen
2013. Clinical data for advanced glucose modeling. Report.

Dyer, J., I. S. Wood, A. Palejwala, A. Ellis, and S. P. Shirazi-Beechey
2002. Expression of monosaccharide transporters in intestine of diabetic humans. *American Journal of Physiology - Gastrointestinal and Liver Physiology*, 282(2 45-2):G241–G248.

Eaton, R. P., R. C. Allen, D. S. Schade, K. M. Erickson, and J. Standefer
1980. Prehepatic insulin production in man: kinetic analysis using peripheral connecting peptide behavior. *J Clin Endocrinol Metab*, 51(3):520–8.

Elleri, D., J. M. Allen, J. Harris, K. Kumareswaran, M. Nodale, L. Leelarathna, C. L. Acerini, A. Haidar, M. E. Wilinska, N. Jackson, A. M. Umpleby, M. L. Evans, D. B. Dunger, and R. Hovorka
2013. Absorption patterns of meals containing complex carbohydrates in type 1 diabetes. *Diabetologia*, 56(5):1108–1117.

Englyst, K. N. and H. N. Englyst
2005. Carbohydrate bioavailability. *British Journal of Nutrition*, 94(1):1–11.

Englyst, K. N., S. Vinoy, H. N. Englyst, and V. Lang
2003. Glycaemic index of cereal products explained by their content of rapidly and slowly available glucose. *British Journal of Nutrition*, 89(3):329–339.

Ercan, N., F. Q. Nuttall, M. C. Gannon, J. B. Redmon, and K. J. Sheridan
1993. Effects of glucose, galactose, and lactose ingestion on the plasma glucose and insulin response in persons with non-insulin-dependent diabetes mellitus. *Metabolism*, 42(12):1560–1567.

Erichsen, L., O. F. Agbaje, S. D. Luzio, D. R. Owens, and R. Hovorka
2004. Population and individual minimal modeling of the frequently sampled insulin-modified intravenous glucose tolerance test. *Metabolism*, 53(10):1349–54.

Evans, A., G. M. Shaw, A. Le Compte, C.-S. Tan, L. Ward, J. Steel, C. G. Pretty, L. Pfeifer, S. Penning, F. Suhaimi, M. Signal, T. Desaive, and J. G. Chase
2011. Pilot proof of concept clinical trials of stochastic targeted (star) glycemic control. *Annals of Intensive Care*, 1(1):1–12.

Fabietti, P. G., V. Canonico, M. O. Federici, M. M. Benedetti, and E. Sarti
2006. Control oriented model of insulin and glucose dynamics in type 1 diabetics. *Medical and Biological Engineering and Computing*, 44(1-2):69–78.

Ferraris, R. P.
2001. Dietary and developmental regulation of intestinal sugar transport. *Biochemical Journal*, 360(2):265–276.

Fisk, L., P. D. Docherty, C. Pretty, and J. G. Chase
2016. Incorporating bolus and infusion pharmacokinetics into the {ICING} insulin model. *Mathematical Biosciences*, 281:1 – 8.

Flint, A., B. K. Moller, A. Raben, D. Pedersen, I. Tetens, J. J. Holst, and A. Astrup
2004. The use of glycaemic index tables to predict glycaemic index of composite breakfast meals. *Br J Nutr*, 91(6):979–89.

Folwaczny, C., R. Wawarta, B. Otto, S. Friedrich, R. Landgraf, and R. L. Riepl
2003. Gastric emptying of solid and liquid meals in healthy controls compared with long-term type-1 diabetes mellitus under optimal glucose control. *Experimental and Clinical Endocrinology and Diabetes*, 111(4):223–229.

Foster-Powell, K., S. H. Holt, and J. C. Brand-Miller
2002. International table of glycemic index and glycemic load values: 2002. *The American Journal of Clinical Nutrition*, 76(1):5–56.

Fraser, R. J., M. Horowitz, A. F. Maddox, P. E. Harding, B. E. Chatterton, and J. Dent
1990. Hyperglycaemia slows gastric emptying in type 1 (insulin-dependent) diabetes mellitus. *Diabetologia*, 33(11):675–680.

Freckmann, G., A. Baumstark, C. Schmid, S. Pleus, M. Link, and C. Haug
2013. Evaluation of 12 blood glucose monitoring systems for self-testing:

System accuracy and measurement reproducibility. *Diabetes Technology & Therapeutics*, 16(2):113–122.

Frost, D. P., M. C. Srivastava, R. H. Jones, J. D. Nabarro, and P. H. Sonksen
1973. The kinetics of insulin metabolism in diabetes mellitus. *Postgrad Med J*, 49:Suppl 7:949–54.

Gale, E. A.
2002. The rise of childhood type 1 diabetes in the 20th century. *Diabetes*, 51(12):3353–3361.

Gannon, M. C., M. A. Khan, and F. Q. Nuttall
2001. Glucose appearance rate after the ingestion of galactose. *Metabolism: Clinical and Experimental*, 50(1):93–98.

Gatewood, L. C., E. Ackerman, J. W. Rosevear, G. D. Molnar, and T. W. Burns
1968. Tests of a mathematical model of the blood-glucose regulatory system. *Computers and Biomedical Research*, 2(1):1 – 14.

Gentilcore, D., R. Chaikomin, K. L. Jones, A. Russo, C. Feinle-Bisset, J. M. Wishart, C. K. Rayner, and M. Horowitz
2006. Effects of fat on gastric emptying of and the glycemic, insulin, and incretin responses to a carbohydrate meal in type 2 diabetes. *Journal of Clinical Endocrinology and Metabolism*, 91(6):2062–2067.

Gerich, J. E.
2010. Role of the kidney in normal glucose homeostasis and in the hyperglycaemia of diabetes mellitus: therapeutic implications. *Diabet Med*, 27(2):136–42.

Goetsch, V. L., B. VanDorsten, L. A. Pbert, I. H. Ullrich, and R. A. Yeater
1993. Acute effects of laboratory stress on blood glucose in noninsulin-dependent diabetes. *Psychosomatic Medicine*, 55(6):492–496.

Goldenberg, J. and A. J. Cummins
1971. The effect of rate of influx and concentration on the absorption rate of glucose by the human small intestine. *Southern Medical Journal*, 64(5):559–564.

González-Ortiz, M., E. Martínez-Abundis, B. R. Balcázar-Muñoz, and S. Pascoe-González
2000. Effect of sleep deprivation on insulin sensitivity and cortisol concentration in healthy subjects. *Diabetes, Nutrition and Metabolism - Clinical and Experimental*, 13(2):80–83.

Guyton, J. R., R. O. Foster, J. S. Soeldner, M. H. Tan, C. B. Kahn, L. Koncz, and R. E. Gleason
1978. A model of glucose-insulin homeostasis in man that incorporates the heterogeneous fast pool theory of pancreatic insulin release. *Diabetes*, 27(10):1027–1042.

Hanazaki, K., M. Munekage, H. Kitagawa, T. Yatabe, E. Munekage, M. Shiga, H. Maeda, and T. Namikawa
2016. Current topics in glycemic control by wearable artificial pancreas or bedside artificial pancreas with closed-loop system. *Journal of Artificial Organs*, 19(3):209–218.

Hannon, T. S., J. Janosky, and S. A. Arslanian
2006. Longitudinal study of physiologic insulin resistance and metabolic changes of puberty. *Pediatric Research*, 60(6):759–763.

Hayes, M. R., E. G. Mietlicki-Baase, S. E. Kanoski, and B. C. De Jonghe
2014. Incretins and amylin: Neuroendocrine communication between the gut, pancreas, and brain in control of food intake and blood glucose. In *Annual Review of Nutrition*, volume 34, Pp. 237–260.

Hinshaw, L., C. D. Man, D. K. Nandy, A. Saad, A. E. Bharucha, J. A. Levine, R. A. Rizza, R. Basu, R. E. Carter, C. Cobelli, Y. C. Kudva, and A. Basu
2013. Diurnal pattern of insulin action in type 1 diabetes implications for a closed-loop system. *Diabetes*, 62(7):2223–2229.

Home, P. D., L. Barriocanal, and A. Lindholm
1999. Comparative pharmacokinetics and pharmacodynamics of the novel rapid- acting insulin analogue, insulin aspart, in healthy volunteers. *European Journal of Clinical Pharmacology*, 55(3):199–203.

Horowitz, M., D. O'Donovan, K. L. Jones, C. Feinle, C. K. Rayner, and M. Samsom
2002. Gastric emptying in diabetes: Clinical significance and treatment. *Diabetic Medicine*, 19(3):177–194.

Hovorka, R., V. Canonico, L. Chassin, U. Haueter, M. Massi-Benedetti, M. Federici, T. Pieber, H. Schaller, L. Schaupp, T. Vering, and M. Wilinska
2004. Nonlinear model predictive control of glucose concentration in subjects with type 1 diabetes. *Physiological Measurement*, 25(4):905–920.

Hovorka, R., K. Kumareswaran, J. Harris, J. M. Allen, D. Elleri, D. Xing, C. Kollman, M. Nodale, H. R. Murphy, D. B. Dunger, S. A. Amiel, S. R. Heller, M. E. Wilinska, and M. L. Evans
2011. Overnight closed loop insulin delivery (artificial pancreas) in adults with type 1 diabetes: crossover randomised controlled studies. *BMJ*, 342.

Hovorka, R., M. Nodale, A. Haidar, and M. E. Wilinska
2013. Assessing performance of closed-loop insulin delivery systems by continuous glucose monitoring: Drawbacks and way forward. *Diabetes Technology and Therapeutics*, 15(1):4–12.

Hustvedt, B. E., A. Christophersen, L. R. Johnsen, H. Tomten, G. McNeill, P. Haggarty, and A. Lovo
2004. Description and validation of the actireg: a novel instrument to measure physical activity and energy expenditure. *Br J Nutr*, 92(6):1001–8.

Insel, P. A., K. J. Kramer, R. S. Sherwin, J. E. Liljenquist, J. D. Tobin, R. Andres, and M. Berman
1974. Modeling the insulin-glucose system in man. *Fed Proc*, 33(7):1865–8.

Johnson, K. M. S., D. S. Edgerton, T. Rodewald, M. Scott, B. Farmer, D. Neal, and A. D. Cherrington
2007. Intraportal glp-1 infusion increases nonhepatic glucose utilization without changing pancreatic hormone levels. *American Journal of Physiology - Endocrinology and Metabolism*, 293(4):E1085–E1091.

Jolliffe, I.
1986. *Principle Component Analysis*, Springer Series in Statistics. Springer New York.

Kameyama, N., C. Maruyama, S. Matsui, R. Araki, Y. Yamada, and T. Maruyama
2014. Effects of consumption of main and side dishes with white rice on postprandial glucose, insulin, glucose-dependent insulinotropic polypeptide and glucagon-like peptide-1 responses in healthy japanese men. *British Journal of Nutrition*, 111(9):1632–1640.

Kamoi, K., Y. Shinozaki, K. Furukawa, and H. Sasaki
2011. Decreased active glp-1 response following large test meal in patients with type 1 diabetes using bolus insulin analogues. *Endocrine Journal*, 58(10):905–911.

Kang, S., J. Brange, A. Burch, A. Volund, and D. R. Owens
1991. Subcutaneous insulin absorption explained by insulin's physicochemical properties. evidence from absorption studies of soluble human insulin and insulin analogues in humans. *Diabetes Care*, 14(11):942–8.

Kar, P., K. L. Jones, M. Horowitz, M. J. Chapman, and A. M. Deane
2014. Measurement of gastric emptying in the critically ill. *Clinical Nutrition*.

Karstoft, K., S. P. Mortensen, S. H. Knudsen, and T. P. J. Solomon
2015. Direct effect of incretin hormones on glucose and glycerol metabolism and hemodynamics. *American Journal of Physiology - Endocrinology and Metabolism*, 308(5):E426–E433.

Khovanova, N. A., I. A. Khovanov, L. Sbano, F. Griffiths, and T. A. Holt
2013. Characterisation of linear predictability and non-stationarity of subcutaneous glucose profiles. *Computer Methods and Programs in Biomedicine*, 110(3):260–267.

Kim, D. Y., Y. S. Jung, R. W. Park, and N. S. Joo
2014. Different location of triaxial accelerometer and different energy expenditures. *Yonsei Medical Journal*, 55(4):1145–1151.

Kirchsteiger, H., J. Jørgensen, E. Renard, and L. Re
2015. *Prediction Methods for Blood Glucose Concentration: Design, Use and Evaluation*. Springer International Publishing.

Klonoff, D. C.
2007. The artifcial pancreas: How sweet engineering will solve bitter problems. *Journal of Diabetes Science and Technology*, 1(1):72–81.

Koivisto, V. and P. Felig
1978. Effects of leg exercise on insulin absorption in diabetic patients. *New England Journal of Medicine*, 298(2):79–83.

Kong, M. F. S. C., I. A. Macdonald, and R. B. Tattersall
1996. Gastric emptying in diabetes. *Diabetic Medicine*, 13(2):112–119.

Kouzi, S. A., S. Yang, D. S. Nuzum, and A. J. Dirks-Naylor
2015. Natural supplements for improving insulin sensitivity and glucose uptake in skeletal muscle. *Frontiers in Bioscience - Elite*, 7E(1):107–121.

Kovacs, L., B. Kulcsar, J. Bokor, and Z. Benyo
2008. Model-based nonlinear optimal blood glucose control of type i diabetes patients. In *2008 30th Annual International Conference of the IEEE Engineering in Medicine and Biology Society*, Pp. 1607–1610.

Kovatchev, B. P., M. Breton, C. Dalla Man, and C. Cobelli
2009. In silico preclinical trials: A proof of concept in closed-loop control of type 1 diabetes. *Journal of Diabetes Science and Technology*, 3(1):44–55.

Kovatchev, B. P., D. J. Cox, L. A. Gonder-Frederick, and W. Clarke
1997. Symmetrization of the blood glucose measurement scale and its applications. *Diabetes Care*, 20(11):1655–8.

Kumar, S. K., P. Khare, A. K. Jaryal, and A. Talwar
2012. Validity of heart rate based nomogram fors estimation of maximum oxygen uptake in indian population. *Indian J Physiol Pharmacol*, 56(3):279–83.

Kurtze, N., V. Rangul, B. E. Hustvedt, and W. D. Flanders
2007. Reliability and validity of self-reported physical activity in the nord-trøndelag health study (hunt 2). *European Journal of Epidemiology*, 22(6):379–387.

Lartigue, S., Y. Bizais, S. Bruley des Varannes, A. Murat, B. Pouliquen, and J. P. Galmiche
1994. Inter- and intrasubject variability of solid and liquid gastric emptying parameters - a scintigraphic study in healthy subjects and diabetic patients. *Digestive Diseases and Sciences*, 39(1):109–115.

Lehmann, E. D. and T. Deutsch
1992. A physiological model of glucose-insulin interaction in type 1 diabetes mellitus. *J Biomed Eng*, 14(3):235–42.

Lehmann, E. D., C. Tarín, J. Bondia, E. Teufel, and T. Deutsch
2009. Incorporating a generic model of subcutaneous insulin absorption into the aida v4 diabetes simulator 3. early plasma insulin determinations. *Journal of diabetes science and technology (Online)*, 3(1):190–201.

Li, J. and J. D. Johnson
2009. Mathematical models of subcutaneous injection of insulin analogues: A mini-review. *Discrete and Continuous Dynamical Systems - Series B*, 12(2):401–414.

Li, J. and Y. Kuang
2009. Systemically modeling the dynamics of plasma insulin in

subcutaneous injection of insulin analogues for type 1 diabetes. *Mathematical biosciences and engineering : MBE*, 6(1):41–58.

Lin, J., N. N. Razak, C. G. Pretty, A. Le Compte, P. Docherty, J. D. Parente, G. M. Shaw, C. E. Hann, and J. Geoffrey Chase
2011. A physiological intensive control insulin-nutrition-glucose (icing) model validated in critically ill patients. *Computer Methods and Programs in Biomedicine*, 102(2):192–205.

Lindholm, A. and L. V. Jacobsen
2001. Clinical pharmacokinetics and pharmacodynamics of insulin aspart. *Clinical Pharmacokinetics*, 40(9):641–659.

Liu, Y., Y. Sun, Q. P. Xue, and J. M. Li
2007. Diagnosis and pathogenic mechanism of diabetic gastroparesis. *World Chinese Journal of Digestology*, 15(3):290–293.

Lloyd, C. E., P. H. Dyer, R. J. Lancashire, T. Harris, J. E. Daniels, and A. H. Barnett
1999. Association between stress and glycemic control in adults with type 1 (insulin-dependent) diabetes. *Diabetes Care*, 22(8):1278–1283.

Lodefalk, M., J. Åman, and P. Bang
2008. Effects of fat supplementation on glycaemic response and gastric emptying in adolescents with type 1 diabetes. *Diabetic Medicine*, 25(9):1030–1035.

Lotz, T. F., J. G. Chase, K. A. McAuley, G. M. Shaw, P. D. Docherty, J. E. Berkeley, S. M. Williams, C. E. Hann, and J. I. Mann
2010. Design and clinical pilot testing of the model-based dynamic insulin sensitivity and secretion test (disst). *Journal of Diabetes Science and Technology*, 4(6):1408–1423.

Lovell-Smith, H. D., T. Kenealy, and S. Buetow
2010. Eating when empty is good for your health. *Medical Hypotheses*, 75(2):172–178.

Lugari, R., C. Dell'Anna, D. Ugolotti, A. Dei Cas, A. Barilli, R. Zandomeneghi, B. Marani, M. Iotti, A. Orlandini, and A. Gnudi
2000. Effect of nutrient ingestion on glucagon-like peptide 1 (7-36 amide) secretion in human type 1 and type 2 diabetes. *Hormone and Metabolic Research*, 32(10):424–428. cited By 52.

Luharuka, R., R. X. Gao, and S. Krishnamurty
2003. Design and realization of a portable data logger for physiological sensing. *IEEE Transactions on Instrumentation and Measurement*, 52(4):1289–1295.

Lunt, H. and L. J. Brown
1996. Self-reported changes in capillary glucose and insulin requirements during the menstrual cycle. *Diabetic Medicine*, 13(6):525–530.

Lustman, P. J., R. J. Anderson, K. E. Freedland, M. De Groot, R. M. Carney, and R. E. Clouse
2000. Depression and poor glycemic control: A meta-analytic review of the literature. *Diabetes Care*, 23(7):934–942.

Macdonald, I. A.
1996. Physiological regulation of gastric emptying and glucose absorption. *Diabetic Medicine*, 13(SUPPL. 5):S11–S15.

Magkos, F., Y. Tsekouras, S. A. Kavouras, B. Mittendorfer, and L. S. Sidossis
2008. Improved insulin sensitivity after a single bout of exercise is curvilinearly related to exercise energy expenditure. *Clinical Science*, 114(1-2):59–64.

Mallad, A., L. Hinshaw, M. Schiavon, C. D. Man, V. Dadlani, R. Basu, R. Lingineni, C. Cobelli, M. L. Johnson, R. Carter, Y. C. Kudva, and A. Basu
2015. Exercise effects on postprandial glucose metabolism in type 1 diabetes: A triple-tracer approach. *American Journal of Physiology - Endocrinology and Metabolism*, 308(12):E1106–E1115.

Mann, T., R. P. Lamberts, and M. I. Lambert
2013. Methods of prescribing relative exercise intensity: Physiological and practical considerations. *Sports Medicine*, 43(7):613–625.

Mansell, E., R. Langdon, P. D. Docherty, S. Schmidt, H. Madsen, J. Bagterp-Jørgensen, and J. G. Chase
2016. Use of non-linear autoregressive correlation to define insulin kinetics and glucose dynamics during subcutaneous aspart infusion in type 1 diabetes. In *2016 New Zealand Society for the Study of Diabetes (NZSSD) Annual Scientific Meeting*, J. Brosnahan, ed.

Mansell, E., H. Lunt, and P. Docherty
2017a. Laboratory diagnosis of gestational diabetes: An in silico investigation into the effects of pre-analytical processing on the diagnostic sensitivity and specificity of the oral glucose tolerance test. *Clinical Biochemistry*, 50(9):506 – 512.

Mansell, E. J., P. D. Docherty, and J. G. Chase
2015a. The detectability of confounding effects in glycemic diary data from in silico patients with diabetes. In *15th Annual Diabetes Technology Meeting 2015*, D. Shilstone, ed.

Mansell, E. J., P. D. Docherty, and J. G. Chase
2015b. The precision of identified variables with respect to multivariable set size in glycaemic data from a virtual type 1 diabetic patient. In *9th IFAC Symposium on Biological and Medical System*, T. Schauer, ed., Berlin, Germany.

Mansell, E. J., P. D. Docherty, and J. G. Chase
2017b. Shedding light on grey noise in diabetes modelling. *Biomedical Signal Processing and Control*, 31:16–30.

Mansell, E. J., P. D. Docherty, J. G. Chase, and B. Benyo
2015c. An eigen-analysis of the relationships between model structure, discrete data, measurement error and resulting parameter identification

distributions. In *9th IFAC Symposium on Biological and Medical System*, T. Schauer, ed., Berlin, Germany.

Mansell, E. J., P. D. Docherty, L. M. Fisk, and J. G. Chase
2015d. Estimation of secondary effect parameters in glycaemic dynamics using accumulating data from a virtual type 1 diabetic patient. *Mathematical Biosciences*, 266:108–117.

Mari, A., J. Wahren, R. A. DeFronzo, and E. Ferrannini
1994. Glucose absorption and production following oral glucose: Comparison of compartmental and arteriovenous-difference methods. *Metabolism*, 43(11):1419–1425.

Markakis, M. G., G. D. Mitsis, G. P. Papavassilopoulos, and V. Z. Marmarelis
2008. Model predictive control of blood glucose in type 1 diabetes: The principal dynamic modes approach. In *2008 30th Annual International Conference of the IEEE Engineering in Medicine and Biology Society*, Pp. 5466–5469.

Mayer-Davis, E. J., R. D'Agostino Jr, A. J. Karter, S. M. Haffner, M. J. Rewers, M. Saad, and R. N. Bergman
1998. Intensity and amount of physical activity in relation to insulin sensitivity the insulin resistance atherosclerosis study. *Journal of the American Medical Association*, 279(9):669–674.

Meneilly, G. S., C. H. S. McIntosh, R. A. Pederson, J. F. Habener, R. Gingerich, J. M. Egan, D. T. Finegood, and D. Elahi
2001. Effect of glucagon-like peptide 1 on non-insulin-mediated glucose uptake in the elderly patient with diabetes. *Diabetes Care*, 24(11):1951–1956.

Mishra, S. and J. Monro
2012. Wholeness and primary and secondary food structure effects on in vitro digestion patterns determine nutritionally distinct carbohydrate fractions in cereal foods. *Food Chemistry*, 135(3):1968–1974.

Monro, J. A.
2013. Kiwifruit, carbohydrate availability, and the glycemic response. In *Advances in Food and Nutrition Research*, volume 68, Pp. 257–271.

Montastier, E., S. Déjean, C. Le Gall, W. H. M. Saris, D. Langin, and N. Viguerie
2014. Adipose tissue cidea is associated, independently of weight variation, to change in insulin resistance during a longitudinal weight control dietary program in obese individuals. *PLoS ONE*, 9(7).

Mourad, F. H. and N. E. Saadé
2011. Neural regulation of intestinal nutrient absorption. *Progress in Neurobiology*, 95(2):149–162.

Mourot, J., P. Thouvenot, C. Couet, J. M. Antoine, A. Krobicka, and G. Debry
1988. Relationship between the rate of gastric emptying and glucose and insulin responses to starchy foods in young healthy adults. *American Journal of Clinical Nutrition*, 48(4):1035–1040.

Nathan, R. S., E. J. Sachar, G. M. Asnis, U. Halbreich, and F. S. Halpern
1981. Relative insulin insensitivity and cortisol secretion in depressed patients. *Psychiatry Research*, 4(3):291–300.

Nesbitt, G. S., M. Smye, B. Sheridan, T. R. J. Lappin, E. R. Trimble, and H. C. R. Grp
2006. Integration of local and central laboratory functions in a worldwide multicentre study: Experience from the hyperglycemia and adverse pregnancy outcome (hapo) study. *Clinical Trials*, 3(4):397–407.

Nguyen, N. Q., T. L. Debreceni, J. E. Bambrick, B. Chia, J. Wishart, A. M. Deane, C. K. Rayner, M. Horowitz, and R. L. Young
2015. Accelerated intestinal glucose absorption in morbidly obese humans: Relationship to glucose transporters, incretin hormones, and glycemia. *Journal of Clinical Endocrinology and Metabolism*, 100(3):968–976.

Nilam, M. E. Alexander, R. Mathur, S. M. Moghadas, and P. N. Shivakumar
2007. Modelling the effect of csii on the control of glucose concentration in type 1 diabetes. *Applied Mathematics and Computation*, 187(2):1476–1483.

Palumbo, P., S. Ditlevsen, A. Bertuzzi, and A. De Gaetano
2013. Mathematical modeling of the glucose-insulin system: A review. *Mathematical Biosciences*, 244(2):69–81.

Pappada, S. M., B. D. Cameron, D. B. Tulman, R. E. Bourey, M. J. Borst, W. Olorunto, S. D. Bergese, D. C. Evans, S. P. A. Stawicki, and T. J. Papadimos
2013. Evaluation of a model for glycemic prediction in critically ill surgical patients. *PLoS ONE*, 8(7).

Parker, R. S., F. J. Doyle, J. H. Ward, and N. A. Peppas
2000. Robust h glucose control in diabetes using a physiological model. *AIChE Journal*, 46(12):2537–2549.

Peplies, J., D. Jimenez-Pavon, S. C. Savva, C. Buck, K. Gunther, A. Fraterman, P. Russo, L. Iacoviello, T. Veidebaum, M. Tornaritis, S. De Henauw, S. Marild, D. Molnar, L. A. Moreno, and W. Ahrens
2014. Percentiles of fasting serum insulin, glucose, hba1c and homa-ir in pre-pubertal normal weight european children from the idefics cohort. *Int J Obes*, 38(S2):S39–S47.

Petersen, S. B., J. M. Lovmand, L. Honoré, C. B. Jeppesen, L. Pridal, and O. Skyggebjerg
2010. Comparison of a luminescent oxygen channeling immunoassay and an elisa for detecting insulin aspart in human serum. *Journal of Pharmaceutical and Biomedical Analysis*, 51(1):217–224.

Pielmeier, U., S. Andreassen, B. S. Nielsen, J. G. Chase, and P. Haure
2010. A simulation model of insulin saturation and glucose balance for glycemic control in icu patients. *Computer Methods and Programs in Biomedicine*, 97(3):211–222.

Pillonetto, G., G. Sparacino, and C. Cobelli
2003. Numerical non-identifiability regions of the minimal model of glucose kinetics: superiority of bayesian estimation. *Mathematical Biosciences*, 184(1):53–67.

Pillonetto, G., G. Sparacino, P. Magni, R. Bellazzi, and C. Cobelli
2002. Minimal model si=0 problem in niddm subjects: nonzero bayesian estimates with credible confidence intervals. *American Journal of Physiology - Endocrinology and Metabolism*, 282(3):E564–E573.

Plank, J., J. Blaha, J. Cordingley, M. E. Wilinska, L. J. Chassin, C. Morgan, S. Squire, M. Haluzik, J. Kremen, S. Svacina, W. Toller, A. Plasnik, M. Ellmerer, R. Hovorka, and T. R. Pieber
2006. Multicentric, randomized, controlled trial to evaluate blood glucose control by the model predictive control algorithm versus routine glucose management protocols in intensive care unit patients. *Diabetes Care*, 29(2):271–6.

Pohjanpalo, H.
1978. System identifiability based on the power series expansion of the solution. *Mathematical Biosciences*, 41(1-2):21–33.

Pories, W. J. and G. L. Dohm
2012. Diabetes: Have we got it all wrong?: Hyperinsulinism as the culprit: surgery provides the evidence. *Diabetes Care*, 35(12):2438–2442.

Prigeon, R. L., S. Quddusi, B. Paty, and D. A. D'Alessio
2003. Suppression of glucose production by glp-1 independent of islet hormones: A novel extrapancreatic effect. *American Journal of Physiology - Endocrinology and Metabolism*, 285(4 48-4):E701–E707.

Quon, M. J., C. Cochran, S. I. Taylor, and R. C. Eastman
1994. Non-insulin-mediated glucose disappearance in subjects with iddm: Discordance between experimental results and minimal model analysis. *Diabetes*, 43(7):890–896.

Radziuk, J., K. H. Norwich, and M. Vranic
1978. Experimental validation of measurements of glucose turnover in nonsteady state. *Am J Physiol*, 234(1):E84–93.

Räikkönen, K., L. Keltikangas-Järvinen, H. Adlercreutz, and A. Hautanen
1996. Psychosocial stress and the insulin resistance syndrome. *Metabolism: Clinical and Experimental*, 45(12):1533–1538.

Ramalho, A. C. R., C. M. Andrade, and F. V. D. O. Prates
2009. Menstrual cycle and glycemic control. *Recent Patents on Endocrine, Metabolic and Immune Drug Discovery*, 3(1):65–68.

Ramkissoon, C. M. and J. Vehí
2015. Emotions and diabetes. In *Lecture Notes in Computer Science (including subseries Lecture Notes in Artificial Intelligence and Lecture Notes in Bioinformatics)*, volume 9044, Pp. 720–727.

Rasmussen, C. H., R. M. Røge, Z. Ma, M. Thomsen, R. L. Thorisdottir, J. W. Chen, E. Mosekilde, and M. Colding-Jørgensen
2014. Insulin aspart pharmacokinetics: An assessment of its variability and underlying mechanisms. *European Journal of Pharmaceutical Sciences*, 62:65–75.

Raue, A., J. Karlsson, M. P. Saccomani, M. Jirstrand, and J. Timmer
2014. Comparison of approaches for parameter identifiability analysis of biological systems. *Bioinformatics*, 30(10):1440–1448.

Raue, A., C. Kreutz, T. Maiwald, J. Bachmann, M. Schilling, U. Klingmüller, and J. Timmer
2009. Structural and practical identifiability analysis of partially observed dynamical models by exploiting the profile likelihood. *Bioinformatics*, 25(15):1923–1929.

Raue, A., C. Kreutz, F. J. Theis, and J. Timmer
2012. Joining forces of bayesian and frequentist methodology: a study for inference in the presence of non-identifiability. *Philosophical Transactions*

of the Royal Society of London A: Mathematical, Physical and Engineering Sciences, 371(1984).

Reinus, J. F. and D. Simon

2014. Gastrointestinal anatomy and physiology : The essentials.

Retnakaran, R. and B. Zinman

2008. Type 1 diabetes, hyperglycaemia, and the heart. *The Lancet*, 371(9626):1790–1799.

Rijkelijkhuizen, J. M., K. McQuarrie, C. J. Girman, P. P. Stein, A. Mari, J. J. Holst, G. Nijpels, and J. M. Dekker

2010. Effects of meal size and composition on incretin, -cell, and -cell responses. *Metabolism: Clinical and Experimental*, 59(4):502–511.

Ritt, J. F.

1950. *Differential Algebra*, volume XXXIII of *American Mathematical Society Colloquium Publications*. New York, N.Y.: American Mathematical Society.

Rizza, R. A., L. J. Mandarino, and J. E. Gerich

1982. Cortisol-induced insulin resistance in man: Impaired suppression of glucose production and stimulation of glucose utilization due to a postreceptor defect of insulin action. *Journal of Clinical Endocrinology and Metabolism*, 54(1):131–138.

Roach, P. and J. R. Woodworth

2002. Clinical pharmacokinetics and pharmacodynamics of insulin lispro mixtures. *Clinical Pharmacokinetics*, 41(13):1043–1057.

Roy, A. and R. S. Parker

2007. Dynamic modeling of exercise effects on plasma glucose and insulin levels. *Journal of Diabetes Science and Technology*, 1(3):338–347.

Rubin, R. R. and M. Peyrot
1999. Quality of life and diabetes. *Diabetes/Metabolism Research and Reviews*, 15(3):205–218.

Rubin, R. R. and M. Peyrot
2001. Psychological issues and treatments for people with diabetes. *Journal of Clinical Psychology*, 57(4):457–478.

Saccomani, M. P.
2013. Structural vs practical identifiability in system biology. In *IWBBIO*, I. Rojas and F. M. O. n. Guzman, eds., Pp. 305–313. Copicentro Editorial.

Saha, S., P. Nag, and M. K. Ray
2014. A complete virtual instrument for measuring and analyzing human stress in real time. In *International Conference on Control, Instrumentation, Energy and Communication, CIEC 2014*, Pp. 81–85.

Salinari, S., A. Bertuzzi, and G. Mingrone
2011. Intestinal transit of a glucose bolus and incretin kinetics: A mathematical model with application to the oral glucose tolerance test. *American Journal of Physiology - Endocrinology and Metabolism*, 300(6):E955–E965.

Samsom, M., L. M. A. Akkermans, R. J. A. Jebbink, H. Van Isselt, G. P. VanBerge-Henegouwen, and A. J. P. M. Smout
1997. Gastrointestinal motor mechanisms in hyperglycaemia induced delayed gastric emptying in type i diabetes mellitus. *Gut*, 40(5):641–646.

Schmidt, S., D. Finan, A. Duun-Henriksen, J. Jørgensen, H. Madsen, H. Bengtsson, J. Holst, S. Madsbad, and K. Nørgaard
2012. Effects of everyday life events on glucose, insulin, and glucagon dynamics in continuous subcutaneous insulin infusion-treated type 1 diabetes: Collection of clinical data for glucose modeling. *Diabetes Technology and Therapeutics*, 14(3):210–217.

Schrack, J. A., E. M. Simonsick, and L. Ferrucci
2010. Comparison of the cosmed k4b2 portable metabolic system in measuring steady-state walking energy expenditure. *PLoS ONE*, 5(2).

Schranz, C., C. Knobel, J. Kretschmer, Z. Zhao, and K. Moller
2011. Hierarchical parameter identification in models of respiratory mechanics. *IEEE Trans Biomed Eng*, 58(11):3234–41.

Schvarcz, E., M. Palmer, J. Aman, M. Horowitz, M. Stridsberg, and C. Berne
1997. Physiological hyperglycemia slows gastric emptying in normal subjects and patients with insulin-dependent diabetes mellitus. *Gastroenterology*, 113(1):60–66.

Scott, C. B.
2006. Estimating energy expenditure for brief bouts of exercise with acute recovery. *Applied Physiology, Nutrition and Metabolism*, 31(2):144–149.

Sensi, S. and F. Capani
1976. Circadian rhythm of insulin-induced hypoglycemia in man. *The Journal of Clinical Endocrinology & Metabolism*, 43(2):462–465.

Shankar, A., R. Klein, B. E. K. Klein, and S. E. Moss
2007. Association between glycosylated hemoglobin level and cardiovascular and all-cause mortality in type 1 diabetes. *American Journal of Epidemiology*, 166(4):393–402.

Sherwin, R. S., K. J. Kramer, J. D. Tobin, P. A. Insel, J. E. Liljenquist, M. Berman, and R. Andres
1974. A model of the kinetics of insulin in man. *Journal of Clinical Investigation*, 53(5):1481–1492.

Siegel, J. A., J. L. Urbain, L. P. Adler, N. D. Charkes, A. H. Maurer, B. Krevsky, L. C. Knight, R. S. Fisher, and L. S. Malmud
1988. Biphasic nature of gastric emptying. *Gut*, 29(1):85–89.

Singh, K. and M. Xie
2003. Bootlier-plot: Bootstrap based outlier detection plot. *Sankhy: The Indian Journal of Statistics (2003-2007)*, 65(3):532–559.

Song, X., M. Huang, and J. Li
2014. Modeling impulsive insulin delivery in insulin pump with time delays. *SIAM Journal on Applied Mathematics*, 74(6):1763–1785. Export Date: 9 May 2016.

Sonnenberg, G. E., F. W. Kemmer, and M. Berger
1990. Exercise in type 1 (insulin-dependent) diabetic patients treated with continuous subcutaneous insulin infusion. *Diabetologia*, 33(11):696–703.

Sorensen, J. T.
1985. *A physiologic model of glucose metabolism in man and its use to design and assess improved insulin therapies for diabetes.* PhD thesis, Massachusetts Institute of Technology.

Sosenko, J. M., J. S. Skyler, J. P. Palmer, J. P. Krischer, L. Yu, J. Mahon, C. A. Beam, D. C. Boulware, L. Rafkin, D. Schatz, and G. Eisenbarth
2013. The prediction of type 1 diabetes by multiple autoantibody levels and their incorporation into an autoantibody risk score in relatives of type 1 diabetic patients. *Diabetes Care*, 36(9):2615–2620.

Steele, R.
1959. Influences of glucose loading and of injected insulin on hepatic glucose output. *Annals of the New York Academy of Sciences*, 82:420–430.

Stephens, E.
2015. Insulin therapy in type 1 diabetes. *Medical Clinics of North America*, 99(1):145–156.

Strath, S. J., D. R. Bassett Jr, D. L. Thompson, and A. M. Swartz
2002. Validity of the simultaneous heart rate-motion sensor technique

for measuring energy expenditure. *Medicine and Science in Sports and Exercise*, 34(5):888–894.

Strath, S. J., A. M. Swartz, J. Bassett D.R, W. L. O'Brien, G. A. King, and B. E. Ainsworth

2000. Evaluation of heart rate as a method for assessing moderate intensity physical activity. *Medicine and Science in Sports and Exercise*, 32(9 SUPPL.):S465–S470.

Sun, S. Z. and M. W. Empie

2012. Fructose metabolism in humans - what isotopic tracer studies tell us. *Nutrition and Metabolism*, 9.

Sunehag, A. L. and M. W. Haymond

2002. Splanchnic galactose extraction is regulated by coingestion of glucose in humans. *Metabolism: Clinical and Experimental*, 51(7):827–832.

Surwit, R. S., M. S. Schneider, and M. N. Feinglos

1992. Stress and diabetes mellitus. *Diabetes Care*, 15(10):1413–1422.

Sykes, K. and A. Roberts

2004. The chester step test-a simple yet effective tool for the prediction of aerobic capacity. *Physiotherapy*, 90(4):183–188.

Szarka, L. A. and M. Camilleri

2009. Methods for measurement of gastric motility. *American Journal of Physiology - Gastrointestinal and Liver Physiology*, 296(3):G461–G475.

Tahrani, A. A., A. H. Barnett, and C. J. Bailey

2013. Sglt inhibitors in management of diabetes. *The Lancet Diabetes and Endocrinology*, 1(2):140–151.

The DIAMOND Project Group

2006. Incidence and trends of childhood type 1 diabetes worldwide 19901999. *Diabetic Medicine*, 23(8):857–866.

The HAPO Study Cooperative Research Group
2008. Hyperglycemia and adverse pregnancy outcomes. *New England Journal of Medicine*, 358(19):1991–2002.

Toffanin, C., H. Zisser, F. J. Doyle Iii, and E. Dassau
2013. Dynamic insulin on board: Incorporation of circadian insulin sensitivity variation. *Journal of Diabetes Science and Technology*, 7(4):928–940.

Torsdottir, I., M. Alpsten, and H. Andersson
1986. Effect of different starchy foods in composite meals on gastric emptying rate and glucose metabolism. ii. comparisons between potatoes, rice and white beans in diabetic subjects. *Human Nutrition: Clinical Nutrition*, 40(5):397–400.

Tranberg, K. G. and H. Dencker
1978. Modeling of plasma disappearance of unlabeled insulin in man. *American Journal of Physiology - Endocrinology and Metabolism*, 235(6):E577.

Uchida, K., R. Matuse, E. Toyoda, S. Okuda, and S. Tomita
1988. A new method of inhibiting glycolysis in blood samples. *Clin Chim Acta*, 172(1):101–8.

Uth, N., H. Sørensen, K. Overgaard, and P. K. Pedersen
2004. Estimation of vo2max from the ratio between hrmax and hrrest - the heart rate ratio method. *European Journal of Applied Physiology*, 91(1):111–115.

Van Cauter, E., K. S. Polonsky, and A. J. Scheen
1997. Roles of circadian rhythmicity and sleep in human glucose regulation. *Endocrine Reviews*, 18(5):716–738.

Velchik, M. G., J. C. Reynolds, and A. Alavi
1989. The effect of meal energy content on gastric emptying. *Journal of Nuclear Medicine*, 30(6):1106–1110.

Veluswamy, S. K., V. Guddattu, and A. G. Maiya
2015. Test-retest reliability of a portable gas analysis system under free living conditions. *Indian Journal of Physiology and Pharmacology*, 59(1):117–120.

Vilsbøll, T., T. Krarup, J. Sonne, S. Madsbad, A. Vølund, A. G. Juul, and J. J. Holst
2003. Incretin secretion in relation to meal size and body weight in healthy subjects and people with type 1 and type 2 diabetes mellitus. *Journal of Clinical Endocrinology and Metabolism*, 88(6):2706–2713.

Visentin, R., C. Dalla Man, Y. C. Kudva, A. Basu, and C. Cobelli
2015. Circadian variability of insulin sensitivity: Physiological input for in silico artificial pancreas. *Diabetes Technology and Therapeutics*, 17(1):1–7.

Ward, W. K., J. R. Castle, and J. El Youssef
2011. Safe glycemic management during closed-loop treatment of type 1 diabetes: the role of glucagon, use of multiple sensors, and compensation for stress hyperglycemia. *Journal of diabetes science and technology*, 5(6):1373–1380.

Wenzel, C., H. G. Wenzel, K. Golka, M. Rutenfranz, and J. Rutenfranz
1990. A comparative study on different methods for the determination of energy expenditure. *International Archives of Occupational and Environmental Health*, 61(8):101–103.

Werner, M., S. H. Brooks, and L. B. Knott
1978. Additive, multiplicative, and mixed analytical errors. *Clinical Chemistry*, 24(11):1895–1898.

Whitley, E. and J. Ball
2002. Statistics review 2: Samples and populations. *Critical Care*, 6(2):143–148.

Wilinska, M. E., L. J. Chassin, H. C. Schaller, L. Schaupp, T. R. Pieber, and

R. Hovorka
2005. Insulin kinetics in type-1 diabetes: Continuous and bolus delivery of rapid acting insulin. *IEEE Transactions on Biomedical Engineering*, 52(1):3–12.

Wong, J., J. G. Chase, C. E. Hann, G. M. Shaw, T. F. Lotz, J. Lin, and A. J. Le Compte
2008a. A subcutaneous insulin pharmacokinetic model for computer simulation in a diabetes decision support role: Model structure and parameter identification. *Journal of Diabetes Science and Technology*, 2(4):658–671.

Wong, J., J. G. Chase, C. E. Hann, G. M. Shaw, T. F. Lotz, J. Lin, and A. J. Le Compte
2008b. A subcutaneous insulin pharmacokinetic model for computer simulation in a diabetes decision support role: Validation and simulation. *Journal of Diabetes Science and Technology*, 2(4):672–680.

Wong, X.-W., J. G. Chase, C. E. Hann, T. Lotz, J. Lin, A. J. Le Compte, and G. M. Shaw
2008c. Development of a clinical type 1 diabetes metabolic system model and in silico simulation tool. *Journal of Diabetes Science and Technology*, 2(3):424–435.

Wong, X.-W., J. G. Chase, A. J. Le Compte, C. E. Hann, J. Lin, and G. M. Shaw
2009. An adaptive clinical type 1 diabetes control protocol to optimize conventional self-monitoring blood glucose and multiple daily-injection therapy. *International Journal of Adaptive Control and Signal Processing*, 23(5):408–434.

Worthington, D. R. L.
1997. Minimal model of food absorption in the gut. *Medical Informatics*, 22(1):35–45.

Wu, H.-i.
2005. A case study of type 2 diabetes self-management. *BioMedical Engineering OnLine*, 4(1):4.

Xiu, F., M. Stanojcic, L. Diao, and M. G. Jeschke
2014. Stress hyperglycemia, insulin treatment, and innate immune cells. *International Journal of Endocrinology*, 2014.

Yardley, J. E., R. J. Sigal, B. A. Perkins, M. C. Riddell, and G. P. Kenny
2013. Resistance exercise in type 1 diabetes. *Canadian Journal of Diabetes*, 37(6):420–426.

Yumiko, Y., K. Takashi, T. Akiko, N. Akiko, H. Makoto, S. Hidehiko, and O. Yoshiyuki
2002. Comparison of accelerometry and oxymetry for measuring daily physical activity. *Circulation Journal*, 66(8):751–754.

Zangheri, M., L. Cevenini, L. Anfossi, C. Baggiani, P. Simoni, F. Di Nardo, and A. Roda
2015. A simple and compact smartphone accessory for quantitative chemiluminescence-based lateral flow immunoassay for salivary cortisol detection. *Biosensors and Bioelectronics*, 64:63–68.

Zibar, K., J. Ćuća, K. Blaslov, T. Bulum, and L. Smirčić-Duvnjak
2015. Difference in glucagon-like peptide-1 concentrations between c-peptide negative type 1 diabetes mellitus patients and healthy controls. *Annals of Clinical Biochemistry*, 52(2):220–225.